NONLINEAR STATIC AND DYNAMIC ANALYSIS OF REINFORCED CONCRETE SUBASSEMBLAGES

by

Filip C. Filippou
Associate Professor

Angelo D'Ambrisi
Research Assistant

Ahmad Issa
formerly, Doctoral Student

Report on Research Conducted
under Grant ECE-8657525
from the National Science Foundation

Report No. UCB/EERC–92/08
Earthquake Engineering Research Center
College of Engineering
University of California, Berkeley

August 1992

ABSTRACT

This study is devoted to the development of improved models and methods for predicting the nonlinear static and dynamic response of reinforced concrete frames. In this respect it is a continuation of the work presented in an earlier study (Filippou and Issa, 1988).

To achieve the general objective new models for reinforced concrete girders were proposed in the earlier study (Filippou and Issa, 1988). Each girder was decomposed into a number of subelements which were connected in series. Each subelement describes a different source of inelastic deformation and energy dissipation in reinforced concrete members. Three subelements were developed in the earlier study: (a) an elastic subelement which models the flexural behavior of the frame member before yielding of the reinforcement; (b) a spread plastic subelement which describes the inelastic flexural behavior of the reinforced concrete member and accounts for the gradual spread of inelastic deformation at the member ends; and (c) a joint subelement modeling the fixed-end rotation that arises at the beam-column interface due to bond deterioration and slippage of reinforcing bars along the anchorage in the joint.

The present study introduces several new subelements. The first is a shear subelement which describes the deformation due to shear and, in particular, due to the shear sliding in the inelastic regions of reinforced concrete members, and complements the list of girder subelements of the earlier study. The other subelements refer to the hysteretic behavior of RC columns and are extensions of the corresponding girder subelements to account for the effect of axial load on the flexural and shear behavior of the member.

The proposed reinforced concrete frame models are implemented in a special purpose computer program for the nonlinear static and dynamic analysis of reinforced concrete frames. A nonlinear solution method which accounts for the possible unbalance of internal forces between the different subelements during the load step and an algorithm for the efficient numerical implementation of this solution strategy was already proposed in the earlier study. This procedure is now extended to include the additional subelements, but, more importantly, to address time varying loads due to ground acceleration. Implementation issues under static and dynamic loading conditions are also addressed in the present study.

The analytical results are compared with experimental information from beam-column subassemblages under cyclic deformation reversals. Only studies related to the effects of

shear and axial load are discussed. These correlation studies complement those presented earlier by Filippou and Issa (1988).

The ability of the proposed models to describe the dynamic response of frame structures that are excited by ground accelerations is evaluated by comparing the analytical results with experimental evidence from a two story one bay reinforced concrete frame that was tested on the shaking table. The effect of bond slip on the local and global dynamic response of the structure is evaluated. The results of the proposed model are compared with those of the widely used one component model in order to assess the ability of the latter to determine the local and global response of reinforced concrete frames.

ACKNOWLEDGEMENTS

This report is part of a larger study on the seismic behavior of reinforced concrete structures supported by Grant ECE-8657525 from the National Science Foundation. This support is gratefully acknowledged. Any opinions expressed in this report are those of the authors and do not reflect the views of the sponsoring agency.

The second author gratefully acknowledges ISRIM - Istituto Superiore di Ricerca sui Materiali Speciali, Terni, Italy and the Italian Dottorato di Ricerca in Meccanica delle Strutture, Bologna, Italy for their financial support during the first and second phase of this research work, respectively.

TABLE OF CONTENTS

CHAPTER 1

INTRODUCTION

1.1 General

In reinforced concrete (RC) frame structures, designed according to current specifications of earthquake resistant design, forces and displacements are expected to greatly exceed those induced by the equivalent static lateral loads stipulated in codes. When these structures are subjected to severe earthquake excitations they are expected to deform well into the inelastic range and dissipate the large seismic energy input into the structure through large but controllable inelastic deformations at critical regions. In order to predict the distribution of forces and deformations in these structures under the maximum credible earthquake that can occur at the site, accurate models of the hysteretic behavior of the different critical regions of the structure are necessary.

Many analytical models have been proposed to date for the nonlinear analysis of reinforced concrete frame structures. These range from very refined and complex local models to simplified global models. Refined analytical models are typically used in predicting the response of small structures or structural subassemblies. On the other hand simplified global models have been typically used in the dynamic response analysis of large structures. While simple component models are unreliable and incapable of simulating the local behavior of critical inelastic regions in the structure and cannot yield accurate estimates of strain or curvature ductilities, the computational cost associated with the use of refined finite element models in nonlinear dynamic response studies of high-rise concrete frames is very high.

In fact, the refined and detailed analysis of critical regions in the structure is impossible without the use of global models which predict the loading history of the particular region. Similarly, the global analysis of structures is impossible without the use of more refined local models which allow the estimation of parameters of the simple component models. The exchange of results between refined local models suitable for detailed analysis of small regions and more simplified component models suitable for global response analysis of multistory structures provides a powerful tool in the study of the seismic response of reinforced concrete structures. It is, therefore, important to bridge the gap between these two

alternatives by providing a platform for the exchange of results between local and global models of RC frame structures. While this is the overall framework of this study, it is not addressed further in this report, but will be the subject of forthcoming studies.

The major sources of deformation in reinforced concrete frame structures are flexural rotation, shear deformation, including shear sliding, and bond slip. The hysteretic load-deformation behavior of frame members arises from a combination of these deformation mechanisms. A rational analysis of the hysteretic behavior of reinforced concrete members needs to be based on the description of all deformation sources and of the interactions between the different mechanisms. This approach permits the determination of the relative contribution of each source of inelastic behavior to the local and global response of reinforced concrete frames. In order to achieve this goal new frame member models are developed in this study. Each member model is made up of different subelements. Each subelement represents a different source of inelastic behavior. The parameters of the subelements are established from first principles, or, otherwise from refined local models or experimental information. The exchange of results between refined local models and simpler global models is accomplished in a crude, manual manner in the present study. More sophisticated ways of exchanging data are left for future studies.

1.2 Review of previous studies

Much effort has been devoted in the last twenty five years to the development of models of inelastic response of reinforced concrete elements subjected to large cyclic deformation reversals. Numerous models incorporating information from experimental investigations and on-field observations of the hysteretic behavior of RC structural elements have been proposed. These range from the simple two-component model with bilinear hysteretic law to refined fiber or layer models based on sophisticated descriptions of the cyclic stress-strain behavior of concrete and reinforcing steel. Since this study focuses on relatively simple models which can be economically used in studying the seismic response of multistory frame structures, only the developments leading to a macroscopic model of inelastic response of RC elements will be briefly reviewed in the following.

The very first inelastic girder model was proposed by Clough et al. (1965). In this model, known as the two-component model, a bilinear elastic-strain hardening moment-curvature relationship is assumed along the girder. The beam model consists of two components acting in parallel: one which is linear elastic and one which is elastic-perfectly plastic with the plastic deformations concentrated in plastic hinges at the ends of the element. The elastic modulus of the first component is equal to the strain hardening modulus $p \cdot EI$ of

the moment-curvature relation, where EI is the pre-yield section stiffness. The elastic modulus of the elasto-plastic component is equal to $q \cdot EI$ where $q = 1 - p$. One of the shortcomings of this model is the difficulty of accounting for the stiffness deterioration of RC elements during cyclic load reversals.

To overcome the problem of stiffness deterioration Giberson proposed another model in 1969 (Giberson 1969). This model is known as the one-component model. It consists of two nonlinear rotational springs which are attached at the ends of a perfectly elastic element representing the girder. All nonlinear deformations of the girder element are lumped in the two rotational springs. This is a simplification of experimental evidence which shows that inelastic deformations spread over a finite region at the ends of the girder. Giberson's model has the advantage that any kind of hysteretic law can be assigned to the nonlinear springs. This fact along with the simplicity of the model accounts for its widespread use in analytical studies to date.

To describe the hysteretic behavior of the nonlinear springs at the ends of the one-component model a hysteretic law is needed. The first such law was proposed by Clough (1965). A more refined hysteresis model was proposed by Takeda et al. (1972). In this model the monotonic behavior is described by a trilinear skeleton curve which accounts for cracking of concrete and yielding of reinforcing steel. The hysteretic behavior is described through a number of rules for unloading and reloading and is based on data obtained from specimens tested in an earthquake simulator. Even though Takeda's hysteretic model was originally proposed for simulating the load-displacement relation of RC subassemblies, it has been widely used since in the description of the hysteretic moment-curvature or moment-rotation relation of RC members.

A different approach to the problem of modeling the seismic behavior of RC girders was proposed by Otani (1974). In this case each beam or column member is divided into two linear elements, one linearly elastic and one inelastic, which act in parallel. One inelastic rotational spring is attached at each end of the member. This spring represents the fixed-end rotation at the beam-column interface due to slip of the reinforcement in the joint. In Otani's model the linear elastic element describes the entire elastic stiffness of the girder; the flexibility matrix of the inelastic element is derived as a function of the location of the point of contraflexure. This approach results in a non-symmetric flexibility matrix, unless one of the following assumptions is made: (a) the inelastic deformations are concentrated at the girder ends, or (b) the contraflexure point is assumed fixed at the midspan of the member. Otani's study recognizes for the first time the importance of fixed-end rotations in predicting the seismic response of RC frame structures.

Mahin and Bertero (1976) reviewed the various definitions of ductility factors in earthquake resistant design. One of the most important questions in this context is the accurate prediction of the rotational ductility demand in structural elements. The study points out how ductility factors for a beam represented by a two-component model must be modified to match those for a beam in which inelastic deformations spread into the member. Since the two-component model substantially underestimates the post-yielding stiffness of a member, the seismic response of the structure will not be predicted accurately. This is particularly true in the case of local response quantities such as inelastic rotations of girders and joints. It does not, therefore, appear reasonable to estimate ductility requirements of RC frame elements on the basis of the results of the two-component model.

Anderson and Townsend (1977) investigated the effect of different hysteretic models on the dynamic response of RC frames. Four different models were used to describe the hysteretic behavior of critical regions of RC members: (a) a bilinear elastic-strain hardening model, (b) a bilinear degrading model with equal unloading and reloading stiffness, (c) a trilinear degrading model with different stiffness for unloading and reloading and (d) a trilinear degrading model for beam-column connections. They studied the effect of reinforcing bar slippage in the joint by inserting a small hinge element of predefined length between the rigid joint element and the flexible girder element. The study shows that the reduction in stiffness of reinforced concrete elements due to inelastic deformations can have a significant effect on the dynamic response of frame structures. Among the different hysteretic models used in the study the trilinear degrading connection model appears to be the most accurate. The study also shows that the use of a degrading stiffness model results in an increase in interstory displacements. This can have a significant effect on the load carrying capacity of the structure due to the P-Δ effect arising from high axial forces.

The first model which accounts for the spread of inelastic deformations into the member was introduced by Soleimani et al. (1979a). In this model a zone of inelastic deformations gradually spreads from the beam-column interface into the member as a function of loading history. The rest of the beam remains elastic. The fixed-end rotations at the beam-column interface are modeled through point hinges which are inserted at the ends of the member. These are related to the curvature at the corresponding end section through an "effective length" factor which remains constant during the entire response history.

The effect of axial load on the yield moment of RC columns has long been recognized by researchers (Kanaan and Powell 1973); however, the effect of axial force on the flexural stiffness of a member was first accounted for in the model proposed by Takayanagi and Schnobrich (1979) in their study of the seismic response of coupled wall systems. The walls and coupling beams are represented by one-dimensional beam elements. The interaction of

bending moment, shear and axial forces is taken into account in the wall elements, while the axial stiffness of the coupling beams is assumed to be infinite, since the horizontal displacements of both walls are approximately equal. Otani's model is selected for modeling the coupling beams with the inflection point assumed fixed at midspan. The beams are connected to the wall elements through a rigid link which accounts for the finite dimensions of the wall. A spring is inserted between the beam element and the rigid link to model the fixed-end rotations due to slip of the reinforcing bars anchored in the wall. The effect of shear in the coupling beams is also taken into account. A modified Takeda model is adopted for the hysteretic behavior of the beam elements. The model accounts for the "pinching" effect during reloading and the strength decay due to loss of shear resistance after crack formation and yielding of the reinforcement in the coupling beams.

The seismic response of a plane frame coupled with a shear wall was studied by Emori and Schnobrich (1981). They conducted nonlinear static analyses under cyclic load reversals and compared the results obtained using different beam models, namely, a concentrated spring model, a multiple spring model and a layer model. The first model is identical to Otani's model. The second is an element composed of several springs acting in series and interconnected by rigid links. This model is thus capable of accounting for the shift of the contraflexure point during the response history. In the third model, which is a modification of the concentrated spring model, a layered element of length L_p is inserted at the ends of the beam. L_p is selected equal to the length of the region where major inelastic action is expected. The layer model can account for the interaction of bending moments and axial forces. It can not account, however, for the effects of shear and slip of reinforcement, unless a spring is inserted at the ends of the beam. Takeda's hysteresis rule has been adopted in all models. The study concludes that the concentrated spring model predicts satisfactorily the inelastic response of RC girders, while a multiple spring model is needed to accurately describe the inelastic behavior of shear walls. If a detailed study of the inelastic response of plastic zones in columns is desired, the authors recommend the use of a layer model.

The applicability of point hinge models in studying the seismic response of structures was investigated in great detail by Anagnostopoulos (1981). His study is limited to flexural members subjected to end moments and uniformly distributed gravity loads. The moment-curvature relation is assumed to be bilinear elastic-strain hardening. The study points out that a point hinge model is incapable of reproducing the gradual change of stiffness of a member in the post-yielding range. The study then focuses attention on the problem of defining the strain hardening ratio of the moment-rotation relation of point hinge models. Anagnostopoulos shows that it is incorrect to set this ratio equal to the strain hardening ratio of the moment-curvature relation, since this considerably underestimates the post-yield

stiffness of flexural members. The study proposes an iterative solution for determining the strain-hardening ratio of the moment-rotation relation of point hinge models.

Several attempts to develop a model of the hysteretic behavior in shear have been made to date. A qualitative model of the hysteretic shear force-deformation relation has been proposed by Celebi and Penzien (1973). The most recent such model has been introduced by Ozcebe and Saatcioglu (1989). This model describes the experimentally observed stiffness degradation and the associated "pinching" of hysteretic loops. Empirically derived expressions are proposed which account for the effect of axial load on the hysteretic behavior.

A complete model for the analysis of seismic response of RC structures was proposed by Banon et al. (1981). The one-component model in its original form describes the nonlinear behavior of the girder. The hysteretic moment-rotation relation is based on a modified Takeda model. In order to reproduce the "pinching" effect due to shear and bond deterioration a nonlinear rotational spring is inserted at each member end. The hysteretic model of the nonlinear springs is based on a bilinear skeleton curve with strength decay under large deformations and includes the effect of "pinching" during reloading. The authors also proposed a set of damage indicators in an effort to quantify the performance of a structure during an earthquake. These indicators describe the state of damage of each element due to large deformation reversals and low-cycle fatigue. The damage indicators are used in the development of a probabilistic model of member resistance. The study concludes that the one-component model is sufficiently accurate in modeling the inelastic response of RC members subjected to severe deformation reversals. It also shows that it is possible to accurately predict the state of damage of RC members using parameters based on deformation ductility and cumulative energy dissipation due to low-cycle fatigue.

The effect of different hysteresis models on the nonlinear dynamic response of a simple concrete specimen was studied by Saiidi (1982). He analyzed four models: elastic-perfectly plastic, elasto-plastic with strain hardening, Clough's model and a new Q-hysteresis model. The first two are very simple, but quite unrealistic for reinforced concrete; the other two are more accurate and differ mainly in the representation of stiffness degradation during unloading and reloading. The performance of the different hysteretic models was evaluated by comparing the results with those obtained using Takeda's model, since its agreement with a large number of experimental data is excellent. Poor agreement with Takeda's model is exhibited by both elasto-plastic models; Clough's model shows relatively good agreement while the Q-hysteresis model shows excellent agreement. The study concludes that stiffness degradation effects during unloading and reloading are very important in determining the

overall response of RC structures, because they affect the amount of energy dissipated by the structure.

In 1983 Meyer et al. (1983) developed another spread plasticity model. The flexibility coefficients of the new model are identical to those of Soleimani's model. The authors proposed a slightly different way of calculating the stiffness of the plastic zone during reloading and used Takeda's model to describe the hysteretic moment-curvature relation. The same model was used in describing the inelastic behavior of beams and columns, with no account of the effect of axial forces on flexural rigidity. Fixed-end rotations are not taken into account in the study. The analytical results are compared with a series of experimental data and show excellent agreement.

An integrated experimental and analytical study on the effect of bond deterioration on the seismic response of RC structures was published by Otani et al. (1985). The model adopted for beams and columns is the one-component model. Takeda's model is used to describe the hysteretic behavior of the elements. A rotational spring is inserted at each member end to model the slip of reinforcement due to bond deterioration; the hysteretic behavior of the spring is described by Takeda's model modified so as to account for the "pinching" effect during reloading. No strength decay is introduced in the monotonic skeleton curve, since experimental data did not provide such evidence.

A model for assessing structural damage in RC structural elements was proposed in a study by Park and Ang (1985). Damage is expressed as a linear function of the maximum deformation and the hysteretic energy absorbed during cyclic load reversals.

In their study of the nonlinear response of plane rectangular frames and coupled shear walls Keshavarzian and Schnobrich (1985) extended the spread plasticity model proposed by Soleimani to column elements. The model accounts for the interaction between bending moment and axial force in determining the strength and stiffness of column elements. The study compares the predictions of different models: in addition to the spread plasticity model, these include the one-component, two-component and multiple spring model. In performing the nonlinear static and dynamic analysis of the structure the element stiffness is linearized at the beginning of each load step. Any nonlinearity which takes place during the load increment is not accounted for and the resulting unbalance forces are neglected. The study concludes that the one-component model is well suited for describing the inelastic behavior of RC girders. It is also noted that the two-component model has the same versatility as the one-component model and yields similar results. The multi-layer model is found very expensive for nonlinear dynamic analysis of multistory structures.

Finally, the study points out that the fluctuation of axial forces in coupled shear walls and in exterior columns of frame structures affects the forces and deformations in individual walls and columns.

In a recent study Roufaiel and Meyer (1987) proposed an extension of the spread plasticity model developed earlier by Meyer et al. (1983). The new model includes the effect of shear and axial forces on the flexural hysteretic behavior based on a set of empirical rules. The hysteretic moment-curvature relation is described by Takeda's model. The variation of axial loads due to overturning moments is not accounted for. The analytical results are compared with available experimental data and show very good agreement. A set of new damage parameters is proposed which correlate well with the residual strength and stiffness of specimens tested in the laboratory.

1.3 Objectives and scope

The general objective of this study is to develop improved models and methods for simulating the nonlinear static and dynamic response of reinforced concrete frames. In this respect this study is a continuation of the work presented in an earlier study (Filippou and Issa, 1988).

To achieve the general objective new reinforced concrete models for reinforced concrete girders were proposed in the earlier study. Each girder was decomposed into a number of subelements which were connected in series. Each subelement describes a different mechanism of hysteretic behavior of reinforced concrete members. Three subelements were developed in the earlier study (Filippou and Issa 1988): (a) an elastic subelement which models the flexural behavior of the frame member before yielding of the reinforcement; (b) a spread plastic subelement which describes the inelastic flexural behavior of the reinforced concrete member and accounts for the gradual spread of inelastic deformations at the member ends; and (c) a joint subelement modeling the fixed-end rotation that arises at the beam-column interface due to bond deterioration and slippage of reinforcing bars along the joint anchorage.

The present study introduces several new subelements in Chapter 2. The first is a shear subelement which describes the deformation due to shear distortion and, in particular, due to shear sliding in the inelastic regions of reinforced concrete members and, so, complements the list of girder subelements of the earlier study (Filippou and Issa 1988). The other subelements refer to the hysteretic behavior of RC columns and are extensions of the corresponding girder subelements to account for the effect of axial load on the flexural and shear behavior of the member.

The proposed reinforced concrete frame models are implemented in a special purpose computer program for the nonlinear static and dynamic analysis of reinforced concrete frames. A nonlinear solution method which accounts for the possible unbalance of internal forces between the different subelements during a load step and an algorithm for the efficient numerical implementation of this solution strategy was already proposed in the earlier study. This procedure is now extended to encompass the additional subelements, but, more importantly, to address time varying loads due to ground acceleration. Implementation issues under static loading conditions are discussed in Chapter 3. Special implementation issues that arise in the context of the numerical time integration strategy are discussed in Chapter 4 where the mass, damping and stiffness representation of the structure is also briefly discussed.

The analytical results are compared with experimental information from beam-column subassemblies under cyclic deformation reversals. Only studies related to the effects of shear and axial load are discussed in Chapter 5. These correlation studies complement those presented earlier by Filippou and Issa (1988).

The ability of the proposed frame model to simulate the dynamic response of frame structures that are excited by ground accelerations is evaluated in Chapter 6 by comparing the analytical results with experimental evidence from a two story one bay reinforced concrete frame tested on the shaking table of the Earthquake Engineering Research Center by Clough and Gidwani (1976). The effect of bond slip on the local and global dynamic response of the structure is evaluated. The results of the proposed model are compared with those of the widely used one component model in order to assess the ability of the latter to establish the local and global response of reinforced concrete frames.

The results of the study are summarized in Chapter 7 which offers general conclusions and recommendations for further research.

CHAPTER 2

MODELS OF REINFORCED CONCRETE FRAME ELEMENTS

2.1 Introduction

In structures designed according to the present state of earthquake resistant design the forces induced in the structure during a major earthquake will exceed the yield capacity of some members and cause large inelastic deformations. These deformations resulting from the combined effect of gravity and lateral loads are concentrated in areas of maximum internal forces which are called critical regions. The different types of critical regions in reinforced concrete frames are shown in Fig. 2.1. In a typical lower story the combined action of high lateral and relatively small gravity loads gives rise to the moment distribution shown in Fig. 2.1 such that critical regions are usually located at the ends of girders and columns and at beam-column joints. In upper stories, on the other hand, inelastic deformations can also occur near the girder midspan.

Critical regions can be classified into different types depending on the internal forces which are induced in them and control their hysteretic behavior (Celebi and Penzien 1973). These types are: regions subjected to flexure, regions subjected to flexure combined with high shear forces and, finally, regions subjected to flexure combined with high shear and axial forces. Beam-column joints are critical regions which are subjected to large shear and axial forces. The forces induced in the different critical regions depend on the structural system, the type of excitation of the structure, the location of the critical region, and the span to depth ratio of the given member.

Since the seismic response of the entire structure depends on the hysteretic behavior of these regions, accurate models of such behavior need to be developed. Ideally these models should be based on the fundamental principles of mechanics using the material properties of concrete and reinforcing steel with due account for crushing and spalling of concrete, bond slip of reinforcement and shear sliding. The discrete nature of flexural and shear cracks should also be taken into consideration. Not only is such a degree of refinement difficult to achieve, but the detailed information obtained from such refined nonlinear analysis is unnecessary in the response description of entire structures (Umemura and

Takizawa 1982). Moreover, the implementation of such models in dynamic response analysis of large structural systems is prohibitively expensive.

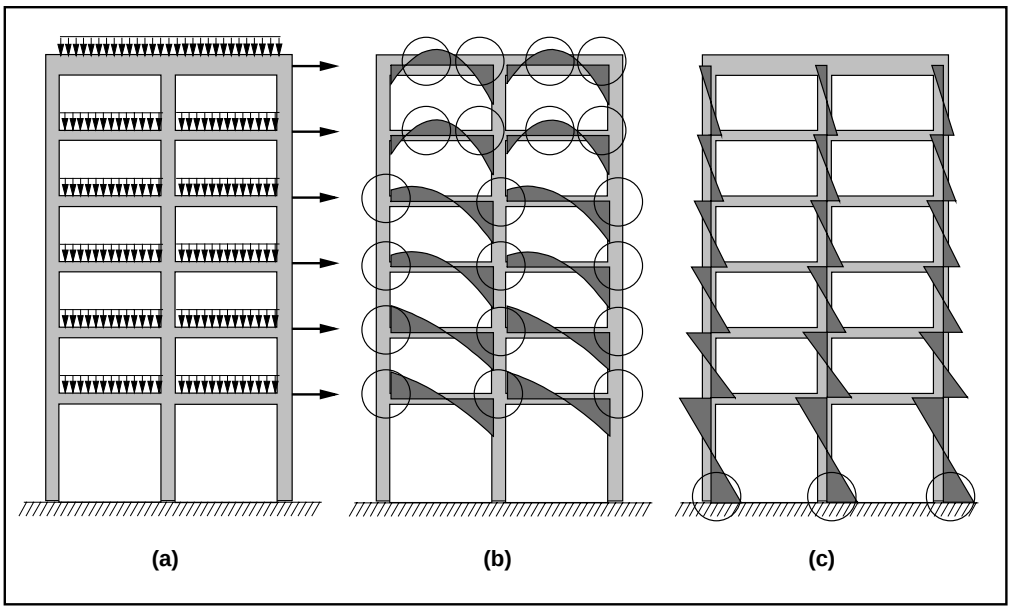

FIGURE 2.1 BENDING MOMENTS IN MOMENT RESISTING FRAMES UNDER COMBINATION OF GRAVITY AND EARTHQUAKE LOADS

A different solution approach consists of developing macroscopic member models of reinforced concrete elements. These are based on approximations of the physical behavior of RC members and vary in their complexity from simple point hinge to more sophisticated layer and fiber models (CEB 1983, Zeris and Mahin 1988, Taucer et al. 1991).

In determining the seismic response of multistory buildings point hinge models have been used extensively because of their simplicity (Umemura and Takizawa 1982). In these models the inelastic behavior of reinforced concrete elements is represented by concentrated springs at the ends of the member. Since it is computationally convenient to use a single spring to describe the inelastic behavior of any type of critical region, several parameters need to be defined for describing the behavior of the springs. These parameters depend on the actions that control the inelastic behavior of the member and are established empirically.

In modeling the hysteretic behavior of RC members under cyclic load reversals phenomenological models of hysteretic behavior are typically used. While only a few parameters are needed to describe the hysteretic behavior when flexure governs the response, many more parameters become necessary in members with complex interactions between bending moment, shear and axial force. These parameters are typically established from a limited set of experimental data. Moreover, the actions arising in a particular critical region

vary depending on the structural system, the strength of the section, the span to depth ratio of the member, and the type of excitation of the structure. Thus the derivation of empirical hysteretic rules, however complex, does not guarantee the general applicability of these rules. It, therefore, appears doubtful that a single hysteretic model can approximate the actual behavior of RC regions over the wide range of possible interactions of bending moment, shear and axial force in structures subjected to earthquake excitations.

Another way of describing the inelastic behavior of RC members is proposed in the present study. This approach consists of identifying the basic mechanisms which control the hysteretic behavior of each type of critical region and, if possible, isolating these in individual subelements. Each girder and column element is then made up of a number of such elements. This approach is, in many respects, similar to the model proposed by Otani (1974) and will be presented in greater detail in the following.

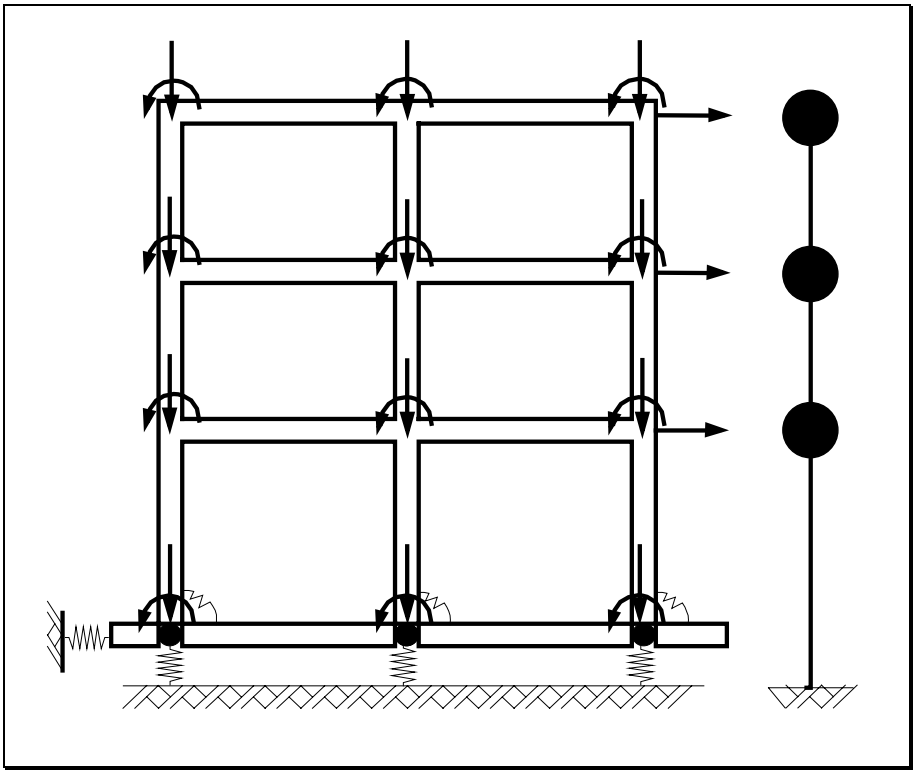

FIGURE 2.2 PROPOSED MODELING OF PLANAR MOMENT RESISTING RC FRAMES

Since the present study is limited to the analysis of planar moment resisting frames (Fig. 2.2), the following basic elements are needed for predicting the nonlinear response of such structures to cyclic excitations: a girder element, a column element, a beam-column joint element and a foundation element. The girder element should also include the effect of the slab. Shear wall or infill panel elements are not dealt with in this study, since attention is

focused on the behavior of bare frames. It is assumed that floor diaphragms are infinitely rigid so that a single degree of freedom represents the lateral displacements of an entire floor in a two-dimensional frame (Fig. 2.2).

The inelastic hysteretic behavior of reinforced concrete members under various loading conditions has been the subject of many experimental investigations in the U.S. and abroad in the last twenty five years. Among the different studies reference will be made in the following to a few conducted at the University of California, Berkeley. These studies have investigated the hysteretic behavior of critical regions under combined bending moment with low shear (Viwathanatepa et al. 1979), under combined bending moment with high shear (Celebi and Penzien 1973), and under the combined action of bending moment, shear, and axial force (Atalay and Penzien 1975). The information presented in these investigations along with experimental evidence from other tests (Gill et al. 1979, Otani et al. 1985, Low and Moehle 1987) will be used in developing the proposed analytical model.

Experimental studies of reinforced concrete frame structures conducted to date conclude that deformations of reinforced concrete girders mainly arise from the effects of flexure, shear, and bond slip of reinforcement. The relative contribution of these sources of deformation to the deflection of reinforced concrete girders depends on the section strength, the geometry of the cross section, the span to depth ratio of the member, and the type of excitation. To account for this fact the girder element is decomposed into individual subelements in the present study. Each subelement represents one of these sources of deformation.

The same sources of deformation control the hysteretic behavior of RC columns. In this case, however, the presence of axial forces becomes a major factor in the description of the hysteretic behavior. Thus, the effect of axial force on the deformations due to flexure, shear, and bond slip needs to be explicitly taken into account in the development of the different column subelements.

Experimental evidence from the hysteretic behavior of beam-column joints (Viwathanatepa et al. 1979, Beckingsale 1980, Otani et al. 1985) shows that joint deformations arise as a result of the shear transfer in the joint and from bond slip of the reinforcing bars anchored in the joint. While beam column joints can be designed and detailed such that joint shear distortions remain small, it is not possible to eliminate fixed end rotations due to bond slip, unless the girder or column reinforcement is detailed so that yielding will occur a certain distance away from the beam-column interface (Al Haddad and Wight 1986). The joint element in this study only accounts for the deformations that arise at the beam-column or column-footing interface due to reinforcement pull-out. Deformations due to shear are presently neglected, but could be readily incorporated in future studies with a

special joint element. Two joint subelements are introduced in this study: (a) the *girder joint element* models the fixed end rotation at the girder ends due to pull-out of the girder reinforcing bars, and is combined with elements which account for other types of deformation at the interface and along the girder span to form the girder superelement, (b) the *column joint element* describes the fixed end rotation at the column ends due to pull out of the column reinforcing bars. Since columns are not expected to deform much into the post yield range, except at the base of the building, little slip of column reinforcement is expected at the beam-column joints, except at the column-foundation interface, where significant pull-out of reinforcing bars can take place. The column joint element is combined with elements which account for other types of deformation at the interface and along the column height to form the column superelement.

Thus, within the scope of this study the moment resisting frame consists of only three types of superelements:

- a girder superelement,
- a column superelement, and
- a foundation superelement.

This subdivision implies that beam-column joint panel zones remain rigid. If it is desired to explicitly include the deformations due to shear cracking in beam-column joints, a panel zone element needs to be added for the purpose.

In reinforced concrete structures subjected to large cyclic deformation reversals, bond deterioration and shear effects give rise to slippage of reinforcing bars anchored in beam-column joints. This leads to an interaction between forces and moments acting at the ends of beams and columns framing into a particular joint (Filippou et al. 1983). If it is desired to explicitly account for the interaction between girder and column moments at beam-column joints, a special joint element needs to be developed. Such interaction is not explicitly accounted for in the present study. A way of implicitly accounting for this effect is presented in Section 2.2.3.

Information about the different elements used in the present study is given in the following sections. First, the girder superelement is described in detail. A more detailed description of the spread plasticity and the joint element is contained in the earlier study by Filippou and Issa (1988). The shear subelement is new and is presented in detail as are the column and foundation superelements. The chapter concludes with the derivation of the stiffness matrix of the entire frame structure.

2.2 Reinforced concrete girder element

In moment resisting frames designed according to current building codes to resist severe earthquake excitations, inelastic deformations are expected to take place at the ends or at midspan of girders and at beam-column joints.

The behavior of critical regions in girders is governed by flexure, shear and the transfer of stresses between reinforcing steel and concrete. When these regions are subjected to cyclic deformation reversals, considerable stiffness deterioration is observed. This can be attributed to several factors the most important of which are:

- the concrete cracking and splitting along reinforcing bars,
- the cyclic deterioration of bond between reinforcing steel and surrounding concrete,
- the shear sliding in regions with cracks running through the depth of the member,
- the crushing and spalling of concrete, and
- the Bauschinger effect of reinforcing steel.

These factors are also responsible for the stiffness deterioration in interior and exterior beam-column joints. In this case, however, the hysteretic behavior of the joints is governed by the large change in bending moments from one face of the joint to the other that causes a combination of high shear and bond stresses. Large bending moments at the girder ends induce yielding of the reinforcement, which, combined with the diagonal cracks induced by shear, leads to slippage of reinforcing bars in the joint. This manifests itself as bar pull-out at the beam-column interface and results in concentrated rotations known as fixed-end rotations at the girder ends. Experimental studies show that fixed-end rotations due to bond deterioration in the joint can contribute up to 50% of the overall deflection of beam-column subassemblages after yielding of the reinforcement (Soleimani 1979).

In addition to fixed-end rotations, the shear stress transfer in the joint leads to diagonal cracks which give rise to panel zone deformations. In general, the mechanism of joint shear resistance is coupled with the problem of stress transfer between reinforcing steel and concrete (Park and Paulay 1984). It is possible, however, to design and detail joints so that the nominal concrete shear stress in the joint remains smaller than a specified limit. This is the approach followed by current design recommendations (ACI 1985). In this case diagonal cracking is kept to a minimum and the shear deformation of the panel zone remains small and can be neglected. By contrast, it is not possible to eliminate fixed-end rotations due to slippage of reinforcing bars in the joint, except by moving the plastic hinge a certain distance away from the beam-column interface through special detailing of the reinforcement (Bertero and Popov 1975, Al Haddad and Wight 1986).

There is now considerable experimental evidence showing that the post elastic response of cyclically loaded ductile beams with conventional detailing of reinforcement can be significantly affected by shear deformations in the plastic hinge zones (Celebi and Penzien 1973). This is especially the case in members with low shear span to depth ratio *a/d*. To account for this effect a relatively simple shear model is developed in this study.

The basic mechanisms of shear transfer are

- direct shear stress transfer in the compression zone of the member,
- shear transfer at the crack due to aggregate interlock,
- shear transfer through dowel action of reinforcement, and
- transfer through shear reinforcement.

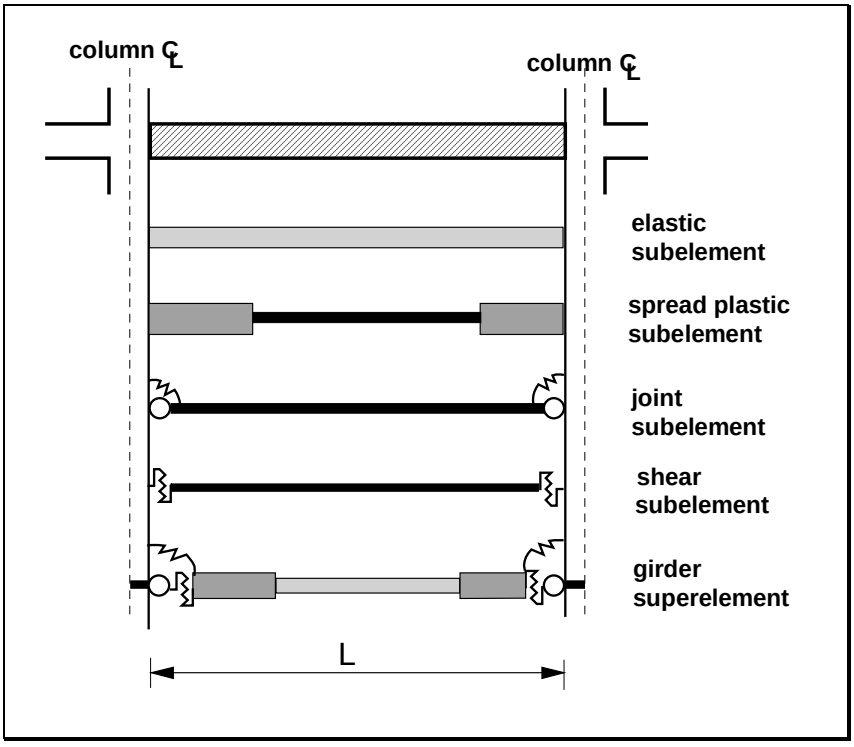

FIGURE 2.3 DECOMPOSITION OF RC MEMBER INTO DIFFERENT SUBELEMENTS

The shear deformations of plastic hinge regions under cyclic loading are largely due to sliding along wide, full depth cracks opened up by large plastic tensile strains in the longitudinal reinforcement. Shear sliding can be significant even when the maximum nominal shear stress is quite moderate (Spurr 1984). Inclined shear cracks combine with flexural cracks and lead to a reduction in the effective shear rigidity of the plastic hinge zone of the member. The overall shear displacement is the result of the combined effect of the rotational and sliding displacements of the loosened pieces of concrete. Both, aggregate

interlock, which is a function of the crack width, and the dowel action of the longitudinal and transverse reinforcement contribute to the sliding resistance of the section.

In order to model as accurately as possible the different mechanisms which contribute to the hysteretic behavior of critical regions in RC girders, the girder element is decomposed into several subelements as shown in Fig. 2.3:

(1) an elastic beam subelement which represents the linear elastic behavior of the girder before yielding of the reinforcement. The girder is assumed cracked and the pre-cracking behavior is neglected in this study,

(2) a plastic beam subelement with plastic hinges at the ends; the length of the plastic hinges is a function of the loading history; this element represents the behavior of the girder in the post-yielding range,

(3) a joint subelement which accounts for the fixed-end rotations at the beam-column interface due to bond deterioration and slip of the reinforcement in the joint, and

(4) a shear subelement which accounts for the shear distortion in the critical regions of the girder and the shear sliding at the beam-column interface.

Fig. 2.3 shows that the beam-column joint panel zone is considered infinitely rigid. If desired, panel zone deformations can be included in the analysis by adding a flexible panel zone element. Such an element has been developed by Kanaan and Powell (1973) for the nonlinear analysis of steel structures.

2.2.1 Linear elastic beam subelement

The linear elastic beam subelement represents the flexural behavior of the girder before yielding of the reinforcement. Its length is equal to the clear span L of the girder and it is assumed to have a constant section stiffness EI along the span. The assumption of a constant section stiffness along the entire span of the girder is clearly an approximation. Reinforcement layout typically varies along the girder with different amounts of reinforcement at the top and bottom of the cross section. When the bending moments act such that the top of the section is subjected to tension, the compression zone is rectangular in shape having a width equal to the width of the web. Part of the slab reinforcement contributes to the tensile force thus significantly increasing the yield strength of the section, but not affecting much the stiffness before yielding. When the bending moments act such that the bottom of the section is subjected to tension, the compression zone is either rectangular or often T-shaped. It is clear from the above that the effective slab width in tension and compression needs to be determined, if the strength and stiffness of the girder element is to be estimated accurately.

In this study the elastic section stiffness *EI* is set equal to the average of the positive (tension at the bottom) and negative (tension at the top) section stiffness at the two girder ends. The elastic section stiffness is determined as the secant stiffness of the moment-curvature relation at yielding of the tension reinforcement. Only the effect of slab in compression has been included in determining the strength and stiffness of the girder based on the effective width specified in ACI 318-83 (ACI 1983). A better model of the effect of slab in tension and compression has been developed by Pantazopoulou (1987). It should be noted that girders spanning between interior columns typically have a symmetric arrangement of reinforcement with respect to the girder midspan. By contrast, exterior girders are likely to have different amounts of reinforcement at each end. In the latter case the average stiffness is determined from the positive and negative section stiffness at each end. The approximation of a constant average section stiffness is certainly unsatisfactory, if it is desired to study the response of the structure under service loads. In the present study attention is focused on predicting the response of the structure under large deformation reversals. Such response is not significantly affected by the stiffness of the structure before yielding. With the assumption of a constant average section stiffness along the span of the elastic beam subelement the flexibility matrix with respect to the member chord is given by the well known expression

$$[\mathbf{f}]_{el} = \frac{L}{6EI} \cdot \begin{bmatrix} 2 & -1 \\ -1 & 2 \end{bmatrix} \tag{2.1}$$

2.2.2 Rigid-plastic beam subelement

The rigid plastic beam subelement accounts for the inelastic flexural deformation of the girder after yielding of the reinforcement. Two different plastic subelements are included in the study:

(a) The first model assumes that all inelastic flexural deformations are concentrated in a hinge of zero length at each end of the girder. The two hinges are connected by an infinitely rigid bar to form the concentrated plastic beam subelement. The combination of the flexibility matrix of this element with that of the elastic subelement results in the one-component model originally proposed by Giberson (1974).

(b) The second model accounts for the gradual spread of inelastic flexural deformations into the girder as a function of loading history. In this an inelastic zone of gradually increasing length is located at each end of the girder. The two inelastic zones are connected by an infinitely rigid bar to form the spread plastic beam subelement. The

combination of the flexibility matrix of this element with that of the elastic subelement results in a model similar to that originally proposed by Soleimani (1979).

The effect of shear and bond on the inclination of cracks and on the curvature distribution in the inelastic zone at the girder ends is approximately taken into account in the spread plasticity model. Such effects cannot be included in the concentrated plastic hinge model in a rational way.

a) Concentrated rigid-plastic beam subelement

In the concentrated plastic subelement, the inelastic flexural deformations which take place at the girder ends after yielding of the reinforcement are represented by a rigid plastic hinge of zero length. The hinge, which is depicted as a nonlinear spring in Fig. 2.4(a), is activated when the moments at the girder ends first exceed yielding. Since all inelastic flexural deformations are lumped at the plastic hinges at the two ends of the girder and the elastic flexural deformations are accounted for in the linear elastic beam subelement, the part of the concentrated plastic subelement which connects the two hinges is infinitely rigid.

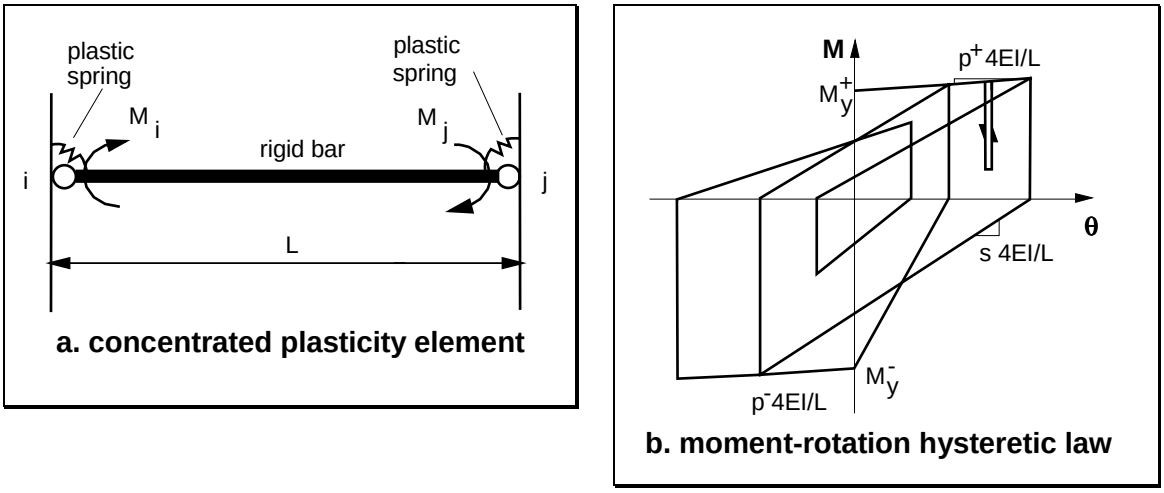

FIGURE 2.4 CONCENTRATED PLASTICITY BEAM SUBELEMENT

It can be easily shown that the off-diagonal elements of the flexibility matrix are zero in this case. The matrix thus reduces to the simple form

$$[\mathbf{f}]_{pl} = \begin{bmatrix} f_i & 0 \\ 0 & f_j \end{bmatrix} \tag{2.2}$$

where f_i and f_j are the flexibility coefficients of the rotational springs at ends *i* and *j*, respectively. The problem of determining the flexibility of the rotational springs has occupied many researchers to date. Otani presented a detailed discussion of the problem (Otani 1974). In order to avoid load path dependency of the flexibility coefficients it is usually assumed that the bending moments are distributed such that the point of inflection remains fixed during the entire load history. In most studies to date the point of inflection is assumed to remain fixed at girder midspan. In this case each half of the member can be viewed as a cantilever beam (Fig. 2.5). If the effect of gravity loads is neglected, the moment distribution is linear (Fig. 2.5b). This corresponds to the cantilever beam being loaded with a concentrated load *P* at the tip (Fig. 2.5c).

To determine the flexibility coefficients f_i and f_j of the concentrated plasticity model the plastic rotation at the root of the cantilever due to the actual curvature distribution is first established for different values of the load *P*. This is rather straightforward, if the moment-curvature relation (M- φ) is known for all sections along the cantilever span. To simplify the calculation the (M-φ) relation is assumed to be bilinear with a single post-yield stiffness (Figs. 2.5d and 2.5e). In spite of the approximations made in Fig. 2.5 the procedure results in a nonlinear flexibility coefficient of the equivalent concentrated spring, because of the gradual spread of inelastic deformations into the cantilever beam. To simplify the moment-rotation relation of the equivalent end spring the actual behavior is replaced by a bilinear moment-rotation relation with constant post-yield stiffness as shown in Fig. 2.4(b). The post-yield stiffness is calculated by equating the plastic rotations for the case that the section at the root of the cantilever reaches the ultimate moment capacity (Fig. 2.5d). In this case the post-yield stiffness k_{sp} of the equivalent rotational spring is

$$k_{sp} = \frac{M_u - M_y}{\theta_{pl}} \tag{2.3}$$

where M_u is the ultimate and M_y the yield moment of the cantilever beam, respectively. θ_{pl} is the plastic rotation of the equivalent concentrated spring. This is equal to the plastic rotation at the root of the cantilever beam which can be readily determined from the curvature distribution in Fig. 2.5(e).

Eq. (2.3) results in an infinite spring stiffness k_{sp} for the case that the end moment does not exceed the yield moment. This is in agreement with the definition of a concentrated rigid-plastic spring subelement which only accounts for the inelastic girder deformations after yielding of the reinforcement.

It is customary to express the rotational spring stiffness k_{sp} in relation to the stiffness term k_{11} of the elastic stiffness matrix of a prismatic beam element. Thus

$$k_{sp} = \frac{4 \cdot EI}{\gamma \cdot L} \tag{2.4}$$

The flexibility matrix of the concentrated plastic beam subelement can now be written by considering Eq. (2.5) at ends *i* and *j* of the element.

$$[\mathbf{f}]_{pl} = \begin{bmatrix} \dfrac{\gamma_i \cdot L}{4 \cdot EI} & 0 \\ 0 & \dfrac{\gamma_j \cdot L}{4 \cdot EI} \end{bmatrix} \tag{2.5}$$

$$[\mathbf{f}]_{pl} = \frac{L}{6 \cdot EI} \cdot \begin{bmatrix} 1.5 \cdot \gamma_i & 0 \\ 0 & 1.5 \cdot \gamma_j \end{bmatrix} \tag{2.6}$$

The coefficients γ_i and γ_j vary as a function of the moment-rotation history of the rotational springs. The moment-rotation relation of the springs is completely defined by two envelope curves which represent the behavior of the springs under positive and negative monotonic loading and a hysteretic model which describes the behavior of the springs under cyclic load reversals (Fig. 2.4b).

The monotonic envelope curves are represented by a bilinear relation which has infinite stiffness for moments not exceeding the yield moment of the end section and a single

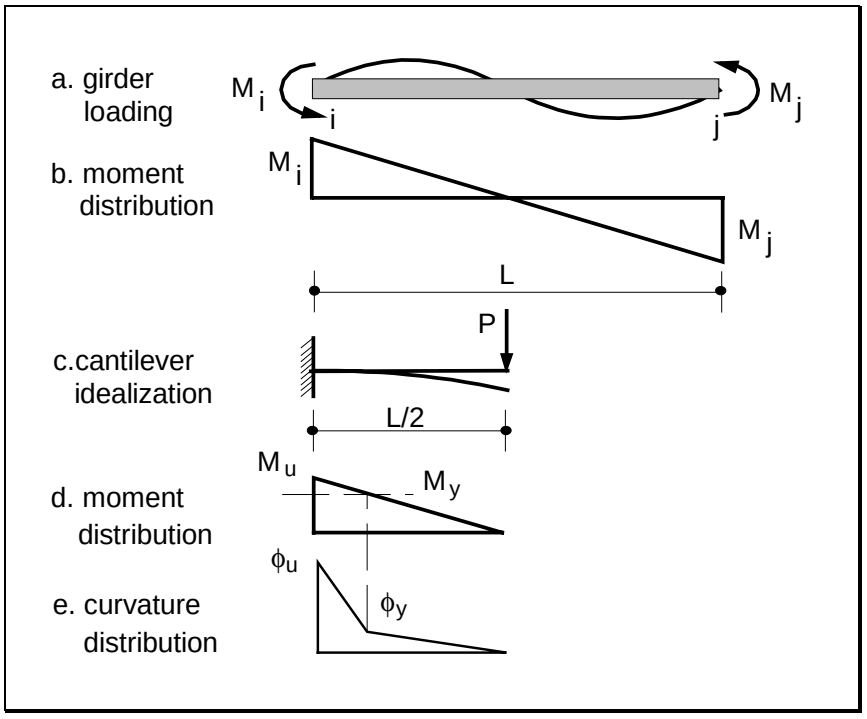

FIGURE 2.5 DERIVATION OF PARAMETERS OF CONCENTRATED PLASTICITY SUBELEMENT

post-yield stiffness for moments larger than the yield moment. The yield moment M_y^+ when the bottom reinforcement is subjected to tension is different from the yield moment M_y^- when the top reinforcement is subjected to tension. The post-yield stiffness $p^+ \cdot 4EI/L$ for positive bending moments is also assumed to be different from the post-yield stiffness $p^- \cdot 4EI/L$ for negative bending moments.

The hysteretic behavior of the rotational springs under cyclic moment reversals is described by Clough's hysteretic model shown in Fig. 2.4(b) (Clough et al. 1965). This model is characterized by the following hysteretic rules:

(a) The unloading stiffness is equal to the initial stiffness before yielding. Since the behavior of the spring is rigid-plastic, this means that the unloading stiffness is infinite and the spring is deactivated during unloading.

(b) Reloading takes place along a line which connects the point at which unloading was completed with the point on the envelope curve in the opposite direction of loading with the maximum previous excursion into the inelastic range.

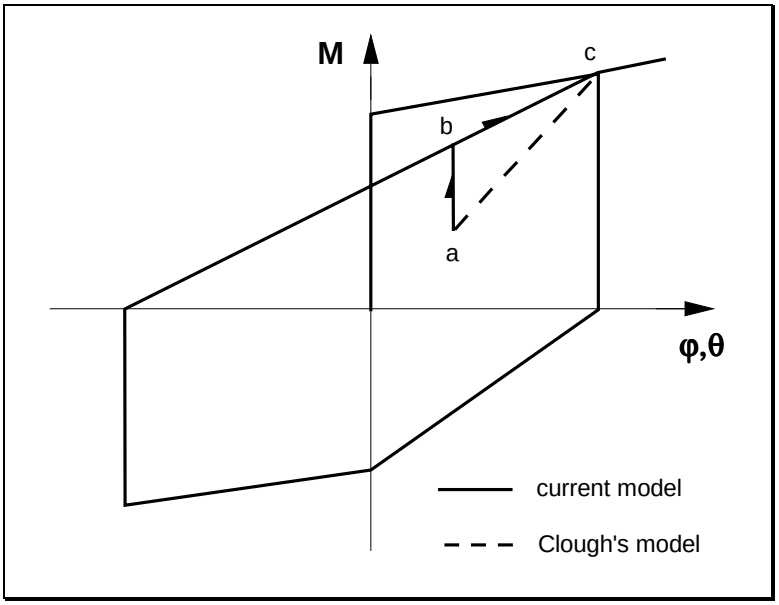

FIGURE 2.6 HYSTERETIC BEHAVIOR OF CURRENT MODEL VS. CLOUGH'S MODEL

The advantage of this model lies in its computational simplicity combined with reasonable accuracy in representing the hysteretic response of RC critical regions whose behavior is controlled by bending. One of the limitations of this model arises from the very steep unloading slope, as was already pointed out by Saiidi (1982).

It should be mentioned here that in the original model reloading after partial unloading takes place along the line which connects the point at which unloading stopped

with the point on the envelope curve in the same direction of loading with the largest previous inelastic deformation (line a-c in Fig. 2.6). Since this behavior is not realistic, the hysteretic model has been modified so that reloading after partial unloading follows an

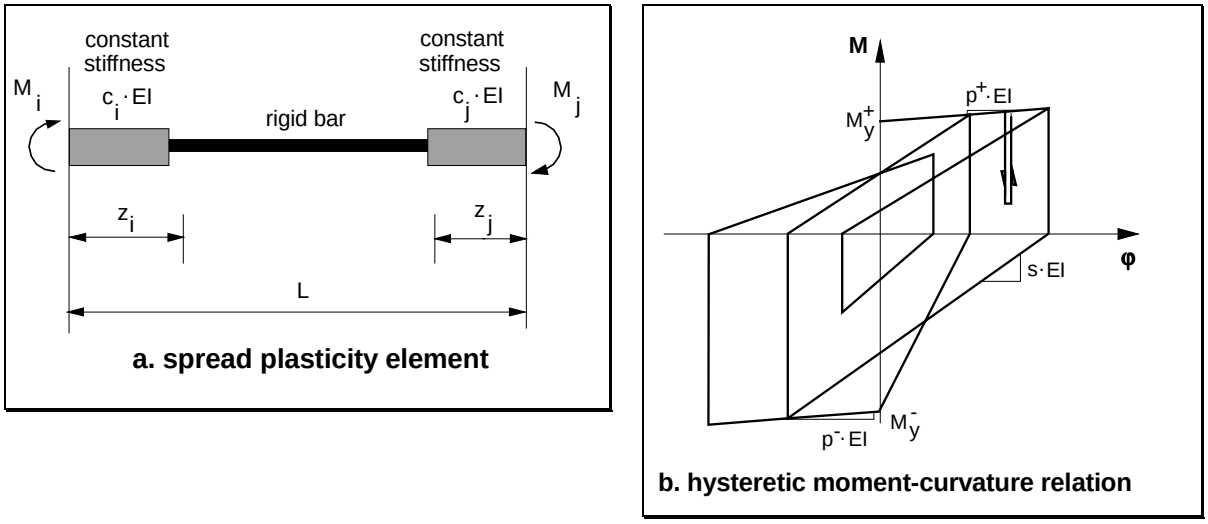

FIGURE 2.7 SPREAD RIGID PLASTIC BEAM SUBELEMENT

infinite slope until reaching the reloading curve which connects the last point of complete unloading with the point on the envelope curve with maximum previous inelastic deformation (line a-b in Fig. 2.6). Upon reaching point b the moment-rotation relation follows the last reloading curve (line b-c in Fig. 2.6).

Based on the hysteretic model of Fig. 2.4(b) the coefficients γ_i and γ_j assume the following values:

- $\gamma = 0$ during initial loading and unloading.
- $\gamma = p$ during strain hardening, where $p \cdot 4EI/L$ is the post-yield stiffness of the moment-rotation relation of the concentrated rotational springs.
- $\gamma = 1/s$ during reloading where $s \cdot 4EI/L$ is the reloading stiffness of the moment-rotation relation of the concentrated rotational springs.

Since the linear elastic and concentrated plastic beam subelements are connected in series, the flexibility matrix of the combined element is obtained by simply adding the flexibility matrices of the two subelements (Eqs. 2.1 and 2.6). Inverting the flexibility matrix of the combined element results in the stiffness matrix of the one-component model, as originally proposed by Giberson (1974).

The main advantage of the concentrated plasticity model is its simplicity and computational efficiency. It has, however, some serious limitations: most importantly it does

not account for the gradual spread of inelastic deformations into the girder. This results in an underestimation of stiffness in the early stages of inelastic deformation. Another limitation of the model lies in the assumption that the point of inflection is fixed at midspan during the entire response history. This is not realistic, particularly, if one considers that the yield moments at the ends of a girder bent in double curvature are not equal, because of unequal amounts of top and bottom reinforcement.

b) Spread rigid-plastic beam subelement

A more refined model of the nonlinear behavior of RC girders was first proposed by Soleimani (1979). A slightly different formulation of the original model was first presented by Filippou and Issa (1988) and is summarized here for the sake of completeness.

Since the deformations of the girder before yielding of the reinforcement are accounted for in the elastic beam subelement, the spread rigid-plastic subelement only accounts for the inelastic girder deformations which take place when the end moments exceed the yield moment.

The spread rigid-plastic beam subelement consists of two regions of finite length where the plastic deformations of the girder take place. These regions are connected by an infinitely rigid bar (Fig. 2.7a). The length of each plastic zone varies during the response history as a function of the moment distribution in the girder. The model thus accounts for the gradual spread of inelastic deformations into the girder and the shift of the inflection point during the response time history.

In the following only the salient features of the spread plasticity girder subelement are presented. More details can be found in Filippou and Issa (1988).

In presenting the features of the spread plastic subelement and the approximations involved in its development it is instructive to look at the case of a cantilever beam loaded by a concentrated load at its tip (Fig. 2.8a). The moment distribution in the cantilever beam (Fig. 2.8b) is identical to the moment distribution caused by lateral loads in the girders of a moment resisting frame between the point of inflection and the beam-column interface, if the effect of gravity loads is neglected (Fig. 2.1).

We are interested in calculating the load-displacement relation at the tip of the cantilever beam after yielding of the reinforcement at the end section. The moment distribution in this case is shown in Fig. 2.8(b). This gives rise to the curvature distribution in Fig. 2.8(c). Curvatures are rather irregular, because of the effects of cracking and tension stiffening between cracks. The strains in the top and bottom reinforcing steel are also affected by the presence of shear stresses in the beam. It is difficult to account for all these effects

when developing simple models of the inelastic behavior of RC members. Several solutions have been proposed in the past. Some researchers have proposed beam shape functions with special weighting schemes which account for the concentration of inelastic deformations at the ends of the girder. Since the shape functions do not change with the response time history, these proposals represent generalizations of the point hinge models and share many of their limitations. Other researchers have subdivided the beam into a number of slices along the span. This approach requires tracing the behavior of each slice during the response time history and is rather costly for nonlinear dynamic analyses of multistory structures. Even so, many of the aforementioned effects of bond deterioration and shear are not taken into account.

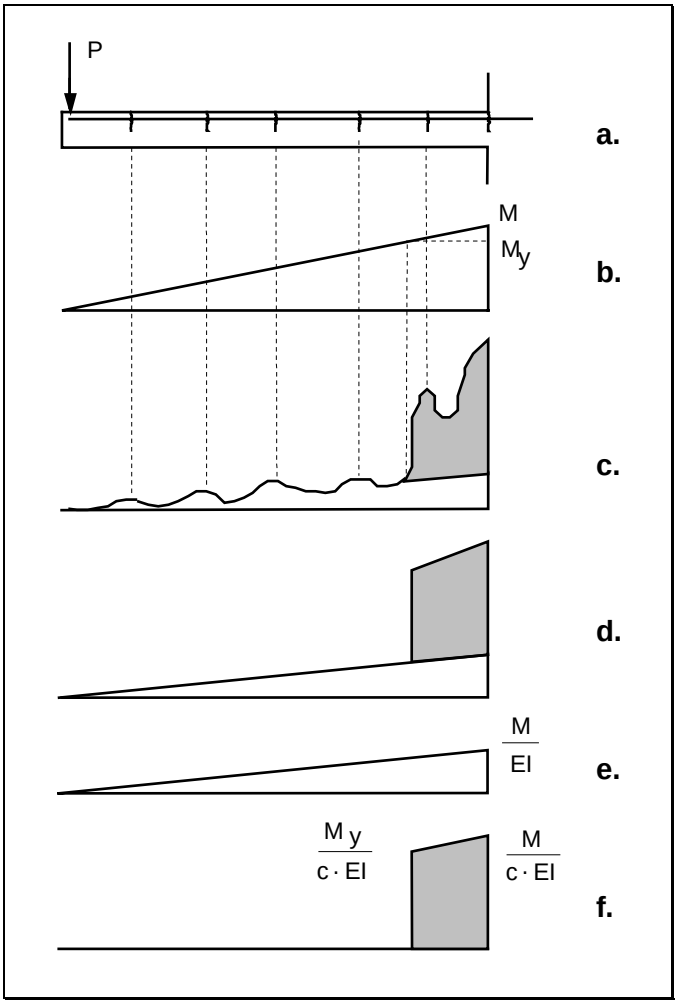

FIGURE 2.8 DEVELOPMENT OF SPREAD PLASTICITY MODEL IN THE CASE OF A CANTILEVER BEAM LOADED BY A CONCENTRATED LOAD AT THE TIP

A possible approximation, which lies between the extremes of point hinge models, on the one hand, and multi-slice or fiber models, on the other, consists of idealizing the curvature distribution as shown in Fig. 2.8(d). This approximation is based on the assumption of an average section stiffness $c \cdot EI$ along the plastic zone of the cantilever beam, where *EI* is the secant stiffness of the end section at yielding of the reinforcement. Subtracting the elastic curvatures which are already accounted for in the elastic subelement (Fig. 2.8e) results in the curvature distribution in Fig. 2.8(f). This curvature distribution lies at the heart of the spread plastic subelement. The assumption of an average effective stiffness of the plastic zone is of considerable importance for the computational efficiency of the model, because it leads to a symmetric stiffness matrix (Filippou and Issa 1988).

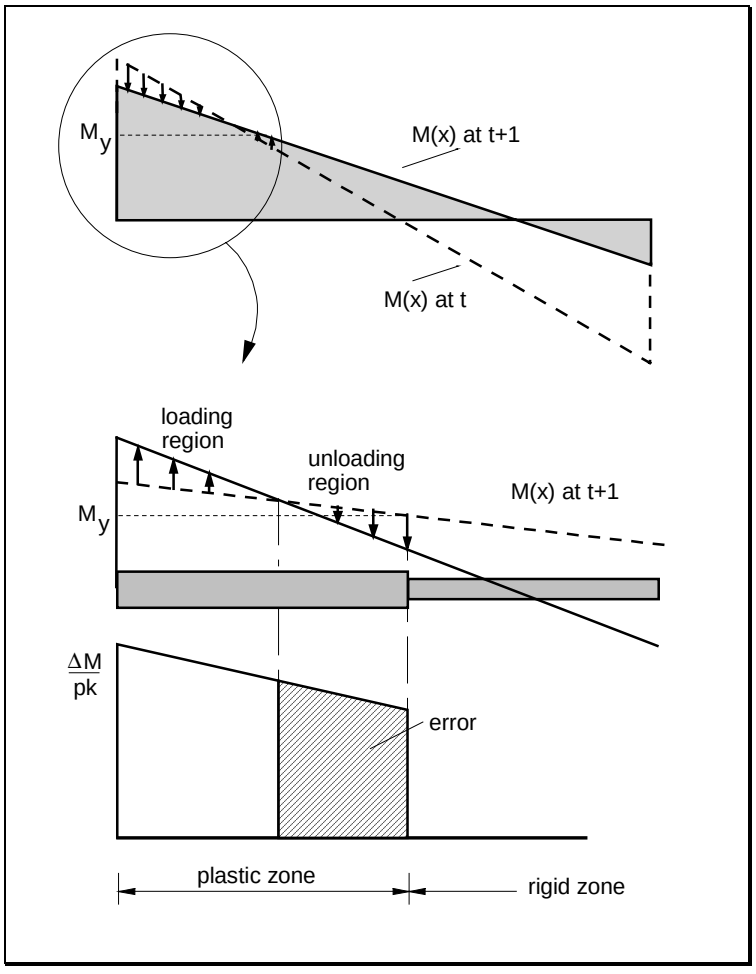

FIGURE 2.9 AN UNUSUALLY LARGE SHIFT IN THE POINT OF INFLECTION DURING A GIVEN LOAD STEP CAUSES UNLOADING ALONG SOME PORTION OF THE PLASTIC ZONE LENGTH

The quality of the approximation of an average section stiffness $c \cdot EI$ along the plastic zone of the subelement depends on the value of *c*. The determination of the value of *c* is relatively simple in the case of a cantilever beam under monotonically increasing load. By neglecting the effect of tension stiffening and assuming that all plastic zone sections exhibit the same bilinear moment-curvature relation we can readily derive *c* (Fig. 2.8f). Under a monotonic load *P* which gives rise to the moment distribution in Fig. 2.8b all plastic zone sections are in the strain-hardening range and have the same stiffness. In this case $c \cdot EI$ is simply equal to the post-yield stiffness of the bilinear moment-curvature relation. It is important to note that the reinforcement layout will not typically vary along the plastic zone length, as long as the zone does not extend beyond the quarter span point. Thus the assumption that all sections in the beam plastic zone possess the same moment-curvature relation is quite accurate.

The determination of the value of *c* becomes more involved, if not impossible, if we consider the effect of load reversals. A number of complications arise in this case:

(a) The point of inflection shifts from one load step to the next. In this case part of the plastic zone is in the loading stage, while another part is unloading (Fig. 2.9).

(b) Different sections in the plastic zone exhibit a different amount of stiffness degradation during reloading. This case is shown in Fig. 2.10 in its simplest form. The cantilever beam in Fig. 2.8 is first loaded in one direction so that part of the beam enters into the strain hardening range. The load at the tip is then reversed. Upon loading in the opposite direction sections along the inelastic zone exhibit different amounts of stiffness deterioration. While it is possible to derive a closed form expression for the curvature distribution in the simple case of Fig. 2.10 (dashed line), such an endeavor is fruitless after the second reloading cycle, even for a bilinear moment-curvature relation.

To accurately represent the hysteretic behavior of the plastic zone during a complex load history requires tracing the response of each section during the entire response time history. Since this is undesirable from the standpoint of computational efficiency, the following key assumptions are made in the spread rigid-plastic zone subelement:

(1) The state of the entire plastic zone is controlled by the state of the section at the beam-column interface. In Fig. 2.9 this means that the entire plastic zone is in the loading stage. This assumption gives rise to a discrepancy between actual and assumed curvature distribution, as shown in Fig. 2.9. This error can be minimized by reducing the size of the load increment and thus avoiding drastic shifts in the point of inflection during a given load step.

(2) The stiffness of the plastic zone is represented by an average effective stiffness $c \cdot EI$ which depends on the stiffness of the section at the beam-column interface.

These two key assumptions associate the behavior of the entire plastic zone with that of the section at the beam-column interface. This reduces substantially the computational effort required for describing the hysteretic behavior of the spread plastic subelement. Instead of a number of sections along the plastic zone, the load history needs to be traced at the two end sections of the element only. In addition, the model has to keep track of the length of the plastic zone at the two ends of the element. The second assumption has the added advantage that it results in a symmetric stiffness matrix.

Since the effective stiffness $c \cdot EI$ of the plastic zone depends on the behavior of the section at the beam-column interface, a hysteretic moment-curvature relation of the end section is needed. This relation is based on two bilinear envelope curves (Fig. 2.7b). Under positive bending moments (tension at the bottom) the section yields at a moment equal to M_y^+, while under negative moments (tension at the top) the yield moment is M_y^-. The post-yield stiffness $p^+ \cdot EI$ for positive bending moments is also assumed to be different from the post-yield stiffness $p^- \cdot EI$ under negative bending moments, as shown in Fig. 2.7b. To describe the behavior of the section under cyclic moment reversals the model originally proposed by Clough et al. (1965) is adopted in this study. The original model has been modified in the same way as described for the moment-rotation relation of the concentrated rigid-plastic subelement (Fig. 2.6b).

Using this model to describe the hysteretic moment-curvature relation of the section at the beam-column interface the value of c is determined as follows:

(1) During strain-hardening of the end section we can assume according to (1) that the entire plastic zone is in the strain-hardening range. Thus $c = p$ where $p \cdot EI$ is the post-yield stiffness of the moment-curvature relation. c thus assumes two different values p^+ or p^- depending on the sign of the end moment.

(2) During unloading of the end section it is assumed that the entire plastic zone is unloading. Since elastic unloading is accounted for by the elastic subelement, this implies that the plastic zone is infinitely rigid and $c = \infty$.

(3) The complications which arise during reloading have already been described. Fig. 2.10 shows that each section has a different reloading stiffness, which is a function of the section's previous response history. In order to limit the number of sections at which the response history needs to be traced the second key assumption of the spread plastic subelement is introduced: it is assumed that the effective stiffness of the plastic zone $c \cdot EI$ is equal to the average of the section stiffness at the ends of the plastic

zone. Since one end is elastic, this implies that only the response time history of the section at the beam-column interface needs to be traced. In this case *c* is equal to

$$\frac{1}{c} = \frac{1}{2} \cdot \left(\frac{1}{s_0} + \frac{1}{\infty} \right) = \frac{1}{2s_0}$$

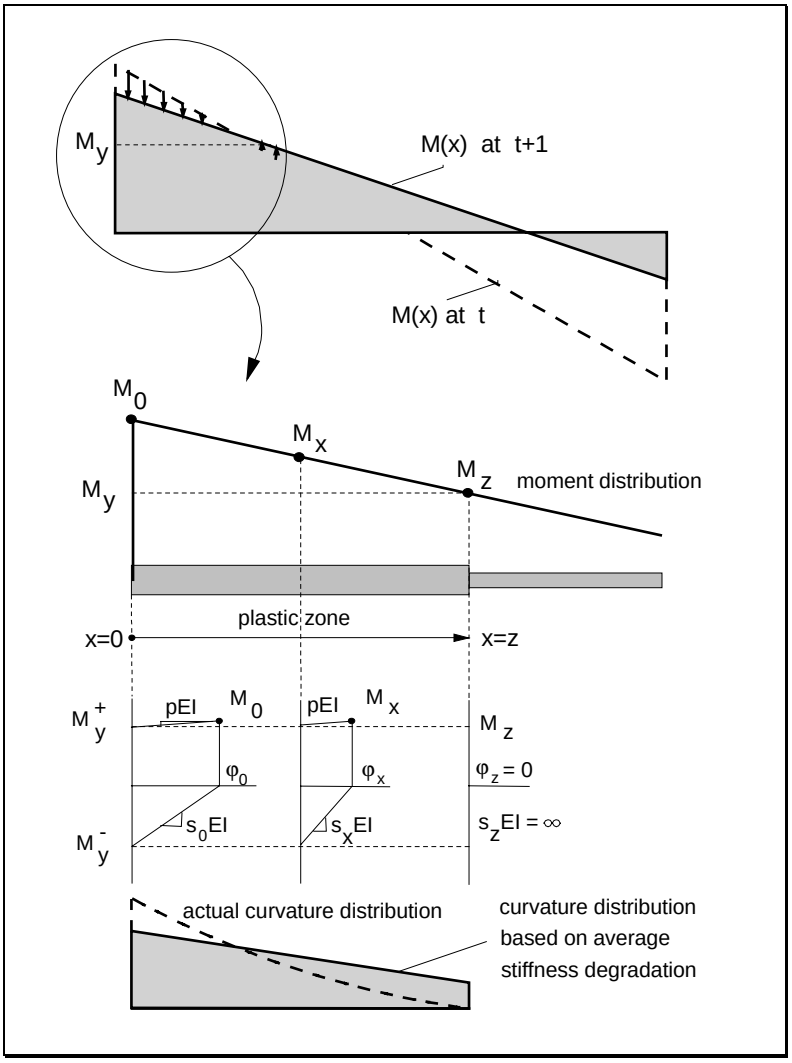

FIGURE 2.10 VARIATION OF STIFFNESS DETERIORATION ALONG THE PLASTIC ZONE LENGTH DURING FIRST UNLOADING AND RELOADING

where $s_0 EI$ is the reloading stiffness of the section at the beam-column interface (Fig. 2.10).

The effect of gravity loads has so far not been accounted for. This effect is considered in the present study in an approximate manner. The girder end moments and shear forces due to incremental lateral load analysis are added to the end moments and corresponding shear forces resulting from a static analysis of the structure under gravity loads. The plastic zone

length at each load step is determined from these end moments and shear forces under the assumption that the shear force remains constant along the entire plastic zone. This implies that the actual gravity load pattern is approximated by the third point loading shown in Fig. 2.11.

This approximation has the computational advantage that the calculation of the current length of the plastic zone z_c can be based on the bending moment and shear force at the girder end, which are readily available. The plastic zone length z_c is then calculated according to (Fig. 2.11b)

$$z_c = \frac{M - M_y}{V} \tag{2.7}$$

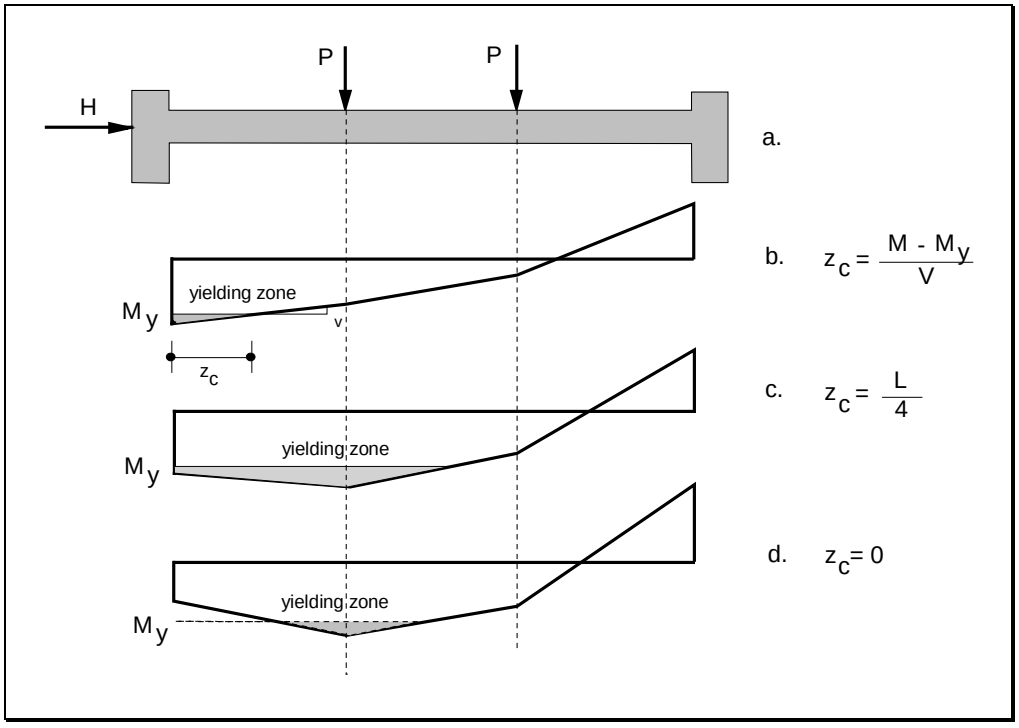

FIGURE 2.11 CALCULATION OF PLASTIC ZONE LENGTH IN TYPICAL CASES

where *M* and *V* are the current values of bending moment and shear force, respectively, at the end of the girder. Eq. (2.7) results in very large values of the plastic zone length if the value of the end shear force is very small. This can happen in the upper stories of high-rise frames where the end shear forces due to lateral loads are small and sometimes act opposite to the shear forces due to gravity loads. In such cases yielding of the girders is, however, limited so that this does not seem to be a real problem in practical cases. Similarly, Eq. (2.7) does not make sense, if the value of the shear force becomes negative (Fig. 2.11c). To prevent

unrealistically large values of the plastic zone length in these cases an upper limit z_{max} is placed on the extent of the plastic zone (Fig. 2.11c):

$$z_{max} = 0.25 \cdot L \tag{2.8}$$

where L is the clear span of the girder. The limit on the extent of the plastic zone is particularly important on account of the likely change in the reinforcement layout that takes place at the quarter span point.

Since the calculation of the plastic zone length depends on the bending moments and shear forces at the girder ends, the spread plastic subelement is unable to recognize yielding that might take place along the girder span (Fig. 2.11d). Plastic zones can, therefore, only form at the girder ends. If hinges are expected to form along the span, then the girder has to be subdivided into several such elements along its length.

It should be noted here that no increase of the current plastic zone length will occur in the extreme case depicted in Fig. 2.12. Consistent with the first key assumption of the model that the behavior of the plastic zone is controlled by the behavior of the corresponding end section, spreading of the plastic zone can only take place while the end section is in the strain-hardening range. Since the end section is unloading in the case of Fig. 2.12, the further extension of the plastic zone length due to considerable decrease in the magnitude of the shear force from one step to the next will not be detected by the model. It should be mentioned, however, that the case depicted in Fig. 2.12 is highly unlikely, when using a reasonably small load step size.

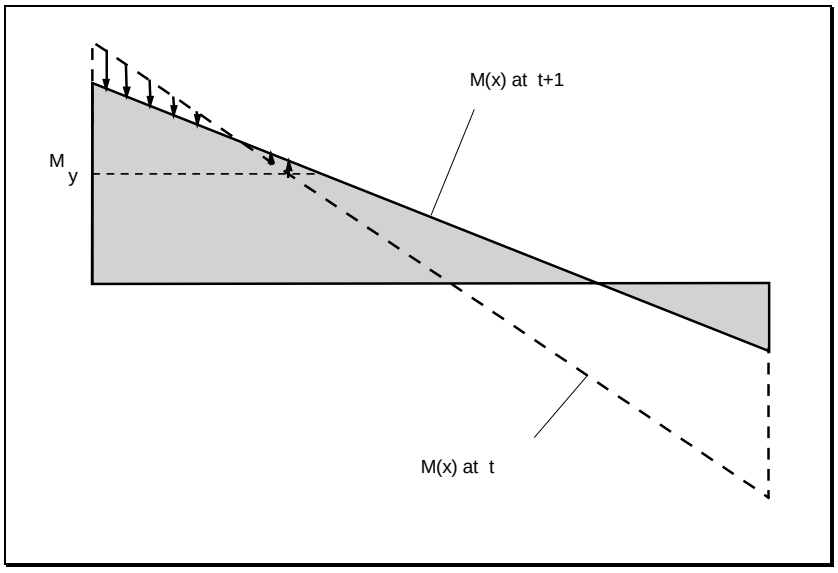

FIGURE 2.12 SPREAD OF THE PLASTIC ZONE WHILE END SECTION IS UNLOADING (NOT ACCOUNTED FOR IN THE MODEL)

The flexibility matrix of the spread plastic subelement as derived in Filippou and Issa (1988) takes the general form

$$[\mathbf{f}]_{pl} = \begin{bmatrix} f_{11} & f_{12} \\ f_{21} & f_{22} \end{bmatrix} \tag{2.9}$$

where

$$f_{12} = f_{21}$$

and

$$f_{11} = \frac{L}{6k} \cdot \left\{ 2\gamma_i \cdot \left[1 - (1 - \xi_i)^3 \right] + 2\gamma_j \cdot \xi_j^3 \right\} \tag{2.10}$$

$$f_{22} = \frac{L}{6k} \cdot \left\{ 2\gamma_j \cdot \left[1 - (1 - \xi_j)^3 \right] + 2\gamma_i \cdot \xi_i^3 \right\} \tag{2.11}$$

$$f_{12} = \frac{L}{6k} \cdot \left[-\gamma_i \cdot (3\xi_i^2 - 2\xi_i^3) - \gamma_j \cdot (3\xi_j^2 - 2\xi_j^3) \right] \tag{2.12}$$

with $k = EI$ and

$$\frac{z}{L} = \xi$$

$$\frac{1}{c} = \gamma$$

It is interesting to note here that the off-diagonal terms f_{12} and f_{21} of the flexibility matrix of the spread plastic subelement are not zero, as is the case in the concentrated plasticity element. This results in coupling between the moments which act at the ends of the element.

2.2.3 Joint subelement

The joint subelement accounts for the fixed-end rotations which arise at the beam-column interface of RC members due to bond deterioration and slippage of reinforcement in the joint and in the girder region adjacent to the joint. Detailed models of this phenomenon have been proposed (Filippou et al. 1983, Filippou 1985). The model used in this study is a simple yet sufficiently accurate phenomenological description of the behavior of beam-column joints observed in previous experimental and analytical studies. The proposed model consists of a concentrated rotational spring located at each girder end. The two springs are connected by an infinitely rigid bar to form the joint subelement (Figs. 2.3 and 2.13a). The moment-rotation relation of the rotational springs is derived using the detailed model by

Filippou et al. (1983) which accounts for the geometry, material properties and reinforcement layout of the connection. A different moment-rotation relation can be prescribed at each connection.

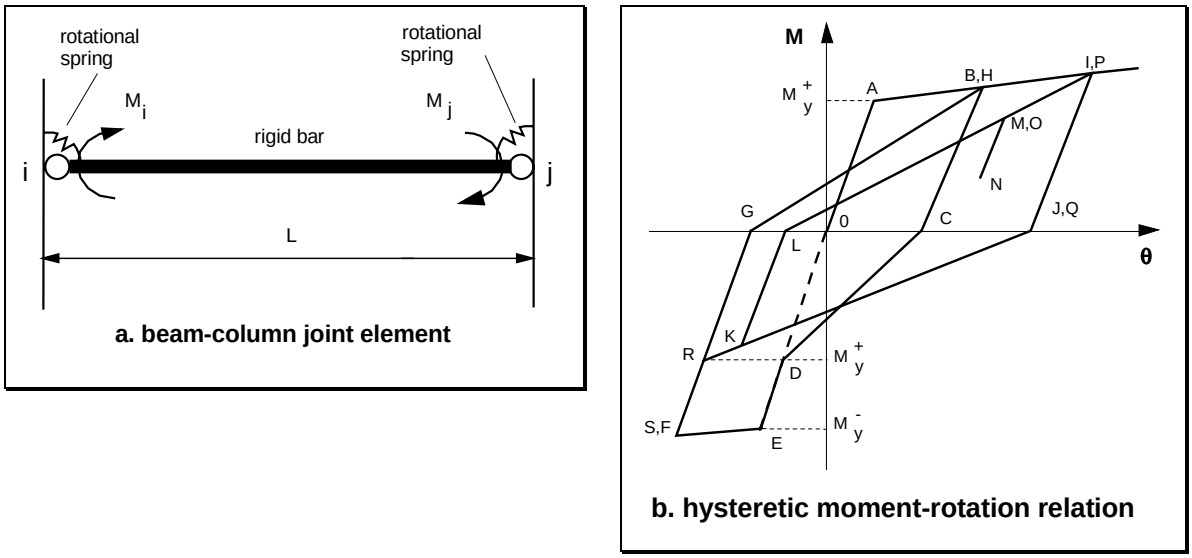

FIGURE 2.13 BEAM-COLUMN JOINT SUBELEMENT

The moment-rotation relation of the rotational springs of the joint subelement is based on a bilinear elastic-strain hardening envelope curve (Fig. 2.13b). Following common design practice the area of the bottom reinforcing bars is typically less than the area of the top reinforcing bars; therefore two envelope curves need to be specified: one pertaining to the "strong side" of the end section, when the top reinforcing bars are subjected to tension, and one pertaining to the "weak side", when the bottom bars are subjected to tension. These envelope curves exhibit different pre-and post-yield stiffness under positive and negative bending moments. Naturally, the yield moment M_y^+ under positive bending moments is different from the yield moment M_y^- under negative bending moments (Fig. 2.13b).

The envelope curves are established with the aid of the joint model in Filippou et al. (1983) once the dimensions of a particular joint and the arrangement of the reinforcement are known. This process takes place as follows: the beam-column joint model which represents a particular connection of the frame under investigation is subjected to monotonically increasing girder end moments. These give rise to concentrated rotations due to reinforcing bar pull-out at the beam-column interface. In the case of interior joints a single loading cycle permits the determination of envelope curves under both positive and negative end moments. This happens, because bending moments caused by lateral loads act at the girder ends of an interior joint so that the bottom bars are pulled at one beam-column interface and pushed at

the other. In the case of exterior joints two different load cases of monotonically increasing girder end moments are required to establish the envelope curves under positive and negative end moments: in one case the *bottom bars* of the end section are subjected to tension, while in the other the *top bars* are subjected to tension.

The study by Filippou et al. (1983) concluded that no unique envelope curve exists in the case of interior and exterior joints. Instead, the envelope curve depends on the load history. Since the elastic stiffness and yield moment do not depend on the load history, this essentially implies that the strain hardening or possibly strain softening slope of the bilinear envelope curve of the rotational springs has to be established as a function of load history. Thus, in order to establish the envelope curve for a particular joint, the load history of this joint must be known in advance. This effect is, however, negligible in properly designed joints and is not taken into account in the present study. If considerable bond deterioration and slippage of reinforcement is expected in the joints of the structure, the effect of load history on the envelope curve of the joint subelement should be taken into account.

The flexibility matrix of the joint subelement takes the simple form

$$[\mathbf{f}]_{jnt} = \begin{bmatrix} f_i & 0 \\ 0 & f_j \end{bmatrix} \tag{2.13}$$

where f_i and f_j are the flexibility coefficients of the concentrated rotational springs at ends *i* and *j*, respectively. These coefficients depend on the monotonic envelope curves of each joint and the model used to represent the hysteretic behavior.

The hysteretic behavior of the rotational springs is described by a special hysteretic model proposed by Filippou (1983). It is derived by modifying Clough's model to account for observations of beam-column joint behavior made during experimental and analytical studies. The rules of this hysteretic model can be summarized as follows (Fig. 2.13b):

(1) unloading takes place along a line parallel to the initial elastic stiffness under moments acting in the same direction (line B-C parallel to 0-A, line K-L, in turn, parallel to 0-E)

(2) reloading on the "weak side" of the joint (G-H) occurs along the line which connects the most recent point of zero moment (G) to the load reversal point on the envelope curve which has the largest previously imposed fixed-end rotation (H),

(3) reloading on the "strong side" of the joint (Q-R-S) follows initially a line Q-R which connects the most recent point of zero moment (point Q) to a point on the unloading curve which initiates at the load reversal point with largest previous fixed-end rotation (point R). This point has a moment equal to the yield moment of the "weak side" of

the joint (M_y^+ in Fig. 2.13b). After reaching this point reloading proceeds along the unloading curve (R-S),

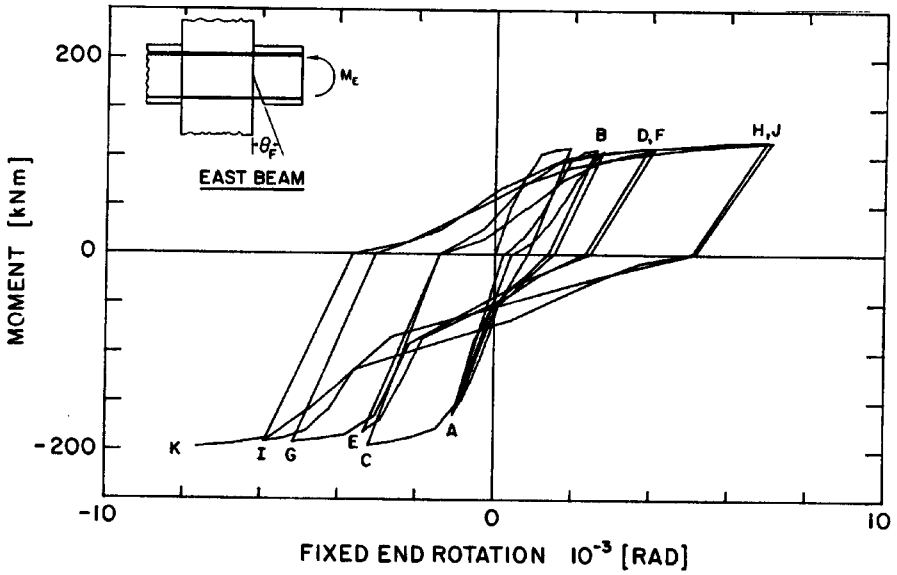

FIGURE 2.14 MOMENT-ROTATION RELATION AT BEAM-COLUMN JOINT INTERFACE (FILIPPOU ET AL. 1983)

(4) incomplete reloading followed by unloading and reloading in the opposite direction takes place along the path J-K-L-M,

(5) incomplete reloading followed by incomplete unloading and reloading in the same direction takes place along the path L-M-N-O-P.

These hysteretic rules are derived from observations of the behavior of joints under cyclic load reversals made during experimental and analytical studies (Filippou et al. 1983) (Fig. 2.14):

(a) no pinching is observed in the hysteretic moment-rotation relation when the bottom reinforcing layer is subjected to tension ("weak side"). In this case the beam-column interface crack remains open through the depth of the end section during the entire moment reversal process. The girder end moment is thus resisted by a force couple in the top and bottom reinforcing steel. This observation is reflected in the second hysteretic rule,

(b) when the top reinforcing layer is subjected to tension ("strong side"), the moment resisted by the section at the beam-column interface cannot exceed the moment carried by the reinforcement with the bottom reinforcing bars yielding in compression, as long as the crack remains open. This moment is approximately equal

to the yield moment in the opposite direction of bending ("weak side"). Since the crack closes when the previously imposed pull-out of the bottom reinforcing bars is overcome, crack closure takes place approximately when the maximum previously imposed fixed-end rotation is exceeded. Once the crack closes, the resisting moment quickly reaches the envelope curve, since the concrete in contact now contributes a significant portion of the compressive force at the section. This observation is reflected in the third hysteretic rule,

(c) it is apparent from the results by Filippou et al. (1983) that the unloading stiffness of the joint moment-rotation relation decreases with increasing deformation. Since, however, no general expression describing the observed decrease in unloading stiffness could be deduced, the simple hysteretic rule that the unloading stiffness remains equal to the initial elastic stiffness is postulated in the present model.

The proposed rules describe well the observed hysteretic behavior of beam-column joints while retaining simplicity and computational efficiency. More refined models of the hysteretic behavior of beam-column joints could be readily incorporated into the girder superelement by simply replacing the hysteretic law of the joint subelement.

It should be noted here that the proposed joint subelement does not explicitly account for the interaction between the moments and forces acting at the girder ends of interior beam-column joints. This interaction is small as long as bond along the reinforcing bars anchored in the joint is not completely destroyed (Filippou et al. 1983). It only becomes pronounced after many severe deformation reversals which are unlikely to occur in well proportioned frames. This interaction is, however, implicitly accounted for in the present model, since the parameters of the envelope curves and the derivation of the hysteretic rules are based on the refined model by Filippou et al. (1983), which explicitly accounts for this interaction. At the same time the present model retains great simplicity in that the flexibility coefficients of each rotational spring in the frame can be derived independently.

2.2.4 Girder shear subelement

The girder shear subelement accounts for the shear distortion of the inelastic zone of the girder as well as the shear sliding at the beam column interface. Different models of shear behavior have been proposed in the literature (Celebi and Penzien 1973, Spurr 1984, Ozcebe and Saatcioglu 1989, Soroushian and Sim 1989). It is not economical to model shear behavior in its full complexity in a frame model developed for the dynamic response analysis of multistory frame structures. Practical limitations are imposed by the scope of the frame element idealization used in the present study and by the lack of quantitative information

about the response of severely cracked concrete under post-yield load reversals. Moreover, the shear response is generally secondary to the flexural response in typical building frame members and, consequently, the same degree of accuracy as for the flexural contribution is not justified for shear.

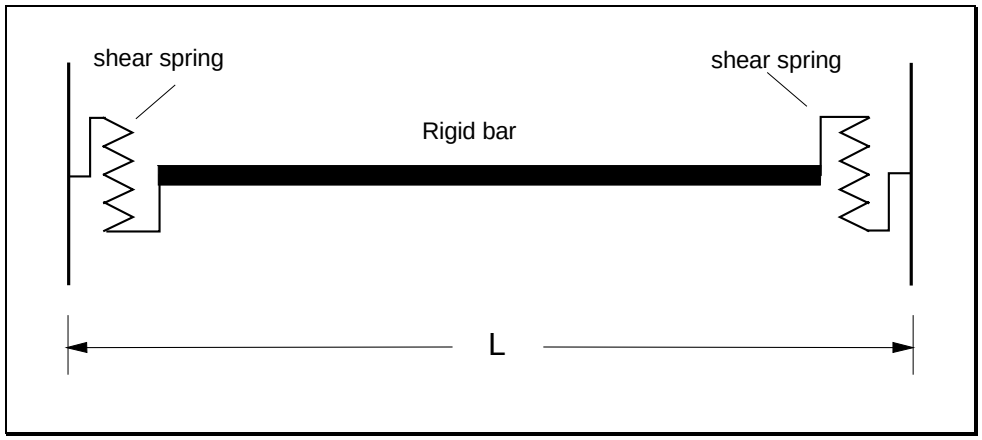

FIGURE 2.15 GIRDER SHEAR SUBELEMENT

The model used in this study is a simple phenomenological description of the shear distortion behavior of reinforced concrete girders subjected to severe cyclic loading. The proposed model consists of a concentrated translational spring of zero dimension located at each girder end. The two springs are connected by an infinitely rigid bar to form the girder shear subelement (Fig. 2.15). It is computationally convenient to express the shear distortion as a function of the end moment

$$\boldsymbol{\theta}_{shr} = [\mathbf{f}]_{shr} \cdot \mathbf{M}$$

where the flexibility matrix of the girder shear subelement $[\mathbf{f}]_{shr}$ takes the simple form

$$[\mathbf{f}]_{shr} = \begin{bmatrix} f_i & 0 \\ 0 & f_j \end{bmatrix} \tag{2.14}$$

where f_i and f_j are the flexibility coefficients of the equivalent concentrated rotational springs at ends *i* and *j*, respectively. These coefficients depend on the monotonic envelope curve and the model used to describe the hysteretic behavior.

The derivation of the monotonic envelope curve is explained with the aid of Figs. 2.16-2.19. The moment distribution in the lower story of a typical moment resisting frame subjected to large lateral loads is shown in Fig. 2.1. If the inflection point is assumed at girder midspan and the effect of gravity loads is neglected, as is the case in most studies to date (Banon et al. 1981), the girder moment and shear diagrams are as shown in Figs. 2.16(a)

and (b), respectively. The shear force V which will give rise to end moment M is given by the expression $V = M/0.5L$ where L is the clear span of the girder. Clearly, the shear force is directly related to the end moment in this case. Assuming that the point of inflection remains fixed at the girder midspan and neglecting the effect of gravity loads leads to a constant ratio between end moment and shear force. Therefore, the shear deformation can be expressed as a function of the end moment. Since the point of inflection is located at the girder midspan, each half of the member can be viewed as a cantilever beam (Figs. 2.16c and 2.16d). Subjecting the cantilever beam to a concentrated load at the tip in Fig. 2.17(a) results in the shear force diagram in Fig. 2.17(b). The shear deformations are distributed according to Figs. 2.17(c) and (d).

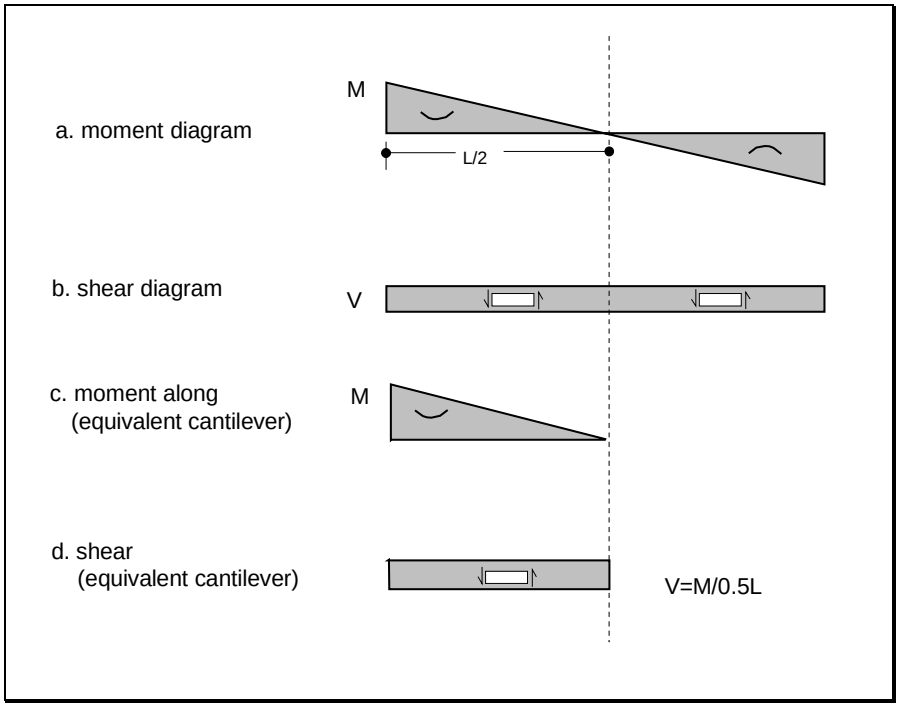

FIGURE 2.16 MOMENT AND SHEAR DIAGRAM OF SHEAR SUBELEMENT

The total shear distortion is found by integration of the shearing strains along the cantilever span

$$\delta_{shr} = \int \frac{V}{G(x) \cdot A^*} dx$$

where G is the shear modulus of concrete and A^* is the effective shear area of the girder. Since $M = (0.5L) \cdot V$

$$\delta_{shr} = \frac{2}{L} \int \frac{M(x)}{G(x) \cdot A^*} dx$$

The relation between the lumped values of δ_{shr} and θ_{shr} is schematically shown in Fig. 2.18:

$$\delta_{shr} = \frac{\theta_{shr} \cdot L}{2}$$

Thus

$$\theta_{shr} = \frac{4}{L^2} \int \frac{M(x)}{G(x) \cdot A^*} dx$$

$$\theta_{shr} = \frac{4M}{L^2} \int \frac{1}{G(x) \cdot A^*} dx$$

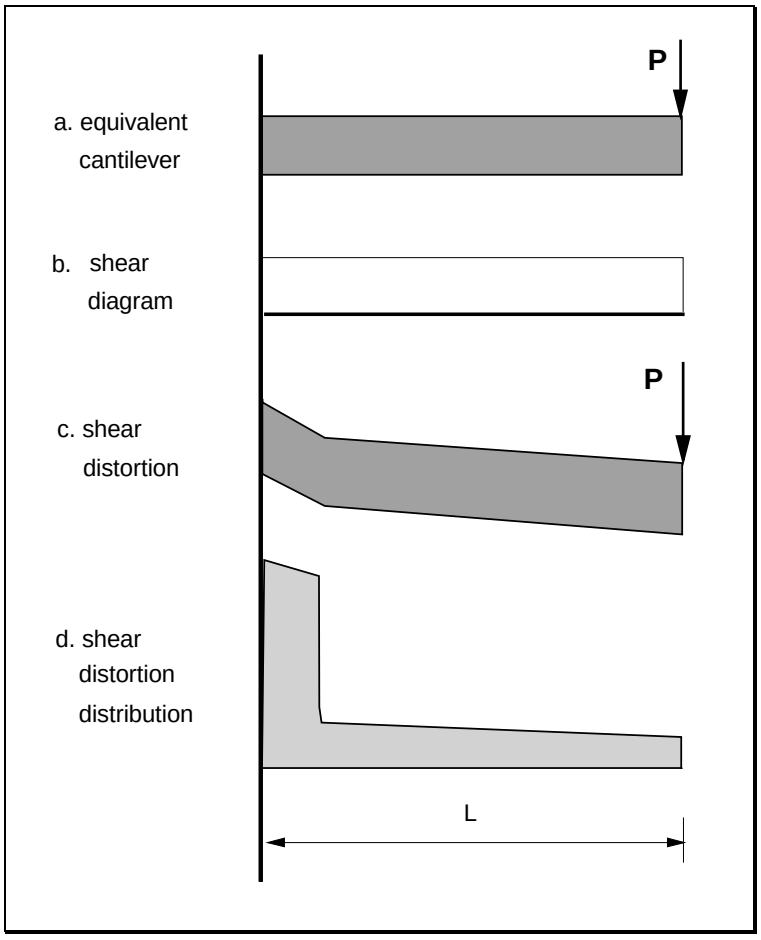

FIGURE 2.17 SHEAR DISTORTION DISTRIBUTION

Thus

$$M = \frac{L^2}{4\int \frac{1}{G(x)\cdot A^*}dx} \cdot \theta_{shr}$$

Before the formation of flexural or diagonal cracks, the behavior of the member can be described with sufficient accuracy on the basis of the theory of elasticity. The shear modulus of concrete can be derived from the well known relationship

$$G = \frac{E}{2(1+\nu)}$$

where E is Young's modulus of concrete and ν is Poisson's ratio.

After diagonal cracking the shear force-shear distortion relation under monotonic loading can be derived either with the method proposed by Küstü (1973) or on the basis of the compression field theory developed by Collins and Mitchell (1980). The latter method is used in this study.

In describing the shear behavior under cyclic load reversals a hysteretic model is needed. The shear hysteretic model for general inelastic section analysis in this study is primarily directed at representing the aggregate interlock and the interaction of shear forces with the opening and closing of the cracks.

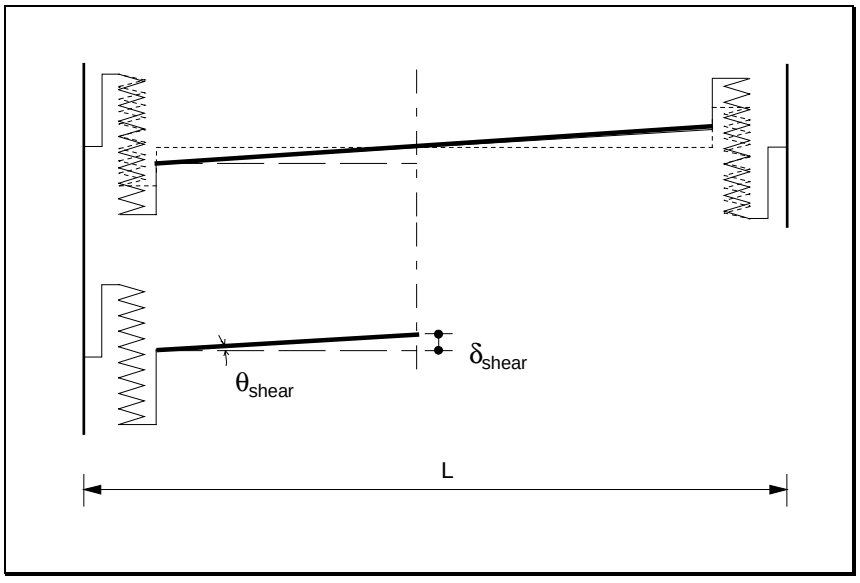

FIGURE 2.18 SCHEMATIC DIAGRAM OF SHEAR SUBELEMENT DEFORMATION

The stiffness degradation model proposed by Clough et al. (1965) cannot be used for the description of the hysteretic shear behavior. In general, the stiffness reduction depends primarily on the magnitude of inelastic load reversals and the number of post-yield load

cycles. It is reported by Celebi and Penzien (1973) that the area enclosed by the hysteresis loops of a beam which is cycled a few times at the same displacement ductility is successively decreased.

Typical shear force-deformation response curves for a reinforced concrete beam with a small shear span to depth ratio are shown in Fig. 2.19 (Celebi and Penzien 1973). It is seen that the pinched shape of the hysteresis loops develops only after the first post-yield load cycle.

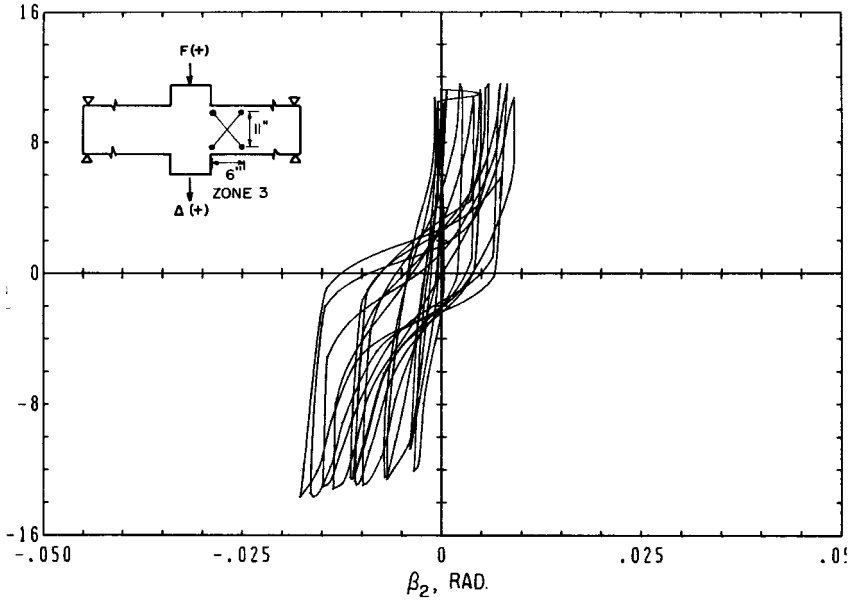

FIGURE 2.19 SHEAR FORCE-SHEAR DISTORTION RELATION (FROM CELEBI AND PENZIEN 1973)

The proposed hysteretic model of shear force-shear deformation relation is derived from experimental results of beams subjected to flexure and shear. This model is based on a set of rules which are shown in Fig. 2.20.

(1) A bilinear monotonic envelope curve (curve **ABC** in Fig. 2.20) is used in this study. A trilinear envelope curve which includes the shear behavior before cracking is not deemed important, since emphasis is placed on the post-yield behavior of RC frames in this study.

(2) The model exhibits a constant initial stiffness until reaching the yield moment M_y of the end section.

(3) Yielding of the shear spring is assumed to take place at the same time as flexural yielding. The assumption of simultaneous shear and flexural yielding is supported by experimental evidence (Ozcebe and Saatcioglu 1989).

(4) Unloading takes place along a line **FG** parallel to the initial stiffness.

(5) After unloading is completed and upon reloading in the opposite direction, there is a significant reduction in stiffness until the crack closes. In this study the point at which the crack closes (point **O**) is determined according to suggestions of Ozcebe and Saatcioglu (1989):

(a) If the member has not been loaded beyond the cracking load M_{cr} in the direction of reloading, the initial reloading path aims at the cracking load M_{cr} on the primary curve (Point **H**) and then follows the primary curve. M_{cr} is the bending moment at which the principal tensile stress is equal to $2\sqrt{f_c'}$.

(b) If M_{cr} has been exceeded in the direction of reloading during previous cycles, reloading up to a moment equal to M_{cr} (point **O**) follows a straight line passing through a point defined by (θ_{max}, M^*) where θ_{max} is the maximum previous equivalent shear rotation and

$$M^* = M_{max} \cdot e^{\frac{-c_1 \cdot \theta_{max}}{\theta_y}}$$

θ_y is the rotation at yield, and M_{max} is the maximum previous moment in the direction of reloading, respectively. Parameter c_1 varies over the small range from 0.20 to 0.35.

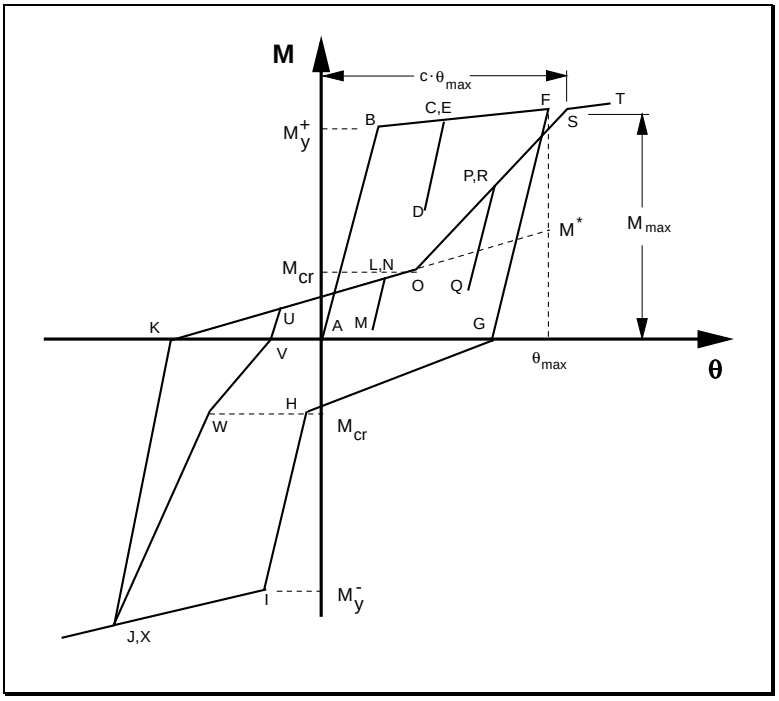

FIGURE 2.20 HYSTERETIC BEHAVIOR OF SHEAR SUBELEMENT

(c) Reloading beyond M_{cr} follows a straight line towards point **S** on the primary envelope curve. Point **S** is determined by multiplying the maximum previous rotation θ_{max} in the same direction of loading by a factor *c*. Thus a new point of maximum rotation towards which reloading occurs is defined on the envelope curve as follows:

$$\theta^{*}_{max} = c \cdot \theta_{max}$$

While Banon et al. (1981) have proposed a value of $c = 1.25$ the correlations of the present study suggest a value of $c = 1.0$.

No strength degradation occurs in the case of cycles that do not cross the zero rotation axis (**U-V-W-X**).

(6) In case a change in load direction occurs during unloading, reloading takes place with a slope equal to the elastic stiffness until the point at which unloading initiated is reached (**C-D-E**), (**L-M-N**), (**P-Q-R**).

The branches of hysteretic behavior between points **K** and **O** and between points **G** and **H** are soft central regions where shear sliding occurs under a small shear force along open full depth cracks. After the cracks close, there is a sharp increase in the shear stiffness (**O-S**, **H-I**). This is followed by a region of small shear stiffness under large rotation values (**S-T**, **I-J** in Fig. 2.20). This stiffness reduction arises from the opening of major inclined flexural-shear cracks caused by increasing plastic tensile strains in the longitudinal reinforcement.

2.2.5 Girder superelement stiffness matrix

The elastic, rigid plastic, joint, and shear subelements are connected in series to form the girder superelement (Fig. 2.3). If needed, additional sources of inelastic behavior can be added in separate subelements in the same manner. Since the constituent subelements are connected in series, the flexibility matrix of the girder superelement $[\mathbf{F}]_g$ can be obtained by simply adding the flexibility matrices of the constituent subelements. Using the convention that upper case letters denote quantities associated with the girder superelement while lower case letters denote quantities associated with the individual subelements we obtain

$$[\mathbf{F}]_g = [\mathbf{f}]_{el} + [\mathbf{f}]_{pl} + [\mathbf{f}]_{jnt} + [\mathbf{f}]_{shr} \tag{2.15}$$

$[\mathbf{f}]_{el}$ denotes the flexibility matrix of the elastic subelement given by Eq. 2.1. $[\mathbf{f}]_{pl}$ denotes the flexibility matrix of either the concentrated rigid plastic (Eq. 2.6) or the spread rigid-plastic subelement (Eqs. 2.9-2.12). $[\mathbf{f}]_{jnt}$ denotes the flexibility matrix of the joint

subelement given by Eq. 2.13. Finally, $[\mathbf{f}]_{shr}$ denotes the flexibility matrix of the girder shear subelement given by Eq. 2.14.

It is important to note that the flexibility coefficients in $[\mathbf{f}]_{pl}$, $[\mathbf{f}]_{jnt}$ and $[\mathbf{f}]_{shr}$ change, because of nonlinearities associated with the moment-curvature or moment-rotation relation and the change of the plastic zone length. Thus $[\mathbf{f}]_{pl}$, $[\mathbf{f}]_{jnt}$ and $[\mathbf{f}]_{shr}$ in Eq. 2.15 represent the current tangent flexibility matrices of the rigid plastic, joint and shear subelement, respectively.

The flexibility matrix of the girder superelement $[\mathbf{F}]_g$ is inverted to obtain the current stiffness matrix $[\mathbf{K}]_g$ in local coordinates. This is then transformed to global coordinates using the transformation matrix $[\mathbf{a}]_b$

$$[\mathbf{K}]_b = [\mathbf{a}]_b^T \cdot [\mathbf{K}]_g \cdot [\mathbf{a}]_b \tag{2.16}$$

where $[\mathbf{K}]_b$ is the tangent stiffness matrix in global coordinates and $[\mathbf{a}]_b$ expresses the transformation of superelement local moments and rotations to nodal forces and displacements in the global coordinate system (Fig. 2.21)

$$\begin{Bmatrix} \Theta_1 \\ \Theta_2 \end{Bmatrix} = [\mathbf{a}]_b \cdot \begin{Bmatrix} \Theta_i \\ \Theta_j \\ v_i \\ v_j \end{Bmatrix} \tag{2.17a}$$

$$\begin{Bmatrix} M_i \\ M_j \\ V_i \\ V_j \end{Bmatrix} = [\mathbf{a}]_b^T \cdot \begin{Bmatrix} M_1 \\ M_2 \end{Bmatrix} \tag{2.17b}$$

where

$$[\mathbf{a}]_b = \begin{bmatrix} 1+e_i & e_j & 1/L & -1/L \\ e_i & 1+e_j & 1/L & -1/L \end{bmatrix} \tag{2.18}$$

$$e_i = \frac{b_i}{L} \tag{2.19a}$$

$$e_j = \frac{b_j}{L} \tag{2.19b}$$

b_i and b_j is equal to half the width of the left and right end beam-column joint, respectively. L is the clear span of the member (Fig. 2.21).

By inverting the sum of the flexibility matrices of the elastic $[\mathbf{f}]_{el}$ and the concentrated plastic subelement $[\mathbf{f}]_{pl}$ given by Eqs. 2.1 and 2.6, respectively, the stiffness matrix of the one-component model as originally proposed by Giberson (1974) results. The addition of flexibility matrices of the elastic $[\mathbf{f}]_{el}$ and spread plastic subelement $[\mathbf{f}]_{pl}$ given by Eqs. 2.1 and 2.10, respectively, yields the flexibility matrix of the spread plasticity model proposed by Soleimani (1979).

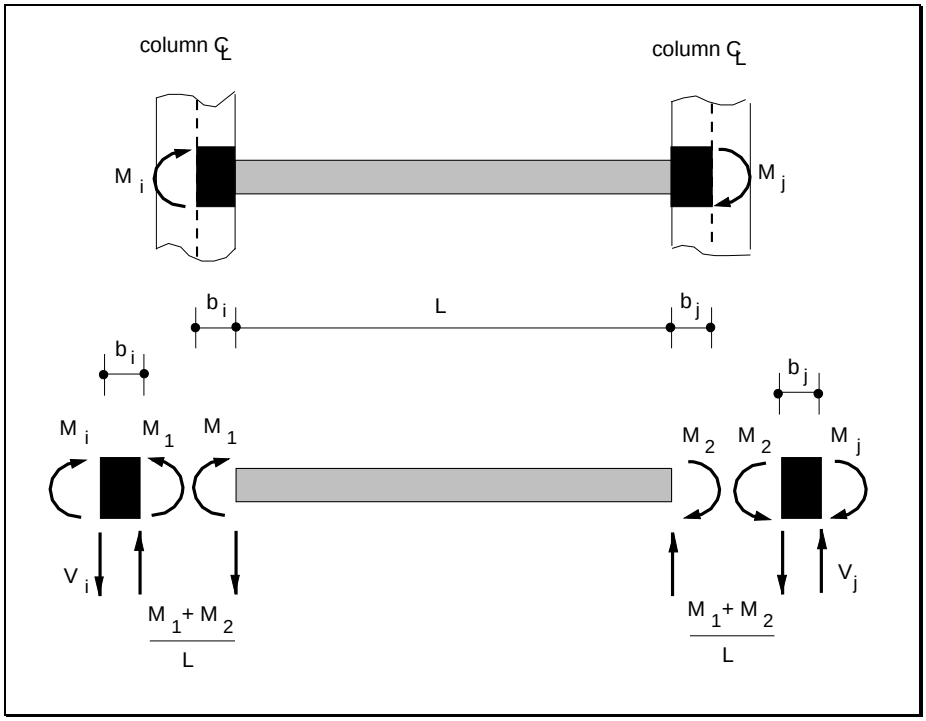

FIGURE 2.21 TRANSFORMATION OF FORCES AND MOMENTS BETWEEN LOCAL AND GLOBAL COORDINATE SYSTEM

2.3 Reinforced concrete column element

In designing reinforced concrete columns to resist severe earthquake excitations, designers favor the strong column-weak girder design concept which aims at dissipating energy in a flexural mode in a large number of hinges in the girders of the structure. Modern design codes attempt to ensure such behavior by requiring that the sum of the moment strengths of columns framing into a beam-column connection exceed the sum of the moment strengths of the girders framing into the same connection along each principal plane of the frame. This may not be sufficient to prevent the formation of plastic hinges in the columns, because of the following factors:

(1) The actual moment strength of the girders will be higher than the nominal strength, because the nominal yield strength of reinforcing steel underestimates the actual strength. Strain hardening under large curvatures will further increase the actual girder strength.

(2) The moment distribution in the columns of moment resisting frames under dynamic loading can be very different from that assumed in design. Points of contraflexure may move away from the column mid-height during the earthquake response time history. This causes moments at the end of particular columns to be higher than those under static loading conditions. Bending moment distributions in columns similar to those shown in Fig. 2.22 are possible (Kelley 1974). In the extreme case that the point of inflection lies outside the column the strength of one column section has to exceed the sum of the moment strengths of the girders framing into the connection.

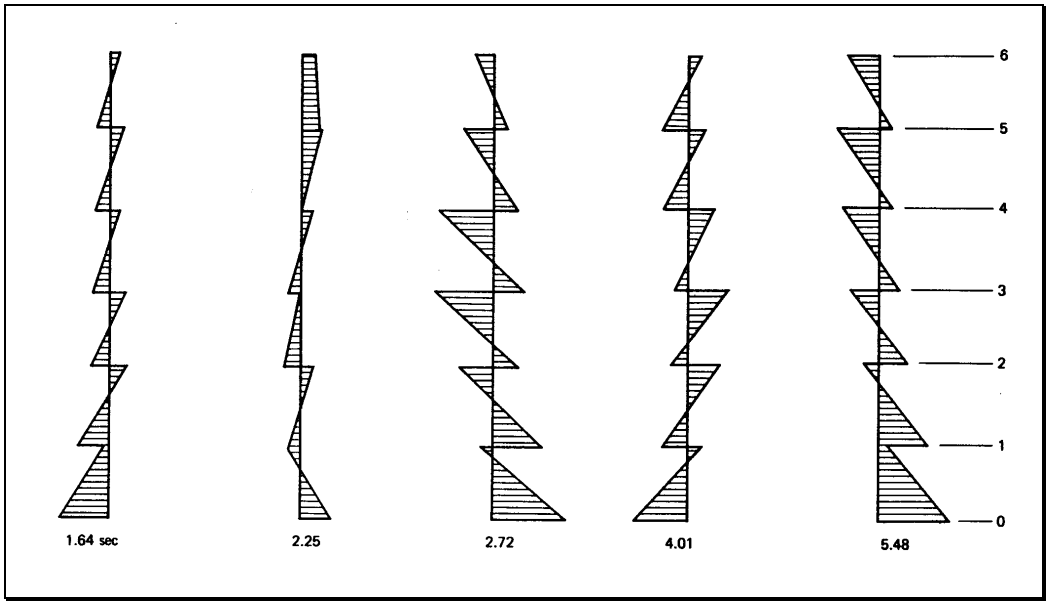

FIGURE 2.22 BENDING MOMENTS IN COLUMNS OF A 12-STORY FRAME RESPONDING NONLINEARLY TO 1940 EL CENTRO EARTHQUAKE (FROM KELLEY 1974)

(3) In the design of structures seismic loading is assumed to act in the direction of one principal axis of the structure at a time. However, the structure is subjected to multiaxial ground accelerations, which give rise to biaxial effects. These can cause yielding of the beams in both directions simultaneously. Since the flexural strength of a square column bent about the diagonal could be 15% less than the flexural strength under uniaxial bending (Gill et al. 1979), multidirectional earthquake loading may result in the columns yielding before the beams.

(4) A complete static collapse mechanism in moment resisting frames requires the formation of plastic hinges in the columns at the base of the building.

Since preventing plastic hinge formation in columns under severe seismic excitations is very difficult, a nonlinear column superelement is developed in this study. Unlike beam elements, the post yield behavior of columns is influenced by axial load. Thus the proposed element must account for the axial force effects on the hysteretic behavior of reinforced concrete members. This effect has been studied over a wide range of axial load levels (Gill et al. 1979, Low and Moehle 1987). These studies have demonstrated that current seismic design provisions for reinforced concrete columns in ductile moment resisting frames guarantee excellent hysteretic behavior up to a displacement ductility of six, even under high axial loads. Excellent hysteretic behavior of reinforced concrete columns under axial load levels up to $0.6 f_c' \cdot A_g$ has been observed (Gill et al. 1979).

The axial load level in mid-rise buildings of typical proportions is, usually, a fraction of the balanced load, since the axial load does not control the size of the column cross section. This is rather controlled by the joint size and drift considerations. Therefore, columns considered in this study are assumed to be subjected to axial loads below the balanced load.

The variation of axial forces in the interior columns of a moment resisting frame is, usually, small, since the axial force caused by the shear in the right hand side beam cancels that caused by the shear of the left hand side beam. This is, especially, true if the frame has bays of approximately equal length. Exterior columns exhibit much larger variation of axial forces than interior columns. Kaba and Mahin (1984) conclude that the assumption of constant axial load will not significantly affect the global response. However, the column shear history under constant axial load might be different from that due to variable load, if axial loads fluctuate greatly in exterior columns. Although the axial load variation in slender moment resisting frames could be important, these effects are not very significant in well designed frame structures of typical dimensions, because columns of typical mid-rise frame buildings are oversized to control drift. The axial load level will, therefore, be a small fraction of the column capacity and the fluctuation of this already small axial load level will not be very significant. Since accounting for axial load variation leads to considerable increase in computational effort, the variation of column axial forces due to lateral load reversals is neglected in this study.

The hysteretic behavior of critical regions in reinforced concrete columns is very sensitive to the presence of shear. If shear stresses are high, consideration should be given to the interaction of shear forces with axial load and bending moment.

Earthquake resistant design philosophy tries to ensure that reinforced concrete

columns fail in a ductile flexural mode and that brittle shear failure is prevented. This requires that the shear strength exceed the flexural capacity of the frame members. Therefore, in moderately tall buildings designed according to current seismic design provisions the lateral deformations of columns result primarily from the effects of flexure and slip of reinforcement (Low and Moehle 1987).

An axial load acting on a reinforced concrete section affects the section stiffness and strength characteristics, as shown in Fig. 2.23. Under compressive axial loads lower than the balanced point, an increase in the level of axial load results in an increase of the flexural strength and stiffness of the column section. If the section is subjected to cyclic curvature reversals, the existence of a high compressive axial load results in pinching of the hysteresis loop due to bond slip and crack opening and closing (Fig. 2.24). If shear effects are small, the higher the axial load the more pronounced is the pinching effect (Kaba and Mahin 1984).

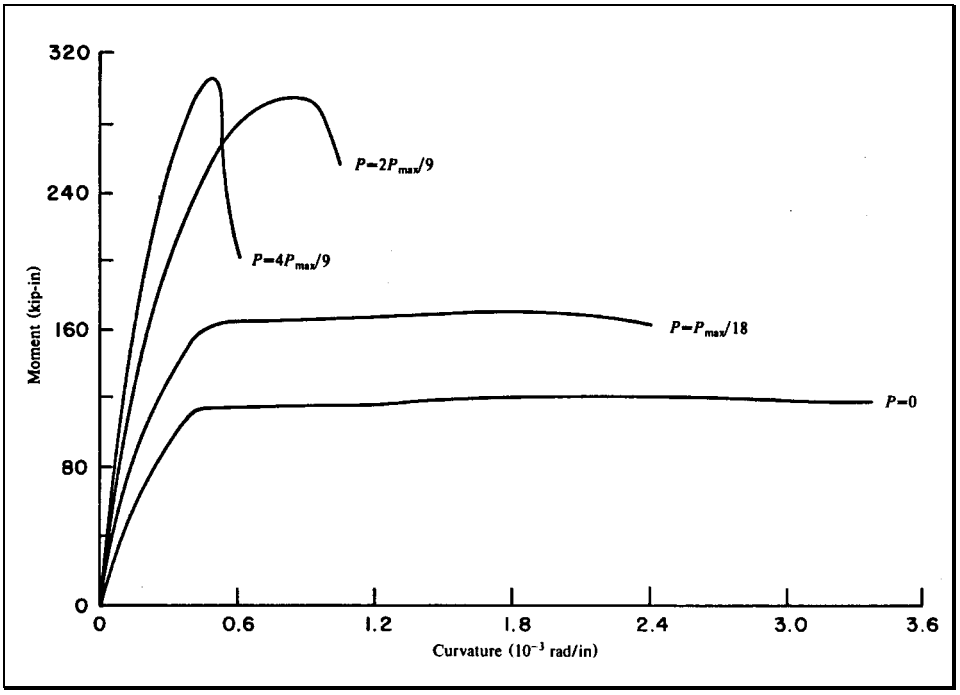

FIGURE 2.23 INFLUENCE OF AXIAL LOAD ON SECTION STRENGTH AND STIFFNESS (FROM KABA AND MAHIN 1984)

Although short columns should be avoided in earthquake resistant design, this does not mean that they do not exist. Short columns are often encountered in the strength evaluation of existing buildings; architectural constraints might also force the structural engineer to accept short columns. Since short columns will attract high shear forces, the shear effect on the hysteretic behavior of axially loaded members is considered in this study.

The hysteretic behavior of critical regions in reinforced concrete columns is significantly affected by the presence of high shear stresses. The hysteretic behavior of reinforced concrete columns subjected to high axial and shear stresses has been investigated experimentally (Küstü 1973, Zagajeski et al. 1978). These studies show that a high axial force can improve the cyclic shear resistance of reinforced concrete columns, since it tends to restrain shear crack widening and thus limits the deterioration of the concrete shear resistance. The beneficial effect of axial load is limited to cases where the axial load does not exceed the balance point load and a sufficient amount of properly detailed transverse reinforcement is provided.

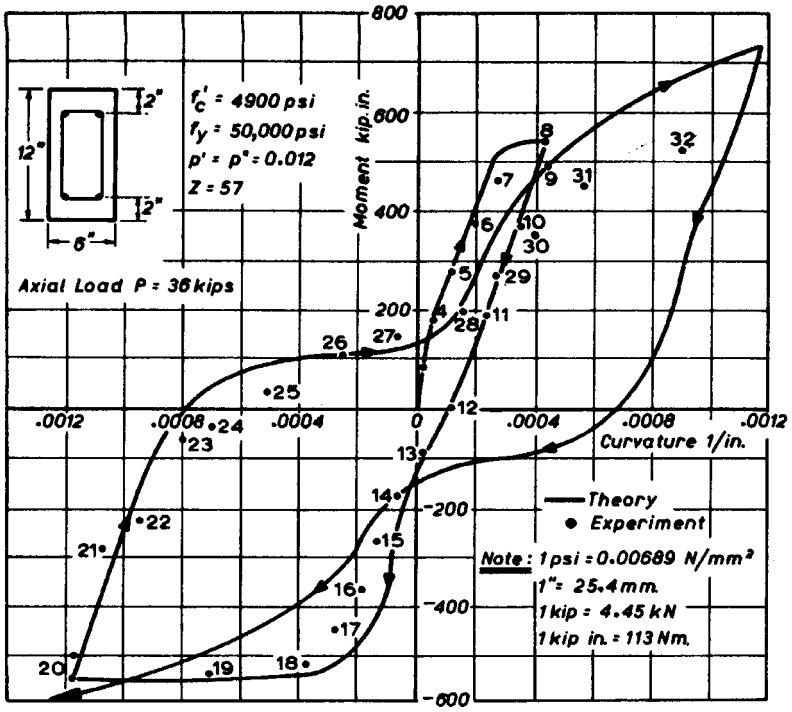

FIGURE 2.24 PINCHING DUE TO BOND-SLIP IN SYMMETRICALLY REINFORCED CONCRETE COLUMN (FROM PARK ET AL. 1972)

Although the concrete contribution to shear resistance increases with axial load, it should be stressed that the shorter the column and the higher the axial load, the larger the possibility of shear failure (Atalay and Penzien 1975, Zagajeski et al. 1978). In general, longer shear spans, smaller axial loads, and larger amounts of properly detailed transverse reinforcement improve the hysteretic behavior of reinforced concrete columns.

In this study the column element is decomposed into different subelements. Each subelement describes a different deformation mechanism affecting the hysteretic behavior of critical regions in columns. This modeling approach permits the prediction of the behavior of

columns subjected to, both, low and high shear stresses. The interaction of axial load, bending moment and shear force with the opening and closing of the cracks is taken into account in the development of the different column subelements. The following subelements are proposed in this study:

(1) An elastic column subelement which represents the linear elastic flexural behavior of the column before yielding of the reinforcement.

(2) A plastic column subelement which describes the flexural behavior of the column in the post-yield range. The element accounts for the spread of plastic deformations into the column as a function of loading history.

(3) A column joint subelement which represents the fixed end rotation due to bond slip at the column ends and accounts for the interaction of bending moment and axial load with the opening and closing of the cracks. This interaction is reflected in the pinching of the hysteretic behavior of the column which increases with increasing axial load, as shown by Kaba and Mahin (1984) for columns subjected to flexure and axial load with low shear stress.

(4) A shear subelement which describes the shear distortion and shear sliding at the column ends. The interaction of shear and axial force with the opening and closing of the cracks is taken into account in this subelement. This is reflected in the pinching of the hysteretic behavior of the subelement which decreases with increasing axial load, as shown in experiments on columns subjected to axial load, shear and bending moment (Atalay and Penzien 1975).

Since the presence of axial load affects the hysteretic behavior of columns with high shear stress differently than that of columns with low shear stress, the introduction of two separate subelements to account for the effect of shear and bond slip, respectively, facilitates the accurate and rational description of the hysteretic behavior of reinforced concrete columns.

The effect of axial load is further accounted for in the derivation of the primary curves for the load-deformation relation of the column subelements. The monotonic envelope curves are derived under constant axial load equal to that caused by gravity loads. This results in an envelope curve which falls in between the stiffer curve resulting from an increase in axial load and the softer curve resulting from a reduction in axial load due to lateral loading reversals (Emori and Schnobrich 1981). As discussed already, the time variation of axial load does not have a significant effect on the seismic response of midrise frames so as to justify the high computational effort needed for its inclusion in the model.

In addition to the effects of shear, flexure, slip of reinforcement and opening and closing of the cracks, the column element includes axial deformations and geometric P-Δ effects as discussed in the following sections.

2.3.1 Linear elastic column subelement

The elastic column subelement describes the linear elastic flexural behavior of the columns before yielding of the reinforcement. The linear elastic flexural stiffness of columns is significantly influenced by the axial load acting on the section. In this model the effect of axial load on the elastic flexural stiffness is taken into account in deriving the primary curve of the moment curvature relation of the column section. Assuming a linear strain variation through the depth of the section the primary moment-curvature relation for a member subjected to constant axial force and gradually increasing bending moment can be derived. The moment-curvature relation is then approximated by a bilinear elastic strain-hardening curve.

The stiffness of the elastic subelement is based on the secant stiffness of the column section at yielding of the reinforcement, which is equal to $EI = M_y / \varphi_y$. To account for the unlikely case that a non-symmetric arrangement of column reinforcement is used the section stiffness is taken as the average between the stiffness under positive and that under negative bending moment. It is assumed that the column element is prismatic and that the longitudinal reinforcement does not change along the height. Splicing of column bars might cause a slightly higher stiffness in a small part of the column; but this effect is not significant.

The elastic flexural stiffness matrix is given by

$$[\mathbf{f}]_{el} = \frac{h}{6EI} \cdot \begin{bmatrix} 2 & -1 \\ -1 & 2 \end{bmatrix} \tag{2.20}$$

where E is the concrete modulus of elasticity of the concrete and h is the clear height of the column.

2.3.2 Rigid-plastic column subelement

The inelastic flexural deformation of the column is modeled in a rigid-plastic subelement. The monotonic envelope curve of the model is based on a bilinear approximation of the moment-curvature relation of the column section under the constant axial load caused by gravity loads. Fig. 2.25 is a typical axial force-moment interaction diagram. Points on the interaction diagram below the balanced point indicate failure by yielding of the reinforcement, while points above correspond to failure by crushing of the

concrete. During the response of typical frame structures to earthquake excitations, column axial forces usually remain below the balanced point and vary in the range shown in Fig. 2.25. In this case the relation between axial force and bending moment can be approximated by the dashed line in Fig. 2.25. The dotted line depicts an interaction relation used in several other investigations. Since, within the expected range of axial load variation, the error associated with either interaction relationship is comparable, the simpler interaction relation is used in this study.

The plastic column subelement is basically the same as the corresponding beam subelement except that the primary curve of the column element is derived with due consideration of the effect of axial load on the yield moment and strain hardening ratio.

Pinching of the hysteretic moment rotation relation is attributed to the opening and closing of the cracks, slip of reinforcement and shear sliding. Since these effects are taken into account in subelements specifically developed for the purpose, the rigid plastic column subelement only describes the inelastic flexural deformations and, consequently, does not exhibit any pinching of hysteretic behavior.

Two different plastic subelement have been developed in this study, one with concentrated plastic deformations and another which allows for the gradual spread of inelastic deformations along the member. These are presented in detail in the following.

a) Concentrated rigid-plastic column subelement

The concentrated rigid plastic column subelement describes the inelastic flexural deformations which take place at the column ends after yielding of the reinforcement. These deformations are modeled by a rigid plastic hinge of zero length similar to the concentrated rigid-plastic springs in the plastic beam subelement. The hinge, which is depicted as a nonlinear spring in Fig. 2.4(a), is activated when the moment at the corresponding column end first exceeds yielding. Since all inelastic deformations are lumped at the plastic hinges at the two ends of the column and the elastic deformations along the member are accounted for in the linear elastic column subelement, the part of the concentrated plastic subelement which connects the two hinges is infinitely rigid.

The flexibility matrix of the subelement takes the simple form

$$[\mathbf{f}]_{pl} = \begin{bmatrix} f_i & 0 \\ 0 & f_j \end{bmatrix} \tag{2.21}$$

where f_i and f_j are the flexibility coefficients of the rotational springs at ends *i* and *j*, respectively. The general method of determining the flexibility of the rotational springs is

described in detail in Section 2.2.2.1. The derivation of the flexibility of the plastic rotational springs is similar to the derivation of the beam rotational springs except that the effect of axial load on the yield moment and the strain hardening stiffness is taken into account.

The main advantage of the concentrated plasticity model is its simplicity and computational efficiency. It has, however, some serious limitations: most importantly it does not account for the gradual spread of inelastic deformations into the column. This results in an underestimation of stiffness in the early stages of inelastic deformation. Another limitation of the model lies in the assumption that the point of inflection is fixed at column mid-height during the entire response history. This is not realistic, particularly, in the dynamic analysis of frames, where columns can be in single curvature at certain stages of the response history depending on the dynamic excitation and the column location in the structure (Fig. 2.22).

b) Spread rigid-plastic column subelement

Since the flexural deformations of the column before yielding of the reinforcement are accounted for in the elastic subelement, the spread rigid-plastic subelement only accounts for the column inelastic flexural deformations which arise when the end moments exceed the yield moment.

The spread rigid-plastic column subelement consists of two regions of finite length where the plastic column deformations take place. These regions are connected by an infinitely rigid bar, as shown in Fig. 2.7(a). The length of each plastic zone varies during the response history as a function of the moment distribution in the column. The model thus accounts for the gradual spread of inelastic deformations into the column and the shift of the inflection point during the response time history.

The features of the spread rigid-plastic subelement and the coefficients of the flexibility matrix are presented in Section 2.2.2.2. The main difference between the column spread plastic subelement and the corresponding beam subelement is the axial load effect on the yield strength and the strain hardening stiffness of the moment curvature of the column section.

The plastic zone length at each load step is determined from the corresponding end moments and shear forces using the assumption that the shear force is constant in the plastic zone.

The general form of the flexibility matrix of the spread plastic column subelement is:

$$[\mathbf{f}]_{pl} = \begin{bmatrix} f_{11} & f_{12} \\ f_{21} & f_{22} \end{bmatrix} \tag{2.22}$$

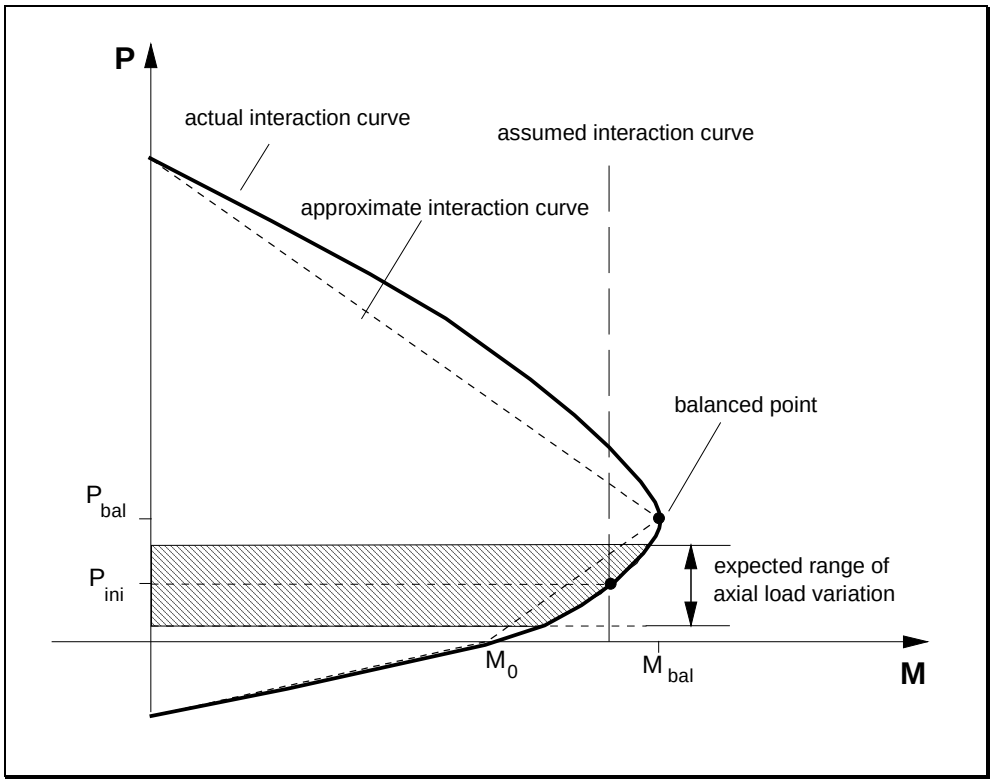

FIGURE 2.25 AXIAL LOAD-BENDING MOMENT INTERACTION DIAGRAM

The coefficients of this flexibility matrix have been derived in Section 2.2.2.2 for the general case and expressions for f_{11}, f_{22} and f_{12} are given in Eqs. 2.10, 2.11, and 2.12, respectively.

2.3.3 Column joint subelement

The column joint subelement models the fixed-end rotation due to bond slip of column reinforcement and the effect of opening and closing of flexural cracks on the moment-rotation relation.

The pinching of the hysteretic moment-rotation relation of RC columns under bending moment and axial load is often quite pronounced. This phenomenon can be illustrated with a study of the interaction of the opening and closing of flexural cracks with the applied bending moment and axial load.

Over a large portion of the cyclic load history of reinforced concrete members, the applied moment is resisted by a steel couple alone (Park and Paulay 1975). This results from large plastic tensile strains in the longitudinal reinforcing steel which cause cracks in the tension zone to remain open while the bending moment is reversed. These cracks will remain

open until the steel in the compression zone yields and forces the crack to partially close. At this stage the concrete starts to contribute a large part of the compressive force and the section stiffness increases considerably (Fig. 2.24). The presence of axial compression in columns means that even for sections with symmetric reinforcement (equal tension and compression steel), the steel in compression yields under a small bending moment and closes the crack. It is clear that the flexural rigidity of the section is reduced when the moment is resisted by a steel couple alone, and that the stiffness increases when the concrete starts to carry part of the compression resultant. The reduction in flexural rigidity of the column section followed by a marked increase in the section stiffness is the cause of pinching of the hysteretic behavior of column sections (Park and Paulay 1975). For columns with small shear stresses, the pinching of the hysteretic loops of the moment rotation relation increases with increasing axial compression (Kaba and Mahin 1984).

The column joint subelement is represented by two rotational springs connected by a rigid bar as is the case for the girder joint subelement. The mechanical characteristics of the column joint springs are, however, different from those of the girder joint subelement because of the effect of axial load. The general form of the flexibility matrix of the column joint subelement is:

$$[\mathbf{f}]_{jnt} = \begin{bmatrix} f_i & 0 \\ 0 & f_j \end{bmatrix} \tag{2.23}$$

The coefficients f_i, and f_j of this flexibility matrix depend on the hysteretic behavior of the springs at column ends *i* and *j*, respectively.

In modeling the hysteretic behavior of the joint subelement, the primary curve is derived with the joint finite element model by Filippou et al. (1983). The joint is subjected to a constant axial load to simulate conditions at the column ends.

The confining effect of other connecting members is included in the derivation of the envelope curve of the column joint subelement. This effect is accounted for in the finite element model by increasing the bond strength as a function of the axial load in the connecting members. Since the axial load of beams connected to the column is negligible in the case of typical frame buildings, the confining effect on the beam-column joint is not very significant, if the effect of girders framing perpendicular to the plane of moment-resisting frame is neglected.

The hysteretic behavior of the column joint springs is shown in Fig. 2.26. It is determined by the following rules (Fig. 2.26):

(1) A bilinear elastic-strain hardening envelope curve (**ABC**) describes the monotonic behavior.

(2) A constant stiffness is assumed until the end section reaches the yield moment M_y.

(3) Unloading takes place along a line **FG** parallel to the initial stiffness.

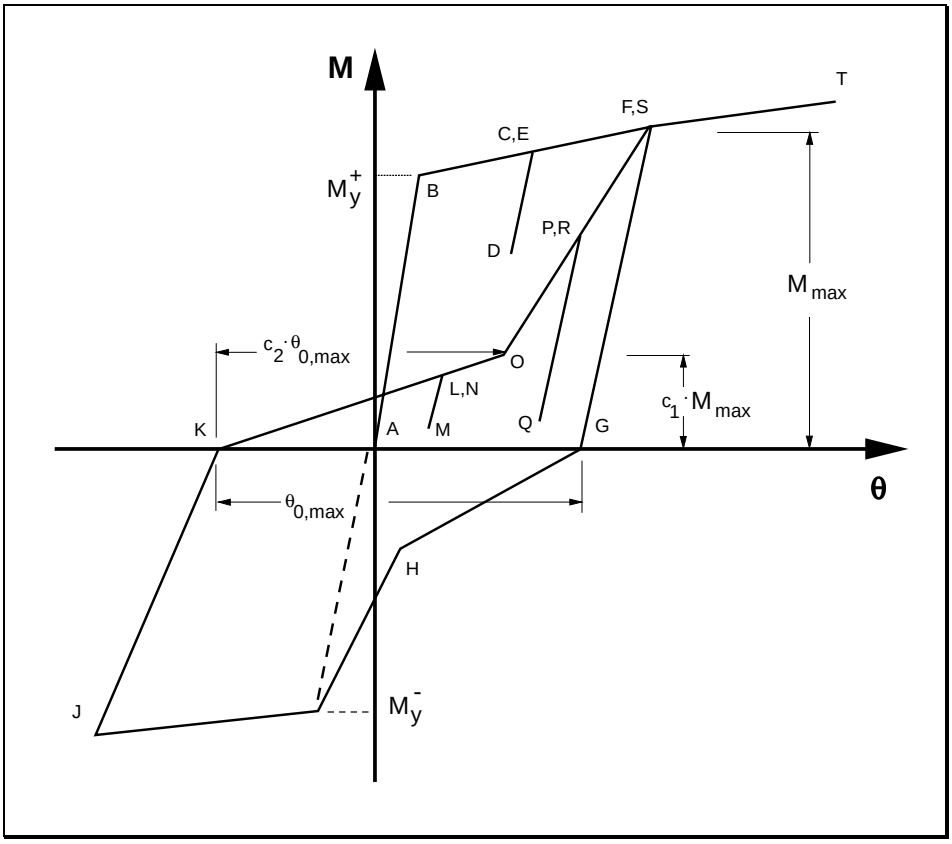

FIGURE 2.26 HYSTERETIC BEHAVIOR OF COLUMN JOINT SUBELEMENT

(4) Once unloading is completed, there is a significant reduction in stiffness caused by crack opening. This stiffness remains in effect until the crack closes (point **O**). The point at which the crack closes, is determined by parameters c_1 and c_2 in Fig. 2.26. These parameters control the amount of pinching of the hysteretic moment-rotation relation of the column joint subelement and depend on the level of axial load. The amount of pinching increases with increasing axial load. Values for these factors are derived from analyses with the joint model by Filippou et al. (1983), as will be discussed in the correlation studies of Chapter 5.

(5) Once the crack closes at point **O** reloading follows a straight line connecting point **O** with the point of maximum previous rotation on the envelope curve (point **S** in Fig. 2.26).

(6) In the case of partial unloading followed by reloading, the loading stiffness is parallel to the elastic stiffness until the point at which unloading started is reached (**C-D-E**),

(**L-M-N**), (**P-Q-R**).

2.3.4 Column shear subelement

The column shear subelement accounts for shear deformations in the columns and the interaction of the opening and closing of the cracks with the shear and axial force. This element describes the effect of shear sliding on the hysteretic load-displacement relation of reinforced concrete columns, which is especially pronounced in short columns. The column shear subelement consists of two concentrated springs connected by a rigid bar.

The flexibility matrix of the column shear subelement takes the simple form of the girder shear subelement

$$[\mathbf{f}]_{shr} = \begin{bmatrix} f_i & 0 \\ 0 & f_j \end{bmatrix} \tag{2.24}$$

where f_i, and f_j are the flexibility coefficients of the shear springs at column ends *i* and *j*, respectively.

The derivation of the properties of the column shear springs is similar to the derivation of the properties of the beam shear springs in Section 2.2.4. In this case, however, the axial load has a strong effect on shear behavior (Atalay and Penzien 1975). Columns with a shear span to depth ratio less than 2 exhibit large shear deformations (Zagajeski et al. 1978).

In members subjected to cyclic shear under constant axial load cyclic stiffness deterioration and pinching of the shear force- displacement relation near zero load is observed (Atalay and Penzien 1975). The stiffness deterioration and pinching effect are less pronounced in columns under high axial loads. The hysteretic rules of the column shear subelement are the same as those used for the beam shear subelement in Fig. 2.21, except that pinching is now dependent on the level of axial load. The value of M^* in Fig. 2.21 depends on the axial load such that lower pinching of the hysteresis loops results under higher axial compression. The following empirical formula for M^* which reflects the effect of axial load on the pinching of the hysteretic shear force-deformation relation is proposed by Ozcebe and Saatcioglu (1989):

$$M^* = M_{max} \cdot e^{\alpha \frac{\theta_{max}}{\theta_y}}$$

$$\alpha = 0.82 \cdot \frac{P}{P_0} - 0.18 < 0$$

P is the axial compressive force, P_0 is the nominal axial load strength of the column, M_{max} is the maximum previous end moment, θ_{max} is the maximum previous shear distortion and θ_y is the shear distortion at yield. The correlations with experimental results in Chapter 5 yield better agreement with a parameter value of 0.18 in the second equation above instead of the value of 0.14 proposed by Ozcebe and Saatcioglu (1989).

The study of two rough, interlocking surfaces which move along the plane of the shear crack indicates that shear displacements need to be much larger than those along the initially uncracked interfaces in order to effectively engage the aggregate particles that protrude from the two faces of the crack. The larger the crack width the larger the shear displacement needed to engage the aggregate particles. The increase in crack width is restrained by the clamping effect of the axial load.

The effect of axial load on the shear behavior of the element is included as follows:

- The axial load increases the yield moment capacity of the column section and, thus, delays the opening of flexural cracks due to yielding of flexural reinforcement. This, in turn, delays the propagation of flexural-shear cracks and results in a reduction of shear sliding. This effect is taken into account in the derivation of the primary curve of the shear subelement.
- The axial load reduces the pinching effect due to sliding. The pinching parameters of the column shear subelement result in a larger amount of pinching with decreasing axial compression.

Although the concrete contribution to shear resistance increases with axial load, a higher compression leads to higher shear forces for axial loads below the balanced point. The axial force-bending moment interaction diagram shows that the yield moment increases from M_0 to M_b as the axial load increases from zero to the balanced point value P_b. Consequently, in a column subjected to an axial load near P_b the shear force at flexural yielding will be larger than the shear force in the same column under a smaller axial load. Increasing the shear force magnitude increases the possibility of brittle shear failure.

2.3.5 Column axial stiffness

The axial stiffness of the column is assumed constant and uncoupled from the bending behavior in this study. Since the dimensions of column cross sections in typical moment frames are controlled by drift considerations, columns are very unlikely to experience yielding under pure compression.

The column axial stiffness matrix with respect to local coordinates is given by

$$\begin{Bmatrix} P_1 \\ P_2 \end{Bmatrix} = \frac{EA}{h} \cdot \begin{bmatrix} 1 & -1 \\ -1 & 1 \end{bmatrix} \cdot \begin{Bmatrix} v_1 \\ v_2 \end{Bmatrix} \tag{2.25}$$

where v_1 and v_2 are the axial displacements at the ends of the column, *EA* is the gross axial stiffness of the cross section and *h* is the column clear height. From consideration of equilibrium and the assumption of rigid joint panel zones it is clear that axial loads and displacements with respect to the girder centerline are the same as those with respect to the column clear height.

2.3.6 Column geometric stiffness

The interaction of large axial forces in the lower story columns of multistory frames with large interstory drifts due to severe lateral loads may result in considerable second-order effects, especially in high rise buildings. For simplicity the local geometric stiffness with respect to the column chord end rotations is neglected. Consideration is given, however, to the global geometric stiffness related to the column end lateral displacements. Assuming a linear displacement function between the column ends in Fig. 2.27 results in the following column centerline geometric stiffness matrix with respect to global coordinates

$$\begin{Bmatrix} F_1 \\ F_2 \end{Bmatrix} = \frac{P}{H} \cdot \begin{bmatrix} 1 & -1 \\ -1 & 1 \end{bmatrix} \cdot \begin{Bmatrix} u_1 \\ u_2 \end{Bmatrix} \tag{2.26}$$

F_1 and F_2 are the lateral forces and u_1 and u_2 are the lateral displacements at the lower and upper column end, respectively, while *P* is the axial compressive force acting on the column. *P* accounts for the effect of gravity loads and overturning moments due to lateral loads. The axial load *P* is assumed to remain constant within a load step.

With the assumption that the floor diaphragm is infinitely rigid in its plane all lateral displacements can be condensed into a single lateral degree of freedom at each story. In this case the geometric stiffness of the individual columns may be combined into the geometric stiffness of the entire story (Fig. 2.27).This is given by

$$\begin{Bmatrix} F_1 \\ F_2 \end{Bmatrix} = \frac{\sum P}{H} \cdot \begin{bmatrix} 1 & -1 \\ -1 & 1 \end{bmatrix} \cdot \begin{Bmatrix} u_1 \\ u_2 \end{Bmatrix} \tag{2.27}$$

u_1 and u_2 are the lateral displacements of the floor below and above the particular story, respectively, and $\sum P$ is the sum of all axial forces in the columns of a particular story.

2.3.7 Column superelement stiffness matrix

The elastic, rigid plastic, joint, and shear subelements of the column are connected in series to form the column superelement (Fig. 2.3). If needed, additional sources of inelastic behavior of the column can be added in separate subelements in the same manner. Since the constituent subelements are connected in series, the flexibility matrix of the column superelement $[\mathbf{F}]_{crd}$ can be obtained by simply adding the flexibility matrices of the constituent subelements. Using the convention that upper case letters denote quantities associated with the column superelement while lower case letters denote quantities associated with the individual subelements we obtain

$$[\mathbf{F}]_{crd} = [\mathbf{f}]_{el} + [\mathbf{f}]_{pl} + [\mathbf{f}]_{jnt} + [\mathbf{f}]_{shr} \tag{2.28}$$

$[\mathbf{f}]_{el}$ denotes the flexibility matrix of the elastic subelement given by Eq. 2.20, $[\mathbf{f}]_{pl}$ denotes the flexibility matrix of either the concentrated rigid plastic (Eq. 2.21.) or the spread rigid plastic subelement (Eqs. 2.10-2.12 and 2.22), $[\mathbf{f}]_{jnt}$ denotes the flexibility matrix of the joint subelement given by Eq. 2.23, and, finally, $[\mathbf{f}]_{shr}$ denotes the flexibility matrix of the shear subelement given by Eq. 2.24.

It is important to note that the flexibility coefficients in $[\mathbf{f}]_{pl}$, $[\mathbf{f}]_{jnt}$, and $[\mathbf{f}]_{shr}$ may change within a load step, because of nonlinearities associated with the moment-curvature or moment-rotation relation and a change in the plastic zone length. Thus $[\mathbf{f}]_{pl}$, $[\mathbf{f}]_{jnt}$, and $[\mathbf{f}]_{shr}$ in Eq. 2.28 represent the current tangent flexibility matrices of the rigid plastic, joint, and shear subelement, respectively.

The flexibility matrix of the column superelement with respect to the chord $[\mathbf{F}]_{crd}$ is inverted to obtain the current stiffness matrix $[\mathbf{K}]_{crd}$ in local coordinates. The column axial stiffness matrix $[\mathbf{K}]_{a}$ with respect to local coordinates is given by Eq. 2.25.

$[\mathbf{K}]_{crd}$ can be readily transformed to global coordinates by applying a transformation matrix $[\mathbf{a}]_{crd}$ similar to $[\mathbf{a}]_{b}$ in Eq. 2.18. Matrix $[\mathbf{a}]_{crd}$ can be derived from $[\mathbf{a}]_{b}$ by replacing *L* by *H* and considering b_i and b_j as half the depth of the beam-column joint at the lower and upper end of the column, respectively.

The transformation of $[\mathbf{K}]_{a}$ in Eq. 2.25 to global coordinates is much more direct, because the rigid offset zones have no effect on axial forces and displacements. Thus, the local axial forces are equal one to one to the corresponding global forces, and the local axial displacements *v* are equal one to one to the corresponding global vertical frame displacements.

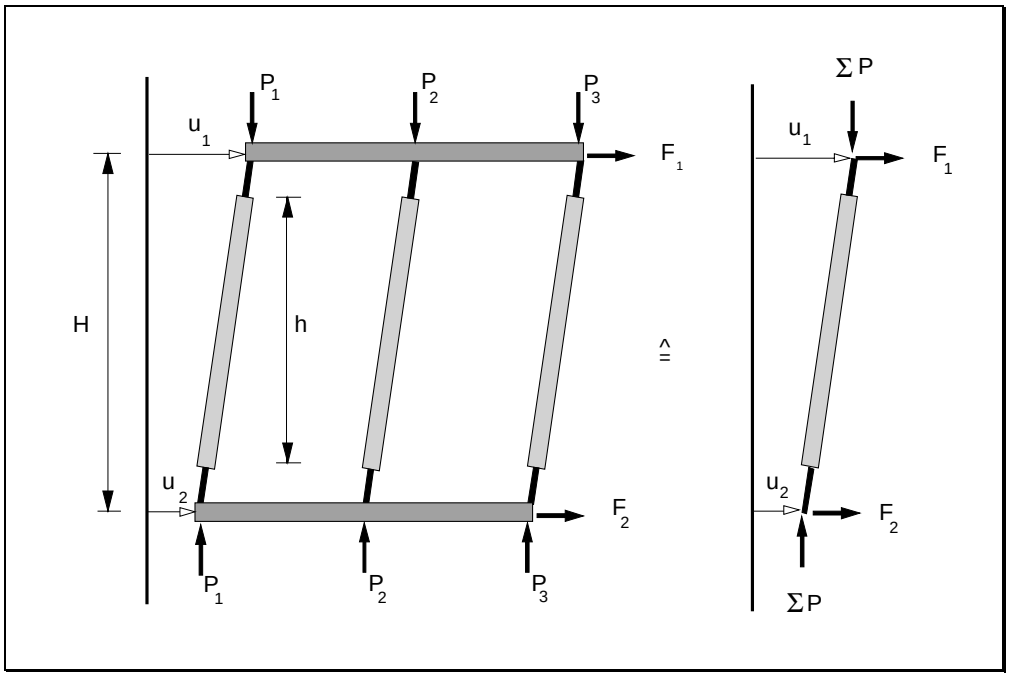

FIGURE 2.27 LINEAR GEOMETRIC STIFFNESS MATRIX OF COLUMN SUBELEMENT

Knowing the chord stiffness transformation matrix $[\mathbf{a}]_{crd}$ and the axial stiffness transformation matrix $[\mathbf{a}]_a$, the stiffness matrix of the column in global coordinates $[\mathbf{K}]_c$ can be obtained with the following operation

$$[\mathbf{K}]_c = [\mathbf{a}]_{crd}^T \cdot [\mathbf{K}]_{crd} \cdot [\mathbf{a}]_{crd} + [\mathbf{a}]_a^T \cdot [\mathbf{K}]_a \cdot [\mathbf{a}]_a \tag{2.29}$$

2.4 Foundation element

Most structures are built on flexible foundations. The flexibility of the foundation influences the response of buildings under static loads and dynamic ground excitations. The effect of the underlying soil not only influences the characteristics of the free field earthquake motion recorded at the surface, but can also interact with the building founded on it to alter the structural response. In this study the structure is subjected to the free field motion, which is applied at the structural supports, and the dynamic response is obtained directly. The effect of the structure on the soil surface acceleration is not accounted for, since this effect is not important in typical building structures.

The foundation element, which is modeled as a spring element, represents vertical, rotational, and lateral displacements of the base of the building associated with settlement, rocking and sliding of the foundation (Fig. 2.2). The stiffness matrix of the foundation

element at the base of each first story column is simply given by

$$[\mathbf{K}]_f = \begin{bmatrix} k_{sv} & 0 & 0 \\ 0 & k_{sh} & 0 \\ 0 & 0 & k_{sr} \end{bmatrix} \tag{2.30}$$

where k_{sv}, k_{sh}, k_{sr} is the vertical, horizontal and rotational stiffness of the spring at the base of the column, respectively. The foundation stiffness coefficients remain constant during the entire response time history.

2.5 Structural stiffness matrix

The first step in the analysis of a moment resisting reinforced concrete frame is the development of a model of the actual structure. This process is schematically illustrated in Fig. 2.28 which shows how the girders and columns of the actual structure are represented by the frame elements in this study. After determining the stiffness matrix of all elements with respect to global coordinates, the stiffness matrix of the entire structural model can be formed using the direct stiffness method. This process can be formally written as

$$[\mathbf{K}] = \sum_{\substack{all \\ elem}} [\mathbf{K}]_b + [\mathbf{K}]_c + [\mathbf{K}]_G + [\mathbf{K}]_f \tag{2.31}$$

where $[\mathbf{K}]$ is the stiffness matrix of the entire structure, $[\mathbf{K}]_b$ is the stiffness matrix of the girder superelement, $[\mathbf{K}]_c$ is the stiffness matrix of the column superelement and $[\mathbf{K}]_f$ is the stiffness matrix of the foundation element with respect to global coordinates. $[\mathbf{K}]_G$ represents the story geometric stiffness matrix defined in Eq. 2.27. The summation in Eq. 2.31 extends over all elements in the structure.

Since the different frame elements exhibit nonlinear behavior either through nonlinearities in material response or through changes in the inelastic zone length, the different stiffness matrices in Eq. 2.31 really represent the tangent stiffness matrices of the various elements. The nonlinear response of the structure to cyclic load or deformation reversals can only be determined through an incremental step-by-step analysis. This process can be expressed by

$$[\mathbf{K}] \cdot \Delta\mathbf{r} = \Delta\mathbf{R} \tag{2.32}$$

where $\Delta\mathbf{R}$ is the vector of load increments which are successively imposed on the structure and $\Delta\mathbf{r}$ is the vector of corresponding displacement increments. $[\mathbf{K}]$ is the current stiffness matrix of the structure.

After solving Eq. 2.32 for the unknown displacement increments $\Delta\mathbf{r}$ the response of the structure to the applied loads is obtained from

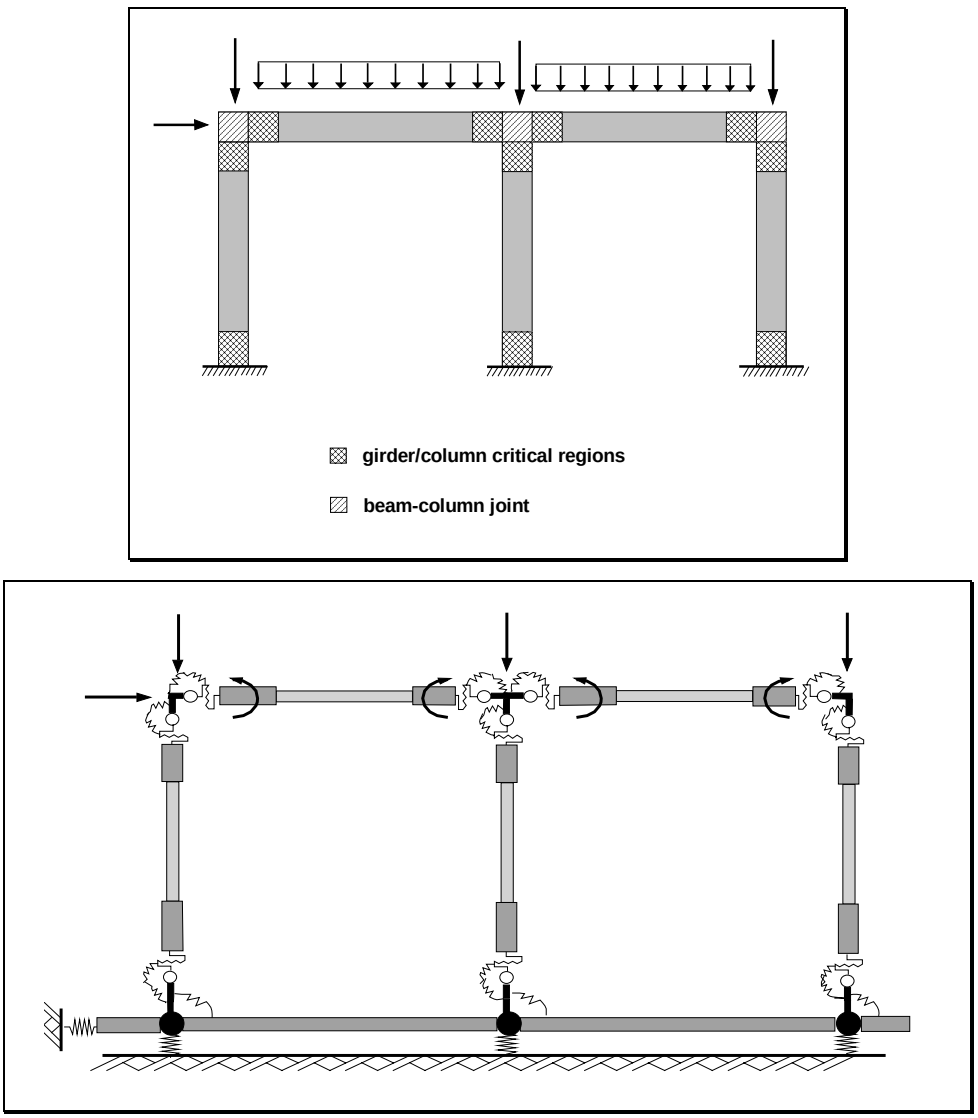

FIGURE 2.28 MODELING OF ONE STORY, TWO BAY FRAME

$$\mathbf{r}_{n+1} = \mathbf{r}_n + \Delta\mathbf{r} \tag{2.33}$$

where $\mathbf{r}_n$ is the vector of structural displacements at the beginning of the current load step and $\mathbf{r}_{n+1}$ the displacement vector at the end. The process is applied step-by-step by starting from a state of no loading and thus no corresponding displacements of the structure.

Depending on the magnitude of load increments it is more or less likely that the stiffness matrix $[\mathbf{K}]$ in Eq. 2.32 will change during the given load step. Thus, Eq. 2.32 has to be solved iteratively. The numerical and computational aspects associated with the solution of Eq. 2.32 will be presented in the next chapter.

CHAPTER 3

NONLINEAR ANALYSIS OF STATIC RESPONSE

3.1 Introduction

This chapter discusses the numerical implementation of the proposed frame elements within the framework of a special purpose program for the nonlinear static and dynamic analysis of planar RC moment-resisting frames. The proposed method of nonlinear analysis is generally applicable. Its implementation is, however, discussed in the context of the static and dynamic response of RC moment-resisting frames. In this chapter the nonlinear analysis algorithm and, in particular, the state determination phase of the solution procedure are discussed in detail. Details of the method specific to the dynamic response analysis are presented in Chapter 4.

The determination of the nonlinear static or dynamic response of the structure evolves around the solution of Eq. (2.32) which yields the displacement increments $\Delta\mathbf{r}$ corresponding to load increments $\Delta\mathbf{R}$. In the static response analysis load increments $\Delta\mathbf{R}$ are directly applied on the structure in a step-by-step manner starting from the unloaded state. In the dynamic response analysis load increments $\Delta\mathbf{R}$ include the effect of inertia and damping forces that are caused by the motion of the structure. In either static or dynamic load case the displacement increments $\Delta\mathbf{r}$ from the solution of Eq. (2.32) are added to the corresponding values at the end of the previous step and the process is repeated until the end of the imposed load or acceleration history. Since the stiffness matrix of the structure is likely to change within a given load step, Eq. (2.32) needs to be solved iteratively.

In order to find out whether the displacement increments $\Delta\mathbf{r}$ cause changes in the stiffness matrix of the structure during a particular load step the corresponding rotation increments $\Delta\boldsymbol{\Theta}$ at the ends of each element need to be determined. This is done by applying Eq. (2.17a) which transforms the global structural degrees of freedom to the local element displacements. The usual procedure at this stage of the nonlinear analysis is the state determination of each element of the structure: the internal moments corresponding to the local rotation increments $\Delta\boldsymbol{\Theta}$ are determined and the stiffness matrix of the element is updated, if necessary. If several elements are connected in series, as is the case in the present study, the state determination process is not straightforward. The basic problem lies in

determining the rotation increments $\boldsymbol{\Delta\Theta}$ that result at the ends of each element in series by only knowing that the sum of all subelement rotations $\boldsymbol{\Delta\theta}$ is equal to the superelement rotation $\boldsymbol{\Delta\Theta}$. As long as no change in stiffness in any one of the elements in series occurs within the load step, the local rotations of each element can be determined from the stiffness of the particular element by making use of the fact that the end moments of all subelements are equal to the end moments of the superelement. If a change of stiffness in any of the elements in series occurs within the load step, then the determination of local subelement rotations requires the development of a new nonlinear analysis procedure. Such a procedure was proposed by Filippou and Issa (1988) and is extended in the present study to encompass the additional girder and column subelements. This procedure is presented in the following in the context of an initial stress formulation of the well-known Newton-Raphson method of nonlinear analysis.

3.2 Brief review of nonlinear solution methods

Several solution schemes have been proposed for solving the nonlinear problem in Eq. (2.32). Some of these methods will be briefly mentioned here as they relate closely with the nonlinear analysis procedure that is proposed. An extensive review and evaluation of solution strategies for statically loaded nonlinear structures is presented in Bergan and Soreide (1973), Haisler and Stricklin (1974) and Simons and Powell (1982).

The basic solution procedure of Eq. (2.32) is the well known Newton-Raphson method. In the Newton-Raphson method, depicted in Fig. 3.1, Eq. (2.32) is solved by a recurrence relation

$$\left[\mathbf{K}_T\right]^k \cdot \boldsymbol{\Delta}\mathbf{r}_n^k = \boldsymbol{\Delta}\mathbf{R}_n^{k-1} = \left(\boldsymbol{\Delta}\mathbf{R}_E\right)_n - \left(\boldsymbol{\Delta}\mathbf{R}_I\right)^{k-1} \tag{3.1}$$

and

$$\mathbf{r}_{n+1}^k = \mathbf{r}_{n+1}^{k-1} + \boldsymbol{\Delta}\mathbf{r}_n^k \tag{3.2}$$

until a suitable norm of the vector on the right hand side of Eq. (3.1) becomes smaller than the specified tolerance. Subscript index *n* refers to the load step, while superscript index *k* refers to the iteration within a particular load step. $\boldsymbol{\Delta}\mathbf{R}_n^{k-1}$ is the difference between $\left(\boldsymbol{\Delta}\mathbf{R}_E\right)_n$, the externally applied load increments at step *n*, and $\left(\boldsymbol{\Delta}\mathbf{R}_I\right)^{k-1}$, the internal resisting load increments.

The basic Newton-Raphson method is not necessarily the most economical solution scheme and does not always provide rapid or reliable convergence. To improve upon some of

the limitations of the basic Newton-Raphson method several modifications have been proposed over the years. Some of these methods involve modifications of the stiffness matrix in Eq. (3.1) and are then classified as Modified Newton or Quasi-Newton methods.

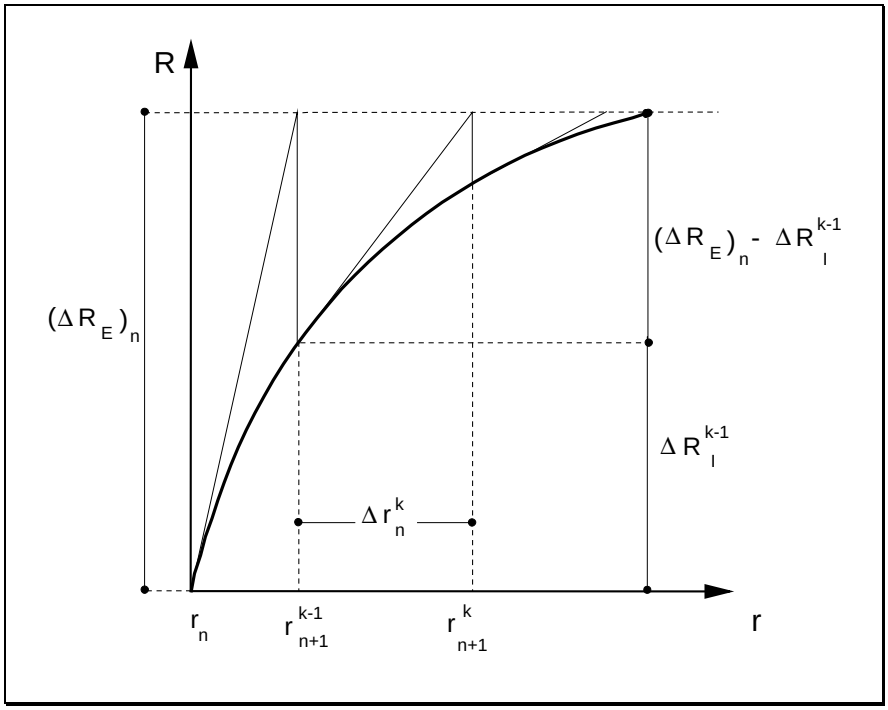

FIGURE 3.1 NEWTON-RAPHSON METHOD OF NONLINEAR ANALYSIS

If large unbalances between external applied loads and internal resisting forces develop, the iteration process might fail to converge. Among the solution schemes that have been proposed to deal with these cases is the event-to-event method (Simons and Powell 1982). In this method the solution advances from one stiffness change or event to the next. The purpose of this strategy is to follow the equilibrium path as closely as possible by updating the stiffness matrix and the state of each element each time a change of stiffness in one of the elements of the structure takes place. This is achieved by predicting the occurrence of the next change of stiffness (event) within a load step and then scaling the load increments by a factor such that the solution just reaches the predicted event.

In the present study the basic Newton-Raphson method is used in solving the nonlinear problem in Eq. (2.32). The method is recast in a different form which is more suitable for the solution of nonlinear structures made up of several elements that are connected in series. Concepts from the event-to-event method are used in addressing the problem of state determination in the case of the gradual spread of the plastic zone that takes place in the

spread plasticity subelement. The proposed algorithm has proved to be efficient and reliable in solving the nonlinear static and dynamic response analysis problems in this study.

3.3 Proposed nonlinear analysis algorithm

Once the stiffness matrix of the entire structure is formed, the problem of determining the response to static or dynamic load increments $\Delta\mathbf{R}$ takes the form of Eq. (2.32)

$$[\mathbf{K}]\cdot\Delta\mathbf{r}=\Delta\mathbf{R}$$

where $[\mathbf{K}]$ is the stiffness matrix. For dynamic loading $[\mathbf{K}]$ is the effective stiffness matrix and $\Delta\mathbf{R}$ is the effective load vector which are defined in Section 4.3 of the following chapter. The solution of Eq. (2.32) using the basic Newton-Raphson method takes the form of Eqs. (3.1) and (3.2).

It is possible to rewrite the basic Newton-Raphson solution scheme such that the displacement increments are always measured from the converged solution in the previous load step *n*. This results in an initial stress version of the Newton-Raphson method, which is better suitable to illustrate the proposed nonlinear state determination process for several elements that are connected in series. To perform the transformation we start from Eq. (3.2). Expressing $\Delta\mathbf{r}_n^k$ in terms of the solution estimates at iteration *k* and *k-1* we get

$$\Delta\mathbf{r}_n^k=\mathbf{r}_{n+1}^k-\mathbf{r}_{n+1}^{k-1} \tag{3.3}$$

Substituting Eq. (3.3) into Eq. (3.1) and solving for $\mathbf{r}_{n+1}^k$ we obtain

$$\begin{aligned}[\mathbf{K}_T]^k\cdot\left(\mathbf{r}_{n+1}^k-\mathbf{r}_{n+1}^{k-1}\right)&=\left(\Delta\mathbf{R}_E\right)_n-\left(\Delta\mathbf{R}_I\right)^{k-1}\\ [\mathbf{K}_T]^k\cdot\mathbf{r}_{n+1}^k&=\left(\Delta\mathbf{R}_E\right)_n-\left[\left(\Delta\mathbf{R}_I\right)^{k-1}-[\mathbf{K}_T]^k\cdot\mathbf{r}_{n+1}^{k-1}\right]\end{aligned} \tag{3.4}$$

By subtracting the term $[\mathbf{K}_T]^k\cdot\mathbf{r}_n$ from both sides of Eq. (3.4) we can solve for the displacement increments relative to the converged solution of the previous load step *n*.

$$\begin{aligned}[\mathbf{K}_T]^k\cdot\left(\mathbf{r}_{n+1}^k-\mathbf{r}_n\right)&=\left(\Delta\mathbf{R}_E\right)_n-\left[\left(\Delta\mathbf{R}_I\right)^{k-1}-[\mathbf{K}_T]^k\cdot\left(\mathbf{r}_{n+1}^{k-1}-\mathbf{r}_n\right)\right]\\ [\mathbf{K}_T]^k\cdot\Delta\bar{\mathbf{r}}_n^k&=\left(\Delta\mathbf{R}_E\right)_n-\left[\left(\Delta\mathbf{R}_I\right)^{k-1}-[\mathbf{K}_T]^k\cdot\Delta\bar{\mathbf{r}}_n^{k-1}\right]\\ &=\left(\Delta\mathbf{R}_E\right)_n-\left(\Delta\mathbf{R}_0\right)^{k-1}\end{aligned} \tag{3.5}$$

$\left(\Delta\mathbf{R}_0\right)^{k-1}$ is the initial load vector used in iteration *k* and $\Delta\bar{\mathbf{r}}_n$ is the increment of the displacement vector with respect to the displacements $\mathbf{r}_n$ at the end of the previous load step.

The graphical representation of the initial stress formulation of the Newton-Raphson method is shown in Fig. 3.2.

At the beginning of a new load step $\left(\Delta\mathbf{R}_0\right)^{k-1}$ is equal to zero and the current displacement vector $\mathbf{r}_n$ and the current tangent stiffness matrix of the structure $\left[\mathbf{K}_T\right]$ are known. Given an external load increment $\left(\Delta\mathbf{R}_E\right)_n$ the solution process starts by solving Eq. (3.5) for the first iteration estimate of the displacement increments $\Delta\bar{\mathbf{r}}_n$.

From $\Delta\bar{\mathbf{r}}_n$ the global displacement increments $\Delta\mathbf{r}_m$ at the ends of each element of the structure can be extracted. The transformation of the global deformation increments $\Delta\mathbf{r}_m$ according to Eq. (2.17a), which is rewritten below for the general case in incremental form, yields the local rotation increments $\Delta\Theta$ at the ends of the girder and column superelement

$$\Delta\Theta = \begin{Bmatrix} \Delta\Theta_1 \\ \Delta\Theta_2 \end{Bmatrix} = \left[\mathbf{a}\right]\cdot\Delta\mathbf{r}_m = \left[\mathbf{a}\right]\cdot\begin{Bmatrix} \Delta\Theta_i \\ \Delta\Theta_j \\ \Delta u_i \\ \Delta u_j \end{Bmatrix} \tag{3.6}$$

where $\left[\mathbf{a}\right]=\left[\mathbf{a}\right]_b$ for girders and $\left[\mathbf{a}\right]=\left[\mathbf{a}\right]_{crd}$ for columns.

The corresponding moment increments at the end of the superelement are

$$\Delta\mathbf{M}_E = \left[\mathbf{K}\right]\cdot\Delta\boldsymbol{\theta} \tag{3.7}$$

where $\left[\mathbf{K}\right]=\left[\mathbf{K}\right]_g$ for girders and $\left[\mathbf{K}\right]=\left[\mathbf{K}\right]_{crd}$ for columns. $\left[\mathbf{K}\right]_g$ and $\left[\mathbf{K}\right]_{crd}$ are the stiffness matrices of the girder and column superelement, respectively. These are defined with respect to local degrees of freedom by inverting the flexibility matrices in Eqs. (2.15) and (2.28) for the girder and column superelement, respectively.

The moment increments at the end of the superelement $\Delta\mathbf{M}_E$ lead directly to the moment increments $\Delta\mathbf{m}_E$ at the ends of each subelement. Since all subelements are in series

$$\Delta\mathbf{M}_E = \left(\Delta\mathbf{m}_E\right)_{el} = \left(\Delta\mathbf{m}_E\right)_{pl} = \left(\Delta\mathbf{m}_E\right)_{jnt} = \left(\Delta\mathbf{m}_E\right)_{shr} \tag{3.8}$$

From the moment increments $\Delta\mathbf{m}_E$ and the current flexibility matrix of each subelement the rotation increments at the ends of each subelement can be determined

$$\Delta\boldsymbol{\theta}_{el} = \left[\mathbf{f}\right]_{el}\cdot\left(\Delta\mathbf{m}_E\right)_{el} \tag{3.9a}$$

$$\Delta\boldsymbol{\theta}_{pl} = \left[\mathbf{f}\right]_{pl}\cdot\left(\Delta\mathbf{m}_E\right)_{pl} \tag{3.9b}$$

$$\Delta\boldsymbol{\theta}_{jnt} = \left[\mathbf{f}\right]_{jnt}\cdot\left(\Delta\mathbf{m}_E\right)_{jnt} \tag{3.9c}$$

$$\Delta\boldsymbol{\theta}_{shr} = \left[\mathbf{f}\right]_{shr} \cdot \left(\Delta\mathbf{m}_{E}\right)_{shr} \tag{3.9d}$$

For the joint, shear and concentrated plasticity subelements the process of state determination is rather straightforward: the local rotation increments at ends *i* and *j*, $\Delta\boldsymbol{\theta}_{pl}$, $\Delta\boldsymbol{\theta}_{jnt}$ and $\Delta\boldsymbol{\theta}_{shr}$, are added to the rotations at the end of the previous load step *n*, $\left(\boldsymbol{\theta}_{n}\right)_{pl}$, $\left(\boldsymbol{\theta}_{n}\right)_{jnt}$ and $\left(\boldsymbol{\theta}_{n}\right)_{shr}$, respectively, to obtain the current total rotations.

$$\left(\boldsymbol{\theta}_{n+1}\right)_{pl} = \left(\boldsymbol{\theta}_{n}\right)_{pl} + \Delta\boldsymbol{\theta}_{pl} \tag{3.10a}$$

$$\left(\boldsymbol{\theta}_{n+1}\right)_{jnt} = \left(\boldsymbol{\theta}_{n}\right)_{jnt} + \Delta\boldsymbol{\theta}_{jnt} \tag{3.10b}$$

$$\left(\boldsymbol{\theta}_{n+1}\right)_{shr} = \left(\boldsymbol{\theta}_{n}\right)_{shr} + \Delta\boldsymbol{\theta}_{shr} \tag{3.10c}$$

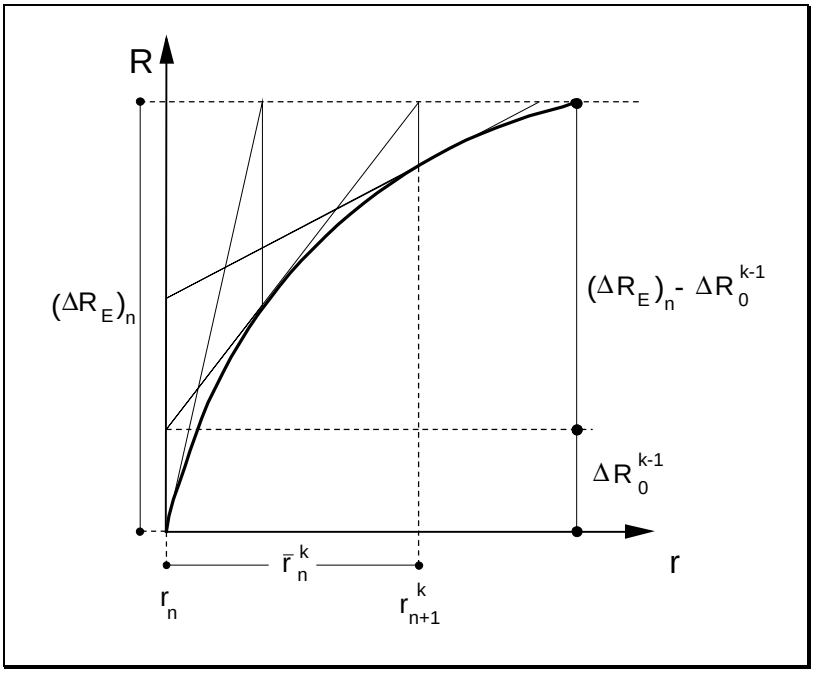

FIGURE 3.2 INITIAL STRESS FORMULATION OF BASIC NEWTON-RAPHSON METHOD

Since the flexibility and stiffness matrices of these subelements are diagonal, the rotational degrees of freedom at the ends of the subelement are uncoupled. Thus, the internal resisting moments

$$\left(\mathbf{m}_{R}\right)_{pl} = \begin{Bmatrix} m_{R,i} \\ m_{R,j} \end{Bmatrix}_{pl}$$

$$\left(\mathbf{m}_{R}\right)_{jnt} = \begin{Bmatrix} m_{R,i} \\ m_{R,j} \end{Bmatrix}_{jnt}$$

$$\left(\mathbf{m}_R\right)_{shr} = \begin{Bmatrix} m_{R,i} \\ m_{R,j} \end{Bmatrix}_{shr}$$

which correspond to total rotations

$$\left(\boldsymbol{\theta}_{n+1}\right)_{pl} = \begin{Bmatrix} \boldsymbol{\theta}_{n+1,i} \\ \boldsymbol{\theta}_{n+1,j} \end{Bmatrix}_{pl}$$

$$\left(\boldsymbol{\theta}_{n+1}\right)_{jnt} = \begin{Bmatrix} \boldsymbol{\theta}_{n+1,i} \\ \boldsymbol{\theta}_{n+1,j} \end{Bmatrix}_{jnt}$$

$$\left(\boldsymbol{\theta}_{n+1}\right)_{shr} = \begin{Bmatrix} \boldsymbol{\theta}_{n+1,i} \\ \boldsymbol{\theta}_{n+1,j} \end{Bmatrix}_{shr}$$

can be independently determined from the corresponding hysteretic moment-rotation relation and the load history at each end of the joint, shear or concentrated plasticity subelement. The incremental vector of internal resisting moments $\left(\Delta\mathbf{m}_R\right)$ can then be determined by subtracting from the current resisting moments those at the end of the previous load step

$$\left(\Delta\mathbf{m}_R\right)_{pl} = \left[\left(\mathbf{m}_R\right)_{n+1} - \left(\mathbf{m}_R\right)_n\right]_{pl}$$

$$\left(\Delta\mathbf{m}_R\right)_{jnt} = \left[\left(\mathbf{m}_R\right)_{n+1} - \left(\mathbf{m}_R\right)_n\right]_{jnt}$$

$$\left(\Delta\mathbf{m}_R\right)_{shr} = \left[\left(\mathbf{m}_R\right)_{n+1} - \left(\mathbf{m}_R\right)_n\right]_{shr}$$

If the difference between the increments of externally applied moments $\left(\Delta\mathbf{m}_E\right)$ and internal resisting moments $\left(\Delta\mathbf{m}_R\right)$ is larger than a specified tolerance at one or both ends, then the flexibility matrix of the corresponding subelement needs to be updated. Because of the change in stiffness, Eqs. (3.9) are no longer valid. Instead these relations have to be modified with the introduction of an initial moment vector $\left(\Delta\mathbf{m}_0\right)$ as follows

$$\Delta\boldsymbol{\theta}_{pl} = \left[\mathbf{f}_u\right]_{pl} \cdot \left(\Delta\mathbf{m}_R - \Delta\mathbf{m}_0\right)_{pl} \tag{3.11a}$$

$$\Delta\boldsymbol{\theta}_{jnt} = \left[\mathbf{f}_u\right]_{jnt} \cdot \left(\Delta\mathbf{m}_R - \Delta\mathbf{m}_0\right)_{jnt} \tag{3.11b}$$

$$\Delta\boldsymbol{\theta}_{shr} = \left[\mathbf{f}_u\right]_{shr} \cdot \left(\Delta\mathbf{m}_R - \Delta\mathbf{m}_0\right)_{shr} \tag{3.11c}$$

where $\left[\mathbf{f}_u\right]$ is the updated flexibility matrix of the corresponding subelement.

Since the flexibility matrices of the joint, shear and concentrated plasticity subelements are diagonal, the whole process of state determination, which consists of Eqs. (3.9)-(3.11) can be

represented graphically for one end of the particular subelement, as shown in Fig. 3.3 for end *i*.

The solution of Eqs. (3.11) for the initial moment vectors $(\Delta\mathbf{m}_0)$ yields

$$(\Delta\mathbf{m}_0)_{pl} = (\Delta\mathbf{m}_R)_{pl} - [\mathbf{k}_u]_{pl} \cdot \Delta\boldsymbol{\theta}_{pl} \tag{3.12a}$$

$$(\Delta\mathbf{m}_0)_{jnt} = (\Delta\mathbf{m}_R)_{jnt} - [\mathbf{k}_u]_{jnt} \cdot \Delta\boldsymbol{\theta}_{jnt} \tag{3.12b}$$

$$(\Delta\mathbf{m}_0)_{shr} = (\Delta\mathbf{m}_R)_{shr} - [\mathbf{k}_u]_{shr} \cdot \Delta\boldsymbol{\theta}_{shr} \tag{3.12c}$$

For the spread plasticity subelement a change of stiffness during a particular load step can be caused by either a change of stiffness in one or both plastic zones or a change in

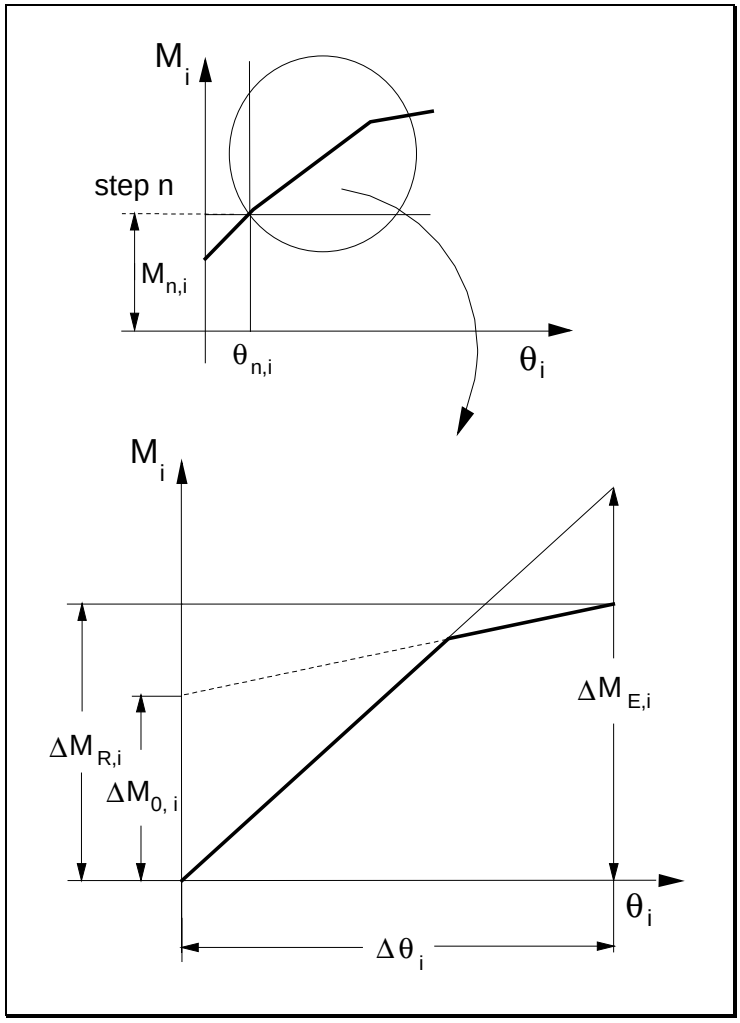

FIGURE 3.3 STATE DETERMINATION AND INITIAL MOMENT CALCULATION FOR JOINT, SHEAR AND CONCENTRATED PLASTICITY SUBELEMENTS

plastic zone length at one or both ends. It is important to note that the flexibility matrix of the spread plasticity subelement is not diagonal and that the rotational degrees of freedom are coupled in this case.

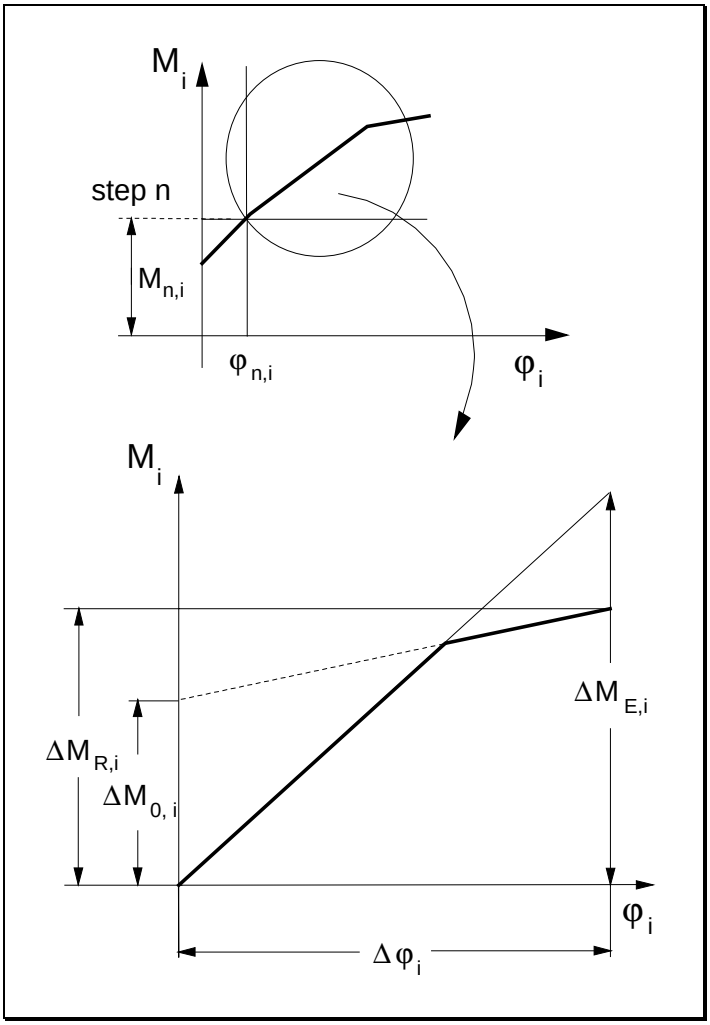

FIGURE 3.4 STATE DETERMINATION AND INITIAL MOMENT CALCULATION FOR SPREAD PLASTICITY SUBELEMENT (STIFFNESS CHANGE)

If only the effective section stiffness changes, the determination of initial moments remains practically the same as presented in Eqs. (3.11) and (3.12). The only difference is that the determination of internal resisting moments now depends on the curvatures at the end sections of the beam subelement instead of the end rotations. Using the concept of average plastic zone stiffness introduced in Chapter 2, the process of state determination is considerably simplified, since the curvature increment $\Delta\varphi$ at each end can be determined

from the external moment increment Δm_E at the same end and does not depend on the curvature increment at the opposite end of the element. Thus

$$\Delta\varphi_i = \frac{\left(\Delta m_{E,i}\right)_{pl}}{c_i \cdot EI} \tag{3.13a}$$

$$\Delta\varphi_j = \frac{\left(\Delta m_{E,j}\right)_{pl}}{c_j \cdot EI} \tag{3.13b}$$

where the indices refer to ends *i* and *j* of the spread plastic subelement.

The curvature increments from Eqs. (3.13) are added to the curvatures at the end of the previous load step to obtain the current curvatures. These are then used to calculate the internal moments $\left(m_R\right)_{n+1}$ of the spread plastic subelement from the moment-curvature relation at each corresponding end (Fig. 3.4). The incremental vector of internal resisting moments $\left(\boldsymbol{\Delta}\mathbf{m}_R\right)$ can now be determined by subtracting from the current resisting moments those at the end of the previous load step

$$\left(\boldsymbol{\Delta}\mathbf{m}_R\right)_{pl} = \left[\left(\mathbf{m}_R\right)_{n+1} - \left(\mathbf{m}_R\right)_n\right]_{pl}$$

exactly as was done in the case of the concentrated plasticity subelement.

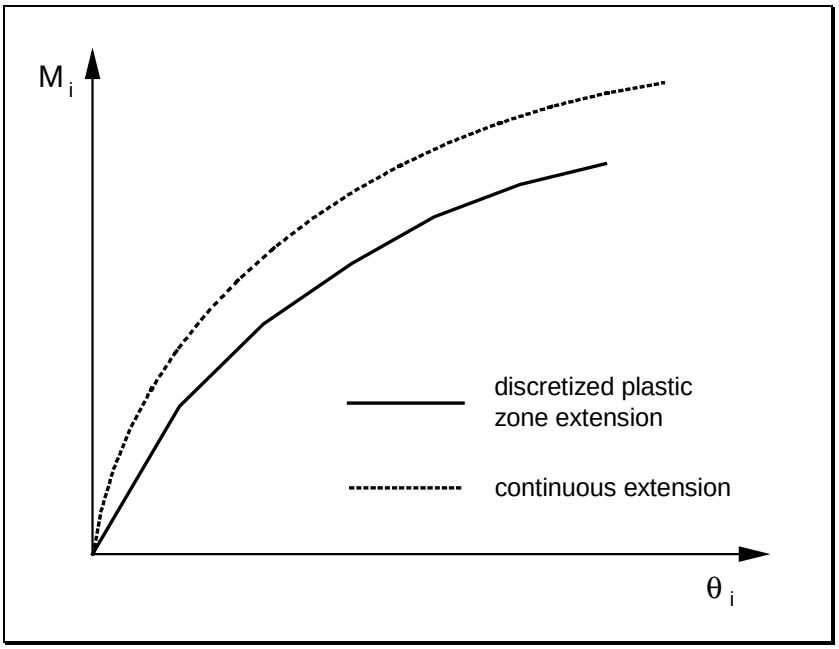

FIGURE 3.5 MOMENT-ROTATION RELATION AT ONE END OF THE SPREAD PLASTIC SUBELEMENT

By comparing the internal moment increments at the two ends of the element $\left(\Delta \mathbf{m}_R\right)_{pl}$ to the external moment increments $\left(\Delta \mathbf{m}_E\right)_{pl}$, it is determined whether a change of stiffness took place during the load step. If such a change is detected, the flexibility matrix of the spread plastic subelement is updated. Since Eq. (3.9b) no longer holds true, initial moments at the ends of the element have to be introduced yielding a relation identical to Eq. (3.11a), which is then solved for the initial moments resulting in Eq. (3.12a).

If the external moment increments in Eqs. (3.7) and (3.8) result in a change in the plastic zone length at one or both ends of the beam subelement, then the process of determining the initial moments becomes considerably more involved.

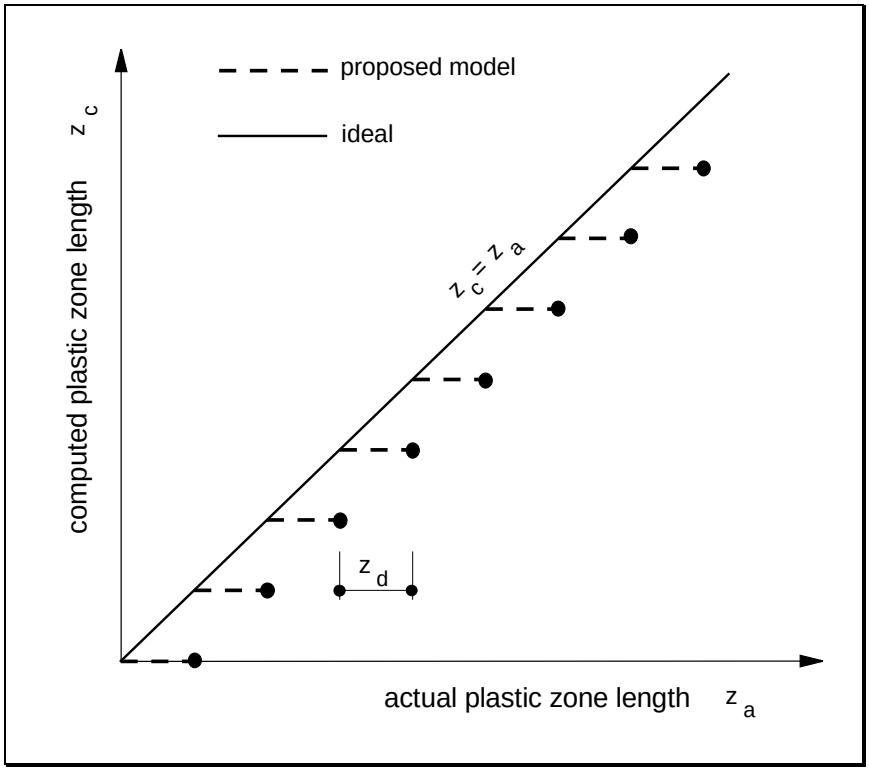

FIGURE 3.6 DISCRETIZATION OF PLASTIC ZONE EXTENSION

To illustrate the complexity of the problem the moment-rotation relation at one end of the spread plastic beam subelement is shown in Fig. 3.5. Since the plastic zone length is a continuous variable the moment-rotation relation is nonlinear, as shown by the broken line in Fig. 3.5. It should also be kept in mind that the moment-rotation relation at one end of the element also depends on the moment acting at the other end, because of the non-zero coupling terms in the element flexibility matrix. This leads to a moment-rotation relation

which is not unique, requiring that both end moments be considered simultaneously. In order to reduce the computational effort the process of plastic zone extension is simplified by assuming that the change in length takes place in discrete increments z_d. The actual plastic zone length z_a thus follows the step function shown dashed in Fig. 3.6. This results in the moment-rotation relation being multi-linear instead of continuous as shown by the solid line in Fig. 3.5. The discrepancy between the actual and the idealized moment-rotation relation in Fig. 3.5 can be reduced by decreasing the size of z_d.

The basic problem in the state determination of the spread plastic subelement now lies in the fact that it is not possible to directly relate rotations with curvatures and, consequently, moments at each end of the element, as is the case in the joint and concentrated plasticity elements. This is illustrated in Fig. 3.7, where $\left(\Delta\theta_i\right)_{pl}$ denotes the increment of end rotation at end *i* of the element caused by external moment increments $\left(\boldsymbol{\Delta}\mathbf{m}_E\right)$.

The internal resisting moment which corresponds to rotation increment $\left(\Delta\theta_i\right)_{pl}$ and is represented by a question mark in Fig. 3.7 cannot be determined for the simple reason that the exact moment-rotation relation (solid line in Fig. 3.7) is not known. This relation depends on the changes in the plastic zone length which cannot be determined without due account of the coupling that exists between the end moments of the element. Another way of looking at the problem is to recall that the resisting moments of the spread plastic subelement are related to the curvatures at the end sections. Since there is no closed form relation between the curvatures at the end sections and the end rotations, the direct determination of the internal resisting moments from the rotation increments $\left(\boldsymbol{\Delta\theta}\right)_{pl}$ is not possible. To solve this problem concepts first introduced in the event-to-event method by Simons and Powell (1982) are used. At the beginning of the load step the plastic zone length z_a at ends *i* and *j* is known

$$z_a = \begin{Bmatrix} z_{a,i} \\ z_{a,j} \end{Bmatrix}$$

Given the external moment increments $\left(\boldsymbol{\Delta}\mathbf{m}_E\right)_{pl}$ the resulting shear increment ΔV can be determined

$$\Delta V = \frac{\left(\Delta m_{E,i} + \Delta m_{E,j}\right)_{pl}}{L} \tag{3.14}$$

Thus the new theoretical plastic zone lengths z_c can be determined from

$$z_{c,i} = \frac{\left(m_{n,i} + \Delta m_{E,i}\right)_{pl} - M_{y,i}}{V_n + \Delta V} \tag{3.15a}$$

$$z_{c,j} = \frac{\left(m_{n,j} + \Delta m_{E,j}\right)_{pl} - M_{y,j}}{V_n + \Delta V} \tag{3.15b}$$

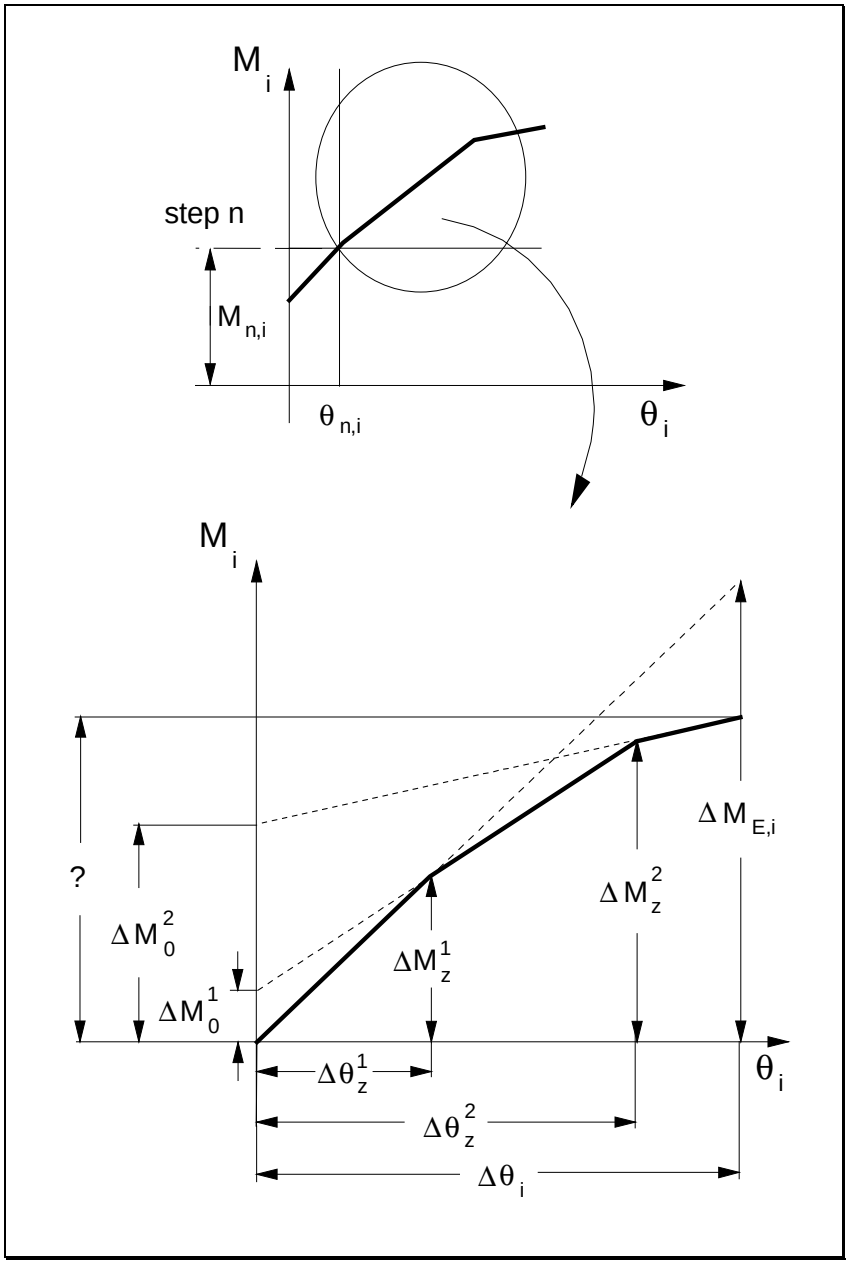

FIGURE 3.7 DETERMINATION OF INITIAL MOMENTS AT END I OF THE SPREAD PLASTICITY ELEMENT FOR CHANGE IN PLASTIC ZONE LENGTH

where M_y is the yield moment (positive or negative) of the end section, $\mathbf{m}_n$ is the vector of end moments of the spread plastic subelement at the end of the previous load step and V_n is given by

$$V_n = \frac{\left(m_{n,i} + m_{n,j}\right)_{pl}}{L} \tag{3.16}$$

The theoretical plastic zone lengths z_c are compared against those at the end of the previous step z_a. If both plastic zone lengths in vector z_c are smaller than those in vector z_a, then no change in plastic zone length has taken place. If an increase in plastic zone length at one or both ends of the beam subelement is detected during the comparison of z_c with z_a, then the corresponding plastic zone length is updated to a new value z_a^N by adding a finite length increment z_d to the plastic zone value z_a at the end of the previous load step (Figs. 3.6 and 3.8)

$$z_{a,i}^N = z_{a,i} + z_d \qquad \text{if} \qquad z_{c,i} > z_{a,i} \tag{3.17a}$$

$$z_{a,j}^N = z_{a,j} + z_d \qquad \text{if} \qquad z_{c,j} > z_{a,j} \tag{3.17b}$$

If the plastic zones at both ends of the spread plasticity subelement extend during a load step, we need to establish which is going to do so first. This is the concept behind the event-to-event method. To do so we make use of the fact that the stiffness of the spread plastic subelement does not change until one of the plastic zones extends. Thus the point of inflection of the moment diagram does not change between the beginning of the load step and the instant when one of the plastic zones first extends. Using this fact we can establish which zone is going to spread first by calculating the moment distribution at the stage when this event takes place (Fig. 3.8). If we assume that the plastic zone length at end *i* will spread first, then the shear force corresponding to a discrete increment of the plastic zone by z_d is

$$V_i^* = \frac{M_{y,i}}{L_i - z_{a,i}^N} \tag{3.18a}$$

where L_i is the distance of the point of inflection from end *i* (Fig. 3.8). This is calculated using the current end moment values (Fig. 3.8)

$$L_i = \frac{m_{n,i} + \Delta m_{E,i}}{m_{n,i} + \Delta m_{E,i} + m_{n,j} + \Delta m_{E,j}} \cdot L \tag{3.18b}$$

If, on the other hand, the plastic zone length at end *j* spreads out first by the discrete increment z_d, then the corresponding shear force is

$$V_j^* = \frac{M_{y,j}}{L_j - z_{a,j}^N} \tag{3.18c}$$

where L_j is the distance of the point of inflection from end *j* given by

$$L_j = \frac{m_{n,j} + \Delta m_{E,j}}{m_{n,i} + \Delta m_{E,i} + m_{n,j} + \Delta m_{E,j}} \cdot L \tag{3.18d}$$

If the plastic zones at both ends of the spread plasticity subelement extend during a load step, then a comparison of the shear force values from Eqs. (3.18a) and (3.18c) establishes which event will take place first. The event to take place first is obviously associated with the smaller shear force value from Eqs. (3.18a) and (3.18c). This value is denoted by V_z.

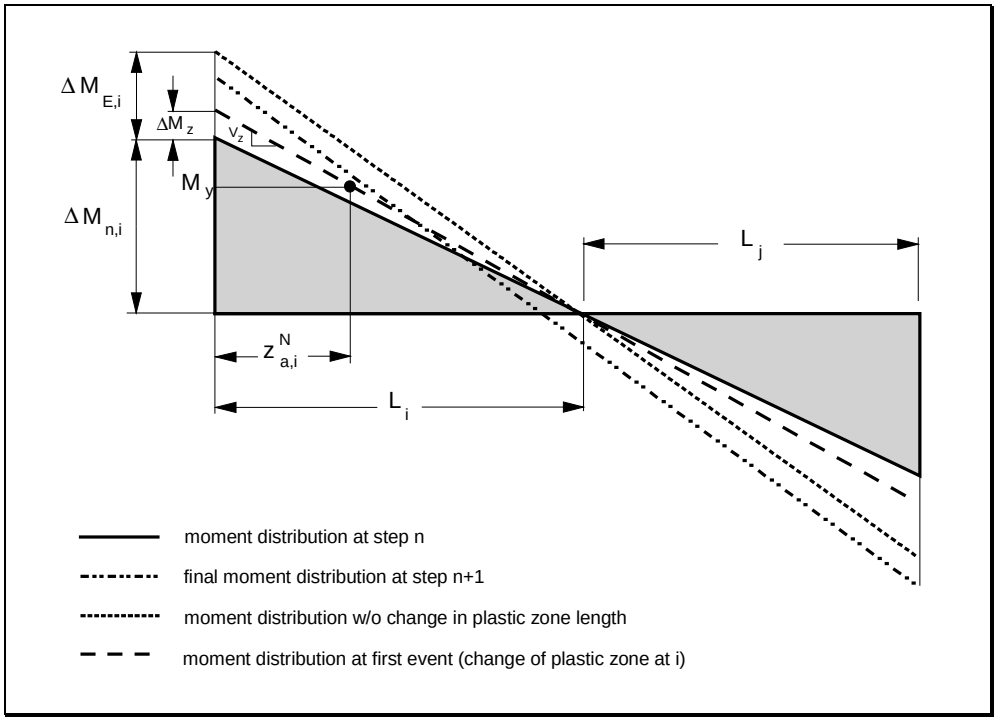

FIGURE 3.8 MOMENT DISTRIBUTION IN SPREAD PLASTICITY ELEMENT DURING A GIVEN LOAD STEP

Making use of the fact that the inflection point does not change until the first event takes place, also permits the determination of the moment and corresponding rotation increments at the ends of the element when the event occurs (Figs. 3.7 and 3.8)

$$\Delta \mathbf{m}_z = \begin{Bmatrix} V_z \cdot L_i \\ V_z \cdot L_j \end{Bmatrix} - \begin{Bmatrix} m_{n,i} \\ m_{n,j} \end{Bmatrix} \tag{3.19}$$

$$\Delta\boldsymbol{\theta}_z = \left[\mathbf{f}\right]_{pl} \cdot \Delta\mathbf{m}_z \tag{3.20}$$

At this point the flexibility matrix of the spread plastic subelement is updated to account for the new plastic zone length. Since the flexibility matrix changes, Eq. (3.20) no longer holds true. Instead, it has to be modified by introducing initial moments $\left(\Delta\mathbf{m}_0\right)_{pl}$ at the ends of the spread plasticity subelement as follows (Fig. 3.7)

$$\Delta\boldsymbol{\theta}_z = \left[\mathbf{f}_u\right]_{pl} \cdot \left(\Delta\mathbf{m}_z - \Delta\mathbf{m}_0\right)_{pl} \tag{(3.21a)}$$

Eq. (3.21a) can be solved for the initial moments resulting in

$$\left(\Delta\mathbf{m}_0\right)_{pl} = \Delta\mathbf{m}_z - \left[\mathbf{k}_u\right]_{pl} \cdot \Delta\boldsymbol{\theta}_z \tag{3.21b}$$

The outlined event-to-event procedure culminating in Eq. (3.21b) thus allows the determination of the initial moments at the ends of the spread plastic subelement, if a change in the length of plastic zone takes place at one or both ends of the beam subelement during the load step. The process was presented for one event only. Since the change of the plastic zone length at one end results in a change in the element flexibility matrix and an unbalance between external and internal end moments, a new iteration needs to be performed until no events are detected during an iteration. This entire process is presented in a summary form at the end of this chapter.

It is important to stress the difference between Eqs. (3.12a) and (3.21b). In the first case no change in plastic zone length takes place. Only the average section stiffness at one or both plastic zones of the element changes. In this case the internal resisting moments $\left(\Delta\mathbf{m}_R\right)_{pl}$ arising from rotation increments $\Delta\boldsymbol{\theta}_{pl}$ are determined by Eq. (3.9b) and are then used in calculating the initial moments. In the second case the internal resisting moments $\left(\Delta\mathbf{m}_z\right)$ *at the instant that the plastic zone at one end of the element extends* are determined. These along with the corresponding end rotations are then used to determine the initial moments at the ends of the spread plasticity subelement.

Once the initial moments at the ends of all subelements in series are determined the initial moments at the ends of the girder or column superelement are established from the following relation

$$\Delta\mathbf{M}_0 = \left[\mathbf{K}\right] \cdot \left\{\left[\mathbf{f}_u\right]_{pl} \cdot \left(\Delta\mathbf{m}_0\right)_{pl} + \left[\mathbf{f}_u\right]_{jnt} \cdot \left(\Delta\mathbf{m}_0\right)_{jnt} + \left[\mathbf{f}_u\right]_{shr} \cdot \left(\Delta\mathbf{m}_0\right)_{shr}\right\} \tag{3.22}$$

where $\left[\mathbf{K}\right] = \left[\mathbf{K}\right]_g$ for girders and $\left[\mathbf{K}\right] = \left[\mathbf{K}\right]_{crd}$ for columns. $\left[\mathbf{K}\right]_g$ and $\left[\mathbf{K}\right]_{crd}$ are the stiffness matrices of the girder and column superelement, respectively. Eq. (3.22) is derived in Appendix A of the report by Filippou and Issa (1988).

The initial moments at the ends of the superelement are finally transformed to the global coordinate system using transformation matrix [**a**].

$$\Delta\mathbf{R}_0 = \left[\mathbf{a}\right]^T \cdot \Delta\mathbf{M}_0 \tag{3.23}$$

where $\left[\mathbf{a}\right] = \left[\mathbf{a}\right]_b$ in the case of girders and $\left[\mathbf{a}\right] = \left[\mathbf{a}\right]_{crd}$ in the case of columns.

Eq. (3.23) gives the vector of initial load increments at the end of the first iteration (Fig. 3.2). These are then subtracted from the vector of external load increments $\left(\Delta\mathbf{R}_E\right)_n$ according to Eq. (3.5) and the process is restarted by applying anew Eqs. (3.6)-(3.23) until the difference between internal resisting and external applied moments at the ends of all subelements is smaller than a specified tolerance. It should be noted that Eqs. (3.9) and (3.13) have to be modified in the second iteration to include the initial end moments from the previous iteration (Fig. 3.7).

A complete description of the iterative process during a particular load step is given in the following algorithm summary where indices are used to denote the iteration process.

3.4 Summary of nonlinear analysis algorithm

For each load step

Step (1) Form the tangent flexibility matrix of all subelements which make up the girder superelement $\left[\mathbf{f}\right]_{el}$, $\left[\mathbf{f}\right]_{pl}$, $\left[\mathbf{f}\right]_{jnt}$, $\left[\mathbf{f}\right]_{shr}$.

Form the tangent flexibility matrix of all subelements which make up the column superelement $\left[\mathbf{f}\right]_{el}$, $\left[\mathbf{f}\right]_{pl}$, $\left[\mathbf{f}\right]_{jnt}$, $\left[\mathbf{f}\right]_{shr}$.

Form the axial stiffness of the column $\left[\mathbf{K}\right]_a$

Form the stiffness of the foundation elements $\left[\mathbf{K}\right]_f$

Step (2) For all girder and column superelements in the structure add the flexibility matrices of the subelements to obtain the flexibility matrix of the superelement in local coordinates:

$$\left[\mathbf{F}\right]_g = \left[\mathbf{f}\right]_{el} + \left[\mathbf{f}\right]_{pl} + \left[\mathbf{f}\right]_{jnt} + \left[\mathbf{f}\right]_{shr}$$

$$\left[\mathbf{F}\right]_{crd} = \left\{ \left[\mathbf{f}\right]_{el} + \left[\mathbf{f}\right]_{pl} + \left[\mathbf{f}\right]_{jnt} + \left[\mathbf{f}\right]_{shr} \right\}_{crd}$$

Step (3) Invert the tangent flexibility matrix of each superelement to obtain the tangent stiffness matrix:

$$[\mathbf{K}]_g = [\mathbf{F}]_g^{-1}$$

$$[\mathbf{K}]_{crd} = [\mathbf{F}]_{crd}^{-1}$$

Step (4) Transform the stiffness matrix of all structural elements to global coordinates:

for girder superelements: $[\mathbf{K}]_b = [\mathbf{a}]_b^T \cdot [\mathbf{K}]_g \cdot [\mathbf{a}]_b$

for column superelements: $[\mathbf{K}]_c = [\mathbf{a}]_{crd}^T \cdot [\mathbf{K}]_{crd} \cdot [\mathbf{a}]_{crd} + [\mathbf{a}]_a^T \cdot [\mathbf{K}]_a \cdot [\mathbf{a}]_a$

Step (5) Assemble the stiffness matrix of all elements into the tangent stiffness matrix of the whole structure (direct stiffness method) including the linear geometric matrix of column elements:

$$[\mathbf{K}_T] = \sum_{elem} [\mathbf{K}]_b + [\mathbf{K}]_c + [\mathbf{K}]_G + [\mathbf{K}]_f$$

Step (6) Given the vector of applied load increments $(\Delta\mathbf{R}_E)_n$ solve for the displacement increments $\Delta\bar{\mathbf{r}}_n$ relative to the converged solution at the previous load step *n*:

$$[\mathbf{K}_T]^k \cdot \Delta\bar{\mathbf{r}}_n^k = (\Delta\mathbf{R}_E)_n - (\Delta\mathbf{R}_0)^{k-1}$$

where *k* is the iteration index, $\Delta\bar{\mathbf{r}}_n^k = \mathbf{r}_{n+1}^k - \mathbf{r}_n$ and $(\Delta\mathbf{R}_0)^{k-1} = 0$ when *k*=1(first iteration).

For each girder and column superelement perform steps **(7)** through **(16)**

Step (7) From the global deformation increments $\Delta\mathbf{r}_m^k$ of each element calculate the local rotation increments $\Delta\boldsymbol{\theta}$:

$$\Delta\boldsymbol{\theta}^k = [\mathbf{a}] \cdot \Delta\mathbf{r}_m^k$$

where $[\mathbf{a}] = [\mathbf{a}]_b$ for girders and $[\mathbf{a}] = [\mathbf{a}]_{crd}$ for columns.

Step (8) Calculate the moment increments at the ends of each superelement:

$$\Delta\mathbf{M}_E^k = [\mathbf{K}]^k \cdot \Delta\boldsymbol{\theta}^k + \Delta\mathbf{M}_0^{k-1}$$

where $[\mathbf{K}] = [\mathbf{K}]_g$ for girders and $[\mathbf{K}] = [\mathbf{K}]_{crd}$ for columns and $\Delta\mathbf{M}_0^{k-1} = 0$ for *k*=1 (first iteration).

Step (9) Since all subelements are in series

$$\Delta\mathbf{M}_E^k = \left(\Delta\mathbf{m}_E\right)_{el}^k = \left(\Delta\mathbf{m}_E\right)_{pl}^k = \left(\Delta\mathbf{m}_E\right)_{jnt}^k = \left(\Delta\mathbf{m}_E\right)_{shr}^k$$

Step (10) Calculate the rotation increments at the ends of each subelement:

$$\Delta\boldsymbol{\theta}_{el}^k = \left[\mathbf{f}\right]_{el}^k \cdot \left(\Delta\mathbf{m}_E\right)_{el}$$

$$\Delta\boldsymbol{\theta}_{pl}^k = \left[\mathbf{f}\right]_{pl}^k \cdot \left(\Delta\mathbf{m}_E - \Delta\mathbf{m}_0^{k-1}\right)_{pl}$$

$$\Delta\boldsymbol{\theta}_{jnt}^k = \left[\mathbf{f}\right]_{jnt}^k \cdot \left(\Delta\mathbf{m}_E - \Delta\mathbf{m}_0^{k-1}\right)_{jnt}$$

$$\Delta\boldsymbol{\theta}_{shr}^k = \left[\mathbf{f}\right]_{shr}^k \cdot \left(\Delta\mathbf{m}_E - \Delta\mathbf{m}_0^{k-1}\right)_{shr}$$

In the case of the spread plastic subelement calculate the curvature increments at the end sections:

$$\Delta\varphi_i^k = \frac{\left(\Delta m_{E,i} - \Delta m_{0,i}^{k-1}\right)_{pl}}{c_i^k \cdot EI}$$

$$\Delta\varphi_j^k = \frac{\left(\Delta m_{E,j} - \Delta m_{0,j}^{k-1}\right)_{pl}}{c_j^k \cdot EI}$$

where $\Delta\mathbf{m}_0^{k-1} = 0$ for $k = 1$ (first iteration).

Step (11) Update the current end rotations/end curvatures and determine the internal resisting moments from the hysteretic moment-rotation/ moment-curvature relations:

$$\left(\boldsymbol{\theta}_{n+1}^k\right)_{pl} = \left(\boldsymbol{\theta}_n^k\right)_{pl} + \Delta\boldsymbol{\theta}_{pl}^k \quad \rightarrow \quad \left(\mathbf{m}_R^k\right)_{pl}$$

$$\left(\boldsymbol{\theta}_{n+1}^k\right)_{jnt} = \left(\boldsymbol{\theta}_n^k\right)_{jnt} + \Delta\boldsymbol{\theta}_{jnt}^k \quad \rightarrow \quad \left(\mathbf{m}_R^k\right)_{jnt}$$

$$\left(\boldsymbol{\theta}_{n+1}^k\right)_{shr} = \left(\boldsymbol{\theta}_n^k\right)_{shr} + \Delta\boldsymbol{\theta}_{shr}^k \quad \rightarrow \quad \left(\mathbf{m}_R^k\right)_{shr}$$

$$\left(\boldsymbol{\varphi}_{n+1}^k\right)_{pl} = \left(\boldsymbol{\varphi}_n^k\right)_{pl} + \Delta\boldsymbol{\varphi}_{pl}^k \quad \rightarrow \quad \left(\mathbf{m}_R^k\right)_{pl}$$

The first relation applies to the concentrated plastic and the last to the spread plastic subelement. The calculation of internal resisting moments takes place at each end of the subelement independently.

Step (12) Calculate the increment of internal resisting moments and the moment unbalance between internal and external moment increments, if any

$$\left(\Delta\mathbf{m}_R^k\right)_{pl} = \left[\left(\mathbf{m}_R^k\right) - \left(\mathbf{m}_R\right)_n\right]_{pl} \quad \rightarrow \quad \left(\Delta\mathbf{m}_U^k\right)_{pl} = \left[\left(\Delta\boldsymbol{\theta}\mathbf{m}_E^k\right) - \left(\Delta\mathbf{m}_R^k\right)\right]_{pl}$$

$$\left(\Delta\mathbf{m}_R^k\right)_{jnt} = \left[\left(\mathbf{m}_R^k\right) - \left(\mathbf{m}_R\right)_n\right]_{jnt} \quad \rightarrow \quad \left(\Delta\mathbf{m}_U^k\right)_{jnt} = \left[\left(\Delta\mathbf{m}_E^k\right) - \left(\Delta\mathbf{m}_R^k\right)\right]_{jnt}$$

$$\left(\Delta\mathbf{m}_R^k\right)_{shr} = \left[\left(\mathbf{m}_R^k\right) - \left(\mathbf{m}_R\right)_n\right]_{shr} \quad \rightarrow \quad \left(\Delta\mathbf{m}_U^k\right)_{shr} = \left[\left(\Delta\mathbf{m}_E^k\right) - \left(\Delta\mathbf{m}_R^k\right)\right]_{shr}$$

If the Euclidean norm of $\Delta\mathbf{m}_U$ exceeds a pre specified tolerance then the flexibility matrix of the corresponding subelement is updated.

Step (13) For the spread plastic subelement calculate the new theoretical length of the plastic zones

$$z_{c,i}^k = \frac{\left(m_{n,i} + \Delta m_{E,i}^k\right)_{pl} - M_{y,i}}{V_n + \Delta V^k} \qquad \text{and} \qquad z_{c,j}^k = \frac{\left(m_{n,j} + \Delta m_{E,j}^k\right)_{pl} - M_{y,j}}{V_n + \Delta V^k}$$

where

$$V_n = \frac{\left(m_{n,i} + m_{n,j}\right)_{pl}}{L} \qquad \text{and} \qquad \Delta V^k = \frac{\left(\Delta m_{E,i}^k + \Delta m_{E,j}^k\right)_{pl}}{L}$$

Compare the theoretical plastic zone lengths against the previous values and update these by a finite increment z_d, if necessary

$$z_{a,i}^N = z_{a,i} + z_d \qquad \text{if} \qquad z_{c,i} > z_{a,i}$$

$$z_{a,j}^N = z_{a,j} + z_d \qquad \text{if} \qquad z_{c,j} > z_{a,j}$$

where $z_d = 0.025 \cdot L$.

If a change in plastic zone length takes place at one or both ends of the spread plastic subelement, determine the end moment and the corresponding end rotation increments when the first event of a change in the plastic zone length is about to take place

$$\Delta\mathbf{m}_z = \begin{Bmatrix} V_z \cdot L_i \\ V_z \cdot L_j \end{Bmatrix} - \begin{Bmatrix} m_{n,i} \\ m_{n,j} \end{Bmatrix} \qquad \text{and} \qquad \Delta\boldsymbol{\theta}_z = \left[\mathbf{f}\right]_{pl}^k \cdot \Delta\mathbf{m}_z$$

where

$$V_z^k = \mathbf{min}\left[\left(V_i^*\right)^k, \left(V_j^*\right)^k\right] = \mathbf{min}\left[\frac{M_{y,i}}{L_i^k - z_{a,j}^N}, \frac{M_{y,j}}{L_j^k - z_{a,j}^N}\right]$$

$$L_i^k = \frac{m_{n,i} + \Delta m_{E,i}^k}{m_{n,i} + \Delta m_{E,i}^k + m_{n,j} + \Delta m_{E,j}^k} \cdot L \qquad L_j^k = \frac{m_{n,j} + \Delta m_{E,j}^k}{m_{n,i} + \Delta m_{E,i}^k + m_{n,j} + \Delta m_{E,j}^k} \cdot L$$

Update the flexibility matrix of the spread plastic subelement to account for the extension of the plastic zone that takes place first.

Step (14) Invert the updated subelement flexibility matrices to obtain the corresponding stiffness matrices. Calculate the initial moments at the ends of each subelement

$$\left(\Delta \mathbf{m}_0\right)_{pl}^k = \left(\Delta \mathbf{m}_R\right)_{pl}^k - \left[\mathbf{k}_u\right]_{pl}^{k+1} \cdot \Delta \boldsymbol{\theta}_{pl}^k$$

$$\left(\Delta \mathbf{m}_0\right)_{jnt}^k = \left(\Delta \mathbf{m}_R\right)_{jnt}^k - \left[\mathbf{k}_u\right]_{jnt}^{k+1} \cdot \Delta \boldsymbol{\theta}_{jnt}^k$$

$$\left(\Delta \mathbf{m}_0\right)_{shr}^k = \left(\Delta \mathbf{m}_R\right)_{shr}^k - \left[\mathbf{k}_u\right]_{shr}^{k+1} \cdot \Delta \boldsymbol{\theta}_{jnt}^k$$

$$\left(\Delta \mathbf{m}_0\right)_{pl}^k = \Delta \mathbf{m}_z^k - \left[\mathbf{k}_u\right]_{pl}^{k+1} \cdot \Delta \boldsymbol{\theta}_z^k$$

The last equation only applies to the spread plastic subelement.

Step (15) Calculate the initial moments at the ends of all superelements

$$\Delta \mathbf{M}_0^k = \left[\mathbf{K}\right]^{k+1} \cdot \left\{ \left[\mathbf{f}_u\right]_{pl}^{k+1} \cdot \left(\Delta \mathbf{m}_0\right)_{pl}^k + \left[\mathbf{f}_u\right]_{jnt}^{k+1} \cdot \left(\Delta \mathbf{m}_0\right)_{jnt}^k + \left[\mathbf{f}_u\right]_{shr}^{k+1} \cdot \left(\Delta \mathbf{m}_0\right)_{shr}^k \right\}$$

where $\left[\mathbf{K}\right] = \left[\mathbf{K}\right]_g$ for girders and $\left[\mathbf{K}\right] = \left[\mathbf{K}\right]_{crd}$ for columns. $\left[\mathbf{K}\right]_g$ and $\left[\mathbf{K}\right]_{crd}$ are the stiffness matrices of the girder and column superelement, respectively.

Step (16) Calculate the initial load vector

$$\Delta \mathbf{R}_0 = \left[\mathbf{a}\right]^T \cdot \Delta \mathbf{M}_0^k$$

where $\left[\mathbf{a}\right] = \left[\mathbf{a}\right]_b$ for girders and $\left[\mathbf{a}\right] = \left[\mathbf{a}\right]_{crd}$ for columns. Go back to **Step 4**, set $k = k+1$ and $k\text{-}1 = k$ and continue until no unbalanced moments occur in **Step 12**.

CHAPTER 4

NONLINEAR DYNAMIC ANALYSIS

4.1 Introduction

This chapter is devoted to aspects related to the nonlinear dynamic analysis method used in the present study. The computational details of the dynamic analysis and the mass and damping idealization of the structure are discussed.

The proposed nonlinear analysis method is applicable to, both, the static and dynamic nonlinear analysis of structures. In this study only the implementation of the method in the context of the nonlinear analysis of moment resisting frames is presented. Since the nonlinear static analysis of frames is just a special case of the dynamic analysis with no damping or inertia forces and with lateral forces applied as concentrated static forces at each floor, details related to the calculation of unbalanced forces and to the process of state determination of individual frame elements were presented in the previous chapter.

The numerical integration strategy for nonlinear dynamic analysis is discussed in this chapter. Questions of accuracy and stability of the numerical integration scheme are only touched upon. Reference is made to more detailed discussions of related integration schemes in the literature (Golafshani 1982, Allahabadi 1987).

In the following discussion special consideration is given to the nonlinearities that can take place within a time step. This is especially important when the deformation contribution of the different subelements to the local and global response of the structure is to be determined. In this study frame members are decomposed into different subelements, which act in series. Each subelement represents a different source of inelastic deformation of frame members. Since each subelement has a unique hysteretic behavior, changes of stiffness in the different subelements do not take place at the same instant. If the sudden change in stiffness of a subelement within the time step is not taken into account, gross inaccuracies in the relative contribution of the different subelements to the local and global response of the structure will result. Moreover, the relative distribution of forces and deformations among the girders and columns of the frame cannot be determined with confidence, if a constant stiffness is assumed within the time step. In addition, unrecoverable numerical instability problems might appear in later time steps. To address this problem a special procedure was proposed in Chapter 3 which accounts for stiffness changes within a time step. This

algorithm is now applied to the dynamic analysis of frame structures. Special problems which arise during this implementation will be discussed in this chapter.

An important aspect of nonlinear dynamic analysis is the selection of time step size. The size of the time step has great effect on the accuracy, stability, and rate of convergence of the solution algorithm. The criteria for selecting the time step size for the proposed solution algorithm will be discussed in this chapter.

For the accurate description of the nonlinear dynamic response of RC frame structures three dimensional models are the best solution. At present the refined three dimensional dynamic analysis of RC buildings is computationally very intensive. This study is limited to two dimensional models of symmetric buildings along one principal axis and determines the response of these models to a ground motion whose direction coincides with this axis.

The features of the two dimensional model are summarized below: (Fig. 2.2.):

- One vertical degree of freedom and one rotational degree of freedom per node as well as one horizontal degree of freedom per floor is assumed.
- The building mass is assumed to be lumped at the floors.
- Mass is assigned to the lateral translational degrees of freedom only, and the rotational inertia is not accounted for.
- Only horizontal ground accelerations are considered.
- Gravity loads are included in the analysis as fixed end moments and shear forces at the girder ends. Joint loads are directly applied as concentrated moments and forces at the nodes. A static analysis is performed before the beginning of the dynamic response analysis.
- The model includes inelastic deformations in girders and columns with due account of the effect of axial load on stiffness and strength.
- Shear effects in girders and columns, the axial deformations of columns and second-order deformations due to P-Δ effects are included in the analysis.
- Finite joint dimensions are used in determining the clear span of members. Fixed end rotations at the beam-column and column-foundation interface due to bond deterioration in the anchorage zone are taken into account.
- The addition of rotational springs at the base of the columns can simulate the condition of hinged, partially fixed or completely fixed supports. Translational springs at the base of the building can simulate sliding, rocking, and settlement of the foundation.
- The frame members are assumed to have infinite ductility, so that failure by attainment of the actual ultimate strength or deformation capacity of the member is not considered.

4.2 Dynamic equilibrium

The equations of motion for multi-degree of freedom systems are given by

$$[\mathbf{M}]\cdot\ddot{\mathbf{r}} + [\mathbf{C}]\cdot\dot{\mathbf{r}} + [\mathbf{K}]\cdot\mathbf{r} = \mathbf{P} \tag{4.1}$$

$\ddot{\mathbf{r}}$ is the relative acceleration, $\dot{\mathbf{r}}$ is the relative velocity, $\mathbf{r}$ is the relative displacement, and the external load vector is $\mathbf{P} = -[\mathbf{M}]\cdot\ddot{\mathbf{r}}_g = -[\mathbf{M}]\cdot\mathbf{1}\,\ddot{a}_g$ in the case of earthquake loading, where $\ddot{a}_g$ is the ground acceleration and $\mathbf{1}$ is a vector of ones. $[\mathbf{M}]$, $[\mathbf{C}]$, $[\mathbf{K}]$ is the mass, damping, and stiffness matrix, respectively. These matrices are described in detail in the following.

4.2.1 Mass matrix

The mass of a structure can be modeled in an equivalent lumped or a consistently distributed matrix (Clough and Penzien 1975). In frame analyses the use of distributed mass is not worth the effort, since the dynamic response is not much affected by the type of idealization (Selna 1977).

In the proposed analytical model only horizontal ground accelerations are considered. Since lateral inertia forces and displacements constitute the dominant effect, mass is assigned to translational horizontal degrees of freedom only and no rotational or vertical translational inertia is included in the model. All permanent weight that moves with the structure is lumped at the appropriate nodes. This includes the dead load and that part of the live load which is expected to be present in the structure during the ground shaking. In regular buildings it is common practice to include 20% of the design live load in the calculation of the mass of the structure, whereas the entire live load is typically included in the mass of warehouse buildings.

Vertical accelerations are ignored, since axial deformations in the columns are rather small. If vertical displacements or accelerations are important, the mass associated with the vertical degrees of freedom has a significant effect on the response, even if vertical ground accelerations are not applied to the frame. This stems from vertical accelerations in flexible frames caused by axial deformations in the columns due to lateral response. In typical building structures the cross-sectional dimensions of columns are determined from drift considerations and anchorage requirements in beam-column joints. This results in columns having so large axial stiffness that vertical inertia can be neglected in typical cases. If the frame is very flexible or all members connected to a particular joint are very slender, then rotational lumped masses at the joints should also be considered.

Since the mass is lumped at the floor level, [**M**] is a sparse diagonal matrix with nonzero terms associated only with the horizontal degrees of freedom. The coefficient values of the mass matrix are assumed to remain constant during the dynamic response of the frame.

4.2.2 Damping matrix

Energy dissipation in the form of damping is commonly idealized in linear elastic dynamic analysis as viscous or velocity proportional for convenience of solution. In reality, damping forces may be proportional to the velocity or to some power of velocity. Alternatively these forces may be of frictional nature, and in some cases they may even be proportional to displacements or relative displacements (Newmark 1959). Once significant yielding takes place, hysteretic damping becomes the major source of energy dissipation. Hysteretic damping is best accounted for directly by the hysteretic load-deformation relation.

The most effective means of deriving a suitable damping matrix is to assume appropriate values of modal damping ratios for all significant modes of vibration of the structure and then compute a damping matrix based on these damping ratios (Clough and Penzien 1975). In this study a Raleigh type mass and stiffness proportional damping of the following form is used

$$[\mathbf{C}] = \alpha \cdot [\mathbf{M}] + \beta \cdot [\mathbf{K}] \tag{4.2}$$

in which α and β are constants derived by assuming suitable damping ratios for two modes of vibration.

Using a normal coordinate transformation of the equations of motion the n-th mode damping ratio is

$$\lambda_n = \frac{\alpha}{2\omega_n} + \beta \frac{\omega_n}{2}$$

where ω_n is the circular frequency of the n-th mode. For mass dependent damping λ_n is inversely proportional to the frequency such that higher modes have little damping. Conversely, stiffness proportional damping is proportional to the frequency of the structure and results in higher damping for higher modes thus decreasing the contribution of higher modes to the response of the structure (Fig. 4.1.).

In nonlinear dynamic analysis the damping matrix can be expressed in proportion to the initial or current tangent stiffness of the structure according to

$$[\mathbf{C}] = \alpha \cdot [\mathbf{M}] + \beta \cdot [\mathbf{K}_0]$$

or,

$$[\mathbf{C}] = \alpha \cdot [\mathbf{M}] + \beta \cdot [\mathbf{K}_T]$$

where $[\mathbf{K}_0]$ is the initial stiffness matrix and $[\mathbf{K}_T]$ is the tangent stiffness matrix.

In this study the first option is used, since the second option can lead to numerical problems and has no advantage over the first option. Moreover, the effect of viscous damping is very small compared to hysteretic damping in the nonlinear dynamic analysis of structures that are subjected to large post-yield deformations.

After selecting the damping ratios for two modes of vibration, the constants α and β can be obtained as follows (Clough and Penzien 1975):

$$\begin{bmatrix} \lambda_m \\ \lambda_n \end{bmatrix} = \frac{1}{2} \cdot \begin{bmatrix} \frac{1}{\omega_m} & \omega_m \\ \frac{1}{\omega_n} & \omega_n \end{bmatrix} \cdot \begin{Bmatrix} \alpha \\ \beta \end{Bmatrix} \tag{4.3}$$

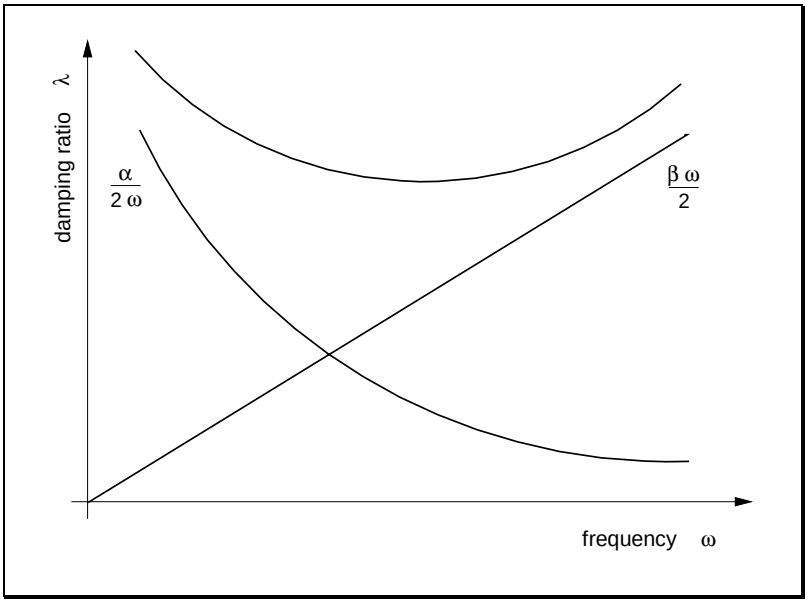

FIGURE 4.1 MASS AND STIFFNESS PROPORTIONAL DAMPING

4.2.3 Stiffness matrix

Complete details of the derivation of the stiffness matrix of the frame model are presented in Chapter 2. The basic idea behind the proposed frame stiffness idealization is to provide a model which is complex enough to approximate the real structure behavior, yet simple enough to be practical in the nonlinear dynamic analysis of large structures. The frame model is a two dimensional idealization of the structural system which consists of column

and girder superelements. These are, in turn, decomposed into different subelements with each subelement representing a particular source of inelastic deformation in the structure.

A complete three-dimensional analysis of RC buildings is a formidable task. Most existing computer programs for nonlinear three-dimensional dynamic analysis do not include a sufficient number of elements to be of use in the simulation of the dynamic response of buildings (Newmark and Hall 1981).

Usually, separate planar models in two orthogonal directions are analyzed for the corresponding component of the ground motion. Care is, however, warranted in planar frame analysis, if strong coupling exists between the lateral motion in two orthogonal directions. Care is also warranted, if significant torsional response is expected as is the case when the mass and stiffness centers of the structure do not coincide or asymmetric inelastic effects take place. In buildings deforming into the inelastic range the stiffness in one direction is affected by the load and deformation history in the other direction. The sequence of application of the two orthogonal components of ground acceleration has, therefore, a large effect on the nonlinear response of the frame.

The proposed frame model aims at predicting the nonlinear hysteretic behavior of plane frames under unidirectional motion and can only provide some insight toward the understanding of the three-dimensional behavior of RC moment resisting frames.

4.3 Numerical integration method

The incremental equations of motion represent the equilibrium of force increments during a time step

$$[\mathbf{M}]\cdot\Delta\ddot{\mathbf{r}}+[\mathbf{C}]\cdot\Delta\dot{\mathbf{r}}+[\mathbf{K}_T]\cdot\Delta\mathbf{r}=\Delta\mathbf{P}$$

After determining the increments of displacement, velocity and acceleration, the solution advances by adding these increments to the corresponding values at the beginning of the time step and by treating the latter as initial conditions for the next step.

In the case of nonlinear systems the equations of motion are solved using a step by step integration method. In the frame model of this study some degrees of freedom with no associated mass can develop velocity dependent damping leading to modes with zero period. An integration method which is unconditionally stable with respect to the integration step size is indispensable in this case. The constant average acceleration method satisfies this requirement and is adopted in this study. The method assumes that within each time step the accelerations associated with all degrees of freedom are the average of the values at the beginning and end of the time step.

This integration method has the following numerical characteristics:

- It is unconditionally stable with respect to time step size.
- It does not introduce spurious damping into the system.
- It is sufficiently accurate for time steps of practical size.

By substituting the mass and stiffness dependent damping matrix into the incremental equilibrium equations we obtain

$$[\mathbf{M}]\cdot\Delta\ddot{\mathbf{r}}+\{\alpha\cdot[\mathbf{M}]+\beta\cdot[\mathbf{K}_0]\}\cdot\Delta\dot{\mathbf{r}}+[\mathbf{K}_T]\cdot\Delta\mathbf{r}=\Delta\mathbf{P} \tag{4.4}$$

Assuming constant acceleration within the time step results in

$$\ddot{\mathbf{r}}=\frac{1}{2}\left(\ddot{\mathbf{r}}_0+\ddot{\mathbf{r}}_1\right)$$

$$\Delta\ddot{\mathbf{r}}=\ddot{\mathbf{r}}_1-\ddot{\mathbf{r}}_0=2\ddot{\mathbf{r}}-2\ddot{\mathbf{r}}_0$$

$$\dot{\mathbf{r}}=\dot{\mathbf{r}}_0+\int\ddot{\mathbf{r}}\cdot dt$$

$$\dot{\mathbf{r}}_1=\dot{\mathbf{r}}_0+\ddot{\mathbf{r}}\cdot\Delta t$$

$$\Delta\dot{\mathbf{r}}=\dot{\mathbf{r}}_1-\dot{\mathbf{r}}_0=\ddot{\mathbf{r}}\cdot\Delta t$$

$$\mathbf{r}=\mathbf{r}_0+\int\dot{\mathbf{r}}\cdot dt$$

$$\mathbf{r}_1=\mathbf{r}_0+\dot{\mathbf{r}}_0\cdot\Delta t+\frac{\ddot{\mathbf{r}}_0\cdot\Delta t^2}{2}$$

$$\Delta\mathbf{r}=\mathbf{r}_1-\mathbf{r}_0=\dot{\mathbf{r}}_0\cdot\Delta t+\frac{\ddot{\mathbf{r}}_0\cdot\Delta t^2}{2}$$

Rearranging in terms of $\Delta\mathbf{r}$ we obtain

$$\Delta\dot{\mathbf{r}}=\frac{2}{\Delta t}\Delta\mathbf{r}-2\dot{\mathbf{r}}_0 \tag{4.5}$$

$$\Delta\ddot{\mathbf{r}}=\frac{4}{\Delta t^2}\Delta\mathbf{r}-\frac{4}{\Delta t}\dot{\mathbf{r}}_0-2\ddot{\mathbf{r}}_0 \tag{4.6}$$

where $\Delta\mathbf{r}$, $\Delta\dot{\mathbf{r}}$ and $\Delta\ddot{\mathbf{r}}$ are the increments of displacement, velocity, and acceleration vectors during the time step Δt, respectively. The subscript 0 indicates quantities at the beginning of the time step.

By combining Eqs. (4.4)-(4.6) and rearranging the results we obtain:

$$\left\{\left(\frac{4}{\Delta t^2}+\frac{2\alpha}{\Delta t}\right)[\mathbf{M}]+\frac{2\beta}{\Delta t}\cdot[\mathbf{K}_0]+[\mathbf{K}_T]\right\}\cdot\Delta\mathbf{r}=\Delta\mathbf{P}+[\mathbf{M}]\cdot\left(2\ddot{\mathbf{r}}_0+\frac{4}{\Delta t}\dot{\mathbf{r}}_0\right)+\{\alpha\cdot[\mathbf{M}]+\beta\cdot[\mathbf{K}_0]\}\cdot 2\dot{\mathbf{r}}_0$$

Defining

$$c_1=\frac{4}{\Delta t^2}+\frac{2\alpha}{\Delta t}$$

$$\mathbf{B} = 2\dot{\mathbf{r}}_0$$

and

$$\left[\mathbf{K}^*\right] = c_1 \cdot \left[\mathbf{M}\right] + \frac{2\beta}{\Delta t} \cdot \left[\mathbf{K}_0\right] + \left[\mathbf{K}_T\right]$$

results in the final form of the dynamic equilibrium equations

$$\left[\mathbf{K}^*\right] \cdot \Delta\mathbf{r} = \Delta\mathbf{P} + \left[\mathbf{M}\right] \cdot \left(2\ddot{\mathbf{r}}_0 + \frac{4}{\Delta t}\dot{\mathbf{r}}_0 + \alpha \cdot \mathbf{B} \right) + \left\{ \beta \cdot \left[\mathbf{K}_0\right] \right\} \cdot \mathbf{B} \tag{4.7}$$

The damping matrix is assumed to be proportional to the initial stiffness $\left[\mathbf{K}_0\right]$ and mass matrix $\left[\mathbf{M}\right]$ i.e. $\left[\mathbf{C}\right] = \alpha \cdot \left[\mathbf{M}\right] + \beta \cdot \left[\mathbf{K}_0\right]$

Since $\left[\mathbf{K}_0\right]$ and [**M**] and do not change during a time step, [**C**] also remains constant The disadvantage of the damping matrix being proportional to the initial stiffness matrix $\left[\mathbf{K}_0\right]$ is the additional storage requirement, since both stiffness matrices, $\left[\mathbf{K}_0\right]$ and $\left[\mathbf{K}_T\right]$, need to be stored in this case.

4.4 Numerical implementation

Buildings subjected to earthquake ground shaking are usually occupied and thus members of the structure are stressed by the combination of the effects of gravity and earthquake ground motion. In this study the building frame model is first subjected to gravity loads, followed by the dynamic analysis for ground accelerations. The building frame model does not have to remain elastic during the static analysis phase, so that initial damage due to other effects prior to the earthquake excitation can be simulated.

The proposed method of nonlinear dynamic analysis is outlined below by referring to the nonlinear algorithm of Chapter 3. The algorithm is subdivided into the following steps:

(1) At the beginning of the time step $\dot{\mathbf{r}}_0$, $\ddot{\mathbf{r}}_0$, α and β are known, where $\dot{\mathbf{r}}_0$ and $\ddot{\mathbf{r}}_0$ are the velocity and acceleration vectors at the beginning of the time step, respectively, and α and β are the damping parameters.

(2) Assemble mass matrix $\left[\mathbf{M}\right]$, which does not change during the analysis.

(3) Assemble the initial stiffness matrix $\left[\mathbf{K}_0\right]$.

(a) This step involves **Steps 1-5** of the nonlinear analysis algorithm in Chapter 3. The initial stiffness matrix $\left[\mathbf{K}_0\right]$ is only formed once. Since the initial stiffness matrix is used in the evaluation of the damping forces, it needs to remain in storage during the entire dynamic analysis.

(b) If a change of stiffness occurs during the time step a new tangent stiffness matrix $[\mathbf{K}_T]$ is assembled.

(4) Determine c_1 and $\mathbf{B}$ from

$$c_1 = \frac{4}{\Delta t^2} + \frac{2\alpha}{\Delta t}$$

$$\mathbf{B} = 2\dot{\mathbf{r}}_0$$

(5) Evaluate the effective stiffness matrix $[\mathbf{K}^*]$

$$[\mathbf{K}^*] = c_1 \cdot [\mathbf{M}] + \frac{2\beta}{\Delta t} \cdot [\mathbf{K}_0] + [\mathbf{K}_T]$$

(6) Evaluate the effective dynamic load vector from

$$\Delta\mathbf{P}^* = \Delta\mathbf{P} + [\mathbf{M}] \cdot \left(2\ddot{\mathbf{r}}_0 + \frac{4}{\Delta t}\dot{\mathbf{r}}_0 + \alpha \cdot \mathbf{B} \right) + \{\beta \cdot [\mathbf{K}_0]\} \cdot \mathbf{B}$$

(7) Solve for the incremental displacement vector $\Delta\mathbf{r}$ from

$$[\mathbf{K}^*] \cdot \Delta\mathbf{r} = \Delta\mathbf{P}^*$$

This step corresponds to **Step 6** of the general nonlinear algorithm in Chapter 3.

(8) Perform **Steps 7 through 16** (state determination) of the general nonlinear algorithm of Chapter 3.

(9) In case of force unbalance go to **Step 3b**.

In case of convergence

(a) Determine the resulting incremental velocity and acceleration vectors from

$$\Delta\dot{\mathbf{r}} = \frac{2}{\Delta t}\Delta\mathbf{r} - 2\dot{\mathbf{r}}_0$$

$$\Delta\ddot{\mathbf{r}} = \frac{4}{\Delta t^2}\Delta\mathbf{r} - \frac{4}{\Delta t}\dot{\mathbf{r}}_0 - 2\ddot{\mathbf{r}}_0$$

(b) Update the initial velocity and acceleration vectors $\dot{\mathbf{r}}_0$, $\ddot{\mathbf{r}}_0$, respectively, from

$$\dot{\mathbf{r}}_0 = \dot{\mathbf{r}}_0 + \Delta\dot{\mathbf{r}}$$

$$\ddot{\mathbf{r}}_0 = \ddot{\mathbf{r}}_0 + \Delta\ddot{\mathbf{r}}$$

(c) Go to Step 3b.

4.4.1 Force unbalance in load deformation relation

If the stiffness is assumed to remain constant during the time step, a force unbalance in the equilibrium equations will arise in cases where the stiffness of some elements changes during the step. A force unbalance resulting from yielding of an element is called overshoot, a force unbalance arising from unloading of an element is called undershoot or backtrack and, finally, a force unbalance due to reloading after unloading is called cross-over. These cases are shown in Fig. 4.2. The problem of force unbalance due to the assumption of constant stiffness during the time step has been discussed by several researchers (Aziz and Roesset 1976). In the case of static analysis the effect of overshooting, backtracking and cross-over can be readily established: the load deformation diagram is elongated in the load direction, but shortened in the deformation direction as shown in Fig. 4.2. The accumulation of this effect overestimates the strength and underestimates the deformation of the structure. In the case of dynamic analysis, on the other hand, the effect of overshooting, backtracking and cross-over, cannot be readily established.

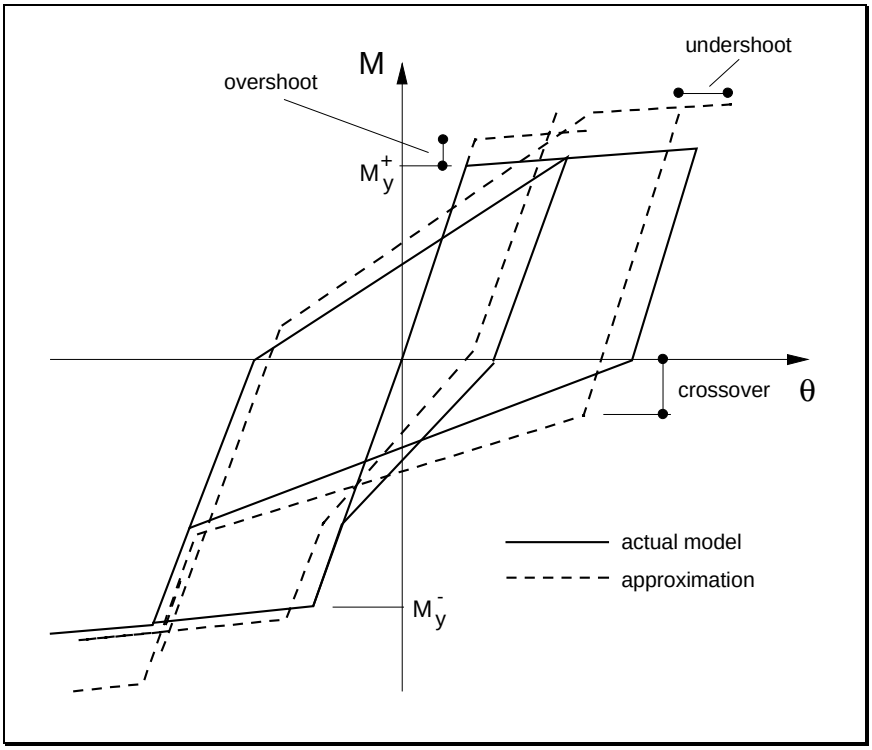

FIGURE 4.2 CASES OF OVERSHOOT, UNDERSHOOT AND CROSSOVER IN HYSTERETIC LOOPS

These effects change the stiffness characteristics of the model. Since the dynamic forces depend on the stiffness, a different dynamic response may result. Thus, by not

accounting for the stiffness change during the time step the maximum response of the structure will increase or decrease depending on the frequency content of the ground motion.

Different approaches of addressing the problem of unbalanced forces have been proposed to date. A summary of the most commonly used methods follows.

(1) The first method essentially ignores unbalanced forces. This method can be further subdivided into three different approaches:

(a) In the first approach the unbalance between applied moments at the ends of the element and resisting moments that correspond to the current deformation based on the load-deformation relation is transformed to global forces which are then applied as corrective loads during the next time step (Kanaan and Powell 1973). It is noted in (Robinson 1989) that the solutions obtained with the corrective force method are unbounded in some cases and can lead to very large errors. Errors of up to 18220% in the maximum response values of a structure with 20 degrees of freedom and a fundamental frequency of 5 Hz have resulted when using a time step size of 0.02, even though the constant acceleration method was used (Robinson 1989).

(b) In the second approach the moments at the ends of the element are set equal to those corresponding to the current deformation based on the load-deformation relation without carrying out the relaxation of the frame, which is physically equivalent to the application of corrective forces (Sharpe 1974).

(c) In the third approach the moments at the end of the time step are used as initial conditions in the following time step, even though they do not satisfy the load-deformation relation of the element. This method completely ignores the unbalance load. Researchers who used this method (Aziz and Roesset 1976) reported errors in the column and girder forces, the ductility demand, the story shear forces and the interstory drift. The largest discrepancy occurs in the calculation of story shear forces. Using different time steps in the nonlinear dynamic analysis of the same frame, no upper bound of member forces was obtained because of backtracking and overshooting (Aziz and Roesset 1976).

With any of these three methods it is questionable whether the selected time step size is small enough to allow for accurate tracking of the load-deformation relation of the member.

(2) **Iteration method.** In this approach an iteration is performed within the time step, if the moment unbalance exceeds a specified tolerance. Among the many iteration schemes proposed in previous studies the most common are:

(a) the Newton Raphson method,

(b) Modified Newton Methods, and

(c) Quasi-Newton methods.

A full description of these methods is given in Simons and Powell (1982).

(3) **Event-to-event method.** The third solution scheme is the event-to-event method. This strategy is suitable for problems that are linear or nearly linear between well defined events. A full discussion of the event-to-event method is given in Simons and Powell (1982). The idea behind the event-to-event method is to closely follow the equilibrium path at all times by updating the stiffness and the state of each element each time a change of stiffness in one of the elements of the structure takes place. This is achieved by predicting the occurrence of the next change of stiffness (event) within a load step and then scaling the load increment by a factor such that the solution just reaches the predicted event. A shortcoming of this method is the increase in the computational cost of each time step, as the number of elements and possible events increases. Its use in the nonlinear dynamic analysis of large structures is, thus, seriously compromised.

The Modified Newton-Method of Chapter 3 proved extremely robust and reliable. Any force unbalance between the different subelements was always resolved within the time step, and equilibrium was thus maintained at all times.

4.4.2 Time step size

In the step by step integration procedure the response of the structure is evaluated in discrete time increments Δt. The following factors must be considered in the selection of the time increment:

- It should be small enough to accurately represent the ground motion. The higher the rate of variation of the applied load the smaller the required time step.
- The accuracy of the numerical integration scheme depends on the size of the time step. If a large time step is selected, some response characteristics that are influenced by higher modes may not be well represented in the analytical results.
- The time step should be small enough to ensure numerical stability. Even though the constant acceleration method is unconditionally stable for linear analysis, there is no proof of unconditional stability in the case of nonlinear analysis.
- The convergence of iterative nonlinear analysis algorithms depends on the time step size. In the algorithm of this study the change of stiffness within the time step is taken into account. If convergence problems arise in certain cases, it is possible to remedy the situation by subdividing the step size, as discussed in Section 4.3.4. In nonlinear

methods which ignore the change of stiffness within the time step a very small step size is required and very often more than one analysis with different time step sizes needs to be performed in order to ensure convergence to the correct solution. The dynamic simulations in this study lead to the conclusion that the total number of time steps required to ensure accuracy of the results is much smaller in the proposed method than in algorithms which do not account for the change of stiffness within the time step. This fact compensates for the added cost associated with the iterative nature of the proposed algorithm.

4.4.3 Numerical problems

When a change of stiffness occurs within a time step, iterations are performed to ensure that equilibrium between applied and resisting forces is satisfied at the end of every time step. Numerical problems which might arise in connection with the proposed algorithm and remedial measures are discussed in the following.

The first problem occurs in the case of Fig. 4.3 which is characterized by a very small stiffness of the load-deformation relation followed by a large stiffness, which, in turn, is followed by a small stiffness. The convergence problems that might arise in this case are illustrated in Fig. 4.3.

(a) Execute Steps 1-9 of the nonlinear algorithm as usual.

(b) At Step 10 of the algorithm, the applied load $\Delta \mathbf{m}_E^k$ results in a very large element deformation increment $\Delta \boldsymbol{\theta}^k$ due to the small stiffness of the element.

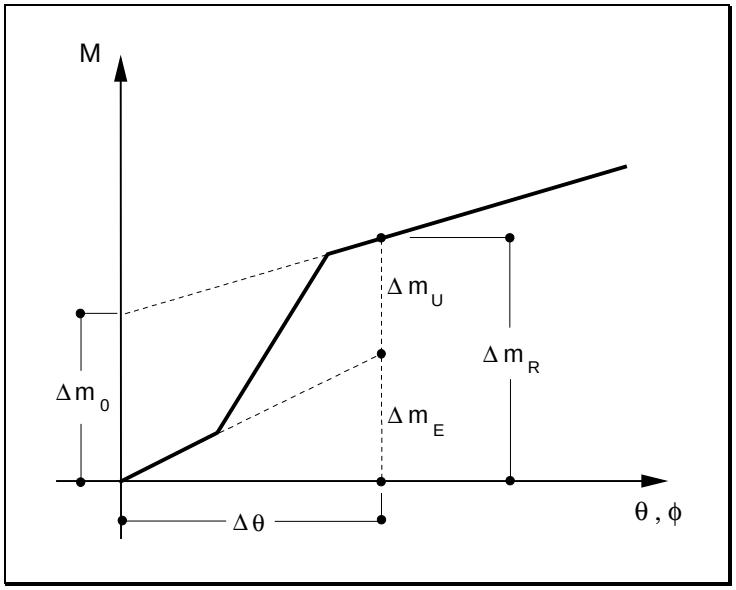

FIGURE 4.3 CASE FOR TIME STEP SUBDIVISION

(c) Steps 11 and 12 are executed to determine the internal resisting moment increment $\Delta\mathbf{m}_R^k$ corresponding to $\Delta\boldsymbol{\theta}^k$. In this case the resulting unbalance moment $\Delta\mathbf{m}_U^k$ is determined from the equations of Step 12 in Chapter 3.

(d) Execute Steps 13-16. In this special case the initial moment $\Delta\mathbf{m}_0^k$ determined from the equations of Step 14 in Chapter 3 will be higher than $\Delta\mathbf{m}_E^k$ (Fig. 4.3).

(e) Set $k = k+1$ at the end of Step 16 and perform a second iteration starting from Step 4 in order to satisfy equilibrium between applied and resisting forces.

(f) Execute Steps 4-9.

(g) Execute Step 10 to determine the value of $\Delta\boldsymbol{\theta}^k$. In this case $\Delta\boldsymbol{\theta}^k$ will correspond to $\Delta\mathbf{m}_E^k - \Delta\mathbf{m}_0^{k-1}$ which is of opposite sign to $\Delta\mathbf{m}_E^k$. This will reverse the loading direction and can lead to numerical problems.

In order to solve this problem a restepping capability is introduced in the nonlinear solution method of Chapter 3. Thus, if no convergence is achieved at the end of the correcting phase, the step size is halved and the iteration process is restarted from the previous converged state. This process is illustrated in Fig. 4.4 for the case of Fig. 4.3.

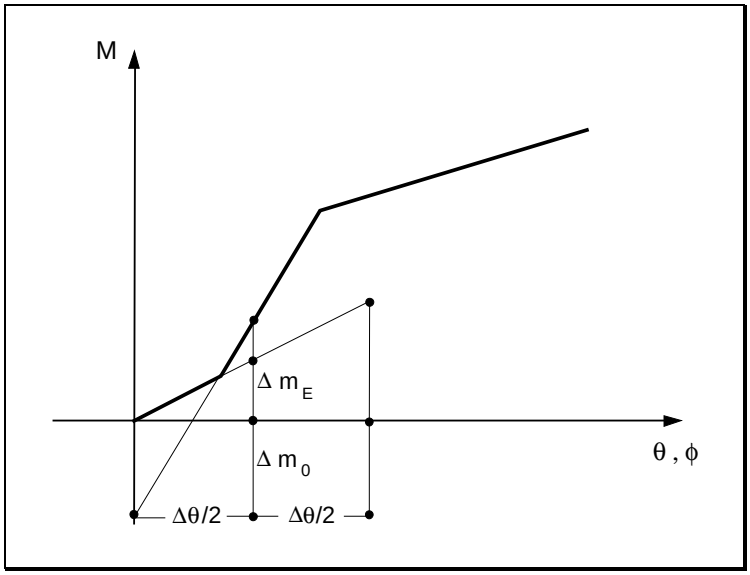

FIGURE 4.4 TIME STEP SUBDIVISION TO ACHIEVE CONVERGENCE

The most dramatic example of the numerical problems that occur in connection with a sudden increase in stiffness is the case of unloading after strain hardening or stiffness degradation. Two methods can be used to solve this problem:

First method. In this case the step is repeated using a very small step size. The step size should be sufficiently small to detect the abrupt change of stiffness. After the unloading stiffness is detected the step is repeated with the original load increment.

Second method. In this case the step is repeated using the unloading stiffness. The first method is necessary, if the unloading stiffness is not known in advance and state determination is required for determining the stiffness. In this case a small load increment suffices for determining the unloading stiffness.

The second method is more economical, if the unloading stiffness is known in advance, which is the case in the present study.

Another numerical problem is associated with “flip flop” of the solution. “Flip flop” is a problem that might appear in nonlinear dynamic analysis. It is characterized by oscillation of the solution between loading and unloading while iterating for convergence within a given time step. “Flip flop” usually occurs when the element tries to unload after strain hardening. In the nonlinear algorithm of this study this problem arises as follows:

The load step starts with the strain hardening stiffness. In the state determination phase of the solution (Step 10 of the nonlinear algorithm in Chapter 3) the subelement deformation is evaluated. If the resulting deformation increment of the subelement is of opposite sign to the previous deformation increment then the step is repeated using the unloading stiffness. In some cases repeating the step with the unloading stiffness reverses again the sign of the deformation increment, such that the original strain hardening stiffness has to be used again in the next step. Repeating the step with the original strain hardening stiffness leads once again to unloading and the process of oscillation between the states of strain hardening and unloading goes on indefinitely during subsequent iterations. The problem of oscillations of the solution between loading and unloading has been encountered in different numerical algorithms (Spurr 1984). To remedy this problem the loading increment needs to be subdivided. In this study the step size is automatically halved until convergence is reached. Once convergence is reached, the remainder of the original time step is applied in the same manner as described for the regular time step. Upon completion of the time step the solution algorithm reverts to the original time step size.

CHAPTER 5

ANALYSIS OF NONLINEAR RESPONSE TO STATIC CYCLIC LOADS

5.1 Introduction

The reinforced concrete girder and column elements and the analytical methods that were presented in the previous chapters are implemented in a special purpose computer program for the nonlinear static and dynamic analysis of reinforced concrete frames. This chapter focuses on analytical correlation studies of the nonlinear static response of frame subassemblages to cyclic alternating lateral loads. The dynamic response of frame subassemblages to earthquake excitations is discussed in the following chapter.

To establish the validity of the proposed girder and column models and the accuracy of the analytical solution methods for determining the nonlinear response of frame structures to cyclic static loads, the program is used in the simulation of the hysteretic behavior of beam-column subassemblages. Four particular specimens were selected. Two specimens have been used in the correlation studies presented by Filippou and Issa (1988). The other two specimens have a small span to depth ratio, so that the effect of high shear plays an important role in the response.

The first such specimen was designed and tested by Celebi and Penzien (1973) to simulate reinforced concrete beams under the combined action of bending moment and shear. This specimen is selected to test the adequacy of the shear subelement and its interaction with the other girder subelements. The specimen had a span to depth ratio of 2.3 and was subjected to a large number of cyclic deformation reversals.

The second specimen was designed by Atalay and Penzien (1975) to simulate reinforced concrete columns under the combined action of bending moment, shear, and axial load. The specimen was designed according to state of the art concepts of earthquake resistant design and was subjected to a large number of inelastic cyclic deformation reversals. This specimen was selected for verification of the ability of the column superelement to predict the hysteretic behavior of reinforced concrete columns under the combined action of axial force, shear and bending moment.

5.2 Correlation with Experimental Studies

5.2.1 Celebi and Penzien (1973) Girder Specimen

In order to test the ability of the proposed models to predict the response of reinforced concrete girders under high shear the results of the model are compared with experimental data from one of the specimens tested by Celebi and Penzien (1973). In the original report the specimen is designated as specimen #12. The design of specimen #12 satisfied the general requirements of Appendix A of the 1971 ACI Code, Special Provisions for Seismic Design. The specimen was tested to study the effect of shear on the behavior of girders. The span to depth ratio of this specimen is 2.31 which means that shear deformations significantly affect the hysteretic behavior.

The specimen was simply supported at both ends and subjected to concentrated lateral loads. The load history is shown in Fig. 5.1, while a simple sketch of the loading setup is shown in Fig. 5.2.

Additional reinforcement was placed in the column stub to increase the effectiveness of bond so that the influence of one side of the joint on the other is minimized. The specimen can, thus, be idealized as two identical cantilevers with half of the load applied at the free end of each (Fig. 5.2). Bond slip of reinforcing steel gives rise to fixed-end rotations at the girder-stub interface due to flexural cracking in the girder end region.

The analytical model used to simulate the behavior of the specimen consists of a girder superelement made up of an elastic subelement, a spread plastic subelement, a joint subelement, and a shear subelement. The properties of the constituent subelements are derived from the material and geometric properties of the specimen reported in Celebi and Penzien (1973). With the measured stress strain relations of concrete and reinforcing steel, the section geometry, and the reinforcement layout of the girder the monotonic moment-curvature relation of a typical girder section can be established

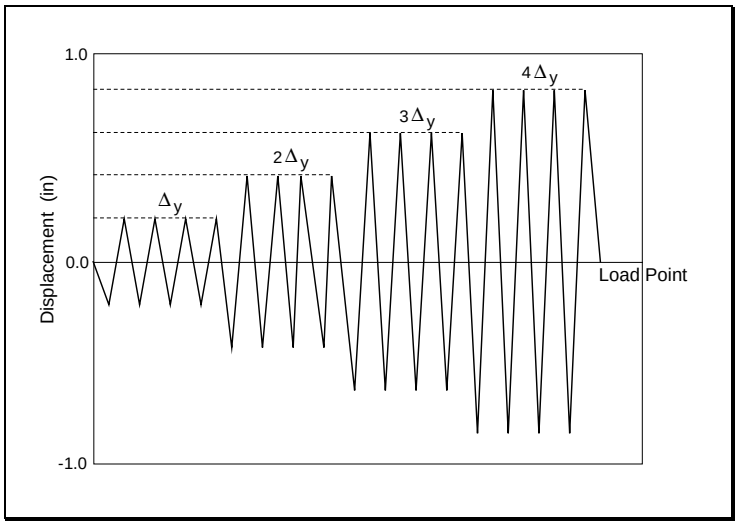

FIGURE 5.1 LOAD HISTORY OF SPECIMEN BY CELEBI AND PENZIEN (1973)

with well known principles of reinforced concrete analysis. The parameters for the elastic and spread plastic subelement are determined from the moment-curvature envelope of the girder end section. The parameters of the joint subelement are determined from the monotonic moment-fixed end rotation envelope. This can be established either with the finite element model by Filippou et al. (1983) or from a simplified analysis of pull-out deformations. The shear subelement describes the shear distortion in the end region of the member and the sliding at the beam-stub interface. The parameters of the shear subelement are also determined from the data in Celebi and Penzien (1973). The parameters of the spread plasticity, the joint and shear subelement are summarized in Table 5.1. Furthermore, a step-by-step derivation of these values is provided in Appendix A.

Fig. 5.3 shows the experimental and analytical lateral load-displacement relation of the specimen. A careful study of the results in Fig. 5.3 leads to the following observations:

- Excellent agreement between analytical predictions and experimental results is generally observed.
- The shear subelement can accurately model the shear effects in the post yield range of response of reinforced concrete girders.
- The pinching of the hysteretic behavior of the girder caused by the interaction of shear forces with the opening and closing of the cracks is predicted well by the analytical model. This effect is very important in short span members and must be taken into account in order to accurately predict the energy dissipation of the member.

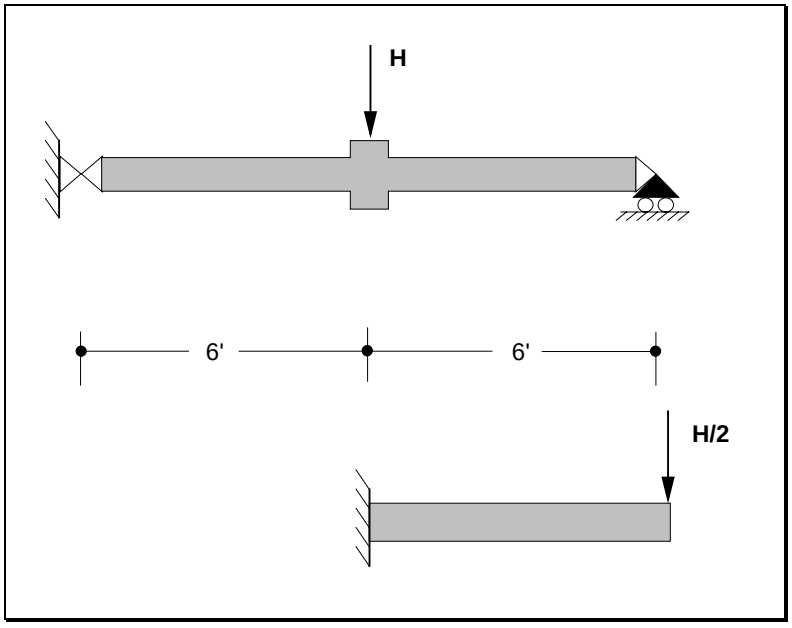

FIGURE 5.2 CANTILEVER EQUIVALENT TO SPECIMEN OF CELEBI AND PENZIEN (1973)

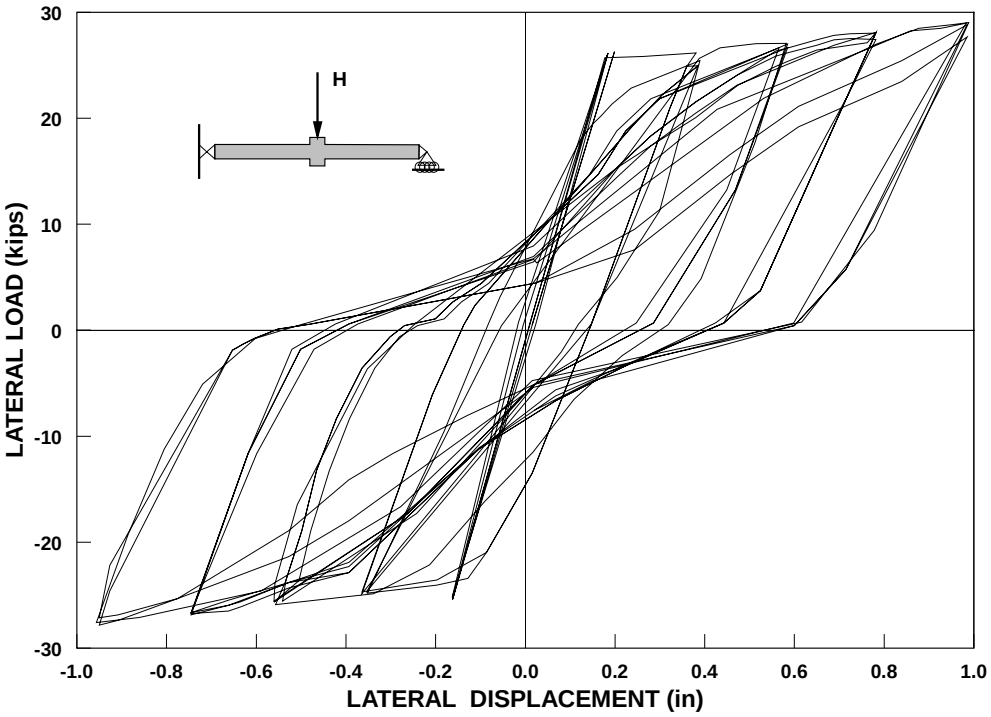

FIGURE 5.3A EXPERIMENTAL RESULTS OF LATERAL LOAD- DISPLACEMENT RELATION OF SPECIMEN #12 (CELEBI AND PENZIEN 1973)

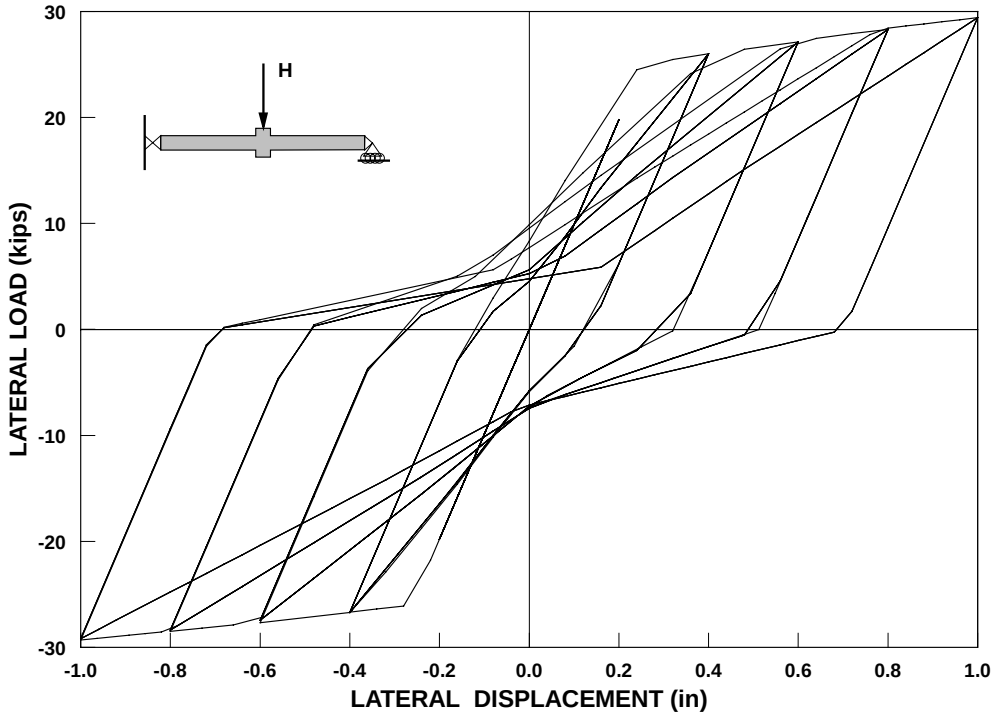

FIGURE 5.3B ANALYTICAL RESULTS OF LATERAL LOAD-DISPLACEMENT RELATION OF SPECIMEN #12 (CELEBI AND PENZIEN 1973)

- The strength degradation is not very significant; nonetheless, it is evident in the experimental results.
- The pre-yield stiffness of the specimen is underestimated in the early stages of loading, because the model does not take into account the stiffness change between the uncracked and cracked state. The model uses instead a secant pre-yield stiffness, since emphasis is placed on predicting the response of RC members under large cyclic deformation reversals. A change to an appropriately defined trilinear envelope curve can be readily accommodated in the model.

CELEBI AND PENZIEN (1973) SPECIMEN							
MOMENTS [k-in]		GIRDER MOMENT-CURVATURE		JOINT MOMENT-ROTATION RELATION		MOMENT-SHEAR ROTATION	
M_{cr}	200	INITIAL STIFFNESS [10^3 k-in^2/rad]	STRAIN HARDENING RATIO	INITIAL STIFFNESS [10^3 k-in/rad]	STRAIN HARDENING RATIO	INITIAL STIFFNESS [10^3 k-in/rad]	STRAIN HARDENING RATIO
M^+	780	2700	0.017	500	0.04	180	0.035
M^-	750	2700	0.017	500	0.04	180	0.035

TABLE 5.1 MODEL PARAMETERS FOR CELEBI AND PENZIEN (1973) SPECIMEN #12

5.2.2 Atalay and Penzien (1975) Column Specimen

To study the adequacy of the proposed model in predicting the hysteretic behavior of reinforced concrete frame elements subjected to the combined action of bending moment, shear, and axial load the behavior of a column specimen tested by Atalay and Penzien (1975) is studied. In the original report (Atalay and Penzien 1975) the specimen is designated as specimen #3. The design of the specimen satisfied the requirements of Appendix A of the 1971 ACI Code, Special Provisions for Seismic Design. The specimen was simply supported at both ends and was subjected to an axial load of 60 kips in addition to cyclic concentrated lateral loads. The load history is shown in Fig. 5.4 and the load setup resembles that in Fig. 5.2 with the addition of an axial load.

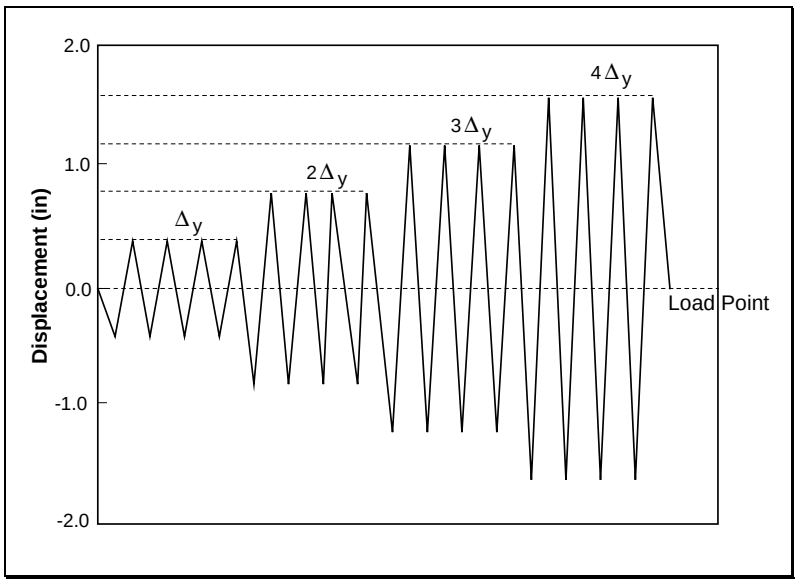

FIGURE 5.4 LOAD HISTORY OF SPECIMEN BY ATALAY AND PENZIEN (1975)

The reinforcing bars were welded to rigid steel plates at the midspan of the specimen to prevent slip of reinforcement and minimize the interaction between the two joint faces. The specimen can, thus, be idealized as two identical cantilevers with half of the load applied at the free end of each (Fig. 5.2).

The analytical model used in the prediction of the behavior of the specimen consists of a column superelement made up of an elastic subelement, a spread plastic subelement, a joint subelement, and a shear subelement. The derivation of the properties of the different constituent subelements is based on the material properties reported in Atalay and Penzien (1975). With the measured stress strain relations of concrete and reinforcing steel, the section geometry, and the reinforcement layout of the column the monotonic moment-curvature relation of a typical section can be established with well known principles of reinforced concrete analysis. The parameters for the elastic and spread plastic subelement are derived by fitting a bilinear envelope curve to the actual monotonic moment-curvature relation of the column end section.

Since the reinforcing bars are welded to the rigid steel plate at midspan, little slip occurs in the joint region. However, a pronounced flexural crack at the column-stub interface was still evident during the test. Therefore, the joint subelement represents the opening and closing of the crack at the column-stub interface and its interaction with the bending moment and axial load. The parameters of the joint subelement are determined from the monotonic moment-fixed end rotation envelope. This can be established either with the finite element model by Filippou et al. (1983) or from a simplified analysis of pull-out deformations.

The shear subelement describes the shear distortion in the end region and the sliding at the column-stub interface. The parameters of the column shear subelement are determined from data reported in Atalay and Penzien (1975).

The parameters of the spread plasticity, the joint and shear subelement are summarized in Table 5.2. Furthermore, a step-by-step derivation of these values is provided in Appendix A.

ATALAY AND PENZIEN (1975) SPECIMEN							
MOMENTS [k-in]		GIRDER MOMENT-CURVATURE		JOINT MOMENT-ROTATION RELATION		MOMENT-SHEAR ROTATION	
M_{cr}	300	INITIAL STIFFNESS [10^3 k-in^2/rad]	STRAIN HARDENING RATIO	INITIAL STIFFNESS [10^3 k-in/rad]	STRAIN HARDENING RATIO	INITIAL STIFFNESS [10^3 k-in/rad]	STRAIN HARDENING RATIO
M^+	916	3960	0.02	300	0.04	1500	0.025
M^-	896	3960	0.02	400	0.04	1500	0.025

TABLE 5.2 MODEL PARAMETERS FOR ATALAY AND PENZIEN (1975) SPECIMEN #3

Due to the P-Δ effect, the strength of the specimen is expressed by the equivalent lateral load

$$H_{eq} = H + \frac{P \cdot \Delta}{h}$$

where H is the applied lateral load, P is the axial load, h is the column height and Δ is the lateral displacement. Fig. 5.5 shows the experimental and analytical equivalent lateral load-displacement relation of the specimen.

A careful study of the results of Fig. 5.5 leads to the following conclusions:

- The agreement between analytical model and experimental data is very good, except at the initial stages of the response. The pre-yield stiffness of the specimen is underestimated in the early stages of loading, because the model does not take into account the stiffness change between the uncracked and cracked state. The model uses instead a secant pre-yield stiffness, since emphasis is placed on predicting the response under large cyclic deformation reversals.
- The pinching effect due to the interaction of flexural cracks with bending moment and axial load and the interaction of diagonal cracks with shear and axial load is predicted satisfactorily. This effect is very important in the accurate prediction of the energy dissipation of column members.

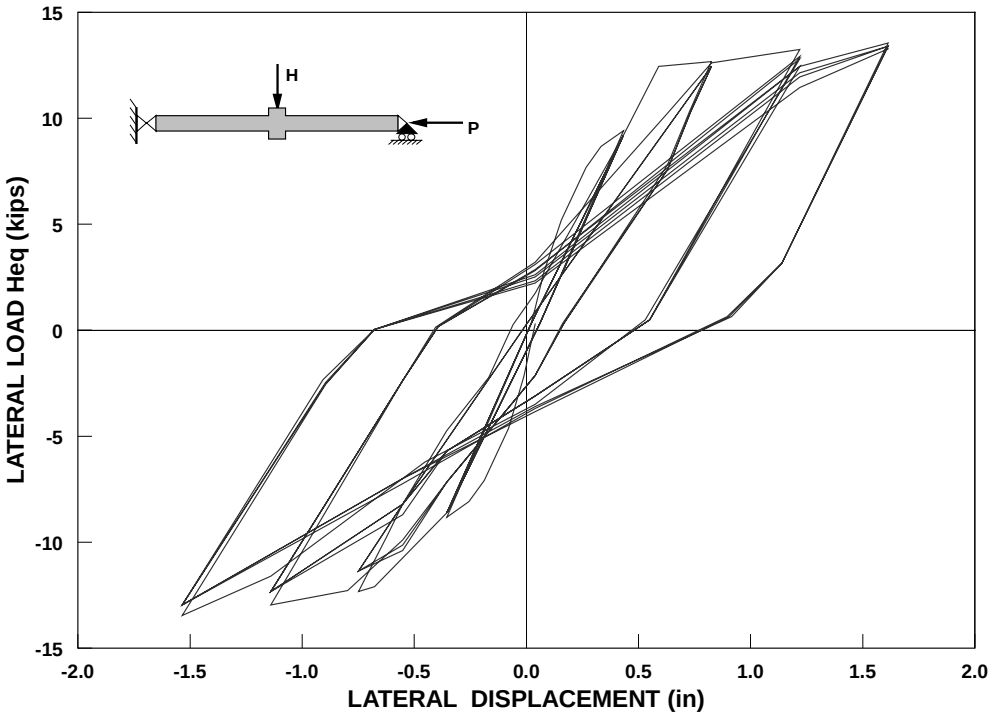

FIGURE 5.5A EXPERIMENTAL RESULTS OF LATERAL LOAD- DISPLACEMENT RELATION OF SPECIMEN #3 (ATALAY AND PENZIEN 1975)

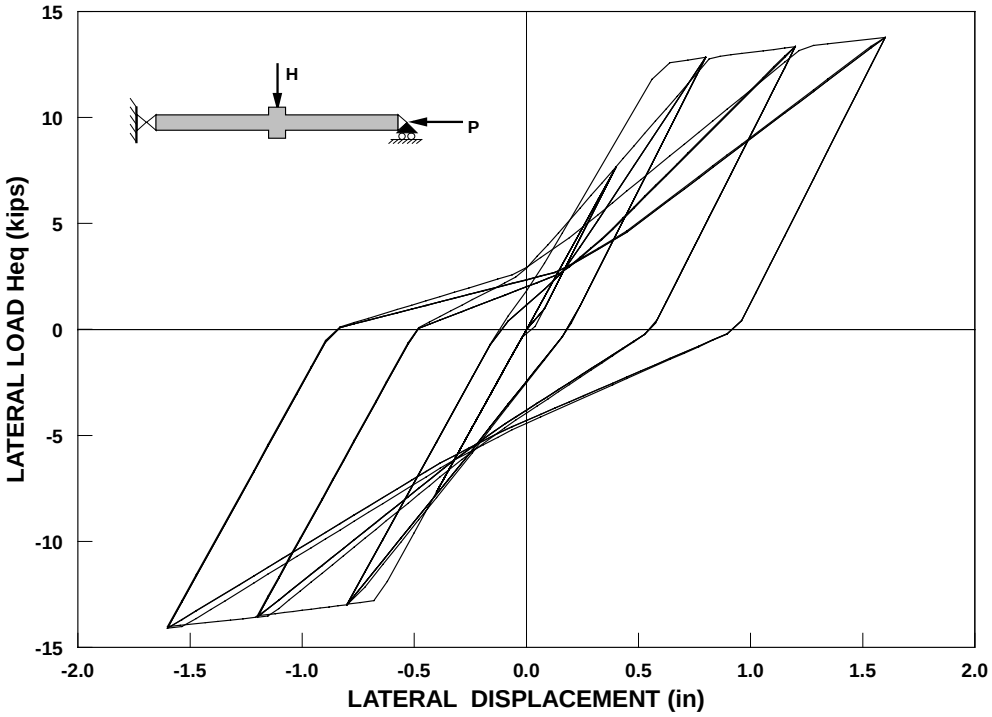

FIGURE 5.5B ANALYTICAL RESULTS OF LATERAL LOAD-DISPLACEMENT RELATION OF ATALAY AND PENZIEN (1975) SPECIMEN #3

CHAPTER 6

CORRELATION STUDIES OF NONLINEAR DYNAMIC RESPONSE OF SHAKING TABLE TEST FRAME

6.1 Introduction

The main purpose of the reinforced concrete frame model and the nonlinear analysis algorithm developed in this study is to allow an accurate prediction of the nonlinear dynamic behavior of reinforced concrete frame structures. To test the adequacy of the proposed frame model and the proposed analytical procedure in predicting the nonlinear dynamic response of frame structures, a complete study of a RC frame which was previously tested on the shaking table is conducted.

This chapter describes the correlation studies of the dynamic response of a one bay two story reinforced concrete frame structure subjected to a simulated strong seismic base motion. The test specimen referred to as RCF2 in Clough and Gidwani (1976) is a 0.7 scale model of a two story office building representative of common design and construction practice. The frame was designed, constructed, and tested by Clough and Gidwani (1976). It was designed according to the 1970 UBC (UBC, 1970) and the 1971 ACI (ACI, 1971) Codes of practice and the design was later verified with reference to the 1979 UBC Code in Blondet et al. (1980). The studies by Clough and Gidwani (1976) describe the philosophy and the procedures involved in the design of the frame structure. Information about material properties of concrete and reinforcing steel as well as other information regarding the test are given in Clough and Gidwani (1976) and will also be referred to in Appendix B, which discusses the derivation of the pertinent model parameters for the test frame.

The test structure was subjected to three consecutive ground acceleration histories on the shaking table at the University of California Berkeley. Each of these motions corresponds to the N69W Taft accelerogram record during the Arvin-Tahachapi earthquake of July 21, 1952, scaled to different peak accelerations, namely 0.095g, 0.57g, 0.65g (Fig. 6.1). These three tests were referred to as W1, W2, W3, respectively. In this study only the second test (W2) is considered, because it demonstrates the performance of a building in good condition when subjected to a ground motion severe enough to cause significant concrete damage and yielding of the reinforcing steel. At the start of the test the structure was slightly cracked from the first test (W1), as might represent the condition of actual structures in service.

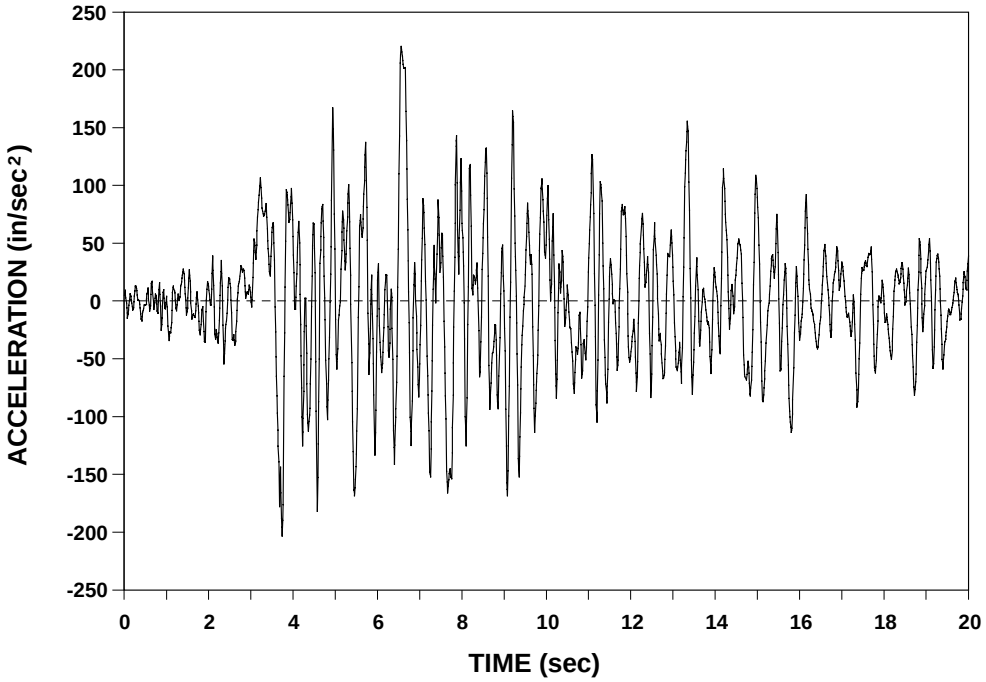

FIGURE 6.1 N69W TAFT ACCELEROGRAM RECORD, JULY 21, 1952, SCALED TO 0.57g

The seismic behavior of the structure is dominated by flexure accompanied by reinforcement slippage and is not much affected by shear and axial loads. This type of behavior is desirable in frame structures that will be subjected to seismic excitations. To represent this behavior, the elastic and spread plastic subelements are used to model flexure, while the joint subelement is used to model the pull-out of reinforcing steel from the base of the test specimen. The shear subelement is not activated in this study, since shear effects are negligible. Bond slippage of reinforcement in RC frames has been the focus of several research studies in the last years. The analytical studies in this chapter address the importance of this effect on the dynamic response of the test frame and methods of including this effect in a nonlinear frame model are discussed. In order to highlight the significance of the pull-out of reinforcing steel in the dynamic response of test frame RCF2, its response is first determined without the pull-out element and the results are subsequently compared with those of the complete model.

The one component model is in extensive use in the nonlinear dynamic analysis of RC frame structures. The analytical studies in this chapter investigate the accuracy of this model in connection with the local and global dynamic response of frame structures.

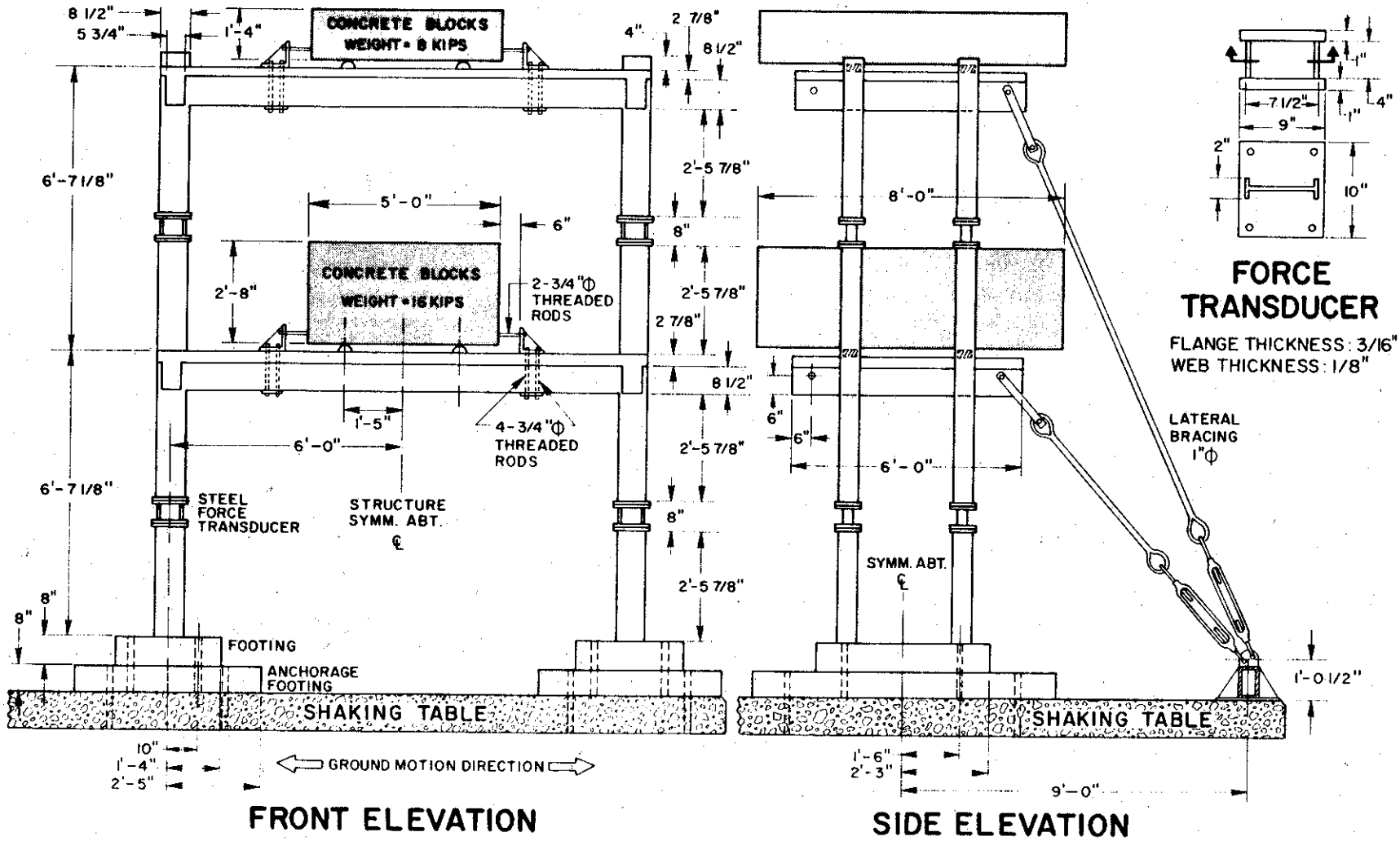

FIGURE 6.2 TEST STRUCTURE AND TEST ARRANGEMENT ON THE SHAKING TABLE OF RCF2 SPECIMEN BY CLOUGH AND GIDWANI (1976)

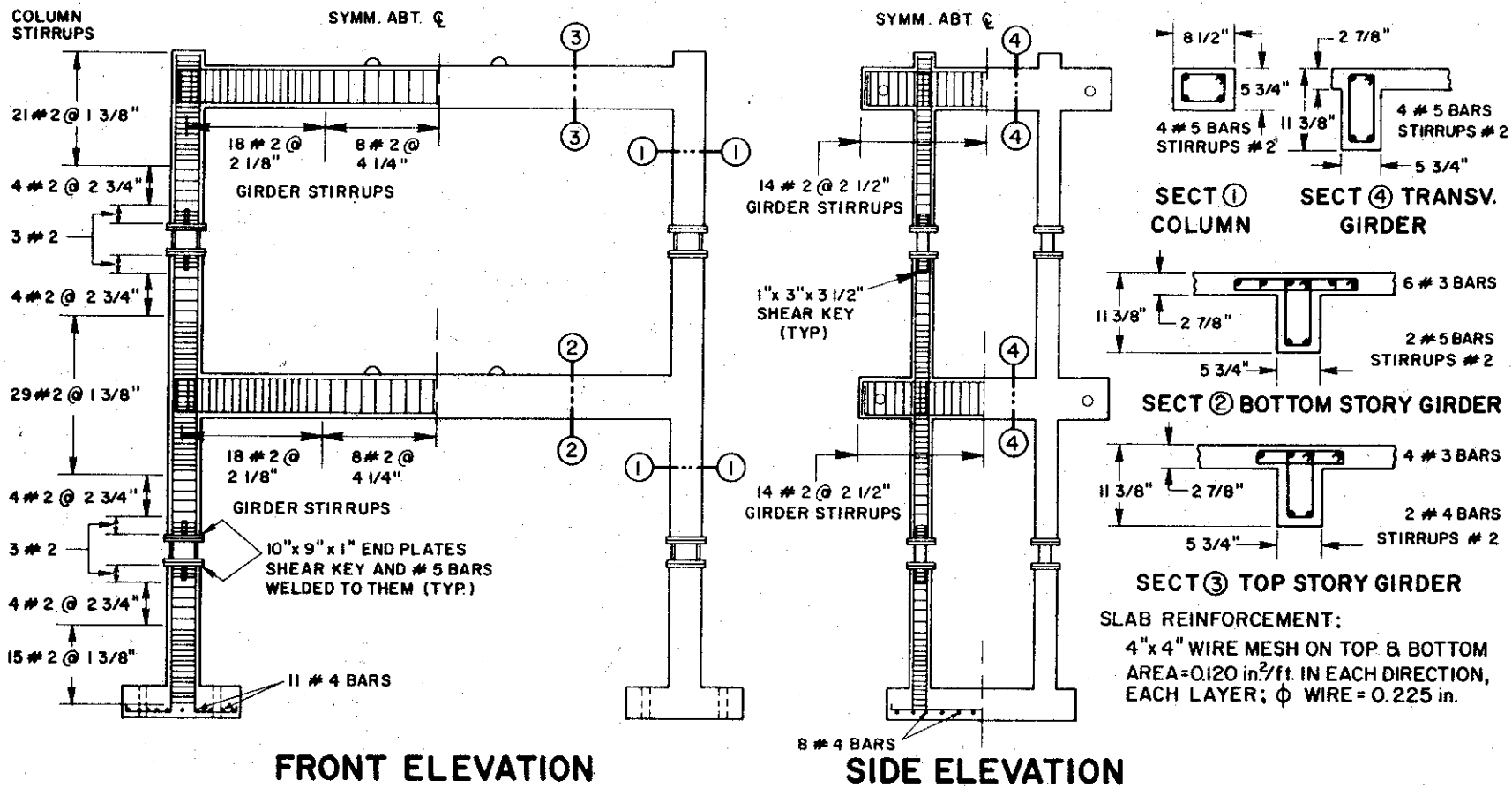

FIGURE 6.3 REINFORCEMENT DETAILS OF RCF2 SPECIMEN BY CLOUGH AND GIDWANI (1976)

6.2 Derivation of Member Properties of RCF2 Test Frame Model

The test structure and test arrangement on the shaking table as well as the reinforcing details of the test structure are shown in Figs. 6.2 and 6.3. A very difficult task in a correlation study between experimental and analytical results is the selection of model parameters that represent the physical state of the test specimen at the beginning of the test and can be derived in a rational manner from first principles of reinforced concrete design. Moreover, from a practical point of view the results of a correlation study are only meaningful, if the model parameters can be derived from information that is readily available during the design phase of a reinforced concrete structure without ad-hoc assumptions. This information pertains to the geometry of the structure and the physical and mechanical characteristics of the building materials.

The difficulty and importance of the task of parameter selection necessitate a more thorough discussion of this subject that is typically the case in similar correlation studies. This is the intent of the subsequent discussion in this chapter and the detailed calculations in Appendix B. Because of the inherent uncertainty about the physical state of the test specimen and the actual physical and mechanical characteristics of the materials in the built specimen, the attempt was made first to establish a reasonable range for each parameter value. This was accomplished with the information about the geometry of the test specimen and the actual material characteristics given by Clough and Gidwani (1976) using first principles of reinforced concrete design. Within this range a trial and error process led to the set of parameter values for each subelement that was used throughout the correlation studies of this chapter.

At the start of the second shaking table test W2 the test frame RCF2 was reportedly undamaged although slightly cracked. Thus, the selection of the initial stiffness of the members in the frame model depends on the state of cracking of the corresponding members in the test frame. While under uncracked conditions a RC member exhibits a stiffness equal to the gross or even transformed section value, this value drops to about one third and starts approaching the fully cracked stiffness value under widespread cracking in the member. The initial stiffness of the frame model establishes its fundamental period of vibration at the start of the test. In the case of test frame RCF2 the fundamental period at the start of the test is close to the range of period values with significant energy input of the base motion (Fig. 6.4). This “tuning” between test structure and base excitation makes the initial stiffness selection of the members in the model a determining factor of the quality of the nonlinear response correlation.

The selection was immensely aided by the thorough measurements of the overall stiffness of the test frame prior to the start of run W2 that were undertaken by Clough and Gidwani (1976). These tests consisted of the measurement of individual flexibility coefficients of the 2 by 2 condensed stiffness matrix of the two story test frame and of snap

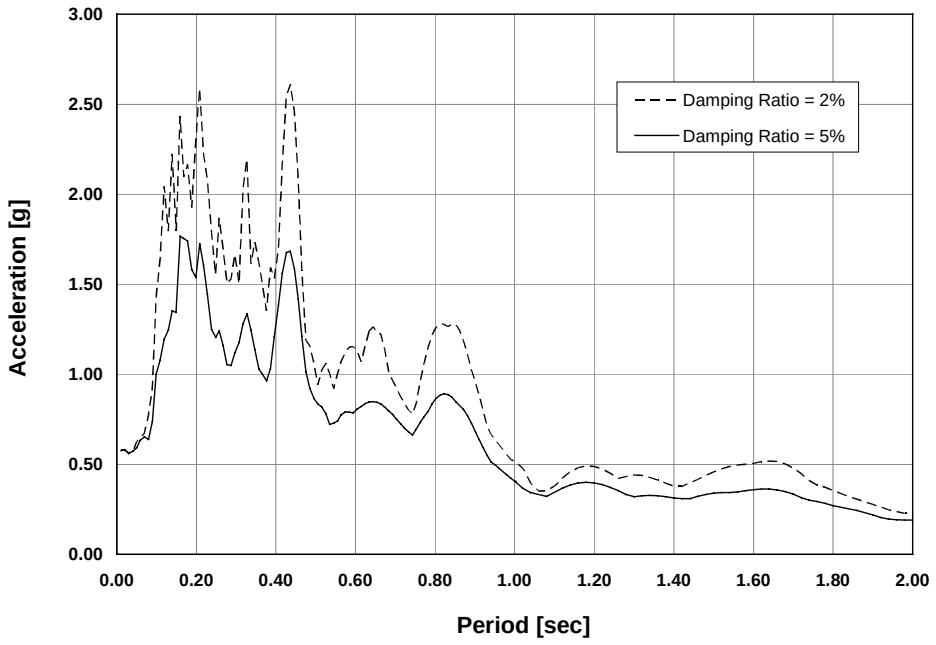

FIGURE 6.4 ACCELERATION RESPONSE SPECTRUM FOR SHAKING TABLE TEST W2

tests. The measured flexibility coefficients yield values of $f_1 = 1.92$ Hz and $f_2 = 6.06$ Hz for the first and second mode of vibration of the test frame, respectively. These values are lower than the corresponding values derived from the snap test which were $f_1 = 2.03$ Hz and $f_2 = 6.70$ Hz for the first and second mode of vibration, respectively. The discrepancy between these two sets of values averages about 6%, but no explanation for this deviation is offered by Clough and Gidwani (1976). At the end of test run W2 the corresponding frequency values from the snap test were $f_1 = 1.88$ Hz and $f_2 = 6.14$ Hz for the first and second mode of vibration, respectively, reflecting the occurrence of damage. This damage was mostly concentrated at the ends of the first story columns.

A study of the experimental results suggests that the snap tests values might be more reliable, and, so, it was decided to adopt the frequency values of $f_1 = 2.03$ Hz and $f_2 = 6.70$ Hz for the first and second mode of vibration, respectively, as the reference values to match. The initial stiffness of the girders and columns of the test frame was calculated with fully cracked moment of inertia and concrete modulus E_c equal to the mean value of those

measured in cylinder tests by Clough and Gidwani (1976). Calculation details are provided in Appendix B. With an initial stiffness equivalent to fully cracked conditions in all frame members the resulting frequency values were $f_1 = 2.19$ Hz and $f_2 = 5.73$ Hz for the first and second mode of vibration, respectively. The good agreement of these values with those measured in the snap tests before the start of shaking table test W2 gives confidence of the good representation of the actual state of the structure before test initiation.

RCF2 FRAME - BOTTOM STORY GIRDERS							
YIELD MOMENTS [k-in]		SPREAD PLASTICITY MODEL		CONCENTRATED PLASTICITY MODEL		JOINT	
		GIRDER MOMENT-CURVATURE RELATION		GIRDER MOMENT-ROTATION RELATION		MOMENT-ROTATION RELATION	
		INITIAL STIFFNESS [10^3 k-in^2/rad]	STRAIN HARDENING RATIO	INITIAL STIFFNESS [10^3 k-in/rad]	STRAIN HARDENING RATIO	INITIAL STIFFNESS [10^3 k-in/rad]	STRAIN HARDENING RATIO
M^+	232	1531	0.012	1531	0.025	200	0.04
M^-	720	1531	0.020	1531	0.038	200	0.04

TABLE 6.1 PARAMETER VALUES FOR BOTTOM STORY GIRDERS IN ANALYTICAL MODEL

RCF2 FRAME - TOP STORY GIRDERS							
YIELD MOMENTS [k-in]		SPREAD PLASTICITY MODEL		CONCENTRATED PLASTICITY MODEL		JOINT	
		GIRDER MOMENT-CURVATURE RELATION		GIRDER MOMENT-ROTATION RELATION		MOMENT-ROTATION RELATION	
		INITIAL STIFFNESS [10^3 k-in^2/rad]	STRAIN HARDENING RATIO	INITIAL STIFFNESS [10^3 k-in/rad]	STRAIN HARDENING RATIO	INITIAL STIFFNESS [10^3 k-in/rad]	STRAIN HARDENING RATIO
M^+	205	1188	0.012	1188	0.025	200	0.04
M^-	640	1188	0.020	1188	0.038	200	0.04

TABLE 6.2 PARAMETER VALUES FOR TOP STORY GIRDERS IN ANALYTICAL MODEL

The damping ratios that were measured in the snap tests before the start of shaking table test W2 were $\xi_1 = 5.77\%$ and $\xi_2 = 2.99\%$ for the first and second mode of vibration, respectively. At the completion of the shaking table test W2 these values had changed to

$\xi_1 = 6.56\%$ and $\xi_2 = 3.46\%$. According to Clough and Gidwani (1976) the greater increase in the damping ratio of the first mode of vibration indicates that the damage during the test was primarily concentrated in a deformation pattern that agrees with the first mode of vibration. In the analytical studies of this chapter a damping ratio of 5% of critical was assumed for the first two vibration modes.

The girder yield moments were determined by Clough and Gidwani (1976) and include the effective width of the floor slab and the effect of compression reinforcement. The values for the analytical studies in this chapter are identical to those reported by Clough and Gidwani (1976) and are summarized in Tables 6.1 and 6.2 for the bottom and top story girders, respectively.

RCF2 FRAME - BOTTOM STORY COLUMNS							
YIELD MOMENTS [k-in]		SPREAD PLASTICITY MODEL		CONCENTRATED PLASTICITY MODEL		JOINT	
		GIRDER MOMENT-CURVATURE RELATION		GIRDER MOMENT-ROTATION RELATION		MOMENT-ROTATION RELATION	
		INITIAL STIFFNESS [10^3 k-in^2/rad]	STRAIN HARDENING RATIO	INITIAL STIFFNESS [10^3 k-in/rad]	STRAIN HARDENING RATIO	INITIAL STIFFNESS [10^3 k-in/rad]	STRAIN HARDENING RATIO
M^+	208	390	0.03	390	0.05	50	0.04
M^-	208	390	0.03	390	0.05	50	0.04

TABLE 6.3 PARAMETER VALUES FOR BOTTOM STORY COLUMNS IN ANALYTICAL MODEL

RCF2 FRAME - TOP STORY COLUMNS							
YIELD MOMENTS [k-in]		SPREAD PLASTICITY MODEL		CONCENTRATED PLASTICITY MODEL		JOINT	
		GIRDER MOMENT-CURVATURE RELATION		GIRDER MOMENT-ROTATION RELATION		MOMENT-ROTATION RELATION	
		INITIAL STIFFNESS [10^3 k-in^2/rad]	STRAIN HARDENING RATIO	INITIAL STIFFNESS [10^3 k-in/rad]	STRAIN HARDENING RATIO	INITIAL STIFFNESS [10^3 k-in/rad]	STRAIN HARDENING RATIO
M^+	194	500	0.03	500	0.05	60	0.04
M^-	194	500	0.03	500	0.05	60	0.04

TABLE 6.4 PARAMETER VALUES FOR TOP STORY COLUMNS IN ANALYTICAL MODEL

For the yield strength of the columns one axial force-bending moment interaction diagram was presented by Clough and Gidwani (1976) and another, significantly different, diagram was presented in a later study by Blondet et al. (1980). Some of these differences are discussed in Appendix B. In the analytical studies of this chapter the latter interaction diagram by Blondet et al. (1980) was adopted, since it is more consistent with the experimental evidence and the actual behavior of the frame during the test.

Blondet et al. (1980) used two different sets of assumptions to arrive at an upper and lower bound of the column strength. The lower bound (denoted as case I in that study) was obtained with the nominal material properties of $f_c' = 4$ ksi for the concrete and $f_y = 40$ ksi for the reinforcing steel and with the introduction of a capacity reduction factor of $\varphi = 0.70$. The upper bound (case II) was obtained with an increase by 25% of the yield strength of the reinforcing steel (thus, $f_y = 50$ ksi) and by eliminating the capacity reduction factor.

The lower bound values of column section strengths (case I) are highly unrealistic, since the calculated ultimate column strength results in about 50% lower shear value than the maximum base shear measured during the shaking table tests. The upper bound values of column section strengths (case II) result in a base shear that is about 18% lower than the corresponding experimental value; the analytical studies of this chapter are, therefore, based on the assumptions on material properties of case II.

The determination of the column strength values is based on the commonly accepted assumptions about reinforced concrete behavior, as also recommended by current codes of practice, such as ACI and UBC: (a) plane sections remaining plane after deformation and thus resulting in linear strain distribution over the cross section; (b) the last assumption also implies perfect bond between reinforcing steel and surrounding concrete; (c) the ultimate strength is attained when the extreme concrete fiber in compression reaches a strain of 0.003; (d) the concrete stress distribution is replaced by a rectangular compressive block as recommended by ACI; and, (e) the stress-strain behavior of reinforcing steel is elasto-plastic.

The column flexural strength values used in the analytical studies of this chapter are derived for an axial force equal to the value that results from the action of gravity loads in the test frame. These values are assumed to be constant over the corresponding column height, since the reinforcement does not vary. These values are also assumed constant during the response time history, which is a reasonable approximation on account of the rather small overturning effect in the two story test frame with a small height to base width ratio. The strength values for the bottom and top story columns are listed in Table 6.3 and 6.4, respectively.

The parameters of the girder and column joint subelements are derived with a simple model that assumes an average effective bond stress along the bar anchorage, as

recommended on pg. 404 of the book by Park and Paulay (1975. The calculation details are presented in appendix B and the resulting stiffness values are summarized in Tables 6.1-6.4.

The values of the monotonic moment-curvature and moment-rotation relations in Tables 6.1-6.4 were derived by first principles and careful study of the experimental results. The strain hardening values of the moment-curvature relation for girders and columns are straightforward to calculate with the basic assumptions used in the determination of the ultimate strength of reinforced concrete sections. The strain hardening values of the joint moment-rotation relation can be obtained with the simple anchorage model by Filippou (1986). Further details of these calculations are provided in Appendix B, while the pertinent values used in the analyses of this chapter are listed in Tables 6.1-6.4. It is characteristic that the strain hardening values of all relations in Tables 6.1-6.4 vary over the small range from 0.012 to 0.05 in good agreement with the values used in previous related studies by Clough and Gidwani (1976) and Filippou and Issa (1988). These values are most profoundly affected by the strain hardening properties of the reinforcing steel, with bond representing the second most important effect.

6.3 Correlation with Experimental Results

In this section the correlations of the analytical results of the proposed model with experimental data of the two story one bay RCF2 test frame are presented. During the shaking table test W2 the specimen was subjected to simulated gravity loading, as shown in Fig. 6.5, and a shaking table signal that corresponded to the N69W Taft accelerogram record during the Arvin-Tahachapi earthquake of July 21, 1952 (Figs. 6.1 and 6.4). The Taft signal was amplified to yield a table motion with a peak acceleration of 0.57g which is strong enough to produce significant damage to the specimen. Moreover, the fundamental period of the test frame at the beginning of the test was approximately equal to 0.5 sec and, thus, was close to the period range of significant energy input of the ground motion, as can be concluded from the acceleration response spectrum in Fig. 6.2.

The small size of the test frame prevented the development of any significant table-test structure interaction, so that this effect is not included in the following analytical results.

The experimental data recorded during the test include the time history of the top and bottom story displacement, top and bottom story shear, and top story drift. In this section a comparison between these experimental data and the analytical results of the proposed model is presented.

The frame model used in the analytical studies consists of two girder and four column superelements. Each superelement, in general, consists of an elastic subelement, spread

plastic subelement, joint subelement, and shear subelement. Since, however, the response of this particular structure is dominated by flexure and pull-out from the base, while shear effects are negligible, the shear subelement is not activated in the following analytical studies.

The following response histories are compared with experimental data:

1. The top floor displacement response history (Fig. 6.6a)
2. The bottom floor displacement response history (Fig. 6.6b)
3. The top interstory drift response history (Fig. 6.6c)
4. The top story shear response history (Fig. 6.6d)
5. The bottom story shear response history (Fig. 6.6e)

A careful study of the results in Fig. 6.6 leads to the following observations:

(1) In general, very satisfactory agreement between experimental and analytical results is observed. The period and general wave form of the response is predicted well with the proposed model. This is an indication that the model represents well the actual strength and stiffness of the structure. In particular, the following model features are instrumental for the good agreement between analytical and experimental results:

   (a) the strain hardening stiffness of the members is not constant but decreases as the loading increases;

   (b) because of the coupling effect between the two ends of each member, the hysteretic moment-rotation relation at each member end changes with the loading history of the structure. The moment-rotation relation at one end of the member depends on section stiffness and plastic zone length at the other end;

   (c) the post yield stiffness of the model is not based on the assumption that the point of inflection is fixed at the midspan of the member as the one component model requires. The post yield stiffness of each member varies with the actual moment distribution during the response time history;

   (d) the bond deterioration and slippage of reinforcing steel is taken into account as a major source of energy dissipation;

   (e) the hysteretic behavior of the members accounts for the stiffness degradation due to the opening and closing of the cracks and the slip of reinforcing steel.

(2) The analytical model is capable of predicting very well the displacement response of the structure (Figs. 6.6a-6.6c). The results correlate better for the top and bottom displacement time history than for the top story drift response history, since interstory drift is the differential of two displacement values.

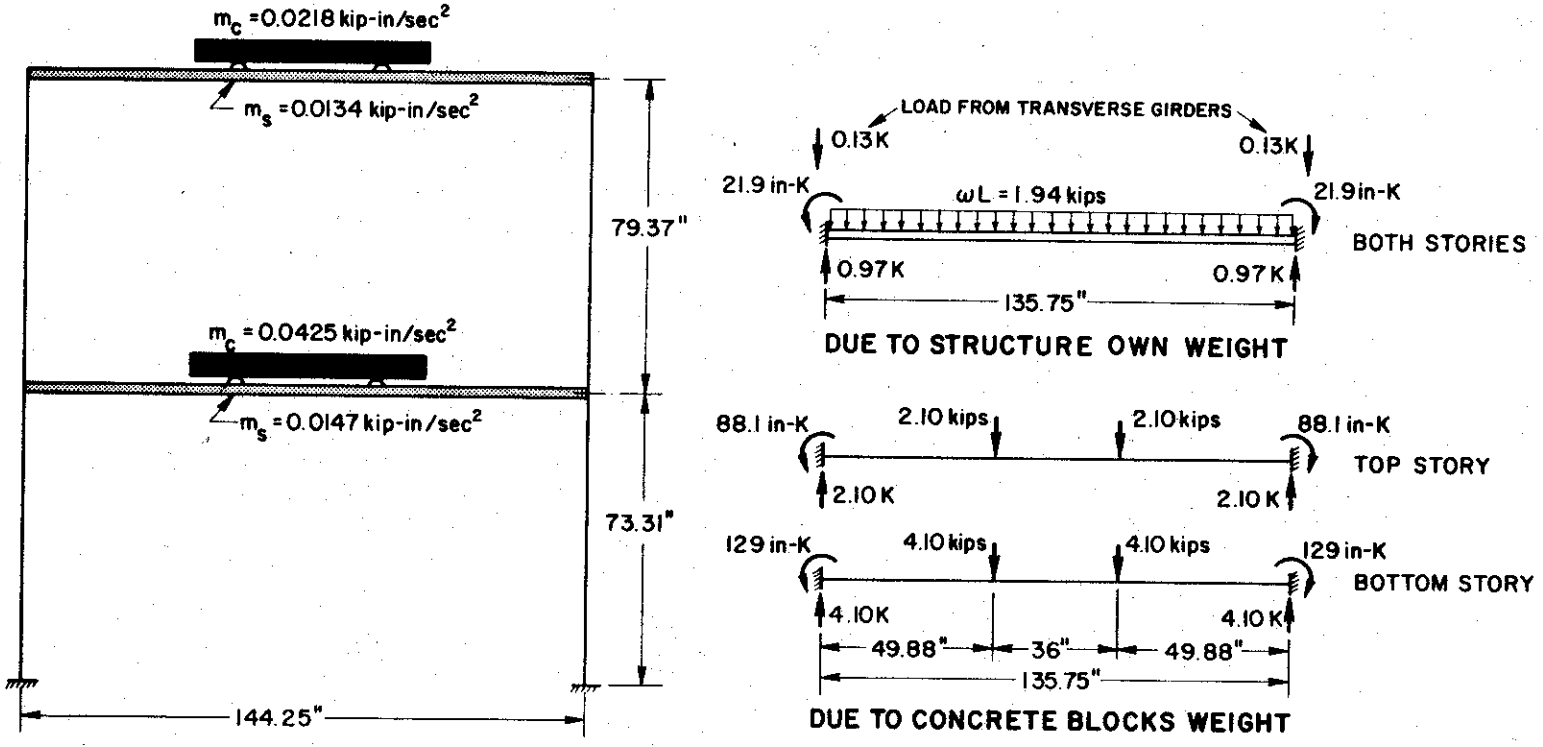

STRUCTURE IDEALIZATION

ASSUME AXIS TO AXIS DIMENSIONS FOR STRUCTURAL ANALYSIS
m_s = STRUCTURE STORY MASS, ASSUMED TO BE LUMPED AT FLOOR LEVEL
m_c = MASS FROM CONCRETE BLOCKS AND ATTACHEMENTS

GRAVITY LOAD FOR EACH GIRDER

ASSUME CLEAR DISTANCE DIMENSIONS TO COMPUTE MOMENTS

FIGURE 6.5 GRAVITY LOAD AND MASS DISTRIBUTION OF RCF2 SPECIMEN BY CLOUGH AND GIDWANI (1976)

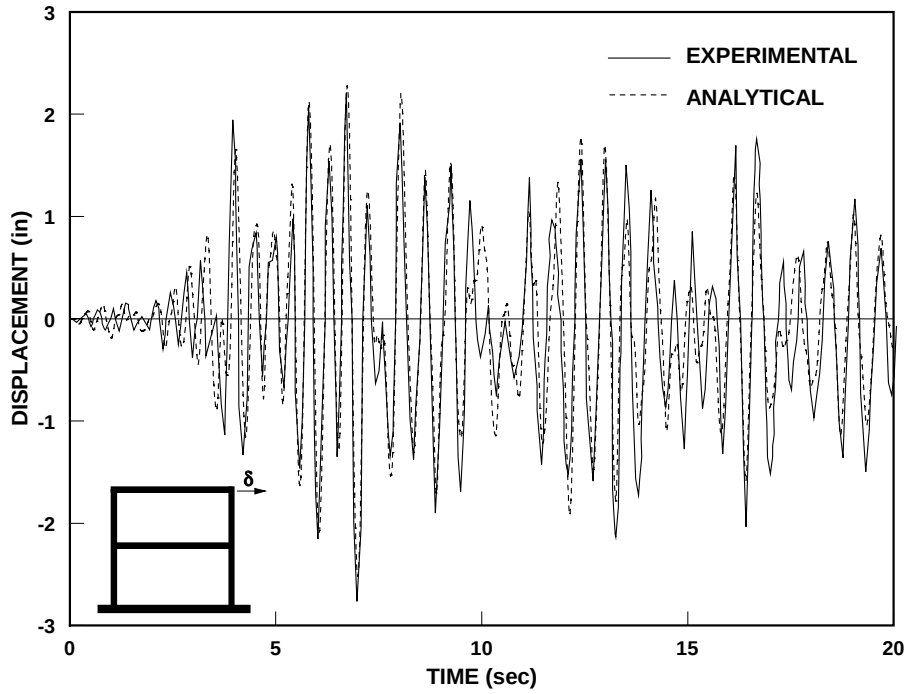

FIGURE 6.6A COMPARISON BETWEEN EXPERIMENTAL AND ANALYTICAL RESPONSE HISTORY OF TOP STORY DISPLACEMENT

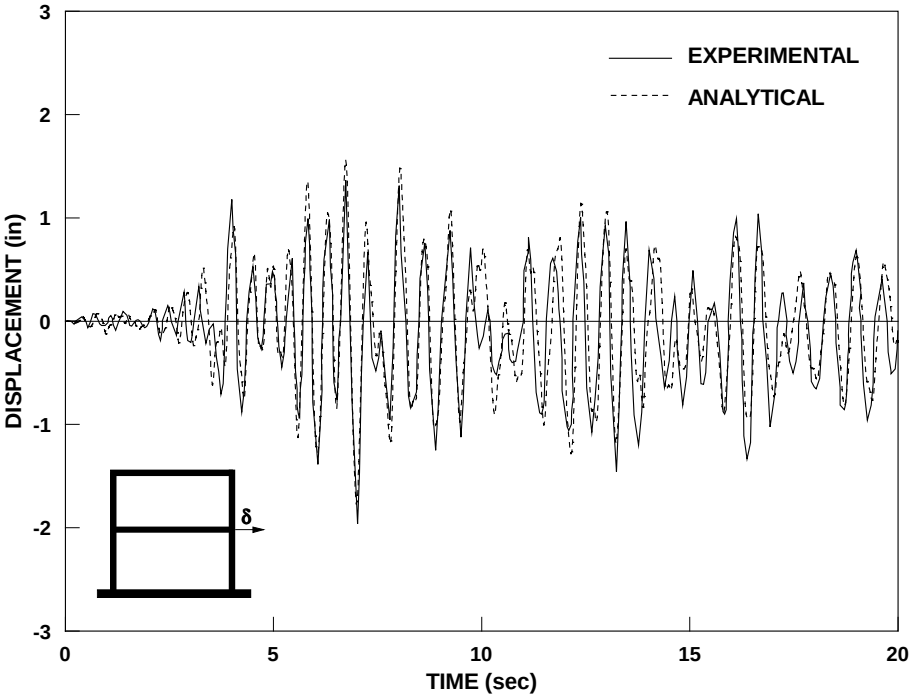

FIGURE 6.6B COMPARISON BETWEEN EXPERIMENTAL AND ANALYTICAL RESPONSE HISTORY OF BOTTOM STORY DISPLACEMENT

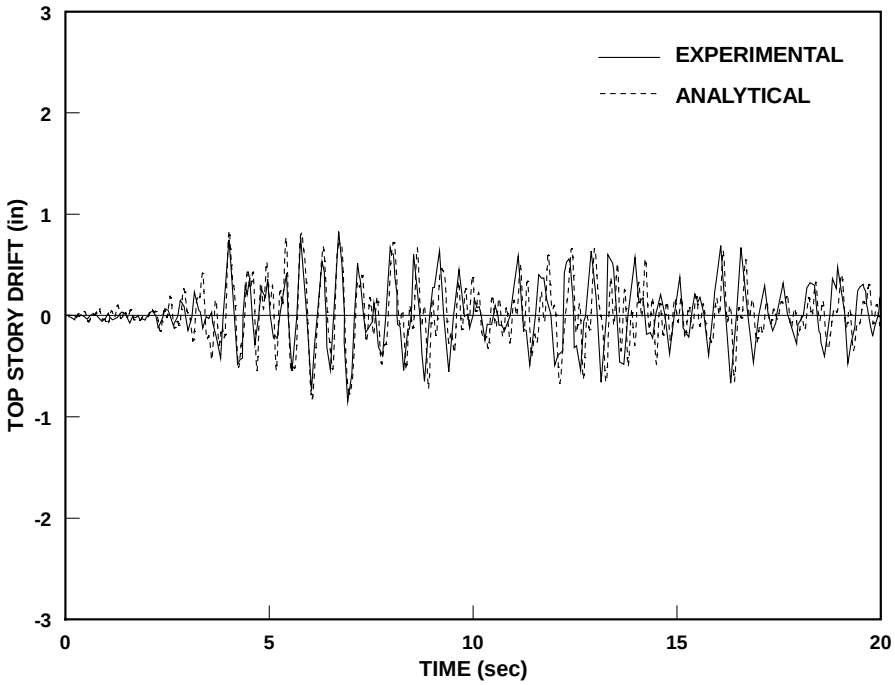

FIGURE 6.6C COMPARISON BETWEEN EXPERIMENTAL AND ANALYTICAL RESPONSE HISTORY OF TOP STORY DRIFT

(3) Although the analytical prediction of the forces that arise in the structure agrees satisfactorily with experimental data (Figs. 6.5d and 6.5e), this agreement is not as good as that observed in the displacement response time history. This might be due to the questionable reliability of the experimental values of the shear response time history, as noted by Clough and Gidwani (1976).

(4) The higher mode effects are much more prominent in the top story shear than in the bottom story shear response history (Figs. 6.5d and 6.5e).

(5) The maximum response of the structure correlates very well in the top and bottom story displacement, drift, and story shear response.

(6) Although the model performed very satisfactorily in predicting the dynamic response of the frame structure, a slight phase shift at some stage of the response, and a discrepancy in the response at the last few cycles of the time history are observed (Fig. 6.6). This discrepancy can be attributed to the following facts:

   (a) The limitations of the model that arise from inadventent simplification of the actual behavior.

   (b) The complexity of the behavior of the reinforced concrete structure and the uncertainty in the measurement of material properties and in the data acquisition during the test.

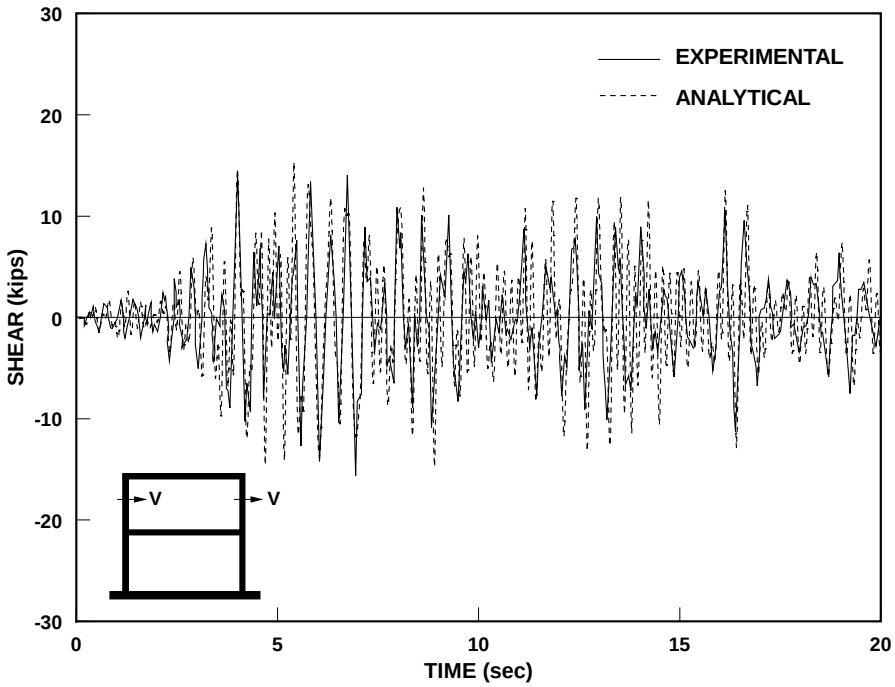

FIGURE 6.6D COMPARISON BETWEEN EXPERIMENTAL AND ANALYTICAL RESPONSE HISTORY OF TOP STORY SHEAR

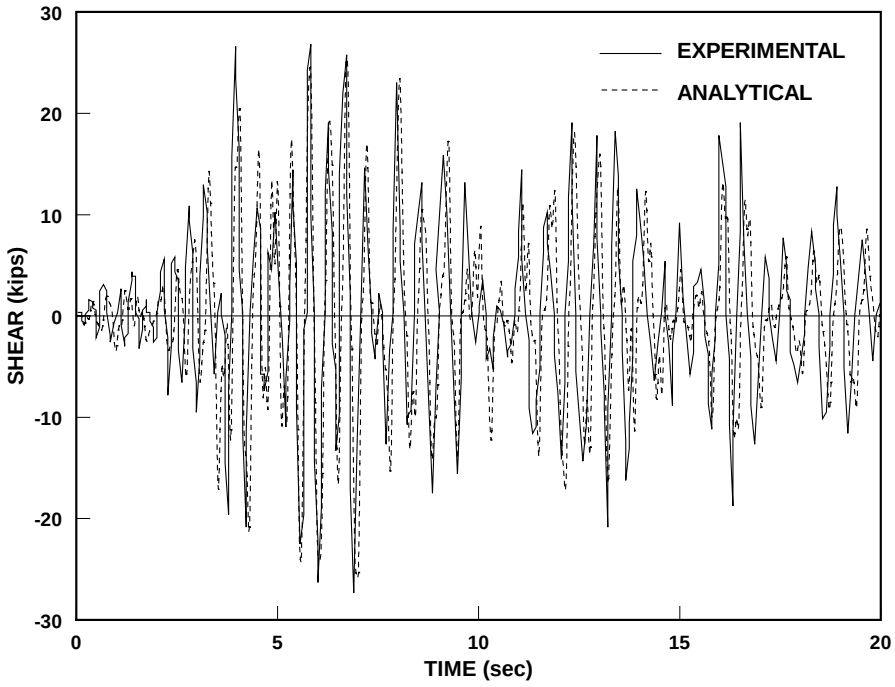

FIGURE 6.6E COMPARISON BETWEEN EXPERIMENTAL AND ANALYTICAL RESPONSE HISTORY OF BOTTOM STORY SHEAR

6.4 Analytical Parametric Studies

After establishing the ability of the proposed model to accurately describe the global and local dynamic response of reinforced concrete frame structures, further analytical studies are conducted in the following. First, the sensitivity of the dynamic response of the test structure RCF2 to the effects of bond slip of reinforcing bars is studied. To accomplish this the dynamic response of the reinforced concrete frame without including the effects of bond slip is compared with the results obtained when bond slip effects are taken into account. Secondly, the ability of the one component model to predict the global and local dynamic response of the test structure RCF2 is investigated by comparing the results for the concentrated plasticity model with those of the spread plasticity model. This comparison is particularly important in view of the wide-spread use of the concentrated plasticity model in the nonlinear dynamic analysis of reinforced concrete frames in practice.

6.4.1 Effect of Reinforcing Bar Pull-Out on the Dynamic Response of Test Frame

This section is devoted to the study of the effects of reinforcement pull-out on the nonlinear dynamic response of test frame RCF2. The most important contribution of this effect arises at the base of the first story columns where the reinforcing bars pull-out from the base that was used to secure the test frame to the shaking table. In order to study the contribution of this effect on the local and global nonlinear dynamic response of the test frame two analyses were conducted: in the first analysis the effect of reinforcement pull-out was included with the aid of the joint subelement in column and girder members. Global response time histories were already compared to the experimental results in the previous section showing excellent agreement. In the second analysis the effect of reinforcement pull-out was excluded from the analysis by deactivating the joint subelement in all frame members. The comparison of the two sets of results is shown in Figs. 6.7-6.10.

Fig. 6.7 shows the dynamic response of the structure to the N69W Taft accelerogram record during the Arvin-Tahachapi earthquake of July 21, 1952, scaled to a peak acceleration of 0.57g. This corresponds to the shaking table test W2 of the two story one bay test frame RCF2. Fig. 6.7 contains the following plots

1. the top floor displacement history (Fig. 6.7a),
2. the bottom floor displacement history (Fig. 6.7b),
4. the top story shear history (Fig. 6.7c),
5. the bottom story shear history (Fig. 6.7d).

Fig. 6.7a shows that maximum top story displacement is about 50% larger when the effect of pull-out from the base is included. The response of the model without the joint

subelement clearly shows the higher stiffness of the system, as reflected by the increase of the fundamental period of the model that includes the joint subelement.

The difference in the displacement time history is equally pronounced for the bottom story displacement in Fig. 6.7b. In fact, a comparison of Fig. 6.7a with Fig. 6.7b reveals that the absolute difference of the maximum displacement between the case which includes the pull-out effect and the case which does not is approximately the same for the top and bottom story displacement. This proves that most of the inelastic deformation of the two story test frame arises in the bottom story and that the effect of joint rotations is almost exclusively concentrated at the base of the frame in the form of pull-out deformations from the footing.

The displacement time histories in Figs. 6.7a and b reveal that the response of the model which does not include the joint rotations dies out in the last five seconds of the test. By contrast, the model that includes the effect of joint rotations continues to respond strongly to the base signal, in good agreement with experimental evidence, where this effect is, in fact, even more pronounced in Figs. 6.6a and b. It is of interest to note that previous studies that have dealt with the dynamic response of test frame RCF2 have failed to capture this effect, because of their inability to correctly represent the different mechanisms of energy dissipation, damage and stiffness deterioration of the frame members.

Figs. 6.7c and d show that the top and bottom story shear is not much affected by the effect of pull-out. Only a slight increase in story shear results when the effect of pull-out is included in the analysis. This is not surprising when the story shear force is regarded as the product of stiffness and interstory displacement. The inclusion of joint rotations increases the fundamental period of the frame and results in larger story displacements, while, at the same time, it decreases the lateral story stiffness. These two effects appear to cancel out in the case of test frame RCF2, so that the inclusion of joint rotations does not affect much the maximum story shear, as is evident in Figs. 6.7c and d.

Figs. 6.8-6.10 provide further details on the response of test frame RCF2. Fig. 6.8 shows the hysteretic relation between top story displacement and bottom story shear. The out-of-phase character of these two variables results in a very irregular relation, which nonetheless shows clearly the difference in energy dissipation between the model that includes the effect of joint rotations and the model that does not. Fig. 6.9 shows the hysteretic relation between bottom story displacement and bottom story shear and is a direct reflection of the hysteretic behavior of the bottom story where most damage takes place in test frame RCF2, as is further corroborated by Fig. 6.10, which depicts the hysteretic behavior of the top story that sustained very little damage. The characteristic “pinching” effect of the hysteretic relation by the inclusion of the pull-out from the base of test frame RCF2 is evident in Fig. 6.9a.

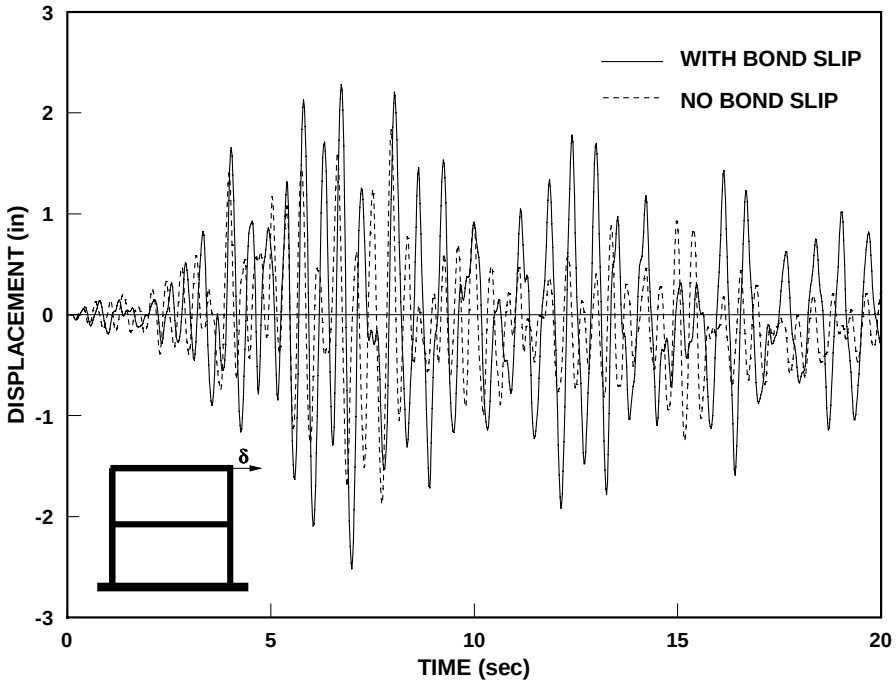

FIGURE 6.7A EFFECT OF BOND SLIP ON FRAME RESPONSE HISTORY OF TOP STORY DISPLACEMENT

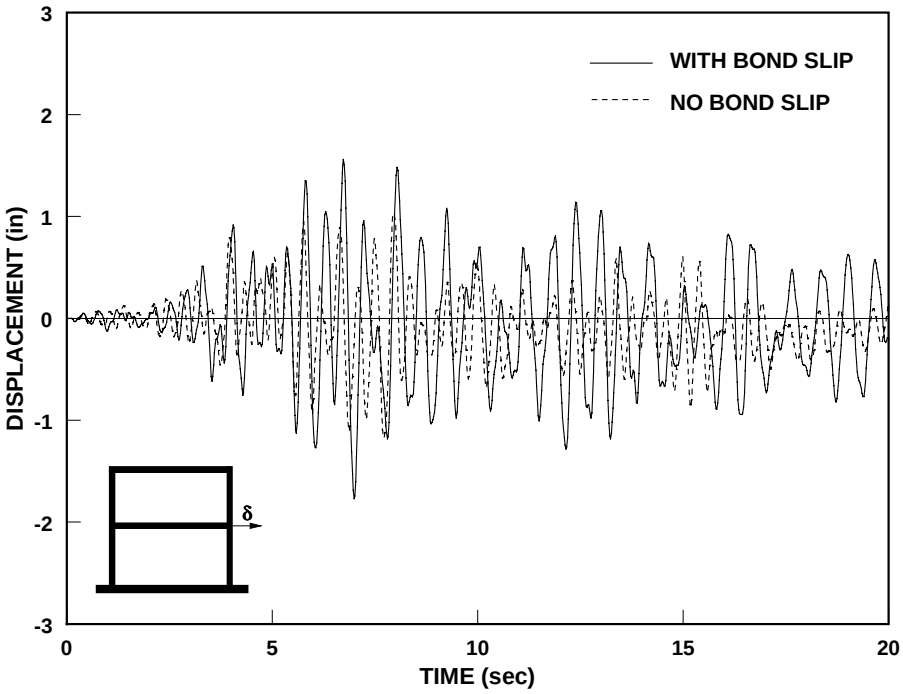

FIGURE 6.7B EFFECT OF BOND SLIP ON FRAME RESPONSE HISTORY OF BOTTOM STORY DISPLACEMENT

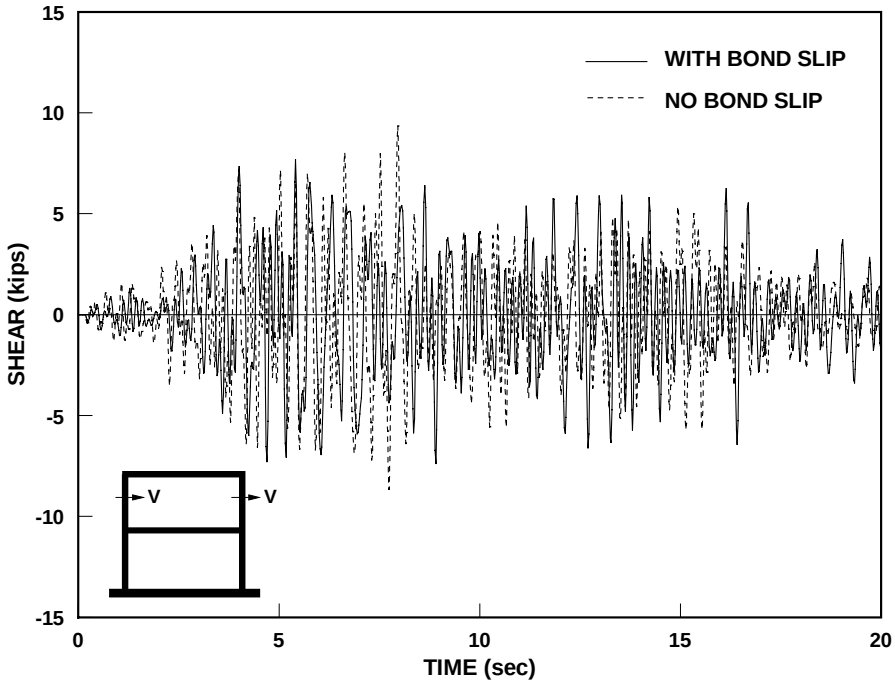

FIGURE 6.7C EFFECT OF BOND SLIP ON FRAME RESPONSE HISTORY OF TOP STORY SHEAR

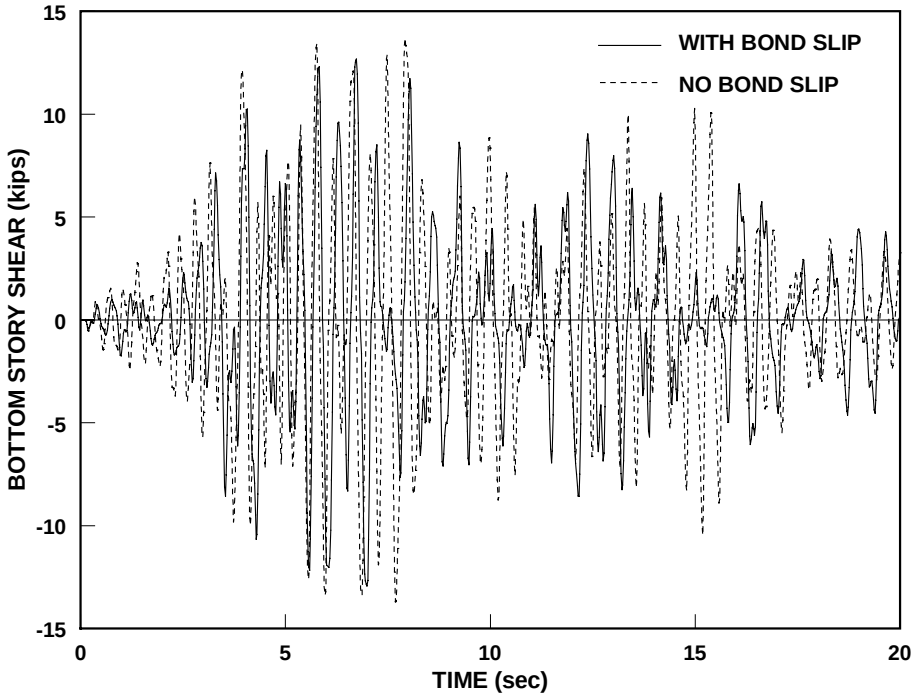

FIGURE 6.7D EFFECT OF BOND SLIP ON FRAME RESPONSE HISTORY OF BOTTOM STORY SHEAR

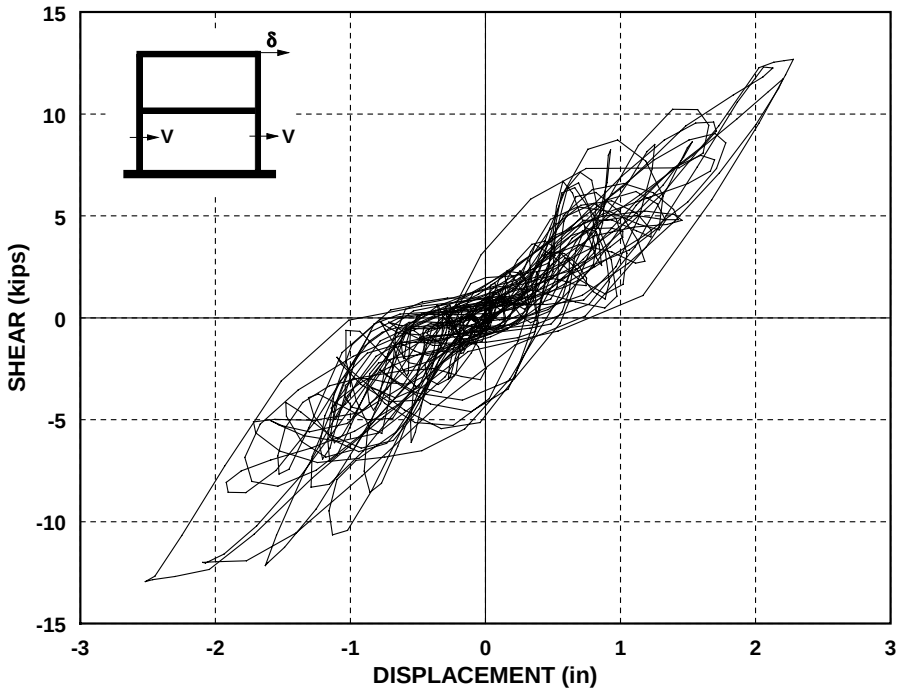

FIGURE 6.8A EFFECT OF PULL-OUT ON BOTTOM STORY SHEAR-TOP STORY DISPLACEMENT HYSTERETIC RELATION - WITH PULL-OUT

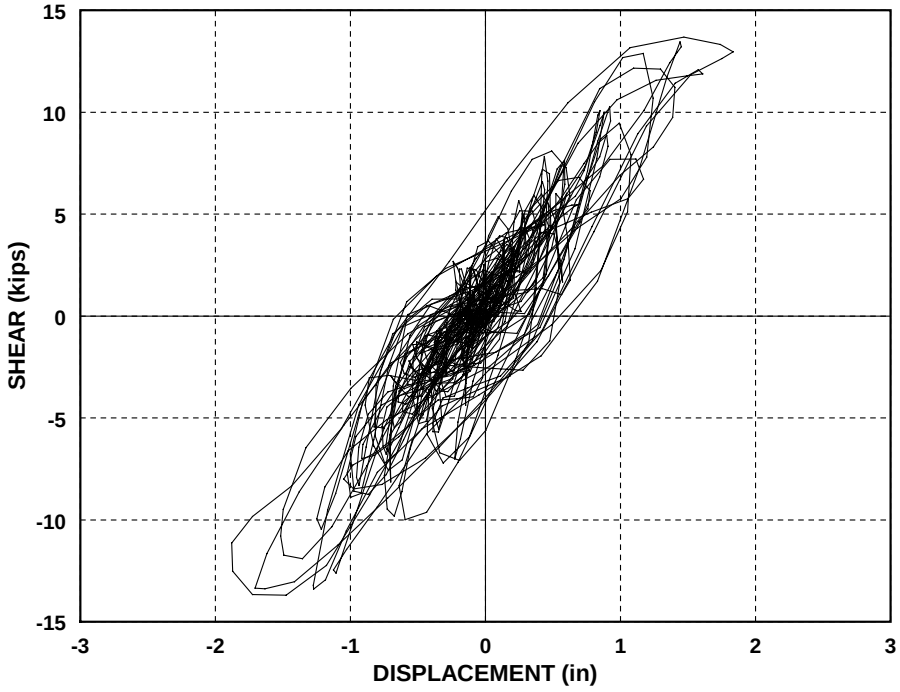

FIGURE 6.8B EFFECT OF PULL-OUT ON BOTTOM STORY SHEAR-TOP STORY DISPLACEMENT HYSTERETIC RELATION - NO PULL-OUT

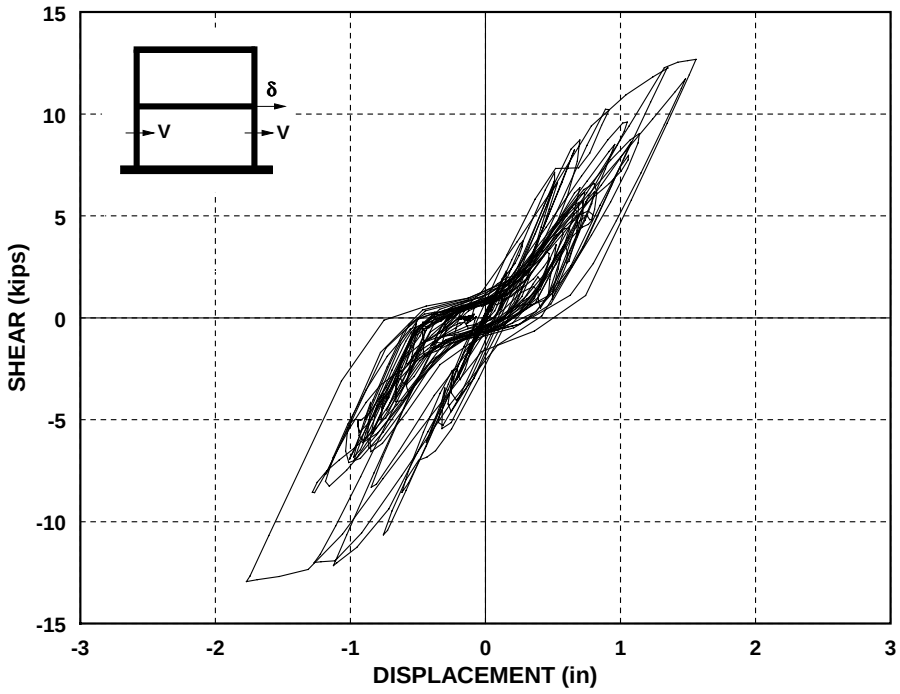

FIGURE 6.9A EFFECT OF PULL-OUT ON BOTTOM STORY SHEAR-BOTTOM STORY DISPLACEMENT HYSTERETIC RELATION -WITH PULL-OUT

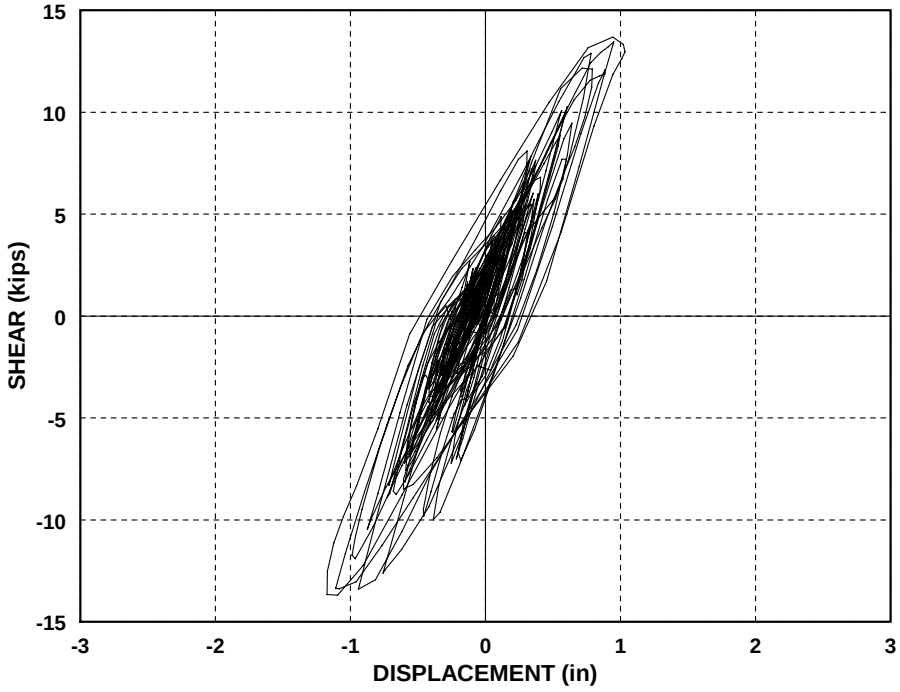

FIGURE 6.9B EFFECT OF BOND SLIP ON BOTTOM STORY SHEAR-BOTTOM STORY DISPLACEMENT HYSTERETIC RELATION - NO PULL-OUT

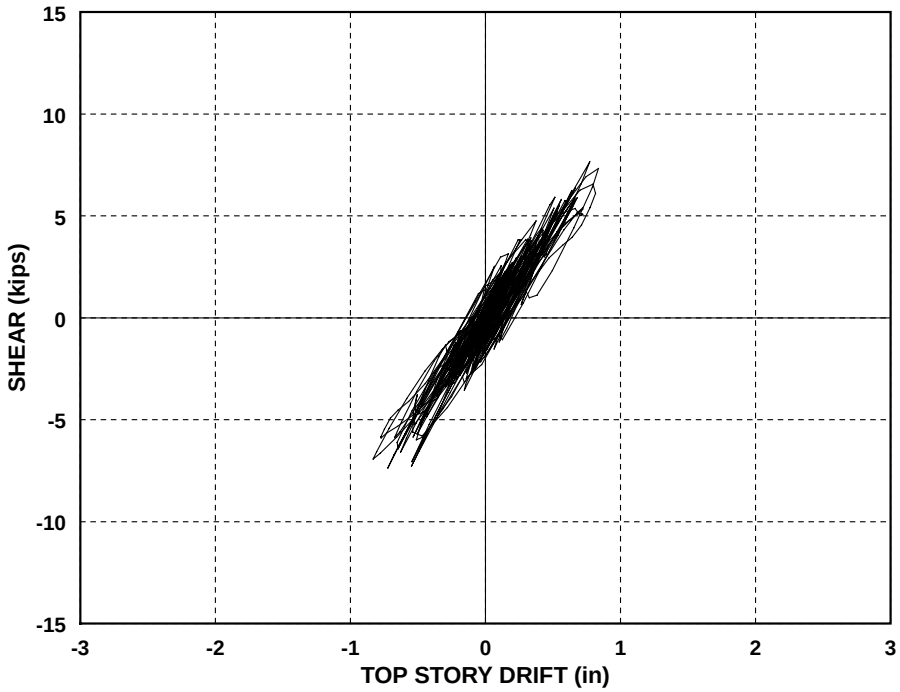

FIGURE 6.10A EFFECT OF PULL-OUT ON TOP STORY SHEAR-TOP STORY DRIFT HYSTERETIC RELATION - WITH PULL-OUT

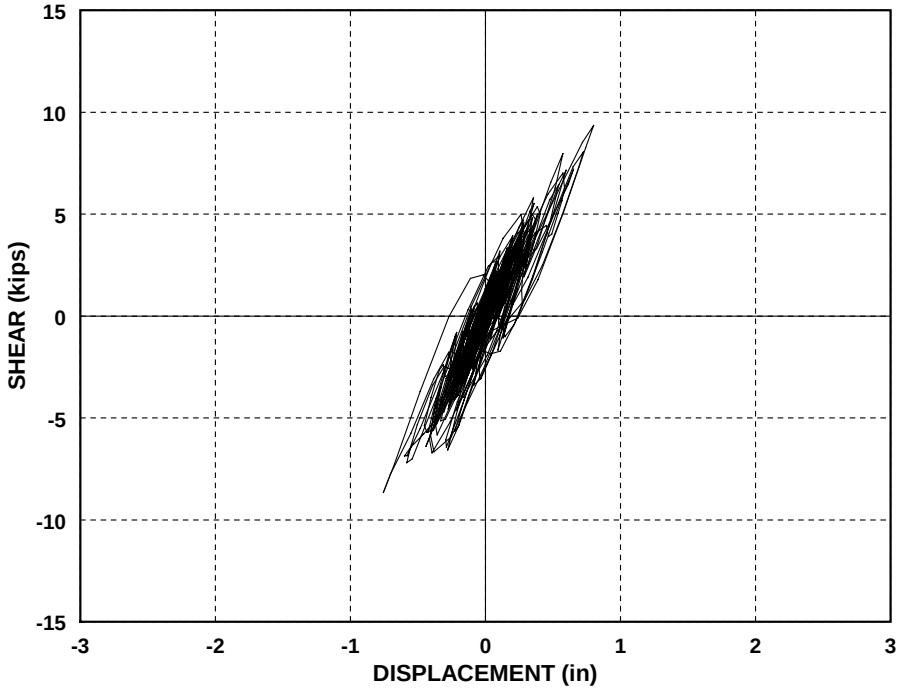

FIGURE 6.10B EFFECT OF PULL-OUT ON TOP STORY SHEAR-TOP STORY DRIFT HYSTERETIC RELATION - NO PULL-OUT

6.4.2 Comparison of Concentrated Plasticity with Spread Plasticity Model

The one component model is in widespread use in the nonlinear dynamic analysis of reinforced concrete frame structures in practice. This section is devoted to studying the ability of the one component model to predict the nonlinear dynamic response of the frame structure RCF2. The dynamic response of frame RCF2 to the 1952 N69W Taft ground motion with a peak acceleration of 0.57g is evaluated using the one component model and the results are compared with those of the spread plasticity model, since these were shown to correlate well with experimental evidence. The accuracy of the concentrated plasticity model in predicting the nonlinear dynamic response of the frame structure can be studied by replacing the spread plasticity subelement with the concentrated plasticity subelement.

The first question to be considered in connection with the concentrated plasticity model is the selection of appropriate values for describing the monotonic moment-rotation relation. The most sensitive and difficult task is the selection of the post yield stiffness of the model. This procedure has been described in detail in Section 2.2.2.1. The strain hardening ratio of the different frame members is determined with this procedure and the values are listed in Tables 6.1 and 6.4. It is important to note that the quality of the analytical results of the model with the concentrated plasticity model depends on the rational determination of its stiffness parameters. The study by Filippou and Issa (1988) presents a parametric study of the effect of these parameters on the global and local response of RC frame subassemblages.

In comparing the ability of the concentrated and spread plasticity model to predict the inelastic flexural response of frame structures, the bond slippage of reinforcement is accounted for by the joint subelement, while the elastic subelement describes the linear elastic flexural behavior along the member. The parameters of the joint and the elastic subelement used in conjunction with the concentrated plasticity model are the same as those used with the spread plasticity model in the studies described in the previous section.

Figs. 6.11-6.14 present the analytical results of test frame RCF2 under the Taft ground acceleration record for the model with the one component model alongside those of the model with the proposed spread plasticity model. The figures show the time history and the global and local hysteretic behavior of the structure.

The following time histories are presented in Fig. 6.11:

1. top floor displacement (Fig. 6.11a),
2. bottom floor displacement (Fig. 6.11b),
3. interstory drift of top story (Fig. 6.11c),
4. top story shear time history (Fig. 6.11d), and
5. bottom story shear (Fig. 6.11e).

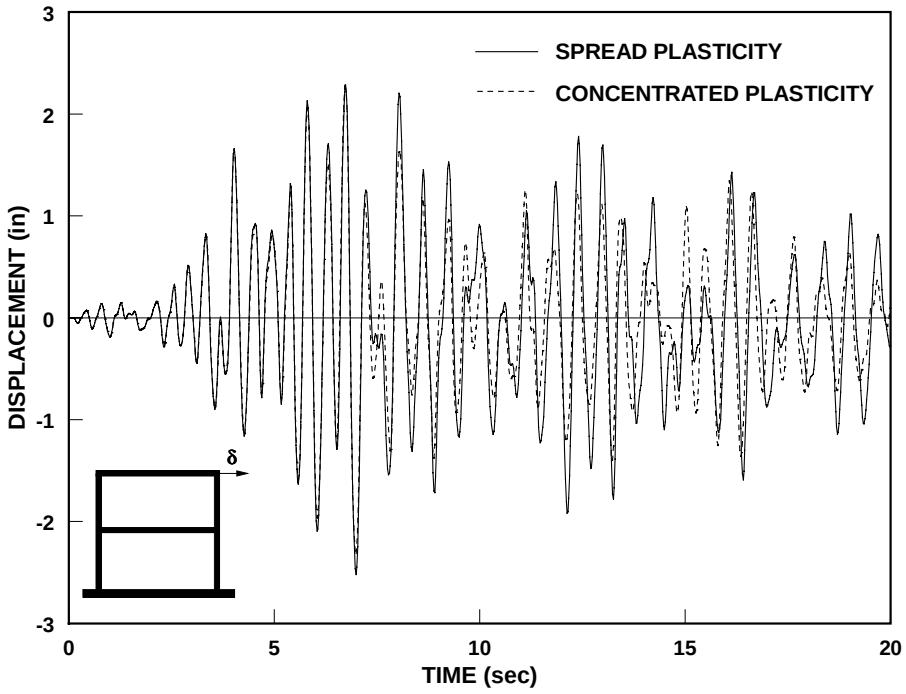

FIGURE 6.11A COMPARISON BETWEEN SPREAD PLASTICITY AND CONCENTRATED PLASTICITY MODELS OF TOP STORY DISPLACEMENT

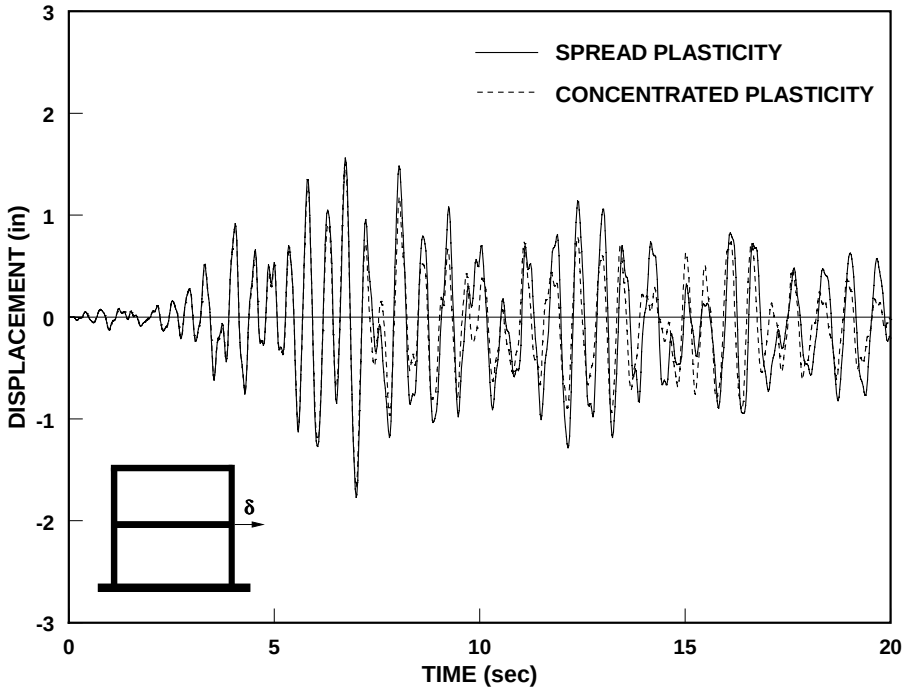

FIGURE 6.11B COMPARISON BETWEEN SPREAD PLASTICITY AND CONCENTRATED PLASTICITY MODELS OF BOTTOM STORY DISPLACEMENT

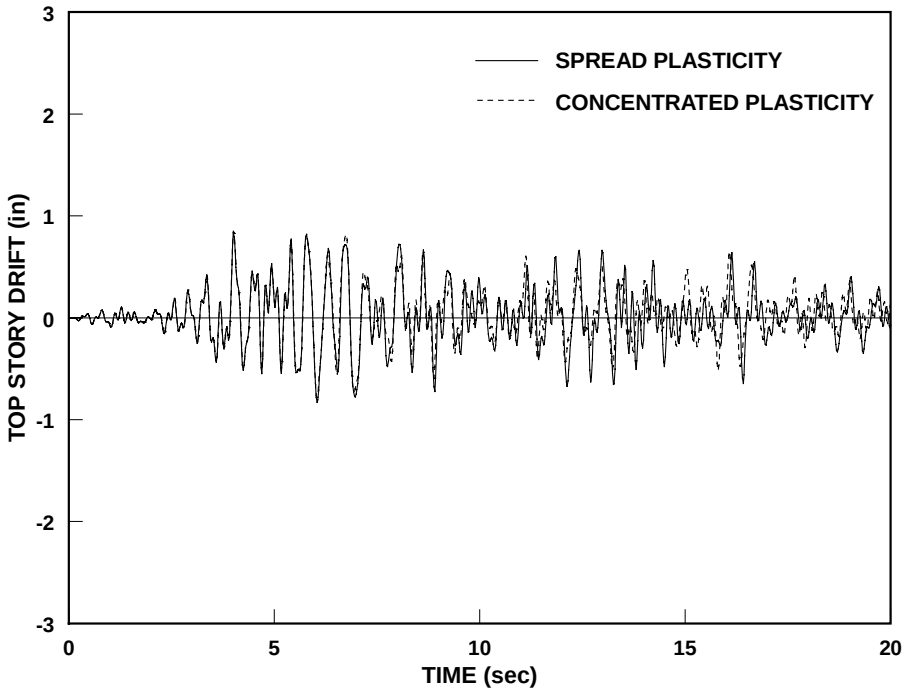

FIGURE 6.11C COMPARISON BETWEEN SPREAD PLASTICITY AND CONCENTRATED PLASTICITY MODELS OF TOP STORY DRIFT

In examining Figs. 6.11-6.14 one should keep in mind that both the spread plasticity and the concentrated plasticity model are used in conjunction with the joint subelement which accounts for the effect of reinforcement slip in the joints and the pull-out from the base of the structure. The following conclusions can be drawn from Fig. 6.11:

(1) Both, the maximum story displacements as well as the maximum story shear values are nearly the same in the two models. Clearly, the careful selection of parameters for the moment-rotation relation of the one component model leads to very satisfactory results under dynamic response conditions.

(2) There is only a notable deviation in the post-peak response of the two models. In fact, the severity of the inelastic excursions in more pronounced for the model with the spread plasticity element, as can be noted in the last ten seconds of the dynamic response in Figs. 6.11a and b. This is also true for the bottom story shear history in Fig. 6.11e.

(3) There is good agreement in the hysteretic behavior of the two models, even though Fig. 6.13 shows a more pronounced “pinching” of the bottom story shear-displacement response for the model with the spread plasticity model. This is due to differences in the reloading stiffness of the two models and the lack of any coupling between the two inelastic end zones of the member in the concentrated plasticity model.

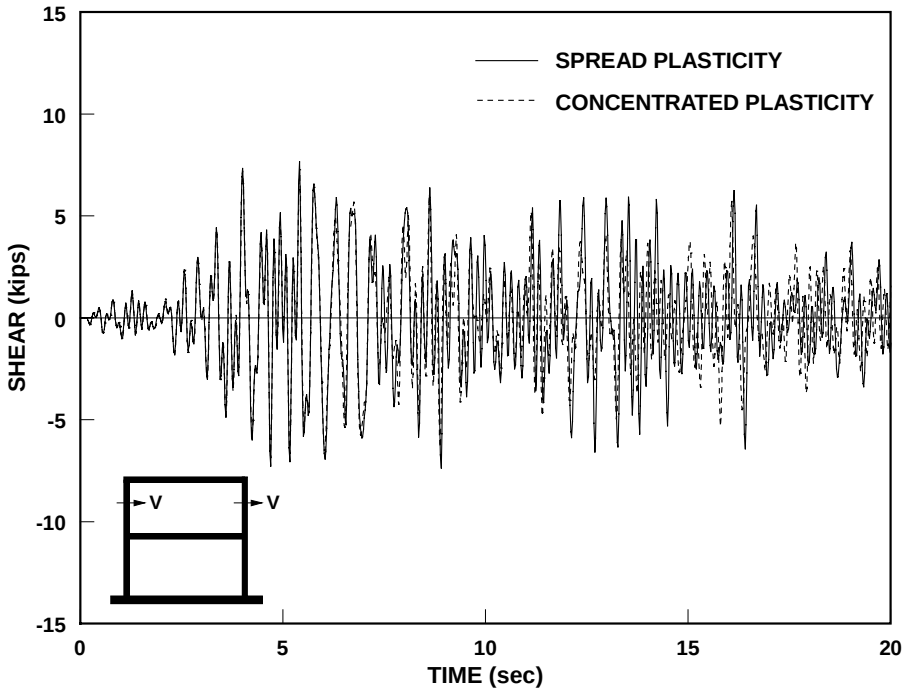

FIGURE 6.11D COMPARISON BETWEEN SPREAD PLASTICITY AND CONCENTRATED PLASTICITY MODELS OF TOP STORY SHEAR

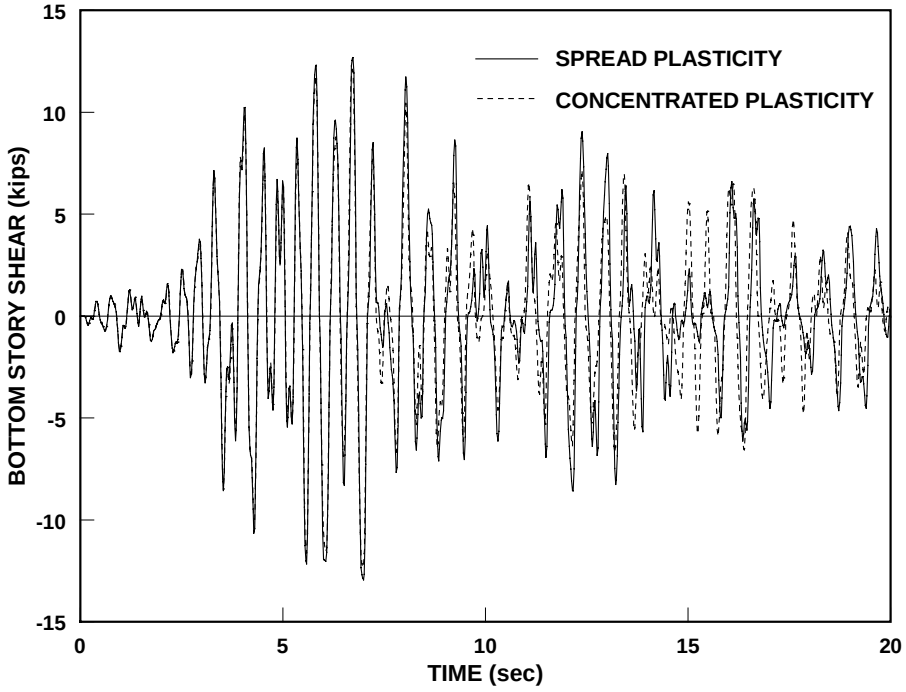

FIGURE 6.11E COMPARISON BETWEEN SPREAD PLASTICITY AND CONCENTRATED PLASTICITY MODELS OF BOTTOM STORY SHEAR

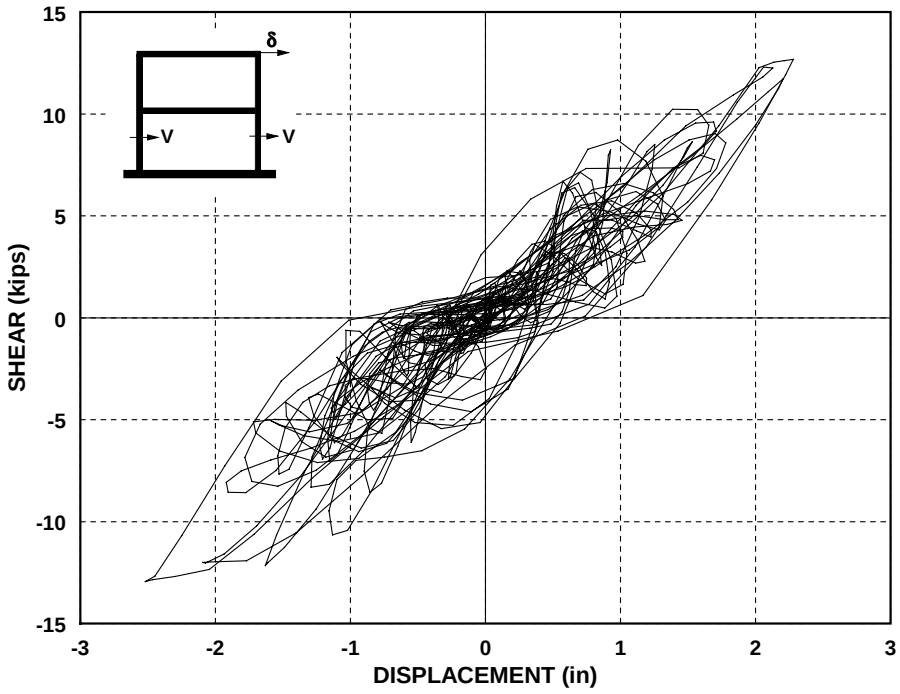

FIGURE 6.12A BOTTOM STORY SHEAR-TOP STORY DISPLACEMENT HYSTERETIC RELATIONSHIP -SPREAD PLASTICITY MODEL

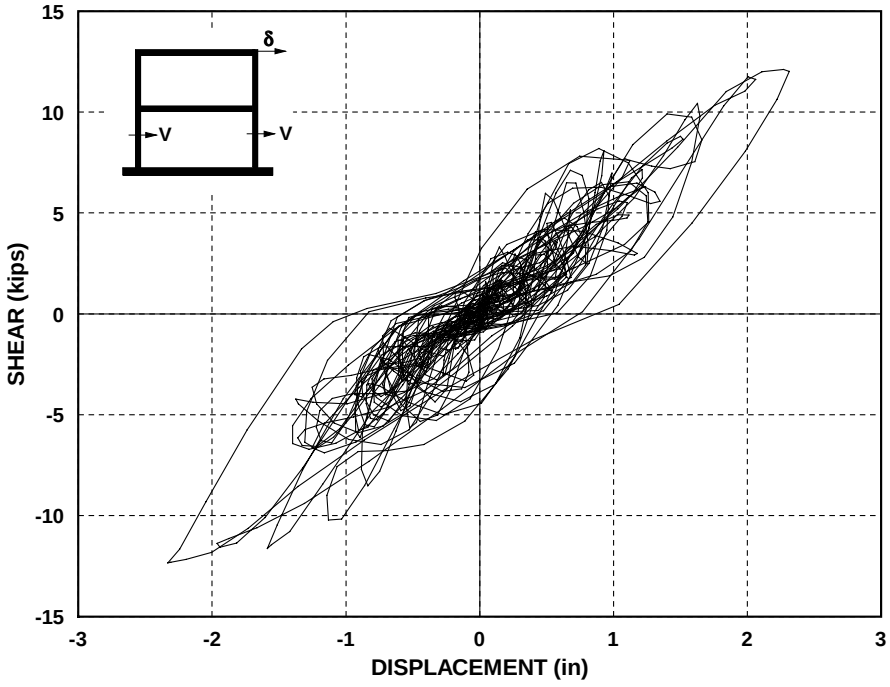

FIGURE 6.12B BOTTOM STORY SHEAR-TOP STORY DISPLACEMENT HYSTERETIC RELATIONSHIP -CONCENTRATED PLASTICITY MODEL

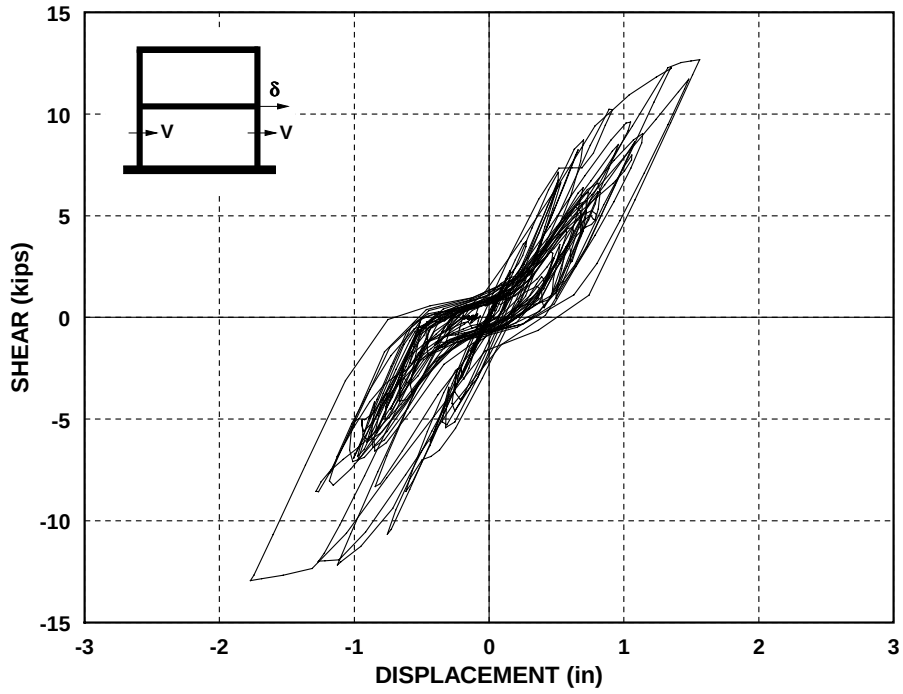

FIGURE 6.13A BOTTOM STORY SHEAR-BOTTOM STORY DISPLACEMENT HYSTERETIC RELATIONSHIP -SPREAD PLASTICITY MODEL

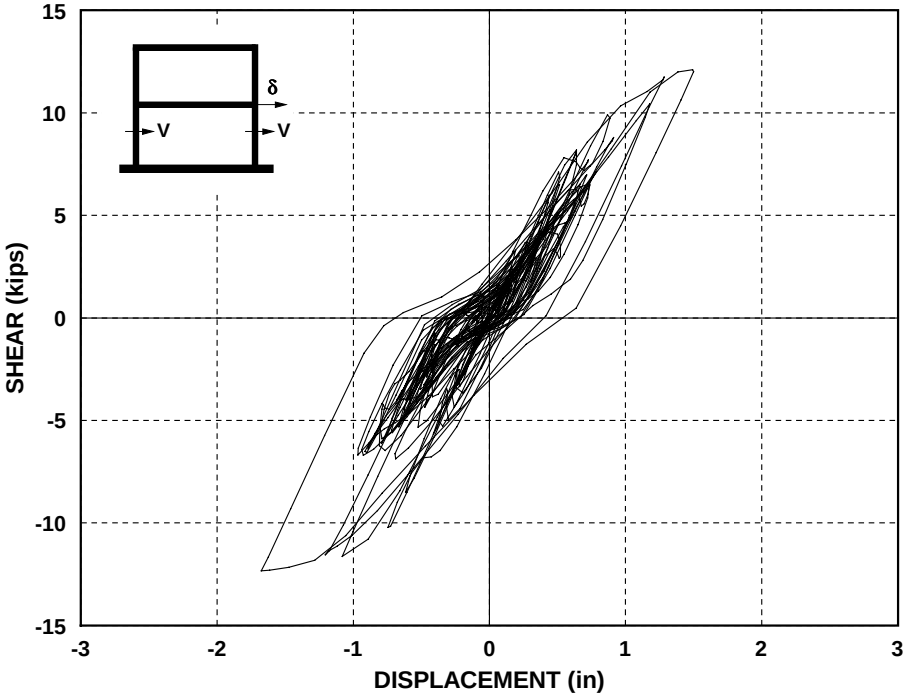

FIGURE 6.13B BOTTOM STORY SHEAR-BOTTOM STORY DISPLACEMENT HYSTERETIC RELATIONSHIP -CONCENTRATED PLASTICITY MODEL

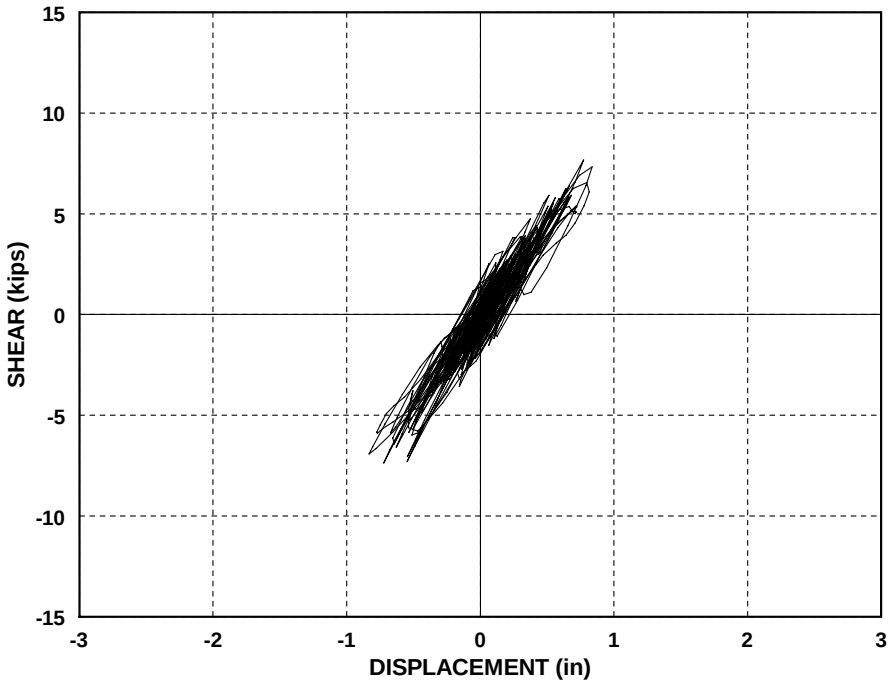

FIGURE 6.14A TOP STORY SHEAR-TOP STORY DRIFT HYSTERETIC RELATIONSHIP -SPREAD PLASTICITY MODEL

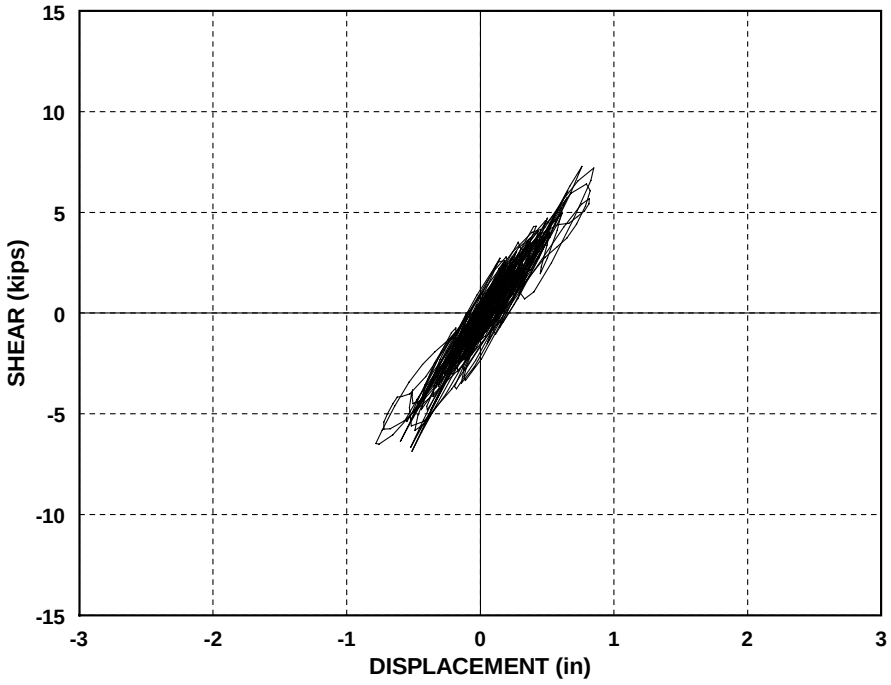

FIGURE 6.14B BOTTOM STORY SHEAR-BOTTOM STORY DISPLACEMENT HYSTERETIC RELATIONSHIP -CONCENTRATED PLASTICITY MODEL

6.5 General Remarks and Discussion

The correlation studies of the proposed model with experimental data from the RCF2 frame proves that the model is able to predict the response of reinforced concrete frame structures subjected to severe dynamic ground shaking while retaining computational efficiency. The analytical predictions of the proposed model correlate well with the experimental data. The displacement response of the structure shows much better agreement with experimental data than the story shear, since the story shear data cannot be considered very reliable (Clough and Gidwani 1976).

The analytical studies presented in this chapter demonstrate that accounting for the fixed-end rotations at the beam-column interface as well as the pull-out from the column base is essential in the dynamic response analysis of RC frame structures during the final design phase, since the bond slip effects alter the global and local response of the structure. The energy dissipation at the beam-column joints constitutes a large portion of the total energy dissipated in the structure. Thus beam-column joints should be designed to have large energy dissipation capacity so as to satisfy the imposed rotation ductility demand.

The study of the local response of the first story column of the structure, in which most of the inelastic deformations are concentrated, shows that neglecting the bond slip effects will considerably overestimate the flexural deformation of the columns. Thus, in order to accurately predict the hysteretic behavior of structural members, the contribution of the joint fixed end rotations to the overall member deformation must be accounted for.

These analytical studies clearly show that the effect of bond slip of reinforcement on the dynamic response of the structure is more complex than its effect on the response to static cyclic load reversals. In the case of dynamic analysis neglecting the effect of bond slip will not necessarily lead to smaller global deformations, as is the case in the static analysis. Rather, the increase in the flexibility of the structure and the energy dissipation due to reinforcement pull-out alters the dynamic response of the structure. However, the increase in the flexibility of the structure due to the bond slip effects does not necessarily result in an increase in the global dynamic response of the structure. This depends on the effect the change in period will have on the spectral acceleration of the ground motion. Therefore, the effect of bond slip on the global response of the structure depends on the dynamic characteristics of the structure and the frequency content of the ground motion.

There is no significant difference in the dynamic response between the model with the concentrated plasticity element and that with the spread plasticity element. This can be certainly attributed to the careful selection of stiffness parameters of the concentrated plasticity element. It is, however, premature at this stage to conclude that the increase in

computational cost of the spread plasticity model over the concentrated plasticity model is not justified. Further comparative studies of the two models, particularly, under conditions of severe strength and stiffness deterioration are required before arriving at a definitive result.

CHAPTER 7
CONCLUSIONS

7.1 Summary

The development of improved analytical methods for predicting the nonlinear static and dynamic response of multistory reinforced concrete frames has been the main objective of this study. A new approach in describing the nonlinear hysteretic behavior of reinforced concrete frame elements has been proposed. This approach consists of isolating the basic mechanisms controlling the hysteretic behavior of girders and columns into individual subelements which are connected in series to form the girder or column superelement. Four particular subelement models were proposed in this study:

(1) a spread plastic subelement which describes the inelastic behavior along the reinforced concrete member accounting for the gradual spread of inelastic deformations at the member ends,

(2) a joint subelement which accounts for the fixed-end rotations that arise at the beam-column interface due to bond deterioration and slippage of reinforcing bars in the beam-column joint region. In case that a substantial axial force is present the joint subelement is capable of describing the interaction of moment and axial force with the opening and closing of flexural cracks,

(3) a shear subelement which describes the sliding in the critical regions and the shear distortion along the member. In case that a substantial axial force is present the shear subelement is capable of describing the interaction of shear and axial forces with the opening and closing of shear cracks,

(4) a flexural subelement which accounts for the linear elastic flexural behavior of the member.

The properties of these elements can be derived from basic principles or refined finite element models.

The monotonic envelope of the spread plastic subelement is derived from the moment-curvature relation of a section in the inelastic region of the frame member. It depends on three values, namely, initial section stiffness, flexural strength and strain hardening ratio and can thus be readily established from first principles. The law governing

the hysteretic behavior of the spread plastic subelement is very simple with no additional parameters introduced. It is based on Clough's hysteretic model.

The properties of the girder and column joint subelements are established using a previously developed refined model of the hysteretic behavior of beam-column joints. The monotonic envelope of the moment-rotation relation depends on three parameters in each direction of bending: the initial stiffness, the yield strength and the strain hardening ratio. The girder joint subelement models the bond deterioration and slip of reinforcement in the beam-column joint. The law governing the hysteretic behavior of this subelement is simple with no additional parameters introduced. It is based on a modification of Clough's hysteretic model so as to account for the characteristic "pinching" effect observed in one direction of bending. The column joint subelement describes the bond deterioration and slip of column reinforcement in the beam-column joint. The law governing the hysteretic behavior of this subelement is based on a modification of Clough's hysteretic model so as to account for the characteristic "pinching" effect observed in columns due to the interaction of axial forces and bending moments with the opening and closing of the beam-column interface crack. The pinching in the column joint subelement depends on the magnitude of the axial force in the member. Higher pinching is introduced as the axial load increases.

The properties of the beam and column shear subelements are established using the compression field theory. The monotonic envelope depends on three parameters: the initial stiffness, the yield strength and the strain hardening ratio. The law governing the hysteretic behavior of the beam shear subelement reflects the pinching effect due to the interaction of shear with the opening and closing of the shear cracks. In the case of the column shear subelement, the higher the magnitude of the axial load the lower the amount of pinching, since the axial load helps in closing the shear cracks.

Since several subelements are connected in series and each of these follows a different hysteretic rule, internal unbalanced moments might arise between these elements at any given load step. The implementation of the proposed girder and column superelement models thus requires the development of a numerical scheme which accounts for these unbalanced moments between subelements. Such a scheme was developed in this study within the framework of a special purpose analysis program for the nonlinear static and dynamic analysis of reinforced concrete moment-resisting frames.

To establish the validity of the proposed models, correlation studies of analytical predictions with experimental evidence were conducted. The experimental evidence included the response of beam-column subassemblages tested under static load reversals as well as the response of a two story one bay frame subjected to strong base excitations on the shaking table.

7.2 Conclusions

A careful analysis of the results of this study leads to the following conclusions:

(1) The proposed modeling approach of decomposing a structural element into subelements connected in series represents a flexible platform for the development of analytical models of any desired level of complexity. Such complexity can be achieved in two ways: first by adding any number of subelements into an existing structural element or, secondly, by refining the hysteretic law of a single subelement. Clearly, a combination of these two schemes is also possible. Studies to date have focused on the second approach adopting a single element and refining the hysteretic law to account for various effects. This study points to the advantages of the first modeling scheme. This approach yields accurate results with relatively simple hysteretic laws which are derived from physical considerations rather than curve fitting.

(2) By isolating mechanisms of hysteretic behavior in separate subelements it is possible to establish improved analytical models of such behavior.

(3) The exchange of results between refined local models suitable for a detailed analysis of small regions and more simplified component models which are suitable for global analysis of multistory structures provides a powerful tool for the study of the seismic response of reinforced concrete structures.

(4) The proposed girder superelement correlates very well with available experimental evidence of the response of beam-column subassemblages to cyclic load reversals. Good agreement with experimental results was observed, both, at the local as well as the global level, in the earlier study of Filippou and Issa (1988).

(5) The proposed column superelement correlates well with available data from experiments on simple specimens subjected to cyclic lateral load reversals and constant axial load. The column element is able to describe the effect of axial load on the strength, stiffness, and the stiffness degradation mechanism of the column.

(6) The proposed girder and column superelements correlate well with available experimental evidence from the dynamic response of a two story one bay frame structure subjected to base excitations corresponding the 1952 N69W Taft record scaled to a peak ground acceleration of 0.57g. Both, story displacement and story shear time history correlate well with experimental results. The good agreement with experimental results indicates that the proposed column and girder superelements are capable of accurately describing the actual strength, stiffness and energy dissipation of RC frame structures. One of the key ingredients of the proposed column and girder

superelements is the stiffness degradation mechanism which proved capable of predicting the actual behavior satisfactorily.

(7) The introduction of two different subelements to account for the effects of shear and bond slip facilitates the accurate and rational consideration of the stiffness degradation mechanism in columns. An increasing axial load reduces the stiffness degradation in members whose behavior is mainly controlled by shear, while it increases the stiffness degradation in members whose hysteretic behavior is controlled by flexure.

(8) In spite of the simplicity of the hysteretic model used in the different subelements, good agreement of the predicted local behavior of beam-column subassemblages with experimental evidence is found. A limitation of the hysteretic models appears to be the value of the unloading stiffness which is consistently higher than observed in experiments.

(9) Neglecting the effects of bond slip of reinforcement can significantly alter the global response of reinforced concrete frame structures subjected to severe base excitations. This, naturally, depends on the frequency content of the base excitations and the dynamic properties of the structure. Neglecting the effect of bond slip underestimates the flexibility of reinforced concrete frames, and thus underestimates the fundamental period of the structure.

(10) The effect of bond slip of reinforcement on the local response of RC frames subjected to severe base excitations is very significant. Neglecting the effect of bond slip in the nonlinear dynamic analysis of reinforced concrete frames leads to an overestimation of the flexural rotation of the frame members.

(11) The reinforcing bar slip at the beam-column joints and the bar pull-out at the base of the first story columns can be a major source of energy dissipation in the structure. It amounts to 20% of the total energy dissipated in the two story one bay structure tested on the shaking table.

(12) The spread plasticity model only approximately accounts for the effect of gravity loads. The effect of gravity loads on the location of plastic hinges is not accounted for. Since inelastic zones are assumed to form at the ends of the member, the girder needs to be subdivided into several elements, if plastic zones can form along the span.

(13) The widely used one-component model shows limitations with respect to the spread plasticity model. These limitations appear in spite of the fact that the fixed-end rotations are modeled in a separate element in the present study. The limitations are:

(a) There is no single rational method for deriving the post-yield stiffness of the moment-rotation relation of the model. In the most commonly used approach the

derivation of the post-yield stiffness is based on the assumption that the point of inflection is located at the member midspan. The stiffness value depends on the magnitude of the bending moment acting at the member end.

(b) The post-yield stiffness depends on the loading history and the structural system.

(c) The earlier study by Filippou and Issa (1988) showed significant differences in the static response of models with the concentrated and spread plasticity element under force control conditions. These differences do not, however, seem to be that significant under displacement control conditions, as might occur under dynamic excitations. The use of either element in the model of a two story subassemblage that was tested on the shaking table resulted in good agreement of the results. Discrepancies between the two models were only observed in the post-peak response of the test frame. Further studies are, however, needed before it can be concluded whether the spread plasticity model offers accuracy advantages that justify its increased computational cost.

(14) It is important to account for the gradual stiffness change in the post yield response of reinforced concrete frame members, the bond slip of reinforcing bars in beam-column joints and the bar pull-out at the base of the frames, especially, in the final design stages. The accurate prediction of the deformation distribution between reinforced concrete members and joints provides valuable information for the detailing of these members.

(15) It is possible to use the one component model for the nonlinear dynamic analysis of RC frame structures in the preliminary design stage. The limitations of the model should, however, be kept in mind in the interpretation of the results of these analyses.

(16) The good agreement of the proposed models with experimental results is achieved with limited computational effort. This is accomplished in three ways:

(a) Each inelastic region possesses a single average effective section stiffness. This concept, originally proposed by Soleimani et. al. (1979) results in a symmetric element stiffness matrix.

(b) The continuous process of plastic zone extension is discretized, as described in Chapter 3.

(c) An efficient nonlinear analysis algorithm is developed which accounts for the nonlinearities due to the gradual spread of the plastic zone length and the coupling between the end moments of the girder.

(17) A new algorithm of nonlinear analysis is proposed. This algorithm is based on the initial stress modification of the Newton-Raphson method. It solves satisfactorily the

problem of possible internal unbalanced moments between the various subelements. These arise, because the subelements are connected in series, while each follows an independent hysteretic rule. Since this situation is encountered in many studies, the algorithm is generally applicable.

(18) The proposed algorithm guarantees within a specified tolerance exact equilibrium between internal resisting moments and external loads at each load step.

7.3 Recommendations for Further Research

(1) The proposed model provides a platform for the addition of new subelements which account for mechanisms of hysteretic behavior that have not been considered in this study.

(2) It is important to extend the proposed hysteretic models to the case of severe damage that can lead to strength dissipation and local failure of individual members in the structure. The proposed analytical method is capable of dealing with the force redistribution in the structure in the presence of strength softening.

(3) The proposed model provides a valuable tool for further studies of the effect of shear and bond in multistory reinforced concrete frames. These studies should also attempt to address the effect of strength softening due to shear and pull-out on the global and local dynamic response.

(4) The effect of various deformation mechanisms on the local and global response of reinforced concrete frame structures under earthquake excitations should be studied in detail. These parametric studies should include structures of different layout and height and several ground motions.

(5) The modeling approach of decomposing a structural element into subelements which represent the basic deformation mechanisms can be extended to shear walls and dual frame-wall systems.

REFERENCES

ACI Committee 318 (1971). Building Code Requirements for Reinforced Concrete, American Concrete Institute, Detroit, MI.

ACI Committee 318 (1983). Building Code Requirements for Reinforced Concrete, American Concrete Institute, Detroit, MI.

ACI-ASCE committee 352 (1985). "Design of Beam-Column Joints in Monolithic Reinforced Structures," *ACI Journal*, v. 82, no. 3.

Allahabadi, R. (1987). "DRAIN-2DX, Seismic Response and Damage Assessment for 2D Structures", Ph.D. Dissertation, University of California, Berkeley.

Anagnostopoulos, S.A. (1981). "Inelastic Beams for Seismic Analyses of Structures", *Journal of the Structural Division, ASCE,* Vol. 107, No. ST7.

Anderson, J.C. and Townsend, W.H. (1977). "Models for RC Frames with Degrading Stiffness", *Journal of the Structural Division, ASCE,* Vol. 103, No. ST12.

American Society of Civil Engineers (1982). "*Finite Element Analysis of Reinforced Concrete Structures*", New York.

Atalay, M. and Penzien, J. (1975). "Behavior of Critical Regions of Reinforced Concrete Components as Influenced by Moment, Shear and Axial Force", *Earthquake Engineering Research Center, Report No. EERC 75-19,* University of California, Berkeley.

Aziz, S.T. and Roesset, J.M. (1976). "Inelastic Dynamic Analysis of Building Frames", *Report No. R76-37, Department of Civil Engineering,* Massachussets Institute of Technology.

Banon, H., Biggs, J.M. and Irvine, M.H. (1981). "Seismic Damage in Reinforced Concrete Frames", *Journal of the Structural Division, ASCE,* Vol. 107, No. ST9.

Beckingsale, C.W. (1980). "Post Elastic Behaviour of Reinforced Concrete Beam-Column Joints," *Research Report 80-20, Department of Civil Engineering,* University of Canterbury, New Zealand.

Bergan, P.G. and Soreide, T. (1973). "A Comparative Study of Different Solution Techniques as applied to a Nonlinear Structural Problem", *Computer Methods in Applied Mechanics and Engineering,* Vol. 2, pp. 185-201.

Bertero, V.V. and Mahin, S.A. (1975). "An Evaluation of Some Methods for Predicting the Seismic Behavior of Reinforced Concrete Buildings", *Earthquake Engineering Research Center, Report No. EERC 75-5,* University of California, Berkeley.

Bertero, V.V. and Popov, E.P. (1975). "Hysteretic Behavior of Ductile Moment Resisting Reinforced Concrete Frame Components", *Earthquake Engineering Research Center, Report No. EERC 75-16,* University of California, Berkeley.

Bertero, V.V. (1979). "Seismic Behavior of Structural Concrete Linear Elements (Beams, Columns) and Their Connections", Introductory Report to Theme II, *AICAP-CEB Symposium, Structural Concrete Under Seismic Actions, Rome 1979;* Comité Euro-International Du Béton, Bulletin D' Information No. 131, Vol. 1, pp. 125-212.

Blondet, J.M., Clough, R.W. and Mahin, S.A. (1980). "Evaluation of a Shaking Table Test Program on Response Behavior of a Two Story Reinforced Concrete Frame", *Earthquake Engineering Research Center, Report No. EERC 80-42,* University of California, Berkeley.

Bresler, B. (1973). "Behavior of Structural Elements," Proceedings of a Workshop on Building Practices for Disaster Mitigation, Boulder, Colorado, Aug., 1972, published by the U.S. Department of Commerce, National Bureau of Standards, Building Science Series No. 6.

Comité Euro-International du Beton (1983). "Response of R.C. Critical Regions under Large Amplitude Reversed Actions", *Bulletin d'Information No. 161,* Lausanne, Switzerland.

Celebi, M. and Penzien, J. (1973). "Experimental Investigation into the Seismic Behavior of the Critical Regions of Reinforced Concrete Components as Influenced by Moment and Shear", *Earthquake Engineering Research Center, Report No. EERC 73-4,* University of California, Berkeley.

Chopra, A.K., Kan. C. (1973). "Effect of Stiffness Degradation On Earthquake Ductility Requirement of Multistory Buildings," *International Journal of Earthquake Engineering and Structural Dynamics,* Vol.2, No. 1.

Clough, R.W., Benuska, K.L. and Wilson, E.L. (1965). "Inelastic Earthquake Response of Tall Buildings", *Proceedings, Third World Conference on Earthquake Engineering, New Zealand,* Vol. 11, New Zealand National Committee on Earthquake Engineering.

Clough, R.W., Benuska, K.L. and Lin, T.Y. (1966). "FHA Study of Seismic Design Criteria for High Rise Buildings", HUDTS-3, Federal Housing Administration, Washington D.C.

Clough, R.W. and Gidwani, J. (1976). "Reinforced Concrete Frame 2: Testing and Analytical Correlation", *Earthquake Engineering Research Center, Report No. EERC 76-15,* University of California, Berkeley.

Clough, R.W. and Penzien, J. (1975). "*Dynamics of Structures*"**,** McGraw Hill Book Co., New York.

Collins, M.P. and Mitchell, D. (1980). "Shear and Torsion Design of Prestressed and Non-Prestressed Concrete Beams", Journal of Prestressed Concrete Institute, Vol. 25, No. 5.

Durrani, A.J. and Wight, J.K. (1982). "Experimental and Analytical Study of Internal Beam to Column Connections Subjected to Reversed Cyclic Loading," *Department of Civil Engineering Report No. UMCE82R3,* University of Michigan, p. 275.

Emori, K. and Schnobrich, W.C. (1981). "Inelastic Behavior of Concrete Frame-Wall Structures", *Journal of the Structural Division, ASCE,* Vol. 107, No. ST1.

Filippou, F. (1983). "Effects of Bond Deterioration on Seismic Response of R/C Frames," *Ph.D. Dissertation,* University of California, Berkeley.

Filippou, F.C., Popov, E.V. and Bertero, V.V. (1983). "Effects of Bond Deterioration on Hysteretic Behaviour of Reinforced Concrete Joints," *Earthquake Engineering Research Center, Report No. UCB/EERC-83/19,* University of California, Berkeley, pp. 191.

Filippou, F.C., Popov, E.P. and Bertero, V.V. (1983). "Modeling of Reinforced Concrete Joints under Cyclic Excitations", *Journal of Structural Engineering, ASCE,* Vol. 109, No. 11.

Filippou, F.C. (1989). "Microcomputer-Aided Design of Reinforced and Prestressed Concrete Elements", *ACI-Special Publication,* State-of-the-Art Computer Applications in Concrete Technology, ACI SP-111.

Gates, W.E. (1977). "The Art of Modeling Buildings for Dynamic Seismic Analysis", *Proceedings of a Workshop on Earthquake Resistant Reinforced Concrete Building Construction,* Vol. II, pp.857-886, University of California, Berkeley.

Giberson, M.F. (1974). "Two Nonlinear Beams with Definition of Ductility", *Journal of the Structural Division, ASCE,* Vol. 95, No. ST7.

Gill, W.D., Park, R. and Priestley, M.J.N. (1979). "Ductility of Rectangular Reinforced Concrete Columns with Axial Loads", *Research Report 79-1, Department of Civil Engineering,* University of Canterbury, New Zealand.

Golafshani, A. (1982). "A Program for Inelastic Seismic Response of Structures", *Ph.D. Dissertation,* University of California, Berkeley.

Mohammad S. Al Haddad and Wight, J.K. (1986). "Feasibility and Consequences of Moving Beam Plastic Hinging Zones for Earthquake Resistant Design of Reinforced Concrete Buildings", *Department of Civil Engineering Report No. UMCE86-1,* University of Michigan.

Haisler, W.E. and Stricklin, J.A. (1974). "Computational Methods for Solving Nonlinear Structural Mechanics Problems", *Proceedings of the International Conference in Nonlinear Mechanics,* University of Texas at Austin.

Humar, J. (1981). "Seismic Response of Reinforced Concrete Frames", *Journal of the Structural Division, ASCE,* Vol. 107, No. ST7, July 1981.

Jirsa, J.O. (1977). "Behavior of Elements and Subassemblages-R.C. Frames", *Proceedings of a Workshop on Earthquake Resistant Reinforced Concrete Building Construction,* Vol. III, pp.1196-1214, University of California, Berkeley.

Kaba, S.A. and Mahin, S.A. (1984). "Refined Modeling of Reinforced Concrete Columns for Seismic Analysis", *Earthquake Engineering Research Center, Report No. EERC 84-03,* University of California, Berkeley.

Kanaan, A.E. and Powell, G.H. (1973). "General Purpose Computer Program for Inelastic Dynamic Response of Plane Structures", *Earthquake Engineering Research Center, Report No. EERC 73-6,* University of California, Berkeley.

Kelly, T.E. (1974). "Some Seismic Design Aspects of Multistory Concrete Frames", *Master of Engineering Report,* University of Canterbury, New Zealand.

Keshavarzian, M. and Schnobrich, W.C. (1984). "Computed Nonlinear Seismic Response of R/C Frame-Wall Structures", *Civil Engineering Studies, Structural Research Series No. 515,* University of Illinois at Urbana-Champaign, Urbana, Ill..

Küstü, Q. (1973). "Behavior of Reinforced Concrete Deep Beam-Column Subassemblages Under Cyclic Loads", *Earthquake Engineering Research Center, Report No. EERC 73-8,* University of California, Berkeley.

Low, S.S. and Moehle, J.P. (1987). "Experimental Study of Reinforced Concrete Columns Subjected to Multiaxial Cyclic Loading", *Earthquake Engineering Research Center, Report No. EERC 87-14,* University of California, Berkeley.

Ma, S.Y., Bertero, V.V. and Popov, E.P. (1976). "Experimental and Analytical Studies on the Hysteretic Behavior of Reinforced Concrete Rectangular and T-Beams," *Earthquake Engineering Research Center, Report No. EERC 76-2,* University of California, Berkeley.

Mahin, S.A. and Bertero, V.V. (1976). "Problems in Establishing and Predicting Ductility in Seismic Design", *International Symposium on Earthquake Structural Engineering*, St. Louis, Missouri, USA.

Meyer, C., Roufaiel, M.S. and Arzoumanidis, S.G. (1983). "Analysis of Damaged Concrete Frames for Cyclic Loads", *Earthquake Engineering and Structural Dynamics*, Vol. 11, pp. 207-228.

NZS 3101-1982 (1982). "Code of Practice for the Design of Concrete Structures", Standards Association of New Zealand, Wellington, Part 1, p. 127, Part 2, p. 156.

Newmark, N.M. (1959). "A Method of Computation for Structural Dynamics", *Journal of the Engineering Mechanics Division, ASCE*, Vol. 85, No. EM3.

Newmark, N.M. and Hall, W.J. (1981). "*Earthquake Spectra and Design*", A Primer, Earthquake Engineering Research Institute, Berkeley, California.

Otani, S. (1974). "Inelastic Analysis of R/C Frame Structures", *Journal of the Structural Division, ASCE*, Vol. 100, No. ST7.

Otani, S., Kitayama, K. and Aoyama, H. (1985). "Beam Bar Bond Stress and Behaviour of Reinforced Concrete Interior Beam-Column Joints", *Second US-NZ-Japan Seminar on Design of Reinforced Concrete Beam-Column Joints*, Tokyo, Japan.

Ozcebe, G. and Saatcioglu, M. (1989). "Hysteretic Shear Model for Reinforced Concrete Members", *Journal of Structural Engineering, ASCE*, Vol. 115, No. 1, Jan. 1989.

Pantazopoulou, S. (1987). "Three-Dimensional Aspects of Nonlinear Response of Reinforced Concrete Structures", *Ph.D. Dissertation*, University of California, Berkeley.

Park, Y.J. and Ang, A.H.S. (1985). "Mechanistic Seismic Damage Model for Reinforced Concrete", *Journal of Structural Engineering, ASCE*, Vol. 111, No. 4.

Park R., Kent, D.C. and Sampson, R.A. (1972). "Reinforced Concrete Members with Cyclic Loading", *Journal of the Structural Division, ASCE*, Vol. 98, No. ST7, July 1972.

Park, P. and Paulay, T. (1975). "*Reinforced Concrete Structures*", John Wiley & Sons, New York.

Park, R. and Paulay, T. (1984). "Joints in Reinforced Concrete Frames Designed for Earthquake Resistance," *Research Report 84-9*, Department of Civil Engineering, University of Canterbury, Christchurch.

Paulay, T. (1977). "Capacity Design of Reinforced Concrete Ductile Frames," *Proceedings of a Workshop on Earthquake-Resistant Reinforced Concrete Building Construction*, University of California, Berkeley, Vol. 3, pp. 1043-1075.

Powell, G.H. (1985). "Notes on Computer Methods for Nonlinear Structural Analysis", Class notes of course CE 223B, University Of California, Berkeley.

Roufaiel, M.S.L. and Meyer, C. (1987). "Analytical Modeling of Hysteretic Behavior of R/C Frames", *Journal of Structural Engineering, ASCE*, Vol. 113, No. 3.

Saiidi, M. (1982). "Hysteresis Models for Reinforced Concrete", *Journal of the Structural Division, ASCE*, Vol. 108, No. ST5.

Sharpe, R.D. (1974). "The Seismic Response of Inelastic Structures", *Ph.D. Dissertation*, University of Canterbury, Christchurch, New Zealand.

Selna, L.G. (1977). "Modeling of Reinforced Concrete Buildings", *Proceedings of a Workshop on Earthquake-Resistant Reinforced Concrete Building Construction,* University of California, Berkeley, Vol. II, pp. 887-937, July 1977.

Simons, J.W. and Powell, G.H. (1982). "Solution Strategies for Statically Loaded Nonlinear Structures", *Earthquake Engineering Research Center, Report No. EERC 82-22,* University of California, Berkeley.

Soleimani, D. (1979a). "Reinforced Concrete Ductile Frames Under Earthquke Loading with Stiffness Degradation", *Ph.D. Dissertation,* University of California, Berkeley.

Soleimani, D., Popov, E.P. and Bertero, V.V. (1979b). "Nonlinear Beam Model for R/C Frame Analysis", *Seventh Conference on Electronic Computation,* St. Louis, Missouri, Aug. 1979, ASCE, New York.

Spurr, S.D. (1984). "Post-Elastic Behavior of Reinforced Concrete Frame Wall Components and Assemblages Subjected to Simulated Seismic Loading", *Ph.D. Dissertation,* University of Canterbury, Christchurch, New Zealand, 1984.

Suko, M., Adams, P.F. (1971). "Dynamic Analysis of Multistory Frames," *Journal of the Structural Division, ASCE,* Vol. 97, No. ST10.

Takayanagi, T. and Schnobrich, W.C. (1979). "Non-Linear Analysis of Coupled Wall Systems", *Earthquake Engineering and Structural Dynamics,* Vol. 7, pp. 1-22.

Takeda, T., Sozen, M.A. and Nielsen, N.N. (1970). "Reinforced Concrete Response to Simulated Earthquakes", *Journal of the Structural Division, ASCE,* Vol. 96, ST12.

Umemura, H. and Takizawa, H. (1982). "Dynamic Response of Reinforced Concrete Buildings", *Document 2, International Association of Bridge and Structural Engineering,* Zürich, Switzerland.

Uniform Building Code (1970). International Conference of Building Officials, Whittier, California.

Viwathanatepa, S., Popov, E.P. and Bertero, V.V. (1979). "Seismic Behavior of Reinforced Concrete Interior Subassemblages", *Earthquake Engineering Research Center, Report No. EERC 79-14,* University of California, Berkeley.

Zagajeski, S.W., Bertero, V.V. and Bouwkamp, J.G. (1978). "Hysteretic Behavior of Reinforced Concrete Columns Subjected to High Axial and Cyclic Shear Forces", *Earthquake Engineering Research Center, Report No. EERC 78-05,* University of California, Berkeley.

Zeris, C.A. and Mahin, S.A. (1988). "Analysis of Reinforced Concrete Beam-Columns under Uniaxial Excitations", *Journal of Structural Engineering, ASCE,* Vol. 114, No. 4.

APPENDIX A
DERIVATION OF MODEL PARAMETERS
FOR SPECIMENS OF CHAPTER 5

This appendix presents a step-by-step derivation of pertinent model parameters for the correlation studies of Chapter 5.

A .1 Specimen #12 by Celebi and Penzien (1973)

A .1 .1 Introduction

The model parameters for the correlation studies of specimen #12 by Celebi and Penzien (1973) are determined from the material properties, the section geometry and the reinforcement layout. This information was extracted from the EERC report by Celebi and Penzien (1973).

A .1 .2 Material Properties

Young's modulus for steel E_S and the initial modulus of concrete E_C are reported in Tables 3 and 4 on pg. 57-58 of the report. The values are:

$$E_C = 3600 \text{ ksi} \qquad E_S = 28700 \text{ ksi}$$

The modular ratio thus is: $n = 8$

A .1 .3 Section properties

Moment of Inertia

The gross section moment of inertia I is determined from the geometry of the section:

$$I = 1110 \text{ in}^4$$

A .1 .4 Parameters of Girder Moment-Curvature Relation

Initial Stiffness

The upper bound of the initial stiffness value is the product of the gross section moment of inertia with the initial concrete modulus E_c. The resulting value is:

$$EI = 3600 \cdot 1110 = 3996 \cdot 10^3 \text{ k–in}^2/\text{rad}$$

Experimental evidence in Fig. 72 of the EERC report by Celebi and Penzien (1973) suggests a lower bound value of approximately

$$EI = \frac{M}{\varphi} = \frac{700}{0.00037} = 1900 \cdot 10^3 \text{ k–in}^2/\text{rad}$$

A value equal to the average between the upper and the lower bound is assumed for the pre-yield stiffness value of the spread plasticity model in the correlation study, since it gave the best agreement with experimental results

$$EI = 2700 \cdot 10^3 \text{ k–in}^2/\text{rad}$$

Yield Moment

Fig. 43 on pg. 102 of the EERC report by Celebi and Penzien (1973) supplies the following yield moment values

$$M_y^+ = 780 \text{ kip–in} \qquad M_y^- = 750 \text{ kip–in}$$

Strain Hardening Ratio

Experimental evidence in Fig. 72 of the EERC report by Celebi and Penzien (1973) yields the following values for the strain hardening stiffness E_{py}^+ under a positive bending moment and the strain hardening stiffness E_{py}^- under a negative bending moment

$$E_{py}^+ = 100/0.0020 = 50000$$

$$E_{py}^- = 150/0.0028 = 53571$$

With these post-yield stiffness values and the assumed initial stiffness the following values result for the strain hardening stiffness ratio η_P under a positive bending moment and the strain hardening stiffness ratio η_N under a negative bending moment

$$\eta_P = 0.018 \qquad \eta_N = 0.019$$

The values that give the best agreement with experimental results in the correlation study are slightly smaller, namely

$$\eta_P = 0.017 \qquad \eta_N = 0.017$$

A .1 .5 Parameters of Joint Moment-Rotation Relation

The parameters of the moment-rotation relation of the joint subelement are determined with the following simple procedure of Park and Paulay (1975, pg. 404).

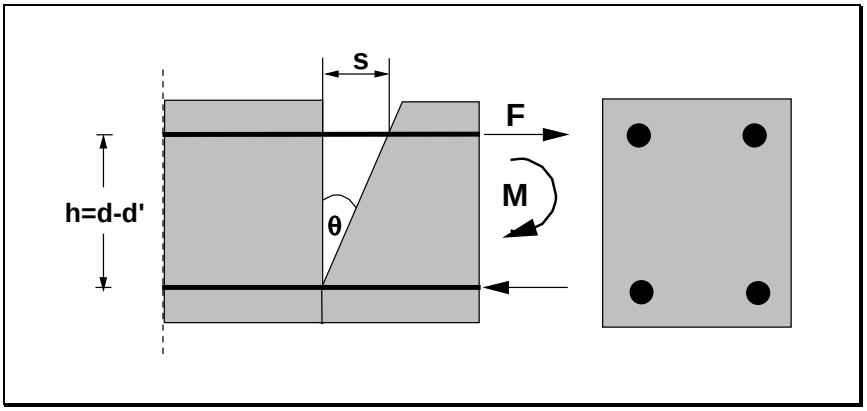

FIGURE A.1 DETERMINATION OF PULL-OUT

The pull-out force *F* in Fig. A.1 is related to the pull-out value *s* by the linear relation

$$F = k \cdot s$$

where *k* is the linear bond stiffness of the reinforcing bar, which can, in turn, be determined with the following relation for a single reinforcing bar

$$k = \frac{E_s \cdot 4\pi \cdot \mu \cdot d_b}{2 f_y}$$

E = steel elastic modulus, μ = average bond stress in anchorage zone, d_b = bar diameter and f_y = yield stress of reinforcing steel.

At yielding of the reinforcing steel the following relations hold (Fig. A.1):

$$F = A_s \cdot f_y$$

$$s = \frac{F}{k}$$

$$\theta \approx \frac{s}{h}$$

$$M \approx F \cdot h$$

where: A_s = total steel area of one layer, h is the distance between top and bottom reinforcing layer in Fig. A.1 and M is the bending moment. The joint pre-yield stiffness then becomes:

$$K_{\text{joint}} = \frac{M}{\theta}$$

Initial Stiffness

For specimen #12 of Celebi and Penzien (1973) the pre-yield stiffness of the joint subelement is determined with the following values:

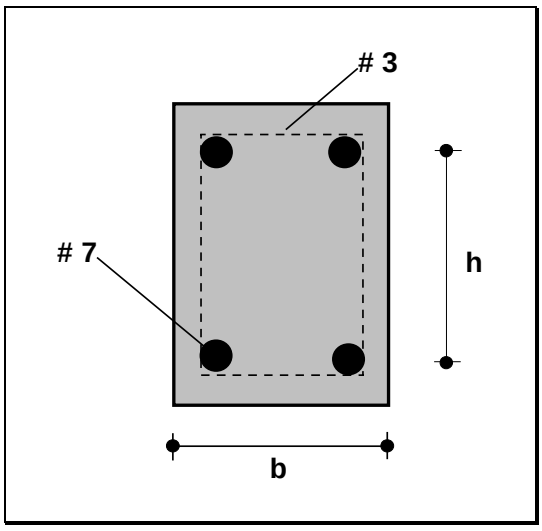

$E_s = 28700 \cdot \text{ksi}$
$\mu = 720 \text{ psi}$
$d_b = 0.875 \text{ in}$
$f_y = 49000 \text{ psi}$
$A_s = 2 \cdot 0.61 \text{ in}^2 = 1.22 \text{ in}^2$
$h = 10.125 \text{ in}$
$b = 9 \text{ in}$

$$k = \frac{28.7 \cdot 10^6 \cdot 4\pi \cdot 0.875 \cdot 720}{2 \cdot 49000} = 2319 \text{ k/in}$$

$$F = A_s \cdot f_y = 0.61 \cdot 49000 = 29.9 \text{ kips}$$

$$s = \frac{F}{k} = \frac{29.9}{2319} = 0.0127 \text{ in}$$

$$\theta = \frac{s}{h} = \frac{0.0127}{10.125} = 12.5 \cdot 10^{-4} \text{ rad}$$

$$K_{\text{joint}} = \frac{M_y}{\theta} = \frac{750}{12.5 \cdot 10^{-4}} = 600 \cdot 10^3 \text{ k-in/rad}$$

The following stiffness value for the joint subelement gave the best agreement in the correlation study:

$$K_{\text{joint}} = 500 \cdot 10^3 \text{ k–in/rad}$$

Strain Hardening Ratio

The following values for the strain hardening stiffness ratio under positive and negative bending moment give the best agreement with experimental results:

$$\eta_P = 0.04 \qquad \eta_N = 0.04$$

A .1 .6 Parameters of Moment-Shear Rotation Relation

The experimental data in Fig. 102 on pg. 161 of the EERC report by Celebi and Penzien (1973) yield the following values:

Cracking Moment

With a tensile strength value of $f_t = 6.8\sqrt{f_c'}$ the value of the cracking moment is:

$$M_{cr} = 190 \text{ kip–in}$$

Initial Stiffness

$$K_{sh} = \frac{M}{\theta} = \frac{F \cdot L / 4}{\theta} = \frac{486}{0.0028} = 173571 \text{ k–in/rad} \approx 174 \cdot 10^3 \text{ k–in/rad}$$

Rounding off the following value is used in the correlation study:

$$K_{sh} = 180 \cdot 10^3 \text{ k–in/rad}$$

Strain Hardening Ratio

$$\eta_P = \frac{54/0.0150}{174 \cdot 10^3} = 0.021$$

$$\eta_N = \frac{54/0.028}{174 \cdot 10^3} = 0.011$$

The following values for the strain hardening stiffness ratio of the shear subelement gave the best agreement with experimental results:

$$\eta_P = 0.035 \qquad \eta_N = 0.035$$

A .2 Specimen #3 by Atalay and Penzien (1975)

A .2 .1 Introduction

The model parameters for the correlation studies of specimen #3 by Atalay and Penzien (1975) are determined from the material properties, the section geometry and the reinforcement layout. This information was extracted from the EERC report by Atalay and Penzien (1975).

A .2 .2 Material Properties

Young's modulus for steel E_S and the initial modulus of concrete E_C are reported in Tables 2.1 and 2.3 on pg. 72 and 74 of the report. The values are:

$$E_C = 3190 \text{ ksi} \qquad E_S = 27350 \text{ ksi}$$

The modular ratio thus is: $n = 7.6$

A .2 .3 Section properties

Moment of Inertia

The gross section moment of inertia I is determined from the geometry of the section:

$$I = 1152 \text{ in}^4$$

A .2 .4 Parameters of Girder Moment-Curvature Relation

Initial Stiffness

The product of the gross section moment of inertia with the initial concrete modulus E_c yields the following initial stiffness value:

$$EI = 3190 \cdot 1152 = 3675 \cdot 10^3 \text{ k–in}^2/\text{rad}$$

The initial stiffness value that gives the best agreement with experimental results is slightly higher than the gross moment of inertia, because of the presence of the axial compression load of 60 kips

$$EI = 3960 \cdot 10^3 \text{ k–in}^2/\text{rad}$$

Yield Moment

The following values for the yield moment are extracted from Table 4.1 on pg. 78 of the EERC report by Atalay and Penzien (1975):

$$M_y^+ = 916 \text{ kip-in} \qquad M_y^- = 896 \text{ kip-in}$$

Strain Hardening Ratio

It is extremely difficult to obtain a strain hardening stiffness ratio from Fig. 4.4 on pg. 127 of the EERC report by Atalay and Penzien (1975):

The following values for the strain hardening stiffness ratio under positive and negative bending moment give the best agreement with experimental results:

$$\eta_P = 0.02 \qquad \eta_N = 0.02$$

A .2 .5 Parameters of Joint Moment-Rotation Relation

Initial Stiffness

Using the same procedure as described earlier for the specimen of Celebi and Penzien the following initial stiffness value results:

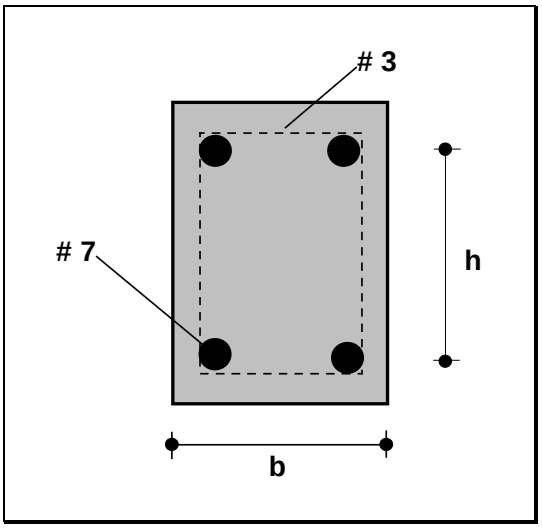

$E_S = 27350 \text{ ksi}$
$\mu = 626 \text{ psi}$
$d_b = 0.875 \text{ in}$
$f_y = 53300 \text{ psi}$
$A_s = 2 \cdot 0.61 \text{ in}^2 = 1.22 \text{ in}^2$
$h = 6.925 \text{ in}$
$b = 12 \text{ in}$

$$k = \frac{27350 \cdot 10^3 \cdot 4\pi \cdot 0.875 \cdot 626}{2 \cdot 53300} = 1766 \text{ k/in}$$

$$F = A_s \cdot f_y = 0.61 \cdot 53300 = 31.98 \text{ kips}$$

$$s = \frac{F}{k} = \frac{31.98}{1766} = 0.0181 \text{ in}$$

$$\theta = \frac{s}{h} = \frac{0.0181}{6.925} = 0.0026 \text{ rad}$$

$$K_{\text{joint}} = \frac{M_y}{\theta} = \frac{900}{0.0026} = 350 \cdot 10^3 \text{ k–in /rad}$$

The following stiffness values give the best agreement with the experimental results:

$$K^{+}_{\text{joint}} = 300 \cdot 10^3 \text{ k–in/rad} \qquad K^{-}_{\text{joint}} = 400 \cdot 10^3 \text{ k–in/rad}$$

Strain Hardening Ratio

The following values for the strain hardening stiffness ratio under positive and negative bending moment give the best agreement with experimental results:

$$\eta_P = 0.04 \qquad \eta_N = 0.04$$

A .2 .6 Parameters of Moment-Shear Rotation Relation

From the experimental data reported in Fig. A.4.c on pg. 210 of the EERC report by Atalay and Penzien (1975) the following values for the parameters of the model result:

Cracking Moment

With a tensile strength value of $f_t = 6.8\sqrt{f_c'}$ and the applied axial compression load of 60 kips the value of the cracking moment is:

$$M_{cr} = 290 \text{ kip–in}$$

Initial Stiffness

$$K_{sh} = \frac{M}{\theta} = \frac{F \cdot L / 4}{\theta} = \frac{324}{0.00025} \approx 1300 \cdot 10^3 \text{ k–in/rad}$$

The value that gives the best correlation with the experimental data is:

$$K_{sh} = 1500 \cdot 10^3 \text{ k–in/rad}$$

Strain Hardening Ratio

The following values for the strain hardening stiffness ratio under positive and negative bending moment give the best agreement with experimental results:

$$\eta_P = 0.025 \qquad \eta_N = 0.025$$

Axial Load Ratio

The axial load ratio is equal to:

$$\frac{P}{P_0}$$

where P = compressive axial force and P_0 = nominal axial strength

For specimen #3 by Atalay and Penzien (1975) the corresponding values are:

$$P = 60 \text{ kips}$$

$$P_0 = f_c \cdot A_c = 4235 \cdot 144 = 610 \text{ kips}$$

so that the following ratio results and is used in the determination of the "pinching" stiffness of the shear subelement in the model

$$\frac{P}{P_0} = \frac{60}{610} = 0.098$$

APPENDIX B

DERIVATION OF MODEL PARAMETERS FOR SHAKING TABLE SPECIMEN RCF2 OF CHAPTER 6

This appendix presents a step-by-step derivation of pertinent model parameters for the correlation studies of Chapter 6.

B .1 Introduction

The model parameters for the correlation studies of the shaking table specimen RCF2 by Clough and Gidwani (1976) are determined from the material properties, the section geometry and the reinforcement layout. This information was extracted from the EERC report by Clough and Gidwani (1976) and the EERC report by Blondet et al. (1980).

B .2 Material Properties

Young's modulus for steel E_S and the initial modulus of concrete E_C are reported in Table 2.1 on pg. 12 of the report by Clough and Gidwani (1976). The values are:

$$E_c = 2640 \text{ ksi} \qquad E_s = 29000 \text{ ksi}$$

The modular ratio thus is: $n = 10.98$

B .3 Parameters of Girder Model

Bottom Story Girders

Moment of Inertia

The value used in the correlation studies is the average cracked moment of inertia. This is determined with the aid of the following information from the EERC Report by Clough and Gidwani (1976). The supplied values of yield moment and curvature in Table 2.3 in Appendix A result in the cracked moment of inertia

$$I_{cr} = \frac{M_y}{E_c \cdot \varphi_y}$$

A single value can then be determined as the average of the cracked moment of inertia under positive and negative bending moments

$$I_{cr,avg} = \frac{I_{cr}^{+} + I_{cr}^{-}}{2}$$

With the information supplied in Table 2.3 the following values result

$$I_{cr}^{+} = 497 \text{ in}^4 \qquad I_{cr}^{-} = 670 \text{ in}^4$$

and the average is

$$I_{cr,avg} = 583.6 \text{ in}^4$$

The following round-off value is used in the correlation studies of Chapter 6

$$I = 580 \text{ in}^4$$

Parameters of Moment-Curvature Relation of Spread Plasticity Model

Initial stiffness

With the values of Young's modulus E_c and moment of inertia I the initial stiffness becomes:

$$EI = 2640 \cdot 580 = 1531200 \text{ k–in}^2/\text{rad}$$

The round-off value used in the correlation study is the same, i.e.

$$EI = 1531 \cdot 10^3 \text{ k–in}^2/\text{rad}$$

Yield Moment

The positive yield moment of the girders is based on the assumption of an effective slab width according to ACI guidelines. The yield moment also accounts for the effect of the compression reinforcement. The participation of the reinforcement within the effective width of the slab is included in the calculation of the negative yield moment. These values are reported in Table 2.3 of the EERC Report by Clough and Gidwani (1976).

$$M_y^{+} = 232 \text{ kip–in} \qquad M_y^{-} = 720 \text{ kip–in}$$

Strain Hardening Ratio

The available experimental data in Clough and Gidwani (1976) are not sufficient to evaluate the strain hardening stiffness ratio η_P under positive bending moment. On the other hand the values in the table on pg. 151 between points 3, 4 and 5 permit the determination of the strain hardening stiffness ratio η_N under negative bending moment. That value is:

$$\eta_N = 0.0195$$

The values for the strain hardening stiffness ratios used in the correlation studies of Chapter 6 are:

$$\eta_P = 0.012 \qquad \eta_N = 0.020$$

Parameters of Moment-Rotation Relation of Concentrated Plasticity Model

Initial Stiffness

The value is the same as for the spread plasticity model, i.e.

$$EI = 1531 \cdot 10^3 \text{ k–in}^2/\text{rad}$$

Yield Moment

The values are the same as for spread plasticity model, i.e.

$$M_y^+ = 232 \text{ kip–in} \qquad M_y^- = 720 \text{ kip–in}$$

Strain Hardening Ratio

Filippou and Issa (1988) conclude in their parametric studies that, in the absence of a better estimate, the strain hardening stiffness ratio for the concentrated plasticity model is approximately equal to twice the strain hardening stiffness ratio of the spread plasticity model (pg. 77-86 and, in particular, pg. 84 in the report). The following values are assumed in the correlation studies of Chapter 6:

$$\eta_P = 0.025 \qquad \eta_N = 0.038$$

For their analytical model Clough and Gidwani (1976) assumed a single strain hardening stiffness ratio of 0.05 on pg. 24 of their report.

Parameters of Joint Moment-Rotation Relation

Initial Stiffness

The following value results with the simple procedure in Appendix A.1.5:

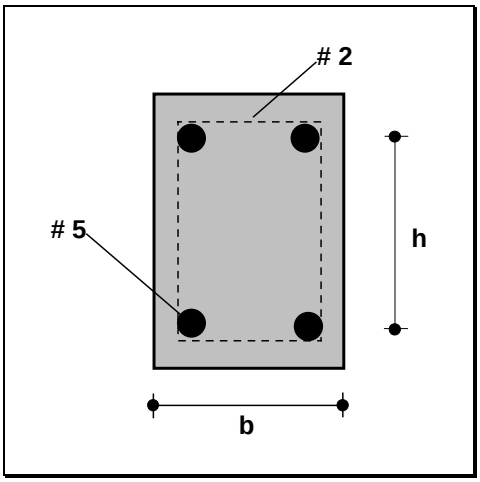

$E = 29800$ ksi
$\mu = 690$ psi
$d = 0.625$ in
$f_y = 41500$ psi
$A_s = 2 \cdot 0.31 \text{ in}^2 = 0.62 \text{ in}^2$
$h = 8.55$ in
$b = 5.75$ in
$h_{slab} = 2.875$ in

$$k = \frac{29.8 \cdot 10^3 \cdot 4\pi \cdot 0.625 \cdot 690}{2 \cdot 41500} = 1946 \text{ k/in}$$

$$F = A_s \cdot f_y = 0.31 \cdot 41500 = 12.865 \text{ kips}$$

$$s = \frac{F}{k} = \frac{12.865}{1946} = 0.0066 \text{ in}$$

$$\theta = \frac{s}{h} = \frac{0.0066}{8.55} = 7.73 \cdot 10^{-4} \text{ rad}$$

$$K_{\text{joint}} = \frac{232}{7.73 \cdot 10^{-4}} = 300 \cdot 10^3 \text{ k-in/rad}$$

The following stiffness value for the joint subelement gave the best agreement in the correlation studies:

$$K_{\text{joint}} = 200 \cdot 10^3 \text{ k-in/rad}$$

Strain Hardening Ratio

The following stiffness value for the joint subelement gave the best agreement in the correlation studies:

$$\eta_P = 0.04 \qquad \eta_N = 0.04$$

Top Story Girders

Moment of Inertia

The value used in the correlation studies is the average cracked moment of inertia. This is determined with the aid of the following information from the EERC Report by Clough and Gidwani (1976). The supplied values of yield moment and curvature in Table 2.3 in Appendix A result in the cracked moment of inertia

$$I_{cr} = \frac{M_y}{E_c \cdot \varphi_y}$$

A single value can then be determined as the average of the cracked moment of inertia under positive and negative bending moments

$$I_{cr,avg} = \frac{I_{cr}^{+} + I_{cr}^{-}}{2}$$

With the information supplied in Table 2.3 the following values result

$$I_{cr}^{+} = 317 \text{ in}^4 \qquad\qquad I_{cr}^{-} = 575 \text{ in}^4$$

and the average is

$$I_{cr,avg} = 446 \text{ in}^4$$

The following round-off value is used in the correlation studies of Chapter 6

$$I = 450 \text{ in}^4$$

Parameters of Moment-Curvature Relation of Spread Plasticity Model

Initial stiffness

With the values of Young's modulus E_c and moment of inertia I the initial stiffness becomes:

$$EI = 2640 \cdot 450 = 1188 \cdot 10^3 \text{ k–in}^2/\text{rad}$$

The round-off value used in the correlation study is the same, i.e.

$$EI = 1188 \cdot 10^3 \text{ k–in}^2/\text{rad}$$

Yield Moment

The positive yield moment of the girders is based on the assumption of an effective slab width according to ACI guidelines. The yield moment also accounts for the effect of the compression reinforcement. The participation of the reinforcement within the effective width of the slab is included in the calculation of the negative yield moment. These values are reported in Table 2.3 of the EERC Report by Clough and Gidwani (1976).

$$M_y^+ = 205 \text{ kip–in} \qquad M_y^- = 640 \text{ kip–in}$$

Strain Hardening Ratio

The available experimental data in Clough and Gidwani (1976) are not sufficient to evaluate the strain hardening stiffness ratio η_P under positive bending moment. On the other hand the average of the values in the table on pg. 152 between points 3, 4 and 5 permit the determination of the strain hardening stiffness ratio η_N under negative bending moment. That value is:

$$\eta_N = 0.022$$

The values for the strain hardening stiffness ratios used in the correlation studies of Chapter 6 are:

$$\eta_P = 0.012 \qquad \eta_N = 0.020$$

Parameters of Moment-Rotation Relation of Concentrated Plasticity Model

Initial Stiffness

The value is the same as for the spread plasticity model, i.e.

$$EI = 1188 \cdot 10^3 \text{ k–in}^2/\text{rad}$$

Yield Moment

The values are the same as for spread plasticity model, i.e.

$$M_y^+ = 205 \text{ kip–in} \qquad M_y^- = 640 \text{ kip–in}$$

Strain Hardening Ratio

Filippou and Issa (1988) conclude in their parametric studies that, in the absence of a better estimate, the strain hardening stiffness ratio for the concentrated plasticity model is

approximately equal to twice the strain hardening stiffness ratio of the spread plasticity model (pg. 77-86 and, in particular, pg. 84 in the report). The following values are assumed in the correlation studies of Chapter 6:

$$\eta_P = 0.025 \qquad \eta_N = 0.038$$

For their analytical model Clough and Gidwani (1976) assumed a single strain hardening stiffness ratio of 0.05 on pg. 24 of their report.

Parameters of Joint Moment-Rotation Relation

Initial Stiffness

The following value results with the simple procedure in Appendix A.1.5:

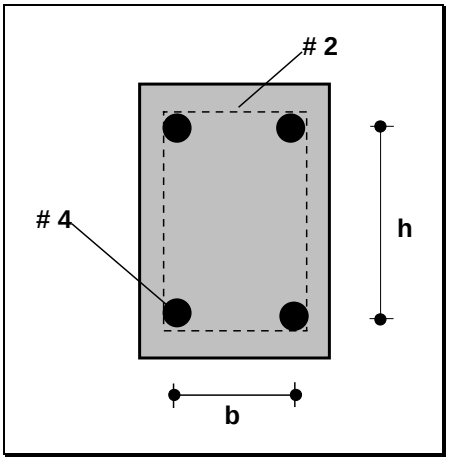

$E = 28000$ ksi
$\mu = 775$ psi
$d = 0.50$ in
$f_y = 56100$ psi
$A_s = 2 \cdot 0.20 \text{ in}^2 = 0.40 \text{ in}^2$
$h = 8.55$ in
$b = 5.75$ in
$h_{slab} = 2.875$ in

$$k = \frac{28 \cdot 10^3 \cdot 4\pi \cdot 0.5 \cdot 775}{2 \cdot 56100} = 1215 \text{ k/in}$$

$$F = A_s \cdot f_y = 0.20 \cdot 56100 = 10.22 \text{ kips}$$

$$s = \frac{F}{k} = \frac{10.22}{1215} = 0.0092 \text{ in}$$

$$\theta = \frac{s}{h} = \frac{0.0092}{8.55} = 0.0011 \text{ rad}$$

$$K_{\text{joint}} = \frac{205}{0.0011} = 186 \cdot 10^3 \text{ k-in/rad}$$

The following stiffness value for the joint subelement gave the best agreement in the correlation studies:

$$K_{\text{joint}} = 200 \cdot 10^3 \ \text{k–in/rad}$$

Strain Hardening Ratio

The following stiffness value for the joint subelement gave the best agreement in the correlation studies:

$$\eta_P = 0.04 \qquad \eta_N = 0.04$$

B .4 Parameters of Column Model

Bottom Story Columns

Moment of Inertia

During test run W1 the first story columns experienced significant cracking. On the contrary, cracking was rather limited for the second story columns (see pg. 113 in Blondet et al. 1980). To represent the extent of cracking in the first columns at the beginning of test run W2 the effective moment of inertia is assumed equal to half the value of the gross moment of inertia

$$I_e = \frac{I_g}{2}$$

where $I_g = 294.3 \ \text{in}^4$ is the gross moment of inertia according to Table 2.2 on page 13 of Clough and Gidwani (1976). Thus,

$$I_e = \frac{294.3}{2} = 147.15 \ \text{in}^4$$

and after rounding-off the following value is used in the correlation studies:

$$I = 148 \ \text{in}^4$$

Parameters of Moment-Curvature Relation of Spread Plasticity Model

Initial stiffness

With the values of Young's modulus E_c and moment of inertia I the initial stiffness becomes:

$$EI = 2640 \cdot 148 = 390720 \ \text{k–in}^2/\text{rad}$$

The round-off value used in the correlation study is the same, i.e.

$$EI = 390 \cdot 10^3 \text{ k–in}^2/\text{rad}$$

Yield Moment

The studies on the shaking table specimen RCF2 by Clough and Gidwani (1976) and by Blondet et al. (1980) supply two different axial force-bending moment interaction diagrams for the columns of the specimen. The characteristic values of the interaction diagram in Clough and Gidwani (1976) are: pure bending moment strength $M_0 = 148.8 \text{ k - in}$, bending moment at balance point $M_B = 352 \text{ k - in}$, axial force at balance point $P_B = 98.4 \text{ kips}$, and axial compression strength $P_0 = 261 \text{ kips}$. The corresponding characteristic values for the interaction diagram for case II in Blondet et al. (1980) are: $M_0 = 180 \text{ k - in}$, $M_B = 320 \text{ k - in}$, $P_B = 70 \text{ kips}$, and $P_0 = 220 \text{ kips}$. The latter interaction diagram appears to be more consistent with the observed experimental behavior of the test frame and is, thus, used as the reference diagram in the following calculations.

Thus, under the assumption of a uniform strength over the column height equal to the ultimate moment capacity that corresponds to a constant axial load under the action of gravity loads, the following yield moment values result for case II (see Table 2.4 on pg. 23 of Blondet et al. 1980):

$$M_y^+ = 208 \text{ kip–in} \qquad M_y^- = 208 \text{ kip–in}$$

Strain Hardening Ratio

The values for the strain hardening stiffness ratios that yield the best agreement with experimental results are:

$$\eta_P = 0.03 \qquad \eta_N = 0.03$$

Parameters of Moment-Rotation Relation of Concentrated Plasticity Model

Initial Stiffness

The value is the same as for the spread plasticity model, i.e.

$$EI = 390 \cdot 10^3 \text{ k–in}^2/\text{rad}$$

Yield Moment

The values are the same as for spread plasticity model, i.e.

$$M_y^+ = 208 \text{ kip–in} \qquad M_y^- = 208 \text{ kip–in}$$

Strain Hardening Ratio

As before, the strain hardening stiffness ratios for the concentrated plasticity model are approximately twice as high as the strain hardening stiffness ratios of the spread plasticity model. The following values are assumed in the correlation studies of Chapter 6:

$$\eta_P = 0.05 \qquad \eta_N = 0.05$$

Parameters of Joint Moment-Rotation Relation

Initial Stiffness

The following value results with the simple procedure in Appendix A.1.5:

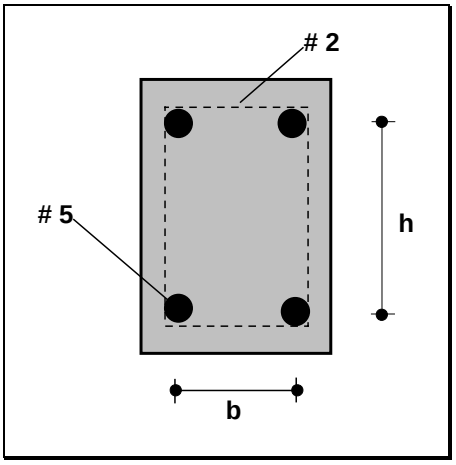

$E = 29000$ ksi
$\mu = 616$ psi
$d = 0.625$ in
$f_y = 41500$ psi
$A_s = 2 \cdot 0.31 \text{ in}^2 = 0.62 \text{ in}^2$
$h = 5$ in
$b = 5.75$ in

$$k = \frac{29 \cdot 10^3 \cdot 4\pi \cdot 0.625 \cdot 616}{2 \cdot 41500} = 1690 \text{ k/in}$$

$$F = A_s \cdot f_y = 0.31 \cdot 41500 = 12.87 \text{ kips}$$

$$s = \frac{F}{k} = \frac{12.87}{1690} = 0.0076 \text{ in}$$

$$\theta = \frac{s}{h} = \frac{0.0076}{5} = 0.00152 \text{ rad}$$

$$K_{\text{joint}} = \frac{208}{0.00152} = 137 \cdot 10^3 \text{ k–in/rad}$$

The following stiffness value for the joint subelement gave the best agreement in the correlation studies:

$$K_{\text{joint}} = 50 \cdot 10^3 \text{ k–in/rad}$$

Strain Hardening Ratio

The following stiffness value for the joint subelement gave the best agreement in the correlation studies:

$$\eta_P = 0.04 \qquad \eta_N = 0.04$$

Top Story Columns

Moment of Inertia

Since the extent of cracking was limited in the second story columns after the completion of shaking table run W1 the following effective moment of inertia value is assumed:

$$I_e = \frac{2}{3} I_g$$

where $I_g = 294.3 \text{ in}^4$ is the gross moment of inertia according to Table 2.2 on page 13 of Clough and Gidwani (1976). Thus,

$$I_e = \frac{2}{3} 294.3 = 196.2 \text{ in}^4$$

and after rounding-off the following value is used in the correlation studies:

$$I = 190 \text{ in}^4$$

Parameters of Moment-Curvature Relation of Spread Plasticity Model

Initial stiffness

With the values of Young's modulus E_c and moment of inertia I the initial stiffness becomes:

$$EI = 2640 \cdot 190 = 501600 \text{ k–in}^2/\text{rad}$$

The round-off value used in the correlation study is the same, i.e.

$$EI = 500 \cdot 10^3 \text{ k–in}^2/\text{rad}$$

Yield Moment

The cross section dimensions for the top story column and the reinforcement layout are the same as for the bottom story columns. The slightly smaller axial load due to gravity loads results in a slightly smaller yield moment according to case II in Table 2.4 on pg. 23 of Blondet et al. (1980):

$$M_y^+ = 194 \text{ kip–in} \qquad M_y^- = 194 \text{ kip–in}$$

Strain Hardening Ratio

The values for the strain hardening stiffness ratios that yield the best agreement with experimental results are:

$$\eta_P = 0.03 \qquad \eta_N = 0.03$$

Parameters of Moment-Rotation Relation of Concentrated Plasticity Model

Initial Stiffness

The value is the same as for the spread plasticity model, i.e.

$$EI = 500 \cdot 10^3 \text{ k–in}^2/\text{rad}$$

Yield Moment

The values are the same as for spread plasticity model, i.e.

$$M_y^+ = 194 \text{ kip–in} \qquad M_y^- = 194 \text{ kip–in}$$

Strain Hardening Ratio

As before, the strain hardening stiffness ratios for the concentrated plasticity model are approximately twice as high as the strain hardening stiffness ratios of the spread plasticity model. The following values are assumed in the correlation studies of Chapter 6:

$$\eta_P = 0.05 \qquad \eta_N = 0.05$$

Parameters of Joint Moment-Rotation Relation

Initial Stiffness

Since the cross section and reinforcement layout are identical the following value results:

$$K_{\text{joint}} = \frac{194}{0.00152} = 128 \cdot 10^3 \text{ k–in /rad}$$

The following stiffness value for the joint subelement gave the best agreement in the correlation studies:

$$K_{\text{joint}} = 60 \cdot 10^3 \text{ k–in/rad}$$

Strain Hardening Ratio

The following stiffness value for the joint subelement gave the best agreement in the correlation studies:

$$\eta_P = 0.04 \qquad \eta_N = 0.04$$